Ultra high-speed transmission using dispersion managed solitons

Lee John Richardson

Doctor of Philosophy

Aston University

July 2001

Aston University

Ultra high-speed transmission using dispersion managed solitons

Lee Richardson

Doctor of Philosophy

July 2001

This thesis presents the results of numerical modelling of ultra high-speed transmission using DM solitons. The theory of propagation in optical fibres is presented with specific reference to optical communication systems. This theory is then expanded to incorporate dispersion-managed transmission and the dispersion managed soliton.

The first part of this work focuses on ultra high-speed dispersion managed soliton propagation in short period dispersion maps. Initially, the characteristics of dispersion managed soliton propagation in short period dispersion maps are contrasted to those of the more conventional dispersion managed regime. These properties are then utilised to investigate transmission at single channel data rates of 80 Gbit/s, 160 Gbit/s and 320 Gbit/s. For all three data rates, the tolerable limits for transmission over 1000 km, 3000 km and transoceanic distances are defined. A major limitation of these higher bit rate systems arises from the problem of noise-induced interactions, which is where the accumulation of timing jitter causes neighbouring dispersion-managed solitons to interact. In addition, the systems become more sensitive to initial conditions as the data rate increases.

The second part of the work focuses on contrasting the performance of a range of propagation regimes, from quasi-linear through to soliton-like propagation, at 40 Gbit/s for both single channel and WDM dispersion managed transmission. The results indicated that whilst the optimal single channel performance was achieved for soliton-like propagation, the optimal WDM performance was achieved for propagation regime that lay between quasi-linear and soliton-like.

Additional key words and phases

Non-linear optics, optical communication systems, non-linear propagation and solitons, dispersion management, optical networks, optical fibres.

Acknowledgement

I would like to thank the supervisors of the project, initially Wladek Forysiak and latterly Vladimir Mezentsev, and also to Professor Keith Blow for providing guidance and inspiration. Additionally, I am also grateful to those with whom I have co-authored papers, namely Sergei Turitsyn, Professor Nick Doran, Jeroen Nijhof, Professor Keith Blow, Vladimir Mezentsev and Wladek Forysiak, for providing stimulating discussion. In addition, I am grateful to Takis Hadjifotiou and his research group at Nortel Networks for both financial support of the project and also for ideas concerning the project.

The funding for this thesis was supported by the United Kingdom Engineering and Physical Research Council (EPSRC) and through a CASE award from Nortel Networks, Harlow laboratories, UK.

Contents

List of Figures

Figure 7.23: A comparison of transmission performance at 40 Gbit/s using 10 ps FWHM pulses. (*dashed line*) hyperbolic secant, (*solid line*) Gaussian and (*dot and dash line*) parabolic. 174

Chapter 1 Introduction

The last two decades have witnessed a rapid growth in the demand for telecommunication services, which in turn, has lead to increased research efforts being focused on optical communications. Transmission using optical fibre shows great potential to meet this increasing demand, as so much of the available bandwidth currently remains unutilised. Of course, the question of effective utilisation is an incredibly important topic and is currently the focus for a vast amount of research [1-5].

In this chapter, we review the types of optical networks and the modulation formats used. We also present an overview of the work included in this thesis.

1.1 Communication networks

In modern times, the telecommunication network covers the vast expanse of the world. In order to achieve such coverage, the network is divided into a hierarchical structure with different levels providing different functionality. The principle structure of the network is shown in Figure 1.1.

Starting at the bottom of the hierarchy in Figure 1.1, the lowest level is the distribution area network. The distribution area network connects end users to a public communications network, facilitating the distribution of signals from local exchanges to the end user.

The access area network sits above the distribution area networks and multiplexes the signals from the end users into higher speed signals. Signals directed in or out of the access area network are routed either from or into the transport network. Typical areas covered by access area networks would be a large city or large conurbation.

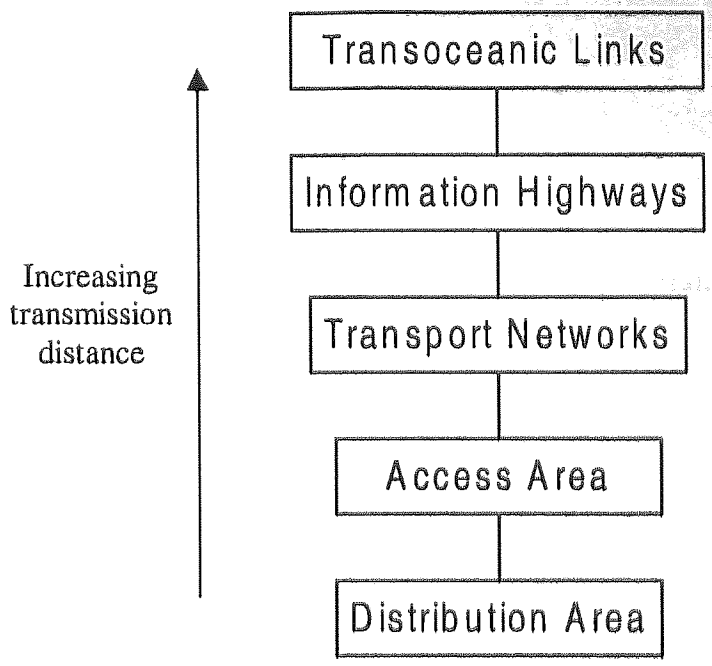

Figure 1.1: Simplified hierarchy of telecommunication networks

The next level in the hierarchy is the transport network, which routes large capacity data without breaking them into component streams. Receiving signals from the access area network, it multiplexes them together and then routes them to their destination. On arrival at the correct destination, the high-speed signals are sent back down to the access level network.

Moving up in the hierarchy, we have information highways. These very high capacity systems connect together different transport area networks. Typically, these networks expand over large geographical areas such as the whole of Europe or the USA.

At the top of the hierarchy are submarine networks, which connect different transport or highway networks across oceans. The main submarine links, such as the Atlantic links connecting Europe with North America, are around 6,000 km in length, and the Pacific links connecting Asia with North America, are round 9,000 km in length.

In the context of this thesis, we are only interested in propagation distances ranging from 1,000 km to 10,000 km. These distances cover the transport area networks, information highways and submarine links. Throughout the thesis, as we have done here, we shall not refer to the network topology, as we assume that all network topologies can be constructed from point-to-point links.

1.2 Data transmission

In the modern era of telecommunications, the nature of the transmitted information has changed from mainly analogue telephony to digital data transmission. Currently, data traffic exceeds telephony traffic and it is predicted that this trend will continue to grow over coming years [6]. Therefore, in this thesis we are concerned solely with digital transmission. Digital data is the representation of information using streams of ones and zeros, with a threshold being used to classify the incoming data signal. The two main modulation formats that are used to transmit optical signals are Return-to-Zero (RZ) and Non-Return-to-Zero (NRZ). With the NRZ format, the pulse width and bit period are identical, so the pulse occupies the whole bit slot and exhibits a rectangular shape. In contrast, RZ pulses only occupy part of the bit period with the pulse intensity returning to zero at the beginning and end of the bit period. Although the NRZ format is more spectrally efficient, better performance is achieved for the RZ modulation format [7-9]. Soliton based optical communications are always RZ format. However, in recent developments other modulation formats have been considered in order to improve the spectral efficiency [10].

1.3 Thesis overview

The aim of this thesis is to investigate ultra high-speed transmission using dispersion managed solitons. In particular, the limitations and robustness of these systems are examined. In chapter 2, we review the theory of pulse propagation in optical fibres. This section reviews some of the limiting factors of optical communication systems. In addition, the concept of both the optical soliton and optical soliton communication systems are introduced.

In chapter 3, we introduce the concept of dispersion management and detail the behaviour of the dispersion managed (DM) soliton. Also we investigate the dynamics of the DM

solitons in the short period dispersion management regime, where DM solitons retain their soliton-like behaviour even for short pulse widths. In addition, we provide an interpretation of how the amplifier placement within dispersion managed systems effects the energy of the DM soliton.

The next three chapters focus on single channel transmission using short period dispersion management. Investigating propagation for long haul to short haul transmission, we optimise the system, and then determine the limitations of the system. Chapter 4 is concerned with 80 Gbit/s transmission, chapter 5 with 160 Gbit/s and chapter 6 with 320 Gbit/s.

In chapter 7, we investigate the important question of whether the DM soliton or quasi linear transmission is the optimal information carrier for high capacity systems. We contrast system performance for four propagation regimes, for both single channel and WDM transmission. The simulation results indicate that for both quasi-linear and DM soliton propagation large inter channel penalties are incurred, whereas for propagation regimes that sit between these regimes the inter channel penalty can be reduced.

Finally, we present the conclusions of the work undertaken in the thesis. Some suggestions for future work are also outline

Chapter 2 Propagation in optical fibres

2.1 Introduction

In this chapter, we review some of the main features of pulse propagation in optical fibres. Initially we focus on the physical properties of optical fibres that are of importance to optical communication systems. We then derive the Non Linear Schrödinger (NLS) equation, which describes the pulse propagation in optical fibres. Next, we consider how non-linear and dispersive effects influence pulse propagation. Finally, we consider soliton propagation in optical fibres and their limitations as information carriers in an optical communication system.

2.2 Properties of optical fibre

In this section, we review the optical fibre, which is the transmission medium used for the work in this thesis. Initially, we examine the construction of an optical fibre, and then review some of its physical properties, with specific emphasis on the application of optical communications.

2.2.1 Fibre characteristics

Step-index fibres are the simplest form of optical fibre, and are constructed from a central core, surrounded by a cladding layer that has a lower refractive index. Therefore, light can be contained in the core through total internal reflection. A schematic representation of a step-index

fibre is shown in Figure 2.1. Such fibres are characterised by the refractive index difference between the core and cladding [11, 12], Δ, defined as

$$\Delta = \frac{n_1 - n_2}{n_1} \tag{2.1}$$

and the normalised frequency V [13], defined as

$$V = k_0 a \left(n_1^2 - n_2^2\right)^{1/2} \tag{2.2}$$

where $n_{1,2}$ are the refractive indices of the core and cladding, k_0 is the wave number, and a is the core radius. Typically $\Delta \approx 3\text{x}10^{-3}$. In this thesis, we are exclusively concerned with single mode fibres, which imposes the condition $V < 2.405$. As a result, we shall discard discussion of any other fibre types.

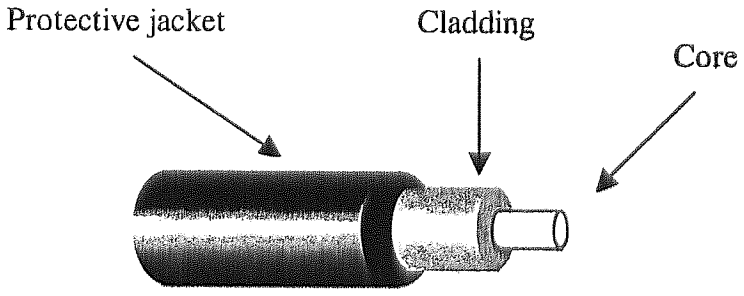

Figure 2.1: Schematic representation of a step index fibre.

2.2.2 Fibre loss

The fundamental limitation of transmission in optical fibres (as with any transmission medium) is the power loss incurred as signals propagate through the fibre. If P_{in} is the launched power,

then after propagation distance L, the output power P_{out} is given by $P_{out} = P_{in}\exp(-\alpha L)$, where α is the attenuation constant or fibre loss. Re-arranging in terms of the fibre loss:

$$\alpha = -\frac{1}{L}\ln\frac{P_{out}}{P_{in}} \tag{2.3}$$

More commonly, fibre loss is quoted in dB/km, in which case α_{dB} is given as:

$$\alpha_{dB} = -\frac{10}{L}\log\left(\frac{P_{out}}{P_{in}}\right) \tag{2.4}$$

where α and α_{dB} are related by $\alpha_{dB} = 10\alpha\log_{10}(e)$.

Attenuation in optical fibres is due to absorption and scattering, and consequently displays frequency dependence. These processes and their relative contributions to the overall fibre attenuation at each wavelength, can be observed in Figure 2.2. Absorption is a complex process phenomenon that is governed by the laws of energy exchange at the atomic level. In the mid-infrared region (above 1.8 μm), the energy is transferred mainly by vibrational transitions, whereas in the ultraviolet region, the absorption is mainly due to electronic and molecular transitions. Scattering loss, the other influential factor, is caused by numerous phenomena. Figure 2.2 shows that Raleigh scattering, which is caused by variations in the refractive index of the transmission medium over distances shorter than the wavelength, is the dominant scattering loss. The resulting loss from Raleigh scattering is proportional to ω^4 (λ^{-4}) and the optimum transmission conditions lie close to the Raleigh lower limit. The presence of the OH absorption peaks limits transmission to three main windows at 0.85 μm, 1.3 μm and 1.5 μm. Modern telecommunications use the 1.5 μm transmission window to take advantage of the low fibre loss of around 0.2 dB/km.

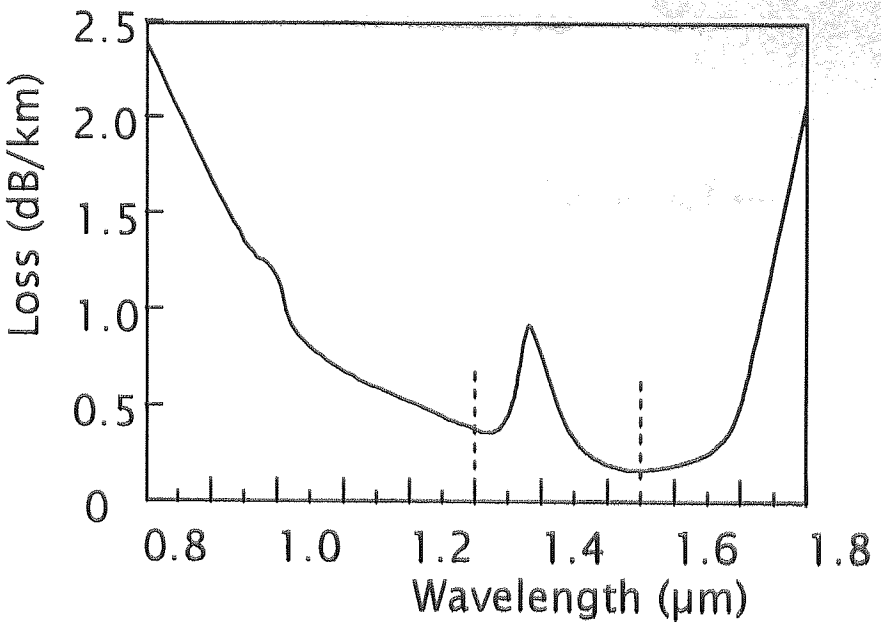

Figure 2.2: Loss charactoristics of standard fibre.

2.2.3 Chromatic dispersion

The frequency dependence of the refractive index $n(\omega)$ of optical fibres, gives rise to chromatic dispersion. The origin of chromatic dispersion is related to the characteristic resonance frequencies at which the medium absorbs the electromagnetic radiation through oscillations of the bound electrons, and far from the medium resonances can be approximated by the Sellmeier equation [11]

$$n^2(\omega) = 1 + \sum_{j=1}^{m} \frac{B_j \omega_j^2}{\omega_j^2 - \omega^2} \tag{2.5}$$

Where ω_j is the resonance frequency and B_j is the strength of the j^{th} resonance, which are obtained from experimental data.

The effect chromatic dispersion has on pulse propagation is to cause the different spectral components of a pulse to experience a different refractive index, which results in pulse

broadening. The effects of fibre dispersion can be analysed by expanding the mode-propagation constant β in a Taylor series about the centre frequency ω_0:

$$\beta(\omega) = n(\omega)\frac{\omega}{c} = \beta_0 + \beta_1(\omega - \omega_0) + \frac{1}{2}\beta_2(\omega - \omega_0)^2 + \cdots \tag{2.6}$$

where

$$\beta_n = \left[\frac{d^n\beta}{d\omega^n}\right]_{\omega=\omega_0} \tag{2.7}$$

The pulse envelope moves at the group velocity $v_g = \beta_1^{-1}$, whilst β_2 is responsible for pulse broadening. These parameters are related to the refractive index through:

$$\beta_1 = \frac{1}{c}\left(n + \omega\frac{dn}{d\omega}\right) = \frac{n_g}{c} = \frac{1}{v_g} \tag{2.8}$$

$$\beta_2 = \frac{1}{c}\left(2\frac{dn}{d\omega} + \omega\frac{d^2n}{d\omega^2}\right) \cong \frac{\omega}{c}\frac{d^2n}{d\omega^2} \cong \frac{\lambda^3}{2\pi c^2}\frac{d^2n}{d\lambda^2} \tag{2.9}$$

where n_g is the group index.

A quantity often used in fibre-optics literature in place of β_2 is the dispersion parameter D given by

$$D = \frac{d\beta_1}{d\lambda} = -\frac{2\pi c}{\lambda^2}\beta_2 \cong -\frac{\lambda}{c}\frac{d^2n}{d\lambda^2} \tag{2.10}$$

2.2.4 Birefringence

Single mode fibres can support two degenerate modes that are dominantly polarised in two orthogonal directions. However, imperfections in the fibre cause a mixing of the two polarisation states by breaking the mode degeneracy. This is the phenomenon of birefringence. Mathematically, the propagation constant β becomes slightly different for each of the polarisations and therefore we introduce propagation constants β_x and β_y for each polarisation. Birefringence causes the polarisation of a monochromatic field to have a periodic evolution during propagation with a beat length:

$$L_b = \frac{2\pi}{\Delta\beta} \tag{2.11}$$

where $\Delta\beta = \beta_x - \beta_y$ is a measure of the fibre birefringence. In other words, the field processes the same state of polarisation at z and $z + L_b$.

Taking the expansion in (2.6), a pulse launched into a fibre, whose state of polarisation does not coincide with one of the modes, broadens due the different group velocities of the modes. This pulse broadening can be measured by a quantity called the differential group delay $[\beta_{1x}(\omega_0) - \beta_{1y}(\omega_0)]z$, whilst the term

$$\Delta\beta_1(\omega_0) = \beta_{1x}(\omega_0) - \beta_{1y}(\omega_0) \tag{2.12}$$

is the polarisation mode dispersion (PMD) of a uniform fibre. However, this is only a simplified model of PMD in a uniform fibre and is not a valid description of real fibres, as important effects such as random mode coupling have been neglected.

2.2.5 Random mode coupling

The phenomenon of random mode coupling [14, 15] arises from the random fluctuations in the fibre structure that induce random power exchange between modes. Therefore, after a short propagation distance (typically a few meters), the power contained in a single mode is randomly distributed between the polarisations modes.

In conventional fibres, random mode coupling is weak, nevertheless coupling cannot be neglected in describing the changing field polarisation [16]. The effect of random mode coupling can be reduced by using high birefringent fibres [17], however cost prevents this from being a practical solution.

2.2.6 Polarisation Mode dispersion

As described in section 2.2.4, polarisation mode dispersion results from the differing group velocity dispersions of the two fibre polarisations. When random mode coupling is also considered, as described in section 2.2.5, the power is randomly distributed between these polarisations. In the simple case of a fibre structure with a constant differential group delay per unit length (deterministic birefringence) plus weak random coupling, then two types of behaviour occurs, depending on the ratio of z and L_h, where L_h is the random mode coupling characterisation length (the distance over which the power is scrambled between the two LP_0 modes).

If the condition $z << L_h$ is satisfied, the random mode coupling has no effect and the differential group delay at the link output is simply $\Delta\tau = \Delta\beta_1 z$. Alternatively if the condition $z >> L_h$, the PMD has a Maxwellian probability written as [18]

$$P(\Delta\tau)^2 = \frac{2\Delta\tau^2}{\sqrt{2\pi\beta_1^6 z^3 L_h^3}} \exp\left(-\frac{\Delta\tau^2}{2\Delta\beta_1^2 L_h z}\right) \qquad 0 \le \Delta\tau < \infty \qquad (2.13)$$

The PMD mean value and standard deviation are given by

$$\langle \Delta\tau \rangle = \sqrt{\frac{8 z L_h}{3\pi}} \Delta\beta_1 , \qquad \sigma_{\Delta\tau} = \sqrt{\frac{(3\pi - 8) z L_h}{3\pi}} \Delta\beta_1 \tag{2.14}$$

An important feature of (2.14) is that the average PMD increases proportionally to $\sqrt{z}$. More commonly, as the transmission distance is variable, PMD is defined as

$$\frac{\langle \Delta\tau \rangle}{\sqrt{z}} = \sqrt{\frac{8 L_h}{3\pi}} \Delta\beta_1 \tag{2.15}$$

with the units ps/√km. The numerical implementation of PMD is discussed in Appendix B.

2.2.7 Nonlinear susceptibility (or fibre nonlinearity)

In general, the evolution of an optical field in a dielectric medium can be given by [19]

$$\nabla^2 \mathbf{E} - \frac{1}{c^2} \frac{\partial^2 \mathbf{E}}{\partial t^2} = -\mu_0 \frac{\partial^2 \mathbf{P}(\mathbf{E})}{\partial t^2} \tag{2.16}$$

where the polarisation $\mathbf{P}$ characterises the medium, and is a function of the electric field. In the case of optical fibre, where the nonlinearity of the medium is weak, the polarisation can be expressed by the Taylor expansion

$$\mathbf{P} \approx \varepsilon_0 \left\{ \chi^{(1)} \mathbf{E} + \chi^{(2)} : \mathbf{EE} + \chi^{(3)} : \mathbf{EEE} \right\} \tag{2.17}$$

where ε_0 is the vacuum permittivity, and $\chi^{(j)}$ (j = 1,2, 3) is the j^{th} order susceptibility. The linear susceptibility $\chi^{(1)}$ represents the dominant contribution to **P** and its effects are included through the refractive index n and the attenuation constant α. The second and third order tensors $\chi^{(2)}$ and $\chi^{(3)}$ are responsible for the nonlinear behaviour. In optical fibres, $\chi^{(2)}$ vanishes as a result of the inversion symmetry at the molecular level of silica glasses. Thus, second-order nonlinear effects are not normally present in optical fibres. The nonlinear behaviour of the optical fibres is mainly due to third order susceptibility $\chi^{(3)}$, which is responsible for phenomena such as third-harmonic generation, four-wave mixing (FWM), and the Kerr effect (nonlinear refraction) [20, 21]. Without special effort in satisfying the phase matching conditions, the non-linear processes which involve the generation of new frequencies (eg third-harmonic generation and FWM) are very inefficient and most of the non-linear effects in optical fibres result from the Kerr nonlinearity. The third order susceptibility is also responsible for stimulated inelastic scattering such as stimulated Raman scattering (SRS) and stimulated Brillouin scattering (SBS), although we shall defer discussion of these phenomena to section 2.7.4.

2.2.8 Kerr effect

The Kerr nonlinearity (also referred to as non-linear refraction) is a phenomenon that refers to the intensity dependence of the refractive index resulting from $\chi^{(3)}$. The refractive index then becomes

$$\hat{n}\left(\omega,|\mathrm{E}|^2\right) = n(\omega) + n_2|\mathrm{E}|^2 \tag{2.18}$$

where $n(\omega)$ is the linear part as shown in (2.5), $|\mathrm{E}|^2$ is the optical field intensity and n_2 is the non-linear-index coefficient given by [20]

$$n_2 = \frac{3}{8n}\mathrm{Re}\left(\chi^{(3)}_{xxxx}\right) \tag{2.19}$$

where Re is the real part and the optical field is assumed to be linearly polarised so that only one component $\chi^{(3)}_{xxxx}$ of the fourth rank tensor contributes to the refractive index. The Kerr effect, depending on the pulse shape, manifests itself in the form of self-phase modulation (SPM), cross-phase modulation (XPM) and four-wave mixing (FWM). These effects will be discussed in more detail in sections 2.5 and 2.7.4.

2.3 Derivation of the Non-linear Schrödinger equation

In this section, we derive the Non-Linear Schrödinger (NLS) equation, which can be used to model short pulse (10 ns ~ 10 fs) propagation in optical fibres, where both non-linear and dispersive effects influence the pulse shape and spectrum. The starting point arising from Maxwell's equations can be given as [22]:

$$\nabla^2\mathbf{E} - \frac{1}{c^2}\frac{\partial^2\mathbf{E}}{\partial t^2} = \mu_0\frac{\partial^2\mathbf{P}_L}{\partial t^2} + \mu_0\frac{\partial^2\mathbf{P}_{NL}}{\partial t^2} \tag{2.20}$$

Where c is the velocity of light, μ_0 is the vacuum permeability, $\mathbf{E}$ is the electric field $\mathbf{E}(r,t)$, and $\mathbf{P}_L$ and $\mathbf{P}_{NL}$ are the linear and non-linear induced polarisations, which are related to the electric field through the dielectric tensors $\chi^{(1)}$ and $\chi^{(3)}$ respectively.

In order to solve (2.20), three simplifying assumptions must be made. Firstly, $\mathbf{P}_{NL}$ can be treated as a small perturbation to $\mathbf{P}_L$. This assumption is valid since optical fibres are only weakly non-linear, the non-linear refractive index is small compared to the refractive index of silica. Secondly, the optical field is assumed to be linearly polarised, therefore its polarisation state does not vary with propagation, and so a scalar approach is valid [23]. Thirdly, the optical

field is assumed to be quasi-monochromatic, i.e. the bandwidth of the field $\Delta\omega$ is much smaller than the carrier frequency ω_0, which is valid for pulse widths > 0.1 ps [24]. As we are concerned with the slowly varying envelope approximation, it is convenient to separate out the rapidly varying part of the electric field, which can be written as:

$$\mathbf{E}(r,t) = \frac{1}{2}\hat{x}\left[\mathbf{E}(r,t)\exp\left(-i\omega_0 t\right) + c.c.\right] \tag{2.21}$$

where $\hat{x}$ is the polarisation vector of the light and *c.c.* is the complex conjugate. Likewise, the polarisation components $\mathbf{P}_L$ and $\mathbf{P}_{NL}$ can be expressed in a similar manner. For pulse widths > 1 ps, the nonlinearity can be assumed to be instantaneous. Therefore, the Fourier transform of the electric field is defined as:

$$\hat{\mathbf{E}}\left(\mathbf{r},\omega-\omega_0\right) = \int_{-\infty}^{\infty}\mathbf{E}(\mathbf{r},t)\exp\left[i\left(\omega-\omega_0\right)t\right]dt \tag{2.22}$$

which satisfies the equation

$$\nabla^2\hat{\mathbf{E}} + \varepsilon(\omega)k_0^2\hat{\mathbf{E}} = 0 \tag{2.23}$$

Where $k_0 = \omega/c$ and $\varepsilon(\omega) = 1 + \chi^{(1)} + \varepsilon_{NL}$ is the dielectric constant whose non-linear part ε_{NL} is given by $\varepsilon_{NL} = {}^3/_4\chi^{(3)}|\mathbf{E}(\mathbf{r},t)|^2$. The dielectric constant can be used to define the refractive index:

$$\hat{n} = n + n_2|\mathbf{E}|^2 \tag{2.24}$$

where $n_2 = \frac{3}{8n}\mathrm{Re}\left(\chi^{(3)}\right)$ is assumed not to change with frequency.

We assume a solution to (2.23) of the form

$$\hat{\mathrm{E}}(r,\omega-\omega_0)=F(x,y)\hat{\mathrm{A}}(z,\omega-\omega_0)\exp(i\beta_0 z) \tag{2.25}$$

where $\hat{\mathrm{A}}(z,\omega-\omega_0)$ is a slowly varying function of z, β_0 is the wave number and $F(x,y)$ is the modal distribution of the fundamental mode in a single mode optical fibre. Substituting (2.25) into (2.23) leads to the following two equations for $F(x,y)$ and $\hat{\mathrm{A}}(z,\omega)$:

$$\frac{\partial^2 F}{\partial x^2}+\frac{\partial^2 F}{\partial y^2}+\left[\varepsilon(\omega)k_0^2-\beta^2\right]F=0 \tag{2.26}$$

$$2i\beta_0\frac{\partial\hat{\mathrm{A}}}{\partial z}+\left(\beta^2-\beta_0^2\right)\hat{\mathrm{A}}=0 \tag{2.27}$$

In (2.27) the second derivative $\partial^2\hat{\mathrm{A}}/\partial z^2$ is neglected since $\hat{\mathrm{A}}(z,\omega)$ is assumed to be a slowly varying function of z. Re-arranging (2.27) and substituting for β^2-β_0^2 gives:

$$\frac{\partial\hat{\mathrm{A}}}{\partial z}=i\left[\beta(\omega)+\Delta\beta-\beta_0\right]\hat{\mathrm{A}} \tag{2.28}$$

Where $\Delta\beta$ can be found from the modal distribution $F(x,y)$ and Δn is the perturbation in the refractive index due to nonlinearity and loss [25]. Δn is given by:

$$\Delta n=n_2|\mathrm{E}|^2+\frac{i\alpha}{2k_0} \tag{2.29}$$

β can be expanded in a Taylor series:

$$\beta(\omega) = \beta_0 + (\omega - \omega_0)\beta_1 + \frac{1}{2}(\omega - \omega_0)^2\beta_2 + \frac{1}{6}(\omega - \omega_0)^3\beta_3 + \ldots \quad (2.30)$$

where

$$\beta_n = \left[\frac{d^n\beta}{d\omega^n}\right]_{\omega=\omega_0} \quad (2.31)$$

Substituting for β and $\Delta\beta$, and taking the inverse Fourier transform, noting that ω-ω_0 is replaced by the operator $i\frac{\partial}{\partial t}$ gives:

$$\frac{\partial A}{\partial z} + \beta_1\frac{\partial A}{\partial t} + \frac{i}{2}\beta_2\frac{\partial^2 A}{\partial t^2} + \frac{\alpha}{2} = i\gamma|A|^2 A \quad (2.32)$$

Where the non-linear coefficient is given by;

$$\gamma = \frac{n_2\omega_0}{cA_{eff}} \quad (2.33)$$

The substitution of $\Delta\beta$ explicitly shows the effects of loss and nonlinearity in equation (2.32). In equation (2.33), A_{eff} is the effective area, which can be found from the modal distribution [26].

Changing to a frame of reference moving with the pulse

$$T = t - \beta_1 Z = t - \frac{Z}{v_g} \quad (2.34)$$

where v_g is the group velocity of the pulse. Therefore, equation (2.32) can be written as

$$i\frac{\partial A}{\partial z} = -\frac{i}{2}\alpha A + \frac{1}{2}\beta_2 \frac{\partial^2 A}{\partial T^2} - \gamma|A|^2 A \qquad (2.35)$$

The three terms on the right hand side of (2.35) are responsible for the effects of absorption, dispersion and nonlinearity on pulses propagating inside optical fibres.

Analysis of the pulse evolution in equation (2.35) can be made by determining the relative contributions of dispersive and non-linear effects. This can be achieved by defining the length scales on which these effects become important. The length scale on which dispersive effects become important is defined as

$$L_D = \frac{T_0^2}{|\beta_2|} \qquad (2.36)$$

where L_D is the dispersion length and T_0 is the initial pulse width. Likewise, the non-linear length can be defined as

$$L_{NL} = \frac{1}{\gamma P_0} \qquad (2.37)$$

where P_0 is the initial pulse power. The relative lengths of L_D and L_{NL} determine which of the effects dominate propagation and can accordingly be classified into four regimes. Considering the case of propagation over a distance L, the first regime is characterised by $L << L_D$ and $L << L_{NL}$. In this regime, neither dispersive nor non-linear effects are important. The second regime is $L \geq L_D$ and $L << L_{NL}$, this regime, where the dispersive effects dominate propagation, will be considered in section 2.4. The third regime is $L << L_D$ and $L \geq L_{NL}$ where non-linear effects dominate propagation, and will be considered in section 2.5. The fourth regime is characterised

by $L \geq L_D$ and $L \geq L_{NL}$, where propagation is dominated by both non-linear and dispersive effects will be discussed in more detail in section 2.6.

2.3.1 Vector non-linear Schrödinger equation

An assumption made in section 2.3, was the field could be treated as being scalar. However, real fibres possess two polarisations, and as discussed in section 2.2.4, the difference in the refractive indexes of these polarisations leads to birefringence [27, 28]. Therefore, a more accurate description of propagation in optical fibres is given by the vector NLS equation [29, 30]:

$$\frac{\partial A_x}{\partial z} + \beta_x' \frac{\partial A_x}{\partial t} + \frac{i}{2}\beta_2 \frac{\partial^2 A_x}{\partial t^2} + \frac{\alpha_x}{2}A_x + i\kappa(z)A_y \exp(-i\Delta\beta z)$$
$$= i\gamma\left(|A_x|^2 + \tfrac{2}{3}|A_y|^2\right)A_x + \frac{i\gamma}{3}A_x^* A_y^2 \exp(-2i\Delta\beta z)$$

$$\frac{\partial A_y}{\partial z} + \beta_y' \frac{\partial A_y}{\partial t} + \frac{i}{2}\beta_2 \frac{\partial^2 A_y}{\partial t^2} + \frac{\alpha_y}{2}A_y + i\kappa(z)A_x \exp(+i\Delta\beta z)$$
$$= i\gamma\left(|A_y|^2 + \tfrac{2}{3}|A_x|^2\right)A_y + \frac{i\gamma}{3}A_y^* A_x^2 \exp(+2i\Delta\beta z) \qquad (2.38)$$

Where $\kappa(z)$ is the random coupling coefficient, $\Delta\beta = \beta_x(\omega_0) - \beta_y(\omega_0)$ is the birefringence parameter and $\alpha_{x,y}$ are the loss values of each polarisation. Equation (2.38) describes propagation in a linearly birefringent fibre.

The equations (2.38) can be simplified further when modelling propagation in optical fibres. The first simplification is to remove the random coupling term $\kappa(z)$, and simulate the random mode coupling numerically, as described in Appendix B. Secondly under the conditions of high and low birefringence the fast rotating terms of equation (2.38) simplify. Under the low birefringence condition, where $\Delta\beta t_0^2 << \beta_2$, the effect of the birefringence is low in the dispersion length, so the exponential terms can be set to 1. Under high birefringence condition,

where $\Delta\beta t_0^2 >> \beta_2$, the exponential terms fluctuate rapidly in the dispersion length and so can be set to 0. The high birefringence conditions are normally met by modern telecommunication fibres. Therefore, applying these simplifications, equation (2.38) becomes

$$\frac{\partial A_x}{\partial z} + \beta_x{}' \frac{\partial A_x}{\partial t} + \frac{i}{2}\beta_2 \frac{\partial^2 A_x}{\partial t^2} + \frac{\alpha_x}{2} A_x = i\gamma\left(|A_x|^2 + \tfrac{2}{3}|A_y|^2\right)A_x$$

$$\frac{\partial A_y}{\partial z} + \beta_y{}' \frac{\partial A_y}{\partial t} + \frac{i}{2}\beta_2 \frac{\partial^2 A_y}{\partial t^2} + \frac{\alpha_y}{2} A_y = i\gamma\left(|A_y|^2 + \tfrac{2}{3}|A_x|^2\right)A_y \qquad (2.39)$$

2.4 Group velocity dispersion

Under the conditions $L \geq L_D$ and $L << L_{NL}$, the effect of group velocity dispersion (GVD) dominates propagation within optical fibres [31]. The main effect of GVD is to cause different frequency components to travel at different velocities causing a pulse to broaden with propagation. For propagation in fibre with a normal dispersion ($\beta_2 > 0$), longer wavelengths travel more quickly, whereas in anomalous dispersion fibre ($\beta_2 < 0$), shorter wavelengths travel more quickly.

The effect of GVD on pulse propagation can be observed in Figure 2.3, which illustrates how the pulse broadens with distance. Also, throughout propagation, the spectrum and energy of the pulse remain unchanged. Neglecting the non-linear terms in equation (2.35), the pulse width after a propagation distance of z, can be predicted using the formula [32]

$$t_1 = t_0\left[1 + \left(\frac{z\beta_2}{t_0^2}\right)^2\right]^{1/2} \qquad (2.40)$$

where t_0 is the initial pulse width and t_1 is the pulse width after propagation over z km. From equation (2.40), it is clear that for an identical β_2, short pulses broaden more quickly.

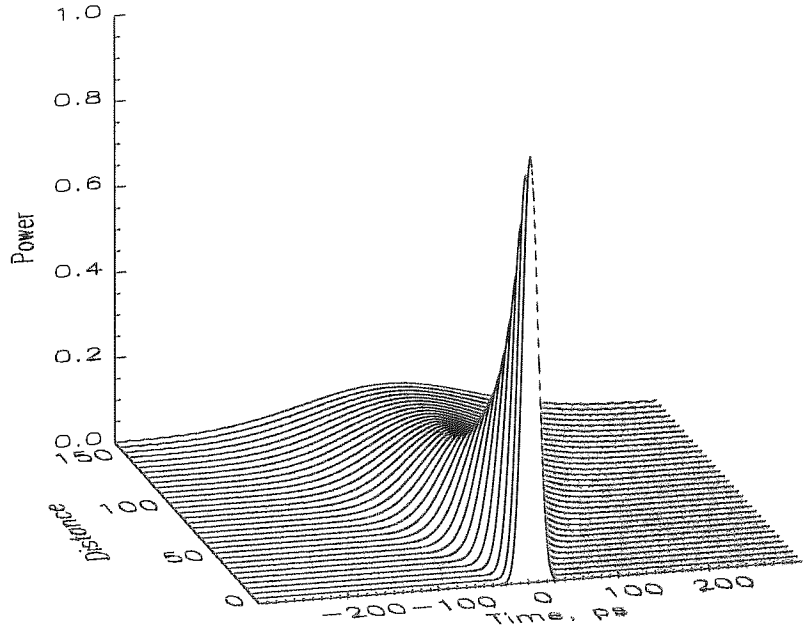

Figure 2.3: A Gaussian pulse broadening with propagation distance for an initial pulse width of 20 ps and $\beta_2 = 10$ ps^2/km

Another type of behaviour can be observed if the initial pulse has a non zero chirp. In the case of the initial chirp being the same sign as the dispersion, then the pulse will broaden more rapidly compared to an initially unchirped pulse. Conversely, if the chirp and dispersion have an opposite sign, then the pulse initially compresses before expanding. In this second case, the frequencies in the leading edge of the pulse are propagating at a lower group velocity than the frequencies at the trailing edge, causing the pulse width and chirp to decrease until the pulse is unchirped. The chirp then changes sign and the broadening behaviour described in the first case begins.

2.4.1 Higher order effects

Whenever the dispersion coefficient $\beta_2 \rightarrow 0$, then higher order terms from the Taylor expansion in equation (2.6) must be considered. The inclusion of the third order dispersion coefficient β_3 complicates the evolution of a propagating pulse [33]. In a similar way as for β_2, the length scale on which the effects due to higher order dispersion become important is defined by [33]

$$L_D' = \frac{t_0^3}{|\beta_3|} \tag{2.41}$$

where t_0 is the initial pulse width. The evolution of a 20 ps pulse through a fibre with $\beta_2 = 0$ and $\beta_3 = 0.2$ ps^3/km is shown in Figure 2.4 at $z = 0$ and $z = 3L_D'$. The effects of the higher order dispersion are to create an asymmetry in the propagating pulse and an oscillating tail. From equation (2.41), it can be seen that these effects are enhanced for short pulse widths.

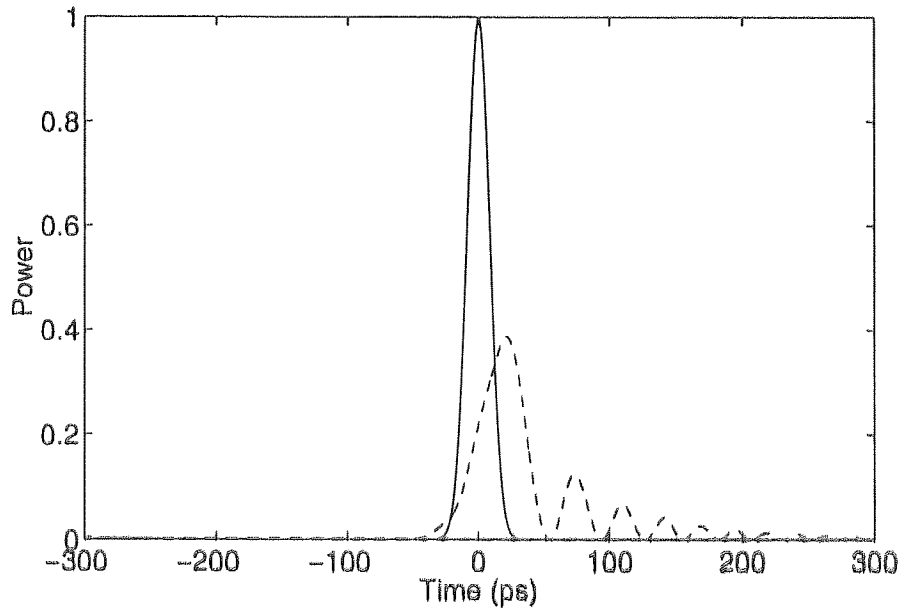

Figure 2.4: The effect of third order dispersion on a propagating pulse. The waveforms are shown at (solid line) $z = 0$ and (dashed line) $z = 3L_D'$.

2.5 Non-linear effects

Under the conditions $L \geq L_{NL}$ and $L << L_D$, the effect of Kerr nonlinearity dominates propagation within optical fibres [34]. The effect of nonlinearity can be investigated by setting $\beta_2 = 0$ in equation (2.35), which yields for the evolution of a pulse [34]:

$$A(z,t) = A(0,t)\exp\left(i\phi_{NL}(z,t)\right) \tag{2.42}$$

Where $A(0,t)$ is the field at $z = 0$ and ϕ_{NL} is the non-linear phase shift given by

$$\phi_{NL}(z,t) = \left|A(0,t)\right|^2\left(z_{eff} / L_{NL}\right) \tag{2.43}$$

$$z_{eff} = \left[1-\exp(-\alpha z)\right]/\alpha \tag{2.44}$$

where z_{eff} is the effective length scale in a lossy system with fibre loss α. Two main effects arise from this nonlinearity: Self-Phase Modulation (SPM) and Cross-Phase Modulation (XPM). SPM produces an intensity dependant phase shift of the pulse's spectrum, whereas XPM is the distortion of one pulse on another that depends on their local intensities. Figure 2.5 illustrates the influence of SPM on the spectral evolution of a 20 ps Gaussian pulse, with $L_{NL} = 5$ km. The temporal evolution remains undistorted due to SPM. However, it can be seen that the spectrum broadens with propagation, with the oscillations in the spectrum arising from the interference of two points of the pulse that have the same instantaneous frequency.

Other non-linear effects not originating from the Kerr nonlinearity include Stimulated Raman Scattering (SRS) [35] and Stimulated Brilliuon Scattering (SBS) [36], which will be discussed in section 2.7.4.

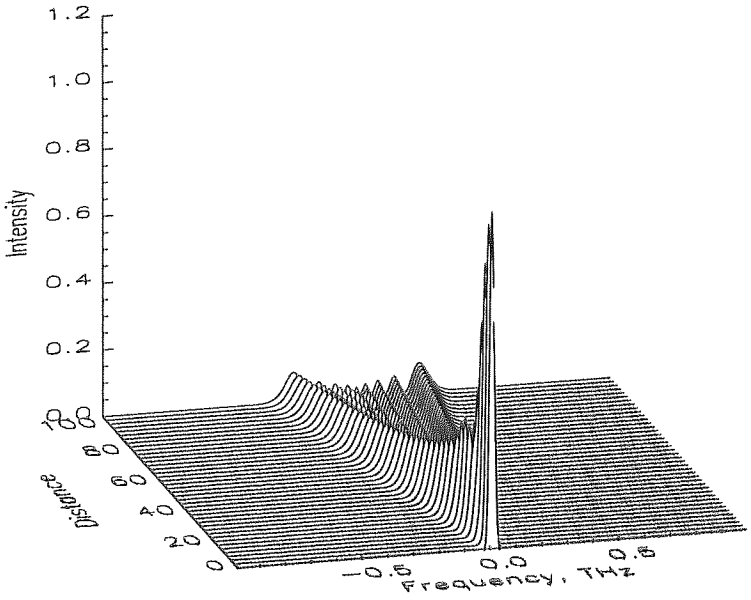

Figure 2.5: The spectrum of a 20 ps Gaussian pulse as it undergoes self-phase modulation, in the absence of fibre dispersion.

2.6 Soliton Solutions of the Non-linear Schrödinger Equation

2.6.1 Introduction

The existence of solitary waves in optical fibres and their subsequent use in optical communication systems, are a direct consequence of two seminal papers published in the early 1970s. The first in 1972 was by Zakharov and Shabat who showed that the NLS equation belongs to a class of equations that could be integrated using the inverse scattering method and admit soliton solutions [37]. The second paper in 1973, by Hasegawa and Tappert, proposed the use of solitons for optical communications [38]. However, it was not until 1980 that solitons were observed under experimental conditions by Mollenauer *et al.* [39].

2.6.2 Soliton propagation in optical fibres

Solitons result from the interplay between the fibre nonlinearity and the anomalous dispersion, creating pulses that can propagate undistorted over long distances. Therefore they exist in a regime such that $L \geq L_D$ and $L \geq L_{NL}$. In its most general form it is given as [40]

$$A(z,t) = \operatorname{sech}(t)\exp(iz/2) \tag{2.45}$$

The corresponding peak power of the soliton is defined as

$$P_0 = \frac{|\beta_2|}{\gamma t_0^2} \tag{2.46}$$

If a hyperbolic secant shaped pulse with a peak power given by equation (2.46) is launched into a lossless fibre then it will propagate over an infinite distance without any change in pulse shape. An example of the propagation of a fundamental soliton can be seen in Figure 2.6, which also shows the evolution of the spectrum and chirp over a single soliton period. The soliton period is defined as

$$Z_0 = \frac{\pi}{2} L_D = \frac{\pi t_0^2}{2|\beta_2|} \tag{2.47}$$

For higher order solitons, this length scale represents the distance over which the soliton returns to its original pulse shape. The soliton period is also the length scale over which the soliton

phase changes by $\pi/2$, although more commonly used is the length over which the phase changes by 2π which is $8Z_0$.

An important factor in soliton propagation is that if a pulse is launched into a fibre that does not have exactly the correct peak power, then over several soliton periods, the pulse will shed radiation and approach the required energy of the soliton. This is an incredibly useful feature, especially in laboratory experiments. Likewise, if the soliton is subject to external perturbations, then again the soliton will regain its initial shape.

(a)

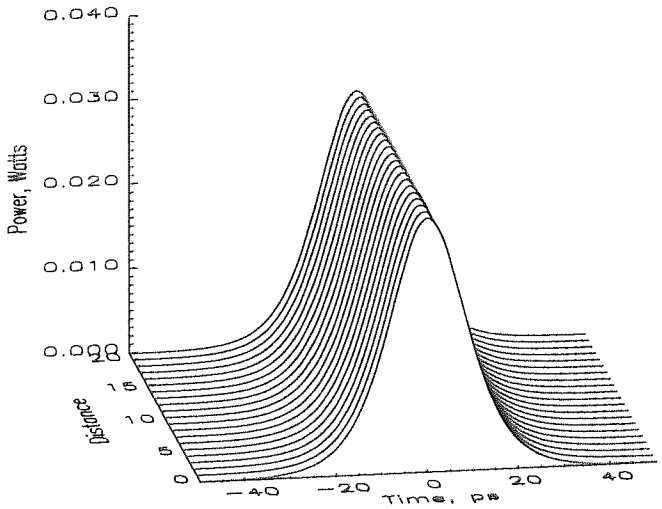

(b)

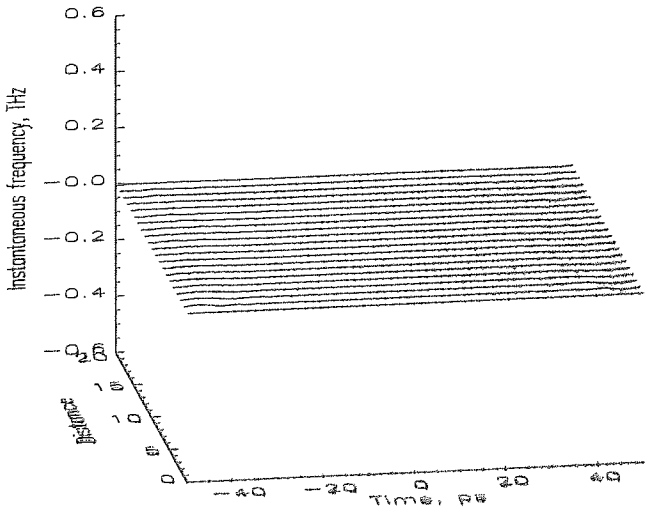

(c)

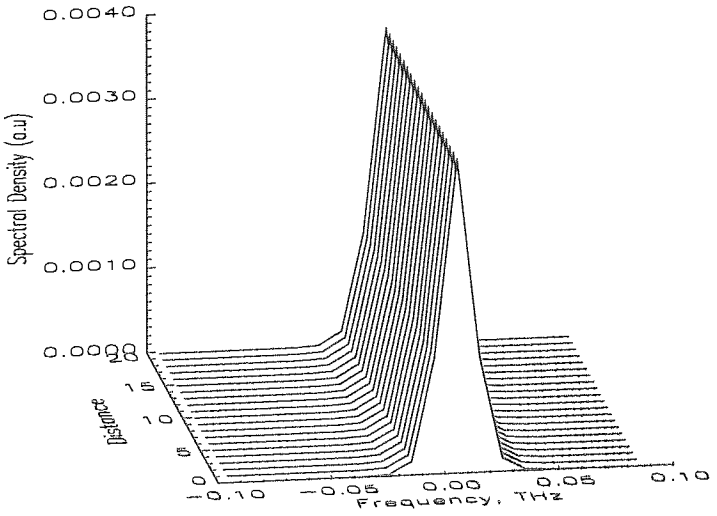

Figure 2.6: The (a) temporal, (b) chirp and (c) spectral solution of the fundamental soliton.

As well as the fundamental soliton, higher order solitons exist where the initial power determines the order of the soliton [41]. The initial conditions of higher order solitons take the form:

$$A(0,t) = N \operatorname{sech}(t) \tag{2.48}$$

where N defines the order of the soliton. For an identical pulse width, a higher order soliton has a peak power that is N^2 times that of a first order soliton. Figure 2.7 demonstrates the evolution of a second and third soliton over a single soliton period. It is apparent, that unlike the fundamental soliton, higher order solitons have a complicated evolution for which the initial pulse shape returns only at the end of the soliton period. This behaviour occurs for higher order solitons because $L_{NL} < L_D$, therefore the pulses become chirped which causes the pulse to split, which then interact and eventually return to the original pulse shape.

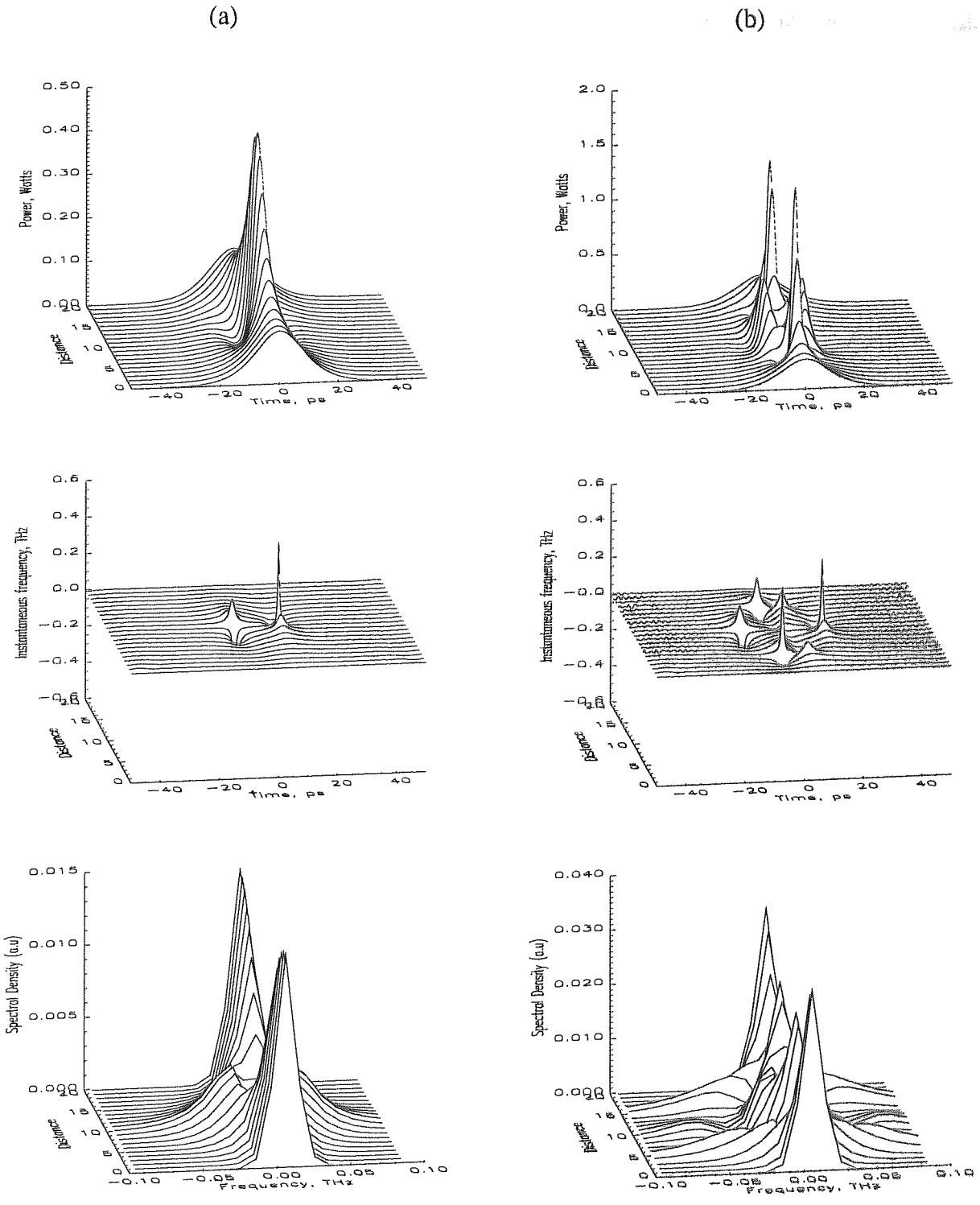

Figure 2.7: The temporal, chirp and spectral evolution of higher order solitons in optical fibre. (a) Second order soliton evolution and (b) third order soliton evolution.

2.7 Soliton based communication systems

Solitons as information carriers, in the conceptual sense, would appear to be the ideal solution for optical communication because of there properties. However, in the transmission environment, there are additional factors that limit performance such as loss, soliton interactions, noise, and higher order non-linear effects. We shall now consider each of these factors in more detail.

2.7.1 Solitons and fibre loss

Although in the strict mathematical sense, solitons cannot exist in the presence of loss, it was found that under certain conditions solitons could in fact propagate in fibres with loss. When solitons propagate through a fibre that contains loss, the balance between the dispersive and non-linear effects no longer holds, as the nonlinearity is continually modified by the fibre loss. A possible solution is to taper the fibre to have an exponential reduction in GVD thus maintaining the non-linear-dispersion balance [42, 43]. Another approach is to just compensate for the fibre loss using amplification. There are two main types of amplification, leading to different soliton propagation, namely Raman amplification and lumped amplification. In the case of Raman amplification, the gain is distributed over a distance beyond the dispersion length, causing the soliton to behave adiabatically i.e. the area occupied by the field envelope stays the same [44, 45]. In the case of lumped amplification, the most common form of which is Erbium Doped Fibre Amplifiers (EFDAs) [46], the soliton behaves non-adiabatically giving rise to the "average" (or "centre guiding") soliton [47, 48]. The average soliton theory shows that as long as the peak power of the pulse averaged over the amplifier span is equal to the first order soliton power, then stable propagation is possible. If the average soliton criteria are not met the propagating pulse breaks up [49].

2.7.2 Soliton interactions

Communication systems based on optical solitons are limited by soliton interactions, which take place through the Kerr nonlinearity [21]. Interactions between solitons results in a loss of information, therefore neighbouring solitons must be well separated in order to minimise these interactions. Interactions have been extensively studied [50-52], and Figure 2.8 shows collision of a pair of solitons. For solitons of equal amplitude and phase, the force between the two solitons is attractive, which causes the solitons to collide. After the collision has taken place the interaction process continually repeats. However, it has been shown that the interaction process is dependant on both the relative magnitudes and phases of the solitons, thus extending the collision distance [53-55].

Figure 2.9 demonstrates the extension of the collision distance between a pair of solitons with a 10 % difference in amplitudes. By comparing Figure 2.9 with Figure 2.8, it can be clearly seen that interactions have been reduced. The effect of having a phase difference between the solitons is illustrated in Figure 2.10, which shows propagation for $\Delta\phi = \pi/2$ and $\Delta\phi = \pi/4$. It can be seen that the introduction of a phase difference causes the solitons to repel each other.

Soliton interactions also occur between solitons of different frequencies, which is the case in WDM systems. Unlike interactions between solitons of the same frequency, the interaction is not periodic, because of the different GVD for each soliton. An interaction between two solitons of different frequencies can be observed in Figure 2.11. The spectral evolution reveals a frequency shift that occurs as the solitons collide, which can be reduced by increasing the frequency separation between the solitons. This frequency shift is caused by the difference in the non-linear shift experienced in the first and second half of the collision process. Other factors that influence the frequency shift are the initial overlap of pulses [56], and the ratio between the collision length and amplification period [57-59].

(a)

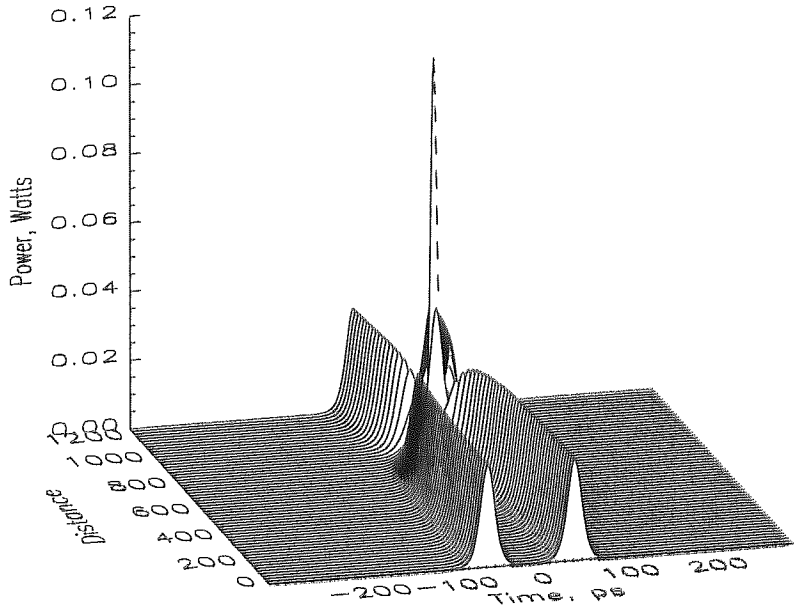

(b)

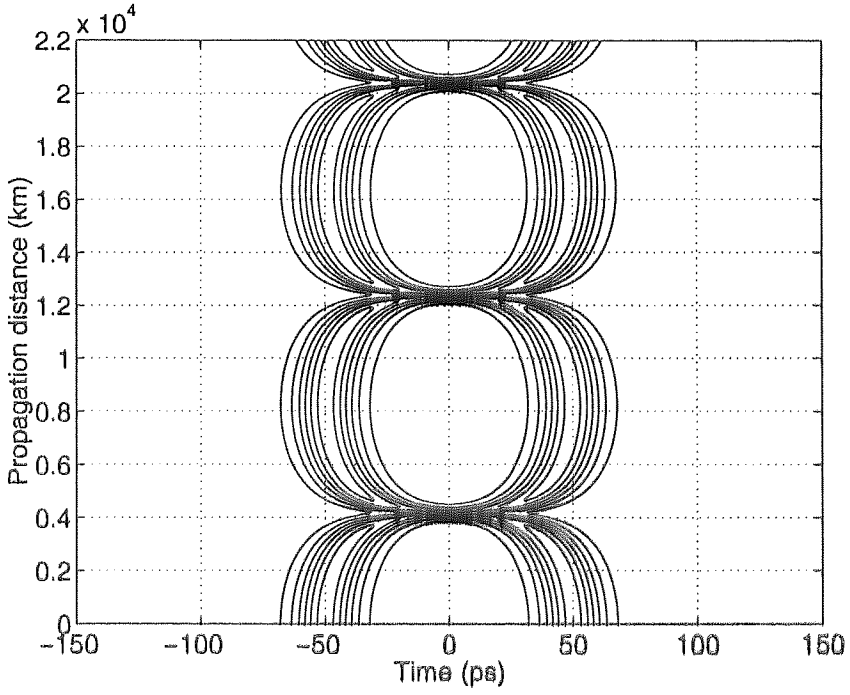

Figure 2.8:The collision of a pair of solitons of equal magnitude and phase. The initial collision is shown in (a) and the repetitive cycle of collisions is shown in (b).

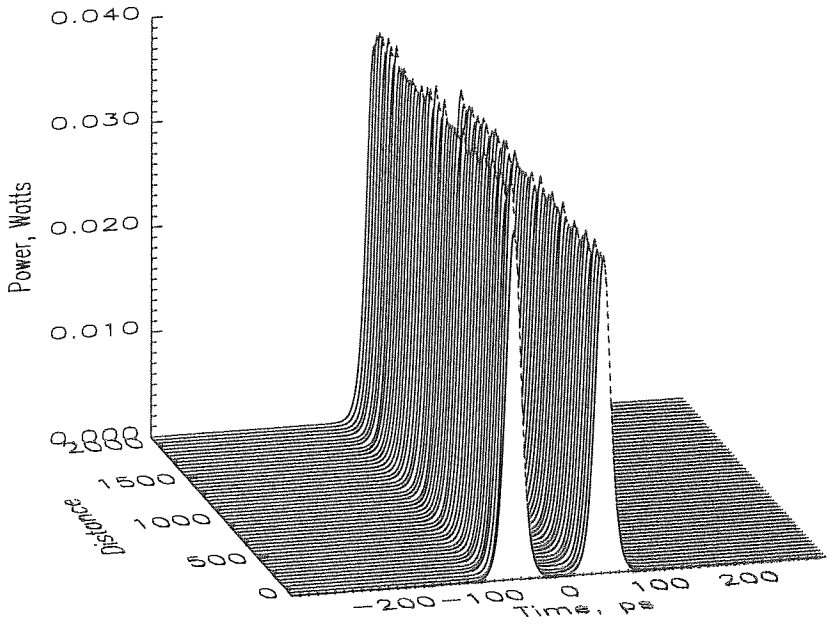

Figure 2.9:Control of soliton interactions by using alternate amplitude solitons, shown is a difference of 10 % in amplitude.

(a)

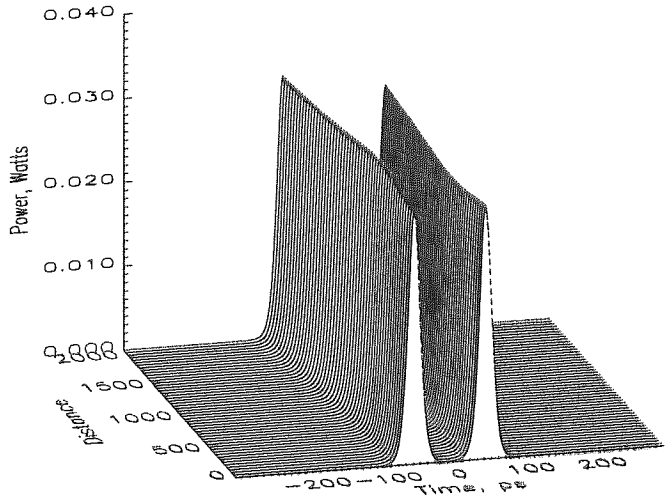

(b)

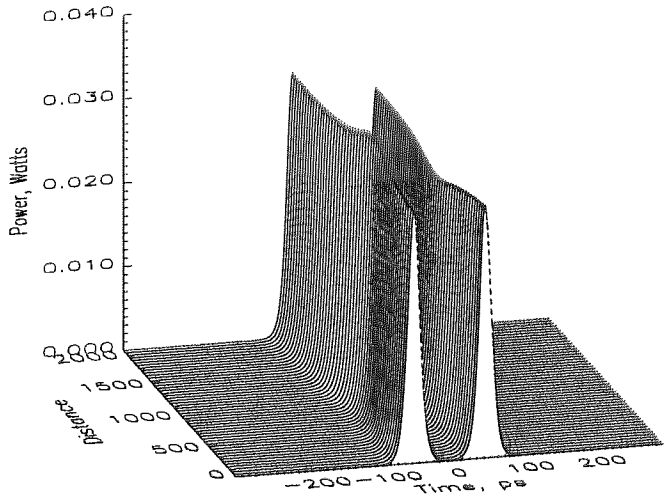

Figure 2.10: Control of soliton interaction using phase control. (a) Phase difference $\Delta\phi = \pi/2$, and (b) phase difference $\Delta\phi = \pi/4$.

(a)

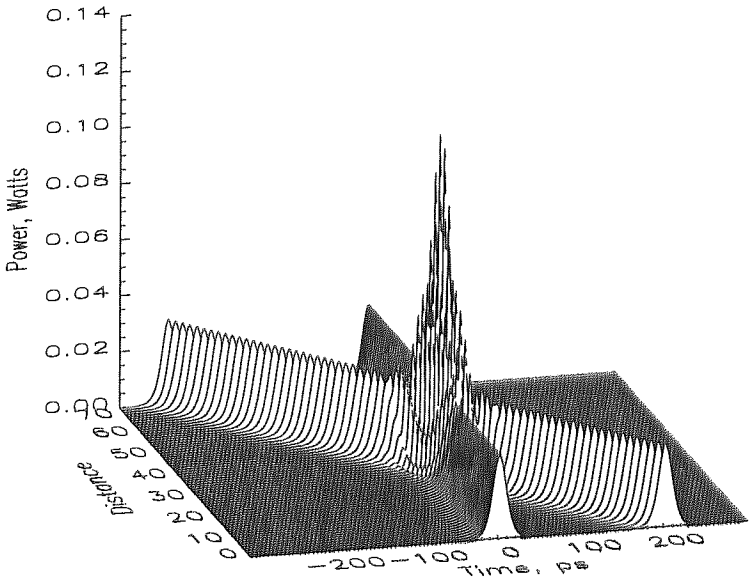

(b)

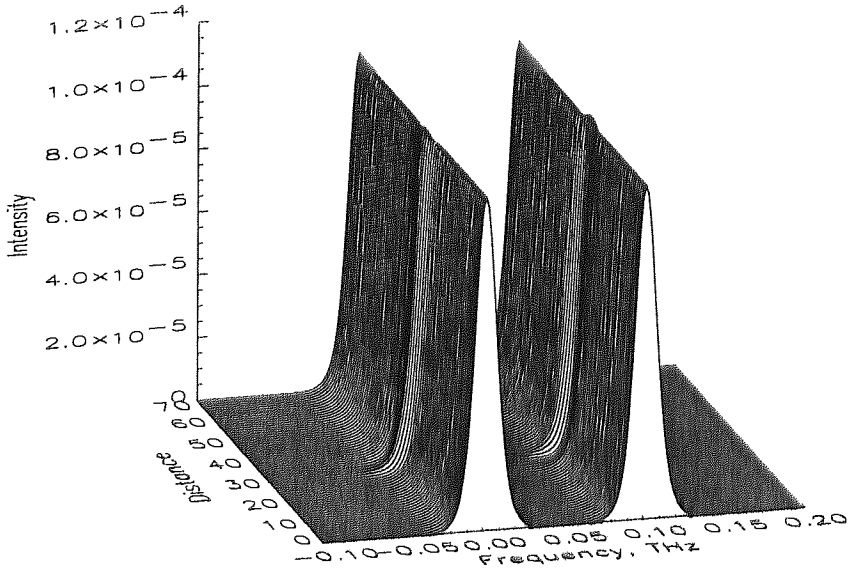

Figure 2.11: The collision of a pair of solitons of different frequencies. (a) temporal evolution and (b) spectral evolution.

2.7.3 Gordon-Haus timing jitter

A major limiting factor of soliton based communication systems is Gordon-Haus (GH) timing jitter [60], which arises from ASE noise, generated by optical amplifiers. GH timing jitter is

caused by the soliton absorbing the ASE noise which induces a random change in the solitons central frequency leading to a timing jitter. After propagation over long distances, these random fluctuations in the central frequency build up, placing a limitation on the maximum possible transmission distance. For idealised amplifiers and average soliton conditions, the transmission distance set by GH timing jitter alone is [61]

$$L_{\max}^{3} \leq 0.1372 \frac{\tau \tau_{bit\tau}^{2} A_{eff} Z_a Q}{n_{sp} \gamma D h (G-1)} \tag{2.49}$$

where τ is the pulse width, $2\tau_{bit}$ is the bit period, Z_a is the amplifier span, γ is the non-linear coefficient of the fibre (cm^2/W) and Q is the average soliton factor given by

$$Q = \frac{\alpha Z_z}{1 - \exp(-\alpha Z_a)} \tag{2.50}$$

which accounts for the variation in soliton amplitude between amplifiers. From equation (2.49), it is clear that the maximum transmission distance L_{max}, increases proportional to $\sqrt[3]{\tau}$, $\sqrt[3]{\tau_{bit}^2}$ and $\sqrt[3]{1/D}$ therefore GH timing jitter can be reduced by reducing the bit rate and dispersion, and increasing the pulse width.

GH timing jitter can be controlled using optical filters, which reduces the build up of ASE noise from the amplifiers. On interaction between the soliton and the filter, the soliton re-centres its spectrum around the central frequency of the filter, which reduces the walk-off from the centre of the bit slot [62-65]. To compensate for the removal of part of the spectrum, additional gain is required, which consequently increases the amplifier noise. With the inclusion of filters, the GH timing jitter only accumulates proportional to $\sqrt{z}$ rather than $\sqrt{z^3}$ as in the unfiltered case.

Further improvements can be achieved by using a chain of filters, which have a central frequency that slides along the chain [66-69]. With solitons aligning their spectrum to the central frequency of the filter, the solitons follow the filters whereas the noise is removed. However, this technique requires more excess gain to compensate for the larger portion of the spectrum that is removed, although narrower filters can be used than in the fixed frequency case.

2.7.4 Higher order non-linear effects

Two further non-linear processes, which have so far been neglected in the discussion, are those of Stimulated Brillouin Scattering (SBS) [36, 70], and Stimulated Raman Scattering (SRS) [35, 71]. SBS is the acoustic interaction between the propagating light wave and the lattice, with the scattered light propagating in the opposite direction to the signal. SBS only significantly affects signals with a very narrow bandwidth, and consequently does not seriously affect soliton based communication systems.

SRS results from the interaction between the light-wave and the infrared optical vibration of the lattice. The incident photons are absorbed, a phonon at an infrared frequency and a photon, with a frequency equal to the difference between the original photon and the phonon, are emitted. Also, a less likely event is that the photon and phonon combine to create an up-shifted phonon. Therefore, SRS creates the growth of side bands in the spectra, with a more intense lower sideband.

The SRS process can be stimulated by a pump signal at the side band frequency so that interactions occur more quickly. Consequently, SRS produces a cumulative effect that can lead to a sequence of scattered sub-sidebands. For short pulse widths (typically < 1 ps), their spectrum becomes wide enough for the pumping of the wavelengths in the edges of the spectrum. This causes a continuous downshift of the average frequency, referred to as the Soliton Self Frequency Shift (SSFS). The rate of SSFS can be given as

$$\frac{d\omega_0}{dz} = \frac{-4\tau_R \beta_2}{15\tau^4} \tag{2.51}$$

where τ_R is the Raman pulse width below which the self frequency shift becomes significant and ω_0 is the central frequency of the soliton. Experimental analysis has shown $\tau_R \approx 1$ ps, therefore in this thesis, as $\tau >> 1$ ps, we use the Generalised Non-Linear Schrödinger equation (GNLS) [72], which accounts for the non-linear response and the Raman gain coefficient of silica optical fibres.

Another effect arising from the $\chi 3$ nonlinearity is Four Wave Mixing (FWM) [73]. FWM is a parametric process which occurs when two waves at frequencies ω_1 and ω_2 interact through a non-linear medium to produce two new waves at frequencies ω_3 and ω_4, such that:

$$\omega_1 + \omega_2 = \omega_3 + \omega_4 \tag{2.52}$$

The phase matching condition, given below, must also be satisfied for efficient conversion:

$$k_3 + k_4 - k_1 - k_2 = 0 \tag{2.53}$$

$$\frac{\left(n_3\omega_3 + n_4\omega_4 - n_1\omega_1 - n_2\omega_2\right)}{c} = 0 \tag{2.54}$$

where k_j is the phase per unit length, n_j the refractive index at frequency ω_j, and c is the speed of light. FWM can cause serious problems in WDM systems during collision between solitons of different channels [74]. It is still possible to generate FWM from initial waves of the same frequency. In this case the conservation of energy and momentum are:

$$\omega_1 + \omega_1 = \omega_3 + \omega_4 \tag{2.55}$$

$$k_3 + k_4 - 2k_1 = 0 \tag{2.56}$$

In this case, the two input frequencies are identical and produce two new frequencies, one up-shifted and one down-shifted. This type of FWM is not possible in soliton systems as the process is only properly phase matched at zero dispersion. However, as we shall see in Chapter 7, this type of FWM is a major limiting factor in quasi-linear RZ transmission systems with low dispersions.

2.7.5 Soliton control techniques

There are a number of techniques that can be used to improve the performance of soliton based transmission systems, we have already seen an example of this in sections 2.7.2 and 2.7.3. Control techniques for transmission systems include amplitude modulation, which can be used to suppress GH timing jitter and reduce interactions. Amplitude modulation works by pushing the central peak of the pulse back into the centre of the bit slot. However, this active technique requires a recovered clock signal and must operate at the transmission rate. Despite the complexity, amplitude modulators have successfully demonstrated an improvement in transmission performance [75-78].

Another control technique is that of phase modulation. Phase modulation works by giving a pulse that moves out of its time slot a chirp. This chirp induces a change in the central frequency of the soliton, which compensates for the original frequency change and the pulse drifts back towards its required position. Phase modulators, therefore, correct for both temporal position and frequency [79-82].

Saturable absorbers are another control technique, which improves SNR, reduces the build up of CW background radiation and reduces interactions [83-85]. Saturable absorbers

remove the low intensity parts of the propagating pulse, where the cut-off intensity is predetermined. Saturable absorbers can be constructed from non-linear polarisation rotation, loop mirrors or from multiple quantum wells [85-89].

Another control technique is optical phase conjugation, which transforms the soliton into its complex conjugate. Optical phase conjugation reverses the chirp that has accumulated in the propagation, and can be placed either at the mid-point of the transmission link or at each amplifier [90]. Optical phase conjugation can reduce interactions [91, 92], GH timing jitter [93, 94], and reverse interactions [92, 95].

Chapter 3 Dispersion Management

3.1 Introduction

Dispersion management has a played a significant role in the explosive growth of system capacity observed in recent years [1, 5, 96-99]. In its simplest form, dispersion management can be defined as the continual variation of the chromatic dispersion within a system. Dispersion management can be used in different ways to achieve slightly different goals. For example, in optical soliton transmission the fibre dispersion can be tailored to follow the exponential loss of the fibre, which can be achieved using a manufactured exponential profile of the fibre dispersion [100-102] or approximated using a step profile using dispersion sections with decreasing magnitudes [103, 104]. More commonly, dispersion management is referred to the case where alternate sign dispersion sections are concatenated to compensate for the large dispersion. Historically, the necessity of dispersion management results from the migration of optical sources from 1.3 μm to 1.55 μm, which meant that the installed optical fibre that had low dispersion at 1.3 μm now had a much larger dispersion at 1.55 μm. It was found that the high local dispersion of Standard Monomode Fibre (SMF) at 1.55 μm (≈ 18 ps/nm/km) could be compensated at each amplifier by a relatively short length of Dispersion Compensating Fibre (DCF) (≈ -80 ps/nm/km). This basic ideal can be extended to more elaborate dispersion management schemes, as described in section 3.5.2. Throughout the remainder of the thesis, we shall confine our discussion of dispersion management to solely refer to the use of alternating sign dispersion fibres, which on average reduce the total dispersion.

In this chapter, we review the Dispersion Managed (DM) soliton, and introduce our own interpretation of short period dispersion management, and the concept of effective average dispersion.

3.1.1 A note on convention

In dispersion managed systems, we normally need to label the individual sections with a subscript to denote whether the dispersion is anomalous or normal, therefore the conventional notation used previously in Chapter 2 must be slightly amended. For dispersion managed systems, the coefficients from equation (2.6), β_1, β_2, β_3 etc will be replaced by $\beta^{(1)}$, $\beta^{(2)}$, $\beta^{(3)}$ thus allowing the subscript for anomalous and normal dispersion sections to be included as $\beta^{(2)}{}_a$ and $\beta^{(2)}{}_n$ respectively.

3.2 The dispersion managed soliton

As stated previously, in this context, dispersion management refers to the compensation of large chromatic dispersion by either a dispersive element or a fibre section that has alternate sign dispersion. In is simplest form dispersion management consists of two equal length sections of fibre which have the same magnitude of chromatic dispersion, but with opposing signs (i.e. one anomalous dispersion fibre section and one normal dispersion fibre section). This is represented schematically in Figure 3.1. Within these dispersion maps, a pulse which exhibits soliton-like properties can exist, called the Dispersion Managed (DM) soliton. Analogous to the classical soliton, the balance between dispersion and nonlinearity needs to achieved, this in turn determines the initial conditions of the DM soliton [105-110]. These initial conditions (shape, width, chirp, energy) can be found using the numerical averaging method of Nijhof *et al.* [111].

An important quantity that is used to determine the characteristics of the DM soliton is the dispersion map strength, S, which can be defined as [105]:

$$S = \frac{\left(\beta_a^{(2)} - \beta_{ave}^{(2)}\right) l_a - \left(\beta_n^{(2)} - \beta_{ave}^{(2)}\right) l_n}{\tau^2} \tag{3.1}$$

where $\beta^{(2)}_{a,n}$ and $l_{a,n}$ are the dispersions and lengths of the anomalous and normal dispersion fibre section respectively, and τ is the minimum pulse width. $\beta^{(2)}_{ave}$ is the average dispersion and is defined as:

$$\beta^{(2)}_{ave} = \frac{\beta^{(2)}_a l_a + \beta^{(2)}_n l_n}{l_a + l_n} \tag{3.2}$$

As with classical solitons, DM solitons show a linear dependence on average dispersion. The map strength, defined in equation (3.1), can be used to indicate the amount of pulse spreading displayed by the DM soliton as it propagates through the map. Also, the shape of the DM soliton is dependant upon S [[106, 112], where for weak S, the DM soliton shape is close to hyperbolic-secant, whereas for strong S, the shape is more Gaussian.

In Ref. [107], it was discovered that the energy of the DM soliton was greater than that of the classical soliton for the same average dispersion. The empirical relationship for the energy enhancement was given as:

$$E_{DM} = E_{sol}\left[1+0.7\left(\frac{\left(\beta^{(2)}_a - \beta^{(2)}_{ave}\right)l_a - \left(\beta^{(2)}_n - \beta^{(2)}_{ave}\right)l_n}{\tau^2}\right)^2\right] \tag{3.3}$$

$$E_{DM} = E_{sol}\left(1+\alpha S^2\right) \tag{3.4}$$

where E_{DM} and E_{sol} are the energies of the DM and first order classical soliton respectively. When fibre loss is included, the relationship in equation (3.3) becomes more complex, this will be discussed in more detail in section 3.6. Additionally, the energy of the DM soliton depends on the depth ($\Delta\beta^{(2)}$) of the dispersion map. It was shown by Nijhof *et al.* [113], that accounting for $\Delta\beta^{(2)}$, the energy of the DM soliton could be more accurately described by

$$\eta^*(S;\delta) = \frac{a\delta}{S}\left(S - b + \sqrt{(S-b)^2 + \frac{cS}{\delta}} \right) \tag{3.5}$$

where a, b and c are normalised dimensionless fitting parameters with the vales $a = 0.2$, $b = 3.7$ and $c = 180$, δ is the normalised depth of the dispersion map, and η is the energy enhancement factor. The dependence of the DM soliton energy on $\Delta\beta^{(2)}$ is quite intuitive, because as $\Delta\beta^{(2)}$ increases, more nonlinearity is required to balance the increased dispersion, hence the DM soliton power increases.

The DM soliton also possesses a remarkable property of being able to propagate at anomalous, zero and normal average dispersions [110, 114-118]. DM solitons can only exist for zero and normal average dispersions for strong S. It was found [110], that for $S < 3.9$ DM solitons only existed for anomalous average dispersions and for $S \geq 3.9$, DM solitons exist for anomalous, zero and normal average dispersions. This phenomenon was eloquently described in Ref. [119], in terms of the effective average dispersion $\beta^{(2)}_{ea}$. The effective average dispersion took into account the pulse bandwidth in each of the fibres, which was greatest in the anomalous dispersion fibre. Therefore, the dispersion induced chirp on the pulse can be anomalous even if the average dispersion is zero or normal. We shall return to the effective average dispersion in section 3.6.1, where we use it to interpret the consequences of amplifier location within dispersion managed systems.

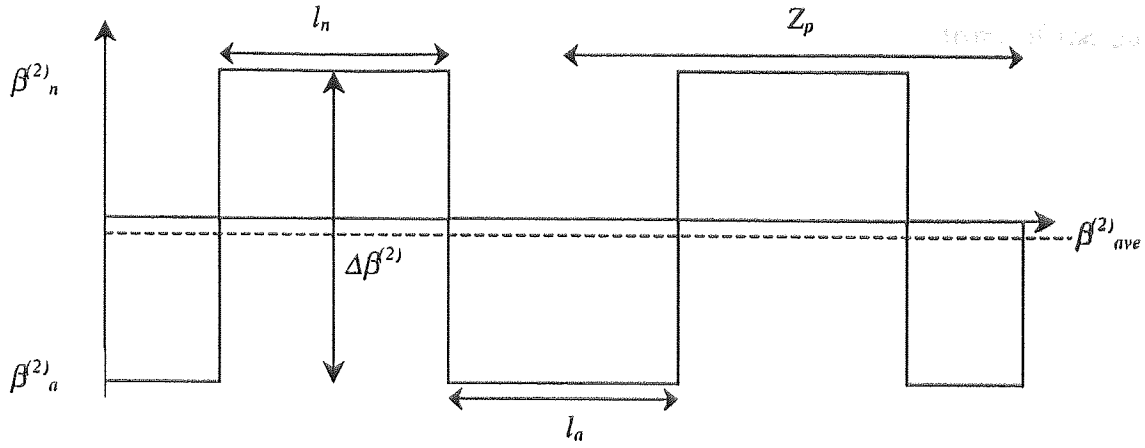

Figure 3.1: Schematic representation of a dispersion map. The lengths of the anomalous and normal dispersion fibre sections are l_a and l_n respectively, $\Delta\beta^{(2)}$ is the depth of the dispersion map, and Z_p the dispersion management period.

3.2.1 Dispersion managed soliton dynamics

Dispersion managed soliton solutions in optical fibres can be found using an averaging method [111]. The dynamics of the DM soliton can be divided into two classes, dependent on the length scale upon which they affect propagation. These two classes are referred to as the fast and slow dynamics [120], with the fast dynamics occurring on a length scale $< Z_p$ and the slow dynamics occurring on a length scale $> Z_p$. Investigating each of these dynamics in turn we start with the fast dynamics.

In dispersion managed systems, we have the case of the local dispersion being much greater than the average dispersion. Therefore, at any point, the powers are low relative to the local dispersion and so dispersive effects dominate. However, nonlinearity still plays an important role. Let us consider what happens when a pulse propagates though a section of anomalous and normal dispersion fibre, neglecting higher order non-linear and dispersive effects, and fibre loss.

Let us assume a chirp free Gaussian pulse is launched into an anomalous dispersion fibre with high local dispersion ($\beta^{(2)}{}_a$) and an energy much less than that of the soliton required for $\beta^{(2)}{}_a$. As described in section 2.4, the pulse broadens with propagation and quickly acquires a

chirp, in which the leading edge is up shifted in frequency and trailing edge is down shifted in frequency. However, the fibre nonlinearity reduces the frequency of the front of the pulse and increases the frequency of the trailing edge of the pulse. Therefore, the extremes of the spectrum are compressed resulting in a decrease in bandwidth.

A Gaussian pulse launched into a normal dispersion fibre, under the same conditions as the previous paragraph, similarly broadens with propagation distance. This time the pulse acquires a chirp, with an opposite sign to that of the anomalous dispersion fibre, in which the leading edge is down shifted in frequency and the trailing edge up shifted in frequency. The nonlinearity has the same effect as in the anomalous dispersion fibre and therefore the bandwidth of the propagating pulse increases.

Therefore, the DM soliton solution is supported by a combination of the dispersive and non-linear effects in each of the anomalous and normal dispersion fibres. More intuitively, the DM soliton evolution over Z_p is shown in Figure 3.2. The periodic expansion and contraction of the DM soliton evolution in Figure 3.2 is referred to as the "breathing" of the pulse. It is clear that after propagating over Z_p, the DM soliton returns to its initial shape.

The behaviour exhibited in Figure 3.2 can best be described using piece-wise analysis, breaking the evolution into three parts: (i) propagation through $l_a/2$, (ii) propagation through l_n and (iii) propagation through $l_a/2$. We consider propagation starting at $l_a/2$ as this corresponds to the location where the DM soliton is unchirped. In the first section, as the initially unchirped pulse propagates through the anomalous dispersion fibre, the pulse broadens (decreasing bandwidth). Observation of the phase plane, Figure 3.3(a), reveals the pulse width and chirp evolution. The rapid chirp acquired by the pulse is clearly visible along with the increasing pulse width. From the phase plane diagram, it can be seen that on entering the normal dispersion fibre section the pulse is chirped. In the second section, Figure 3.3(b), we observe that initially both the pulse width and the chirp decrease (increasing bandwidth) until the chirp undergoes a sign reversal that results in the pulse broadening again (decreasing bandwidth). On entering the third

section, Figure 3.3(c), the chirp is such that it causes the pulse width to decrease, thus returning to its initial conditions.

Observation of Figure 3.2(b), which shows the DM soliton on a logarithmic scale, reveals the rather curious shape of the DM soliton. At the locations in the dispersion map where the chirp free points occurs, it can be seen that the DM soliton appears to have oscillatory tails. This observation was first made by Turitsyn *et al.* [106], who described the structure of the DM soliton in terms of two parts: a central section (or core) and the oscillatory tails.

In the previous paragraphs, we were concerned with the DM soliton evolution over Z_p, where we observed the DM soliton has an identical pulse shape at beginning and end of Z_p. The slow dynamics are concerned with the evolution of the returning DM soliton shape. An example of the evolution of the slow DM soliton dynamics can be seen in Figure 3.4, which shows propagation in both linear and logarithmic scales. The slow dynamics illustrate that the DM soliton evolution is extremely stable for propagation on a terrestrial scale. However, if the DM soliton was subjected to an external perturbation then it is likely that we would observe an evolution in the slow dynamics. Additionally, if the exact DM soliton shape were not launched, then we would observe a periodic evolution of the slow dynamics. This is often the case when a Gaussian or hyperbolic secant shaped pulse, with the same initial conditions are used to approximate a DM soliton.

(a)

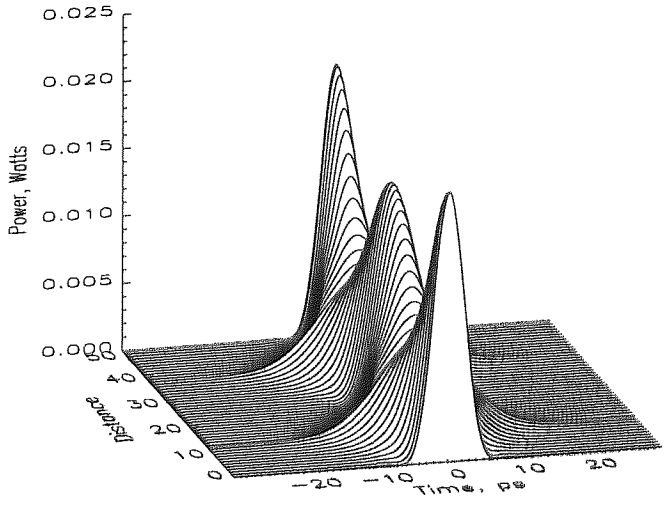

(b)

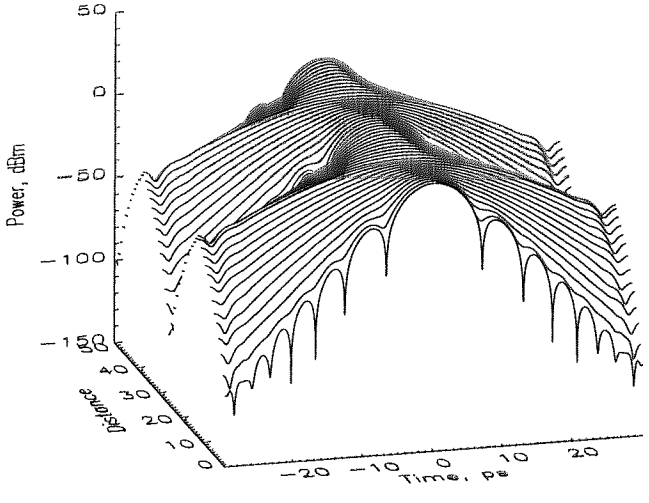

Figure 3.2: DM soliton evolution over a single dispersion management period, shown in (a) linear scale and (b) logarithmic scale.

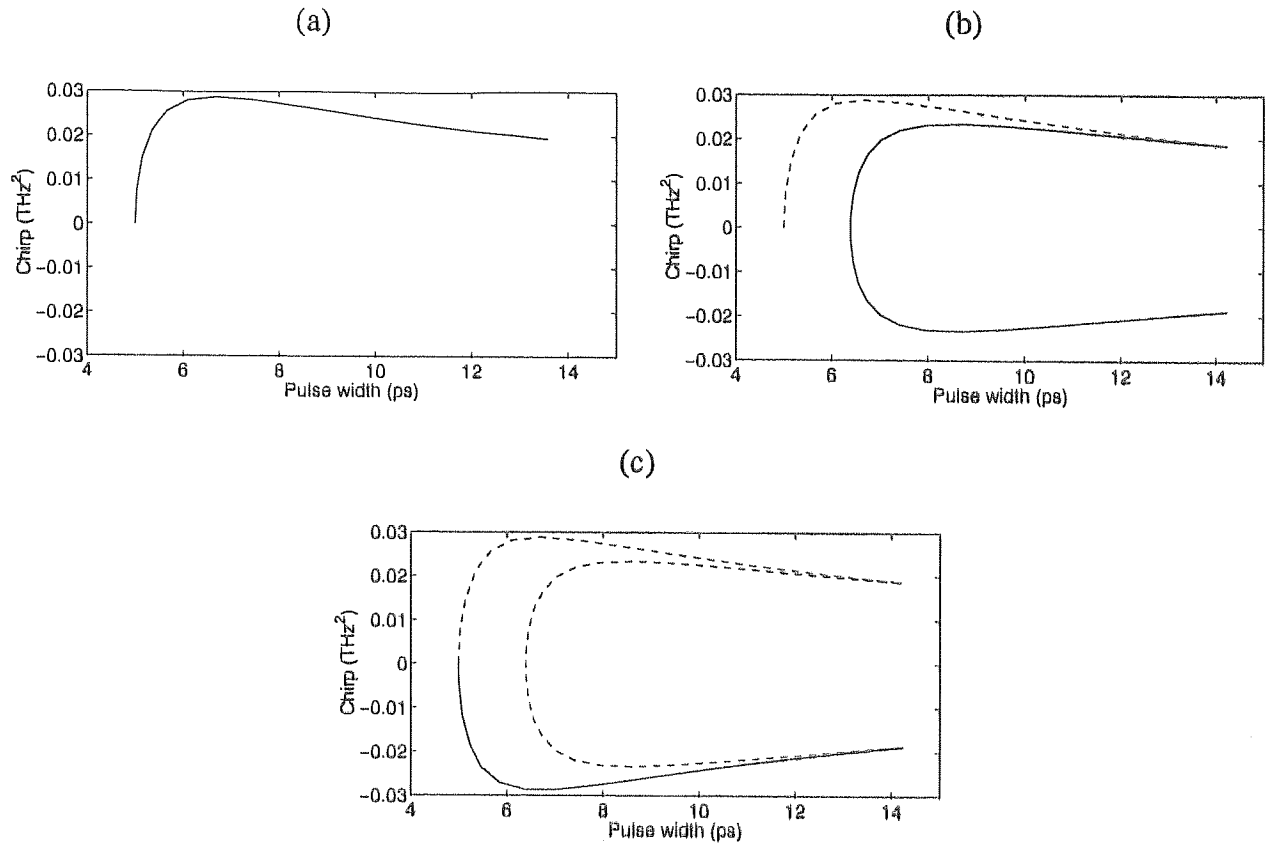

Figure 3.3: DM soliton evolution over Z_p shown in the phase plane. (a) Propagation over $l_a/2$, (b) propagation over l_a and (c) propagation over $l_a/2$.

(a)

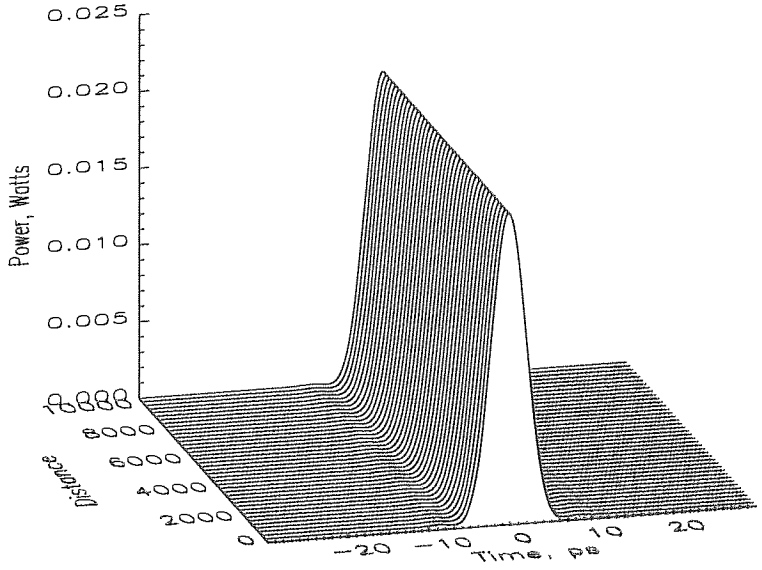

(b)

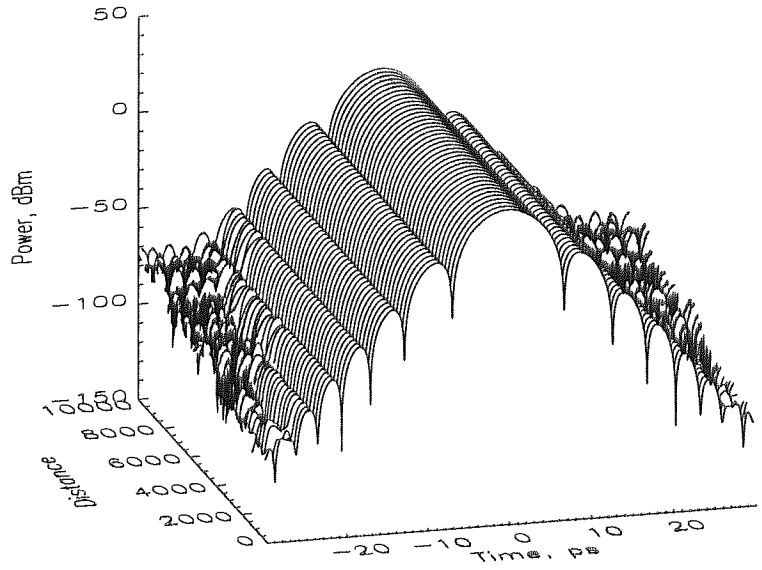

Figure 3.4: Evolution of the slow DM soliton dynamics showed stroboscopically at the mid-point of the anomalous dispersion fibre. (a) Linear scale and (b) logarithmic scale.

3.3 Properties of DM solitons

As described in section 3.2, the DM solitons possess a greater energy than the classical soliton for the same path-average dispersion. With the introduction of fibre loss and amplification into the transmission system, see section 3.6.1, this enhanced energy of the DM soliton benefits performance relative to the classical soliton. In section 2.7.3, we described that the effect of amplification noise in transmission systems, manifests itself in the form of reduced SNR and Gordon-Haus timing jitter.

The dependence of SNR on propagation can be given by [121]:

$$SNR = \frac{E_0 Z_a}{\eta_{sp}(G-1)h\,\nu Z} \tag{3.6}$$

Where E_0 is energy at the output of the amplifier, Z_a is the amplifier span, η_{sp} is the spontaneous emission factor of the amplifier, G is the gain, h is Planks constant and ν is the frequency. Therefore, it is clear from equation (3.6) that SNR $\propto$ E_0, which illustrates the improved SNR of DM solitons compared to classical solitons.

The effect of Gordon-Haus timing jitter on DM solitons is somewhat more complex as it is dependent on many factors [122-126] including the bandwidth of the pulse. The Gordon-Haus timing jitter after n amplifiers can be given by [121]:

$$\left\langle \delta t^2 \right\rangle = \frac{2\eta_{sp}(G-1)h\nu}{E_0}\left(\sum_{i=1}^{n}\Omega_i^2\beta_i^2 + \frac{\pi^2}{12}ZZ_a\tau_{\min}^2\right) \tag{3.7}$$

where Ω^2_i is the quadratic bandwidth, β_i is the cumulative dispersion after the i^{th} amplifier and τ_{min} the minimum pulse width. From equation (3.7), it can be seen that the timing jitter is

dependant on the bandwidth of the pulse at the point of amplification and inversely dependant on the DM soliton energy. Relative to the classical soliton, the cumulate dispersion is also much lower in dispersion managed systems.

3.4 Interactions between DM solitons

Analogous to classical solitons, DM solitons exhibit an interactive force between co-propagating pulses that significantly degrades the performance of transmission systems. It is therefore understandable that a lot of research has been focused on understanding the interaction process of DM solitons [104, 127-137]. The interaction process of DM solitons, whilst similar in nature to that of classical solitons detailed in section 2.7.2, some fundamental differences remain. One difference arises from the shape of the DM solitons, which is hyperbolic secant-like for weak S and Gaussian-like for stronger S. In the case of Gaussian shaped pulses, the leading and trailing edges fall off more rapidly, which means that the effect of pulse tails on interactions is reduced. Another difference results from the dynamic breathing of the DM soliton as it propagates through the link. As the DM soliton breathes, the temporal separation between the pulses varies, which can increase interactions. Another difference is due to the chirped tails of the DM soliton, which means that the tails do not necessarily interfere constructively.

Interactions between DM solitons are, unsurprisingly, dependant on S, which was defined in equation (3.1), which are minimised for $S \approx 1.65$ [127]. The type of interaction is also dependant on the map strength, for $S < 1.65$, the interactive force between the DM solitons is repulsive whereas for $S > 1.65$, the interactive force is attractive. The region $S > 1.65$, is where interactions are strongest, however, it has been shown that for $S > 50$ the collision distance actually increases [138]. However, for $S > 50$, the DM solitons behave more as quasi-linear pulses which are discussed in Chapter 7. In addition, when fibre loss is considered, the amplifier location within the dispersion map is also a critical determining factor in the strength of the interactions [137].

3.5 Scaling in dispersion managed systems

So far, we have neglected the effects of fibre loss. When fibre loss is taken into account, it adds an extra dimension of scaling into the DM soliton propagation. The dynamics of the propagating DM soliton are significantly affected by the length scale of the periodic loss and amplification (Z_a), and the dispersion management period (Z_p). The scaling in dispersion managed systems can be conveniently categorised into two main groups based on their properties.

3.5.1 Conventional dispersion management regime

We define the conventional dispersion management regime as $Z_a \leq Z_p$, although it is possible to still further divide this into the two further subclasses defined by $Z_a = Z_p$ and $Z_a < Z_p$. These subclasses are shown schematically in Figure 3.5. The case $Z_a = Z_p$ is the so-called "resonance model" [139] and is currently the most common form of dispersion managed system, partially due to upgrading of installed systems. Another reason the common occurrence of this dispersion management regime is that the dispersion map is identical between each amplifier. In this case, the DM solitons are periodic in both Z_p and Z_a.

The other subclass is $Z_a < Z_p$, also called long period dispersion management, as the dispersion management period is long compared to the amplifier span. In this regime, the DM soliton dynamics are close to those of the lossless regime. However, if we assume a practical amplifier spacing (40 km – 80 km) and use of commercially available fibre types, then in this regime, Z_p is incredibly large, yielding high map strengths at the pulse widths required for transmission at ≥ 20 Gbit/s. As was discussed in section 3.4, interactions increase for large values of S.

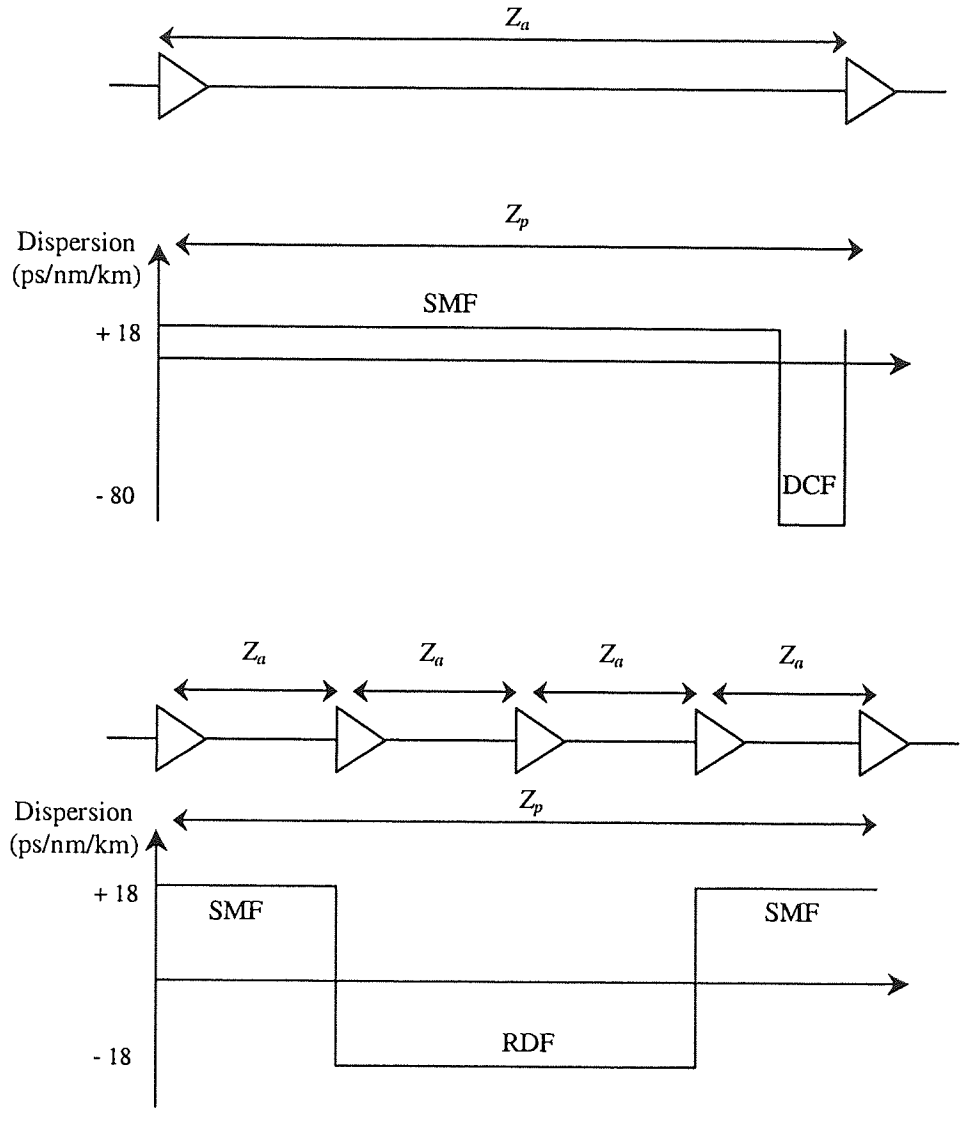

Figure 3.5: Schematic representation of scaling in dispersion managed systems. (top) The resonance model where $Z_a = Z_p$ and (bottom) long period dispersion management where $Z_a < Z_p$.

3.5.2 Short period dispersion management regime

At high transmission rates, which require short pulses, the dispersion management regimes detailed in section 3.5.1 become prohibitive because of the associated increases in pulse energy and breathing that lead to increased interaction [127]. Nevertheless, short pulses can be supported if S is kept low enough. For practical amplifier spacings, S can be controlled by reducing the local dispersion, but in the conventional dispersion management regime, the local

dispersion rapidly approaches the average dispersion, and the maps become less effective in reducing four-wave-mixing impairments. An alternative approach is to use short period dispersion management [140-143], characterised by $Z_p << Z_a$. An n section Short Period Dispersion Map (SPDM) can be seen in Figure 3.6 where n denotes the number of alternate-sign dispersion sections per amplifier spacing. In these maps (which have also been referred to as short-scale dispersion maps [140] and dense periodic fibre maps [144]), the lengths of the dispersion sections $l_{1,2}$ can be significantly reduced, making it possible to sustain short pulses in dispersion maps with high local dispersion at map strengths that avoid significant penalties from interactions.

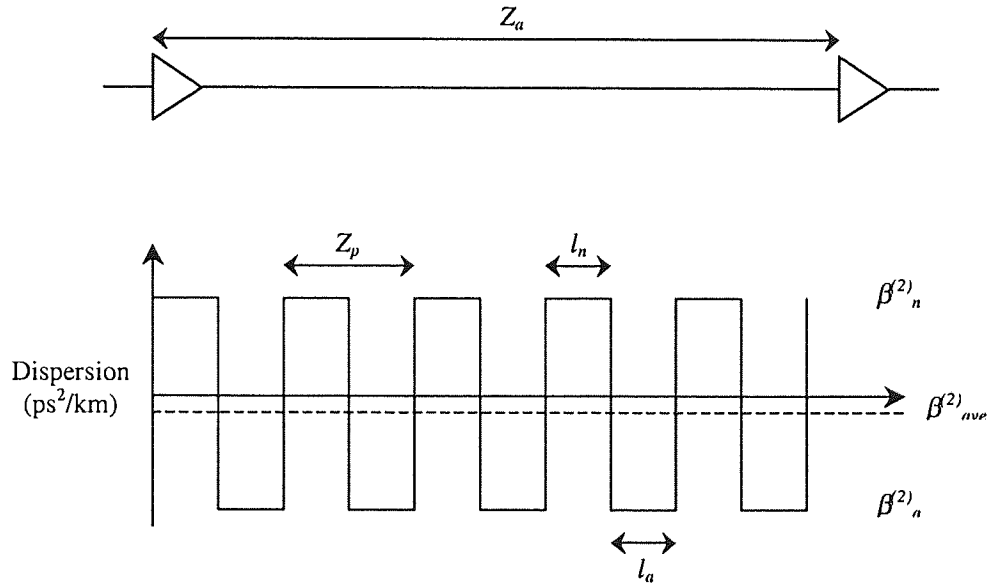

Figure 3.6: A schematic representation of an n-section SPDM that is characterised by $Z_p << Z_a$.

As mentioned in section 3.2, DM soliton solutions of the NLS equation can be found in SPDMs using an averaging method [111]. As an example, Figure 3.7(a) illustrates the pulse width dynamics over a single amplifier period for an eight-section SPDM and a conventional two-section dispersion map. In both cases the map strength is fixed to be S = 4, the average dispersion $\beta^{(2)}_{ave}$ = -0.02 ps^2/km, and the minimum pulse width in the amplification period is τ_{min} = 2.5 ps. Throughout, we consider Z_a = 0 corresponds to the start of the anomalous dispersion

fibre and the fibre loss is 0.2 dB/km. The stability of the DM solitons in these maps is verified by propagation of the solutions over 10,000 km.

Figure 3.7 shows that the DM soliton dynamics in the SPDM are different from those in the two-step dispersion map. This is principally because the pulse energy is reduced in each period of the SPDM, owing to fibre loss. Therefore the DM soliton dynamics are no longer periodic in Z_p (as they are in the lossless case), but they are periodic in Z_a. Figure 3.7 illustrates the regular form of the pulse width evolution over Z_a, which displays a convergence of the pulse width minima, and a global minimum that occurs in the first anomalous fibre section. Such regular dynamics are in contrast to the non-uniform behaviour observed previously for small S [140] in SPDMs, and are consistent with an exponential reduction in the nonlinearity across the amplifier span. This reduction is reflected in Figure 3.7(b), which shows the bandwidth evolution over Z_a. For the eight-section SPDM we observe large spectral variations in the leading sections that diminish as the non-linear effect becomes less dominant.

We now consider the effects of amplifier position within the dispersion map on the stable pulse energy. Figure 3.8 compares the energy enhancement factors of the stable pulses in the eight-section SPDM and the conventional two-section map, for the parameter values given previously. The enhancement factor (η) is taken as the ratio of the DM soliton energy to the conventional average (or centre guiding) soliton energy [47] for the same average dispersion and (minimum) pulse width. It is apparent that, although the shape of the energy dependence in both maps is broadly similar, for the SPDM the absolute value of the energy is greater on average, and the relative variation is much smaller. In both cases the maximum energy occurs when the amplifier is placed toward the end of the anomalous dispersion fibre, a feature that is observed in all the dispersion maps investigated.

(a)

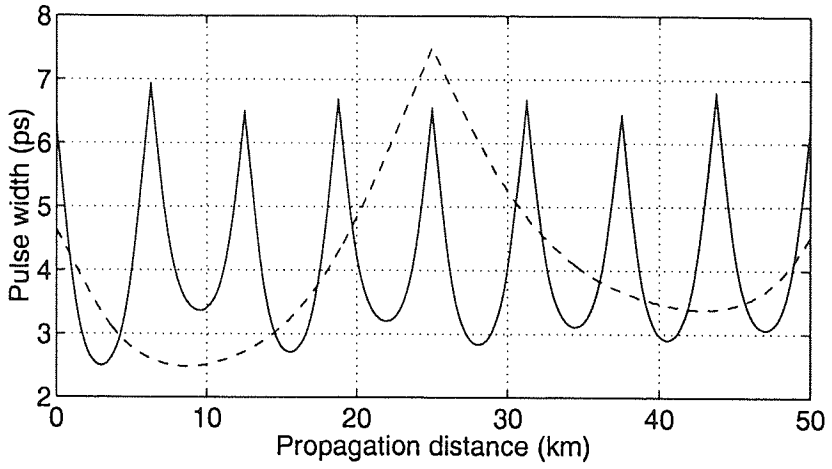

(b)

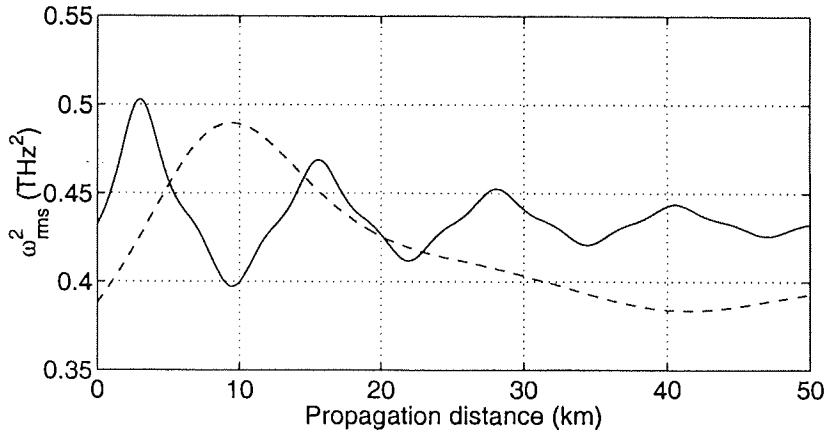

Figure 3.7: DM soliton dynamics for an eight-section SPDM (solid line) and a conventional two-section dispersion map (dashed line) with the amplifier positioned at the start of the anomalous dispersion fibre section ($Z_a = 0$). (a) Pulse width dynamics over Z_a. (b) Spectral bandwidth evolution over Z_a.

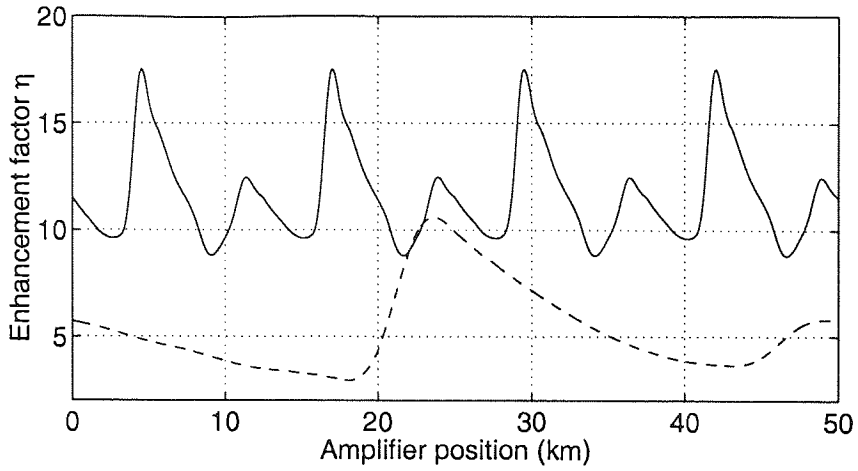

Figure 3.8: Energy enhancement as a function of amplifier position within Za for an eight-section SPDM (solid line) and a conventional two-section dispersion map (dashed line).

The results of Figure 3.8 are summarised and extended in Figure 3.9, which plots the minimum and maximum energy enhancement factors as a function of the number of dispersion sections for values up to $n = 32$. In Figure 3.9(a) we can clearly observe for $S = 2$ a gradual increase and convergence of the minimum and maximum DM soliton energies as n increases. The increase in energy enhancement can be explained in terms of the increase in map depth, $\delta = \Delta\beta^{(2)}/|\beta^{(2)}_{ave}|$, which scales linearly with n. It has been shown previously that in lossless systems the DM soliton energy is dependant on the map depth, as well as the map strength [113]. Figure 3.9(a) confirms that a similar dependence holds for stable solutions obtained in SPDMs (including loss) for weak S. For large enough n, however, we find only pseudo-periodic solutions, similar to those observed by Favre *et al.* [145], at certain amplifier locations toward the end of the anomalous fibre, which occur at lower values of n with increasing S. The influence of these solutions is visible in Figure 3.9(b), in which we can observe for $S = 4$ a divergence in the minimum and maximum energies. Justification of their inclusion in Figure 3.9(b) results from their stable propagation over tens of thousands of kilometres.

(a)

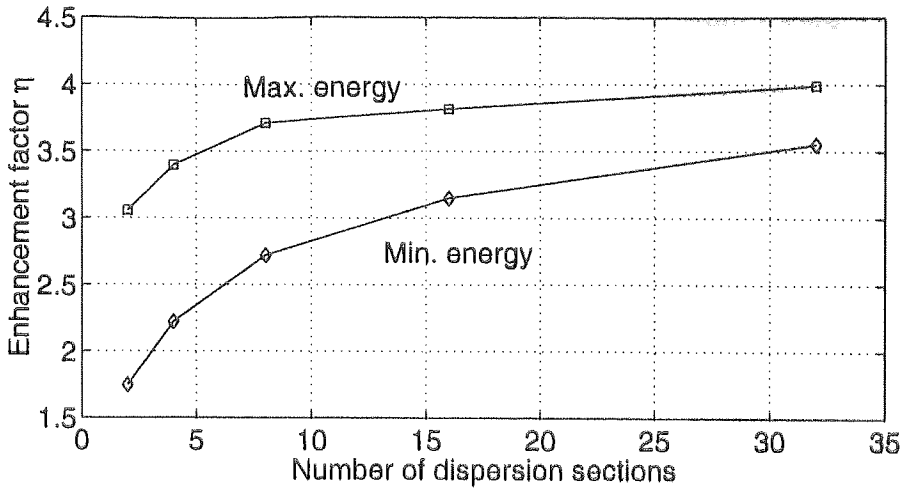

(b)

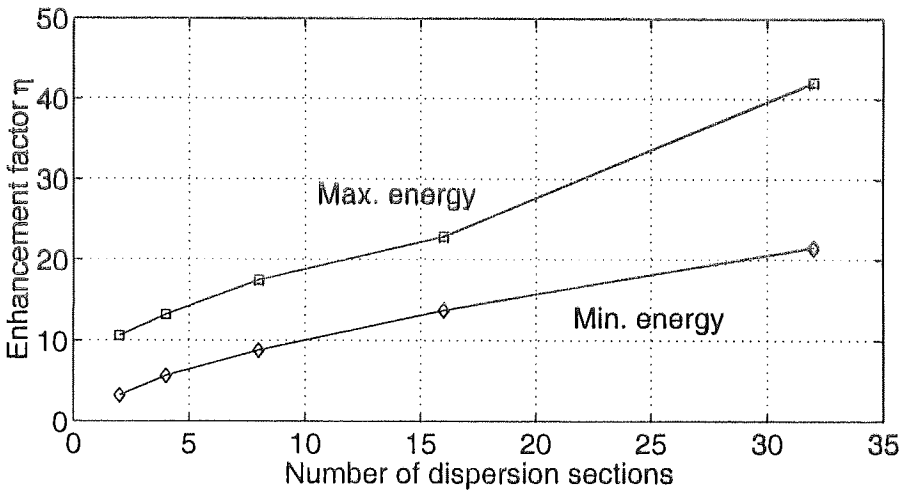

Figure 3.9: Minimum and maximum energy variation of the DM soliton as a function of the number of dispersion sections per amplifier spacing. (a) $S = 2$, (b) $S = 4$.

Next, we determine how interactions are influenced by the number of dispersion sections in a SPDM. Figure 3.10 shows how the collision distance of a pair of DM solitons changes as a function of amplifier position for an eight-section SPDM and a conventional two-section map with $S = 4$. Once again, there is a broad similarity between the forms of these curves, however, the collision distance is greater for the two-section system, and the variation of this distance is much smaller in the eight-section map. In each case, there is a strong inverse correlation between the pulse energy and the collapse distance, as noted previously for two-section dispersion maps [136]. Thus, the increased interactions in the SPDM can be attributed to the greater enhanced energy of the DM soliton (a similar correlation holds for the reduced

variation). However, note that, for the amplifier positioned at 0 km, Figure 3.10 shows that the collision distances for both dispersion maps are similar, although from Figure 3.8 it can be seen that the pulse energy in the SPDM is more than twice that in the two-section map.

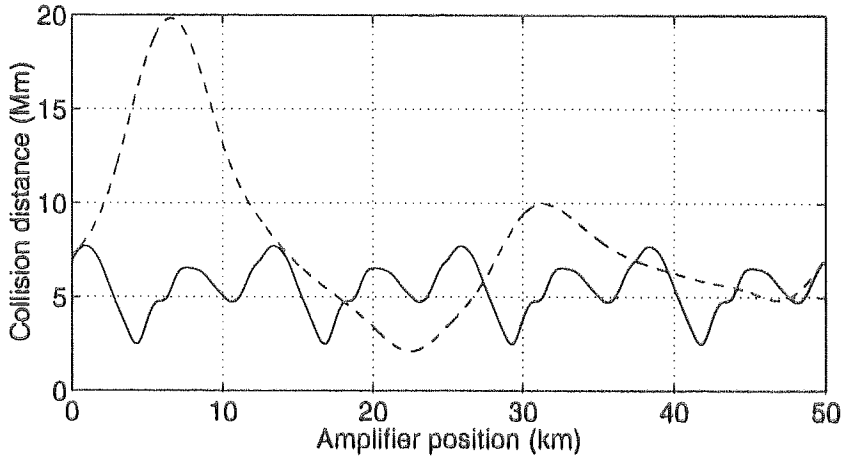

Figure 3.10: Dependence of the collision distance on the amplifier position with Z_a, for a pair of pulses separated by 20 ps (equivalent to 50 GHz transmission).

In this section, we have compared the characteristics of DM solitons in the conventional dispersion management regime, with a regime characterised by having a dispersion management period that is much shorter than the amplification period. We have shown that DM solitons in SPDMs exhibit regular dynamics over a single amplifier span and possess a greater energy enhancement factor, for fixed S, compared to a conventional dispersion map. This additional energy enhancement is a direct result of the increased local dispersion. We have found that for weak S, as n increases, the variations in energy reduce and thus we approach a regime similar to that of the lossless model. Contrasting behaviour was observed for strong S, where we observe increasing variations in energy as n increases. Shown also are the increased interactions in SPDMs that result from greater energy enhancement of the DM solitons.

3.6 Implications of amplifier placement in dispersion managed systems

Having introduced the notion of scaling in dispersion managed systems, we then investigate how propagation of DM solitons is influenced by the location of the amplifier within the dispersion map.

3.6.1 Interpretation of the energy variations due to amplifier positioning

The implication of the amplifier location within the dispersion map on propagating DM solitons was first considered by Chin *et al.* [146]. They concluded that the insertion of periodic loss and amplification into a dispersion managed system decreased the energy enhancement factor (η) of the DM soliton. A later paper [147], then reported that η in fact increased with periodic loss and amplification. Investigating a dispersion map constructed from 2 equal length sections, where the amplification period (Z_a) is equal to the dispersion management period (Z_p) we illustrate how the effective average dispersion ($\beta^{(2)}_{ea}$) can be used to interpret the energy variations observed as the amplifier occupies different positions within the dispersion map.

A characteristic of DM soliton propagation in the time domain is that the pulse undergoes periodic expansion and compression, which results in chirping. In the spectral domain, these expansions and contractions of the pulse effectively alter the dispersion. It was shown by Nijhof *et al.* [119], that in fact by balancing the non-linear and dispersive contributions, DM solitons create an effective or non-linear average dispersion that is greater than the linear average dispersion of the map $\beta^{(2)}_{ave}$. This can be used to explain some of the interesting properties of DM solitons, such as enhanced energy and propagation for normal linear average dispersions. Derived previously [119, 148] the effective average dispersion can be expressed as

$$\beta_{ea}^{(2)} = \frac{\langle \beta^{(2)}(z)\Omega^2(z) \rangle}{\langle \Omega^2(z) \rangle} \tag{3.8}$$

where $\beta^{(2)}{}_{ea}$ is a piecewise function describing the local dispersion, $\Omega^2(z)$ is the spectral bandwidth of the propagating pulse and < > implies averaging over the period.

In the case of propagation through a lossless dispersion map, the DM soliton energy remains invariant, which means the nonlinearity is constant. Consequently, for a fixed map strength (S) and minimum pulse width (τ_{min}) only a single DM soliton solution exists. The introduction of fibre loss and periodic amplification modifies the nonlinearity as the pulse propagates through the dispersion map. Therefore, for a fixed map strength (S) and minimum pulse width (τ_{min}), adjustment of the amplifier position within the dispersion map results in a unique bandwidth evolution.

(a)

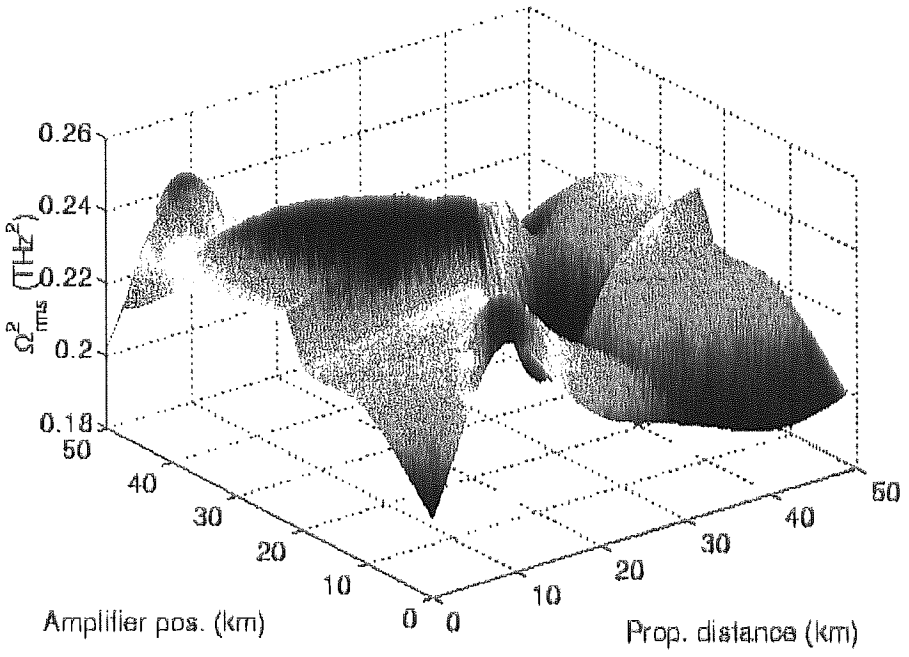

(b)

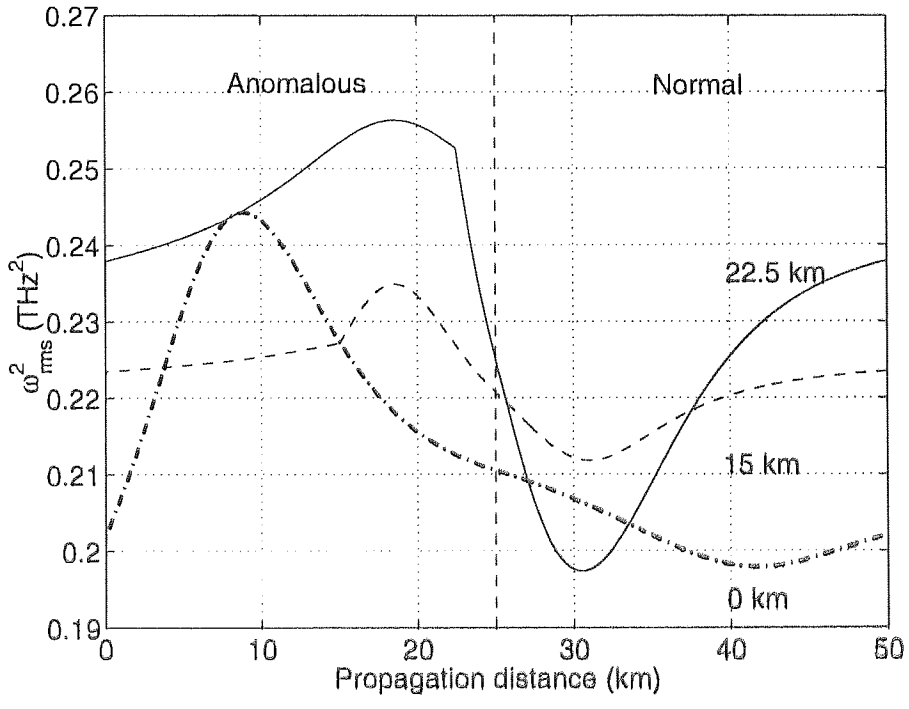

Figure 3.11: Evolution of the RMS bandwidth for a DM soliton over a single dispersion management period. (a) Bandwidth evolution shown as a function of amplifier position within the dispersion map, and (b) bandwidth evolution shown for 3 specific amplifier positions.

Initially, we investigate the different bandwidth evolutions that arise from changing the position of the amplifier within the dispersion map. Again, stable periodic DM soliton solutions are found through numerical integration of the NLS and application of the averaging method of Nijhof *et al.* [111]. Figure 3.11(a) illustrates the bandwidth evolution over a single dispersion management period as the amplifier occupies different positions within the dispersion map. The bandwidth evolution for three specific amplifier positions is shown in Figure 3.11(b). The RMS bandwidth has been used in Figure 3.11, as the pulses used are not exactly Gaussian. It is clear that with the amplifier placed at 22.5 km, the bandwidth in the anomalous fibre is far in excess of the bandwidth in the normal fibre. Moving the amplifier to 15 km, the bandwidths in each fibre section are now more even and with the amplifier positioned at 0 km, we again observe a greater bandwidth in the anomalous dispersion fibre relative to the normal dispersion fibre. These bandwidth evolutions are then used to numerically evaluate $\beta^{(2)}_{ea}$ with the aid of equation (3.8). The effective average dispersions for the amplifier locations in Figure 3.11(b) are shown by symbols in Figure 3.12. The corresponding average dispersions are -0.26 ps^2/km (0 km), -0.12 ps^2/km (15 km) and -0.29 ps^2/km (22.5 km).

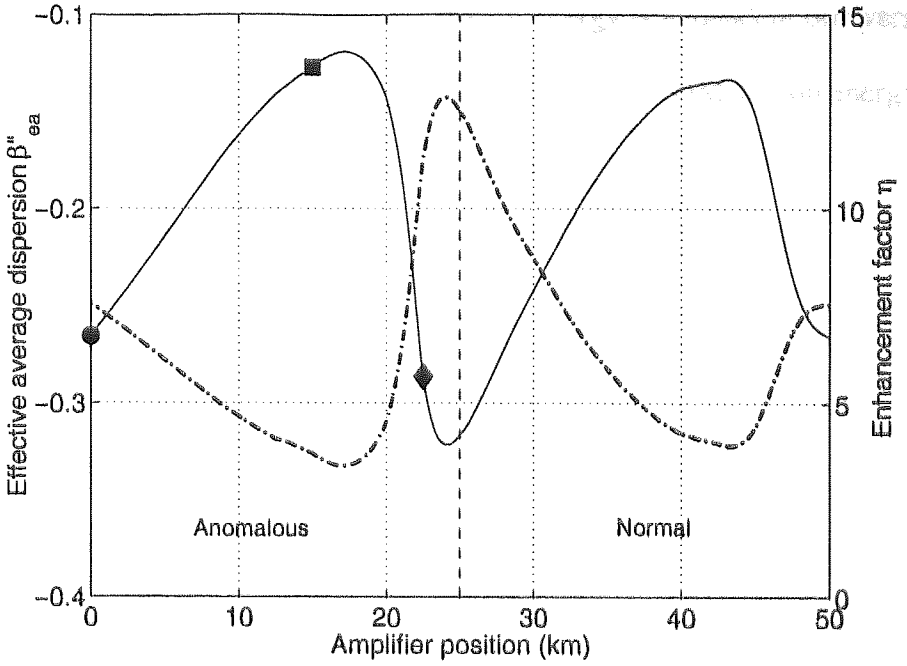

Figure 3.12: Correlation between amplifier location, effective average dispersion and energy enhancement for $S = 4$ and $\tau_{min} = 5$ ps. Symbols: amplifier position = 0 km (circle), 15 km (square), and 22.5 km (diamond).

The importance of the concept of effective average dispersion is highlighted by Figure 3.12. This figure shows how the effective average dispersion ($\beta^{(2)}_{ea}$) and the energy enhancement factor (η) of the DM soliton depend on amplifier location within the dispersion map. Observation of Figure 3.12 suggests a strong inverse correlation between the effective average dispersion and the enhancement factor of the DM soliton. More formally, we can calculate the cross-correlation coefficient, defined as

$$\rho_{1,2} = \frac{\frac{1}{N}\sum_{n=0}^{N-1} x_1(n)\, x_2(n)}{\frac{1}{N}\left[\sum_{n=0}^{N-1} x_1^2(n) \sum_{n=0}^{N-1} x_2^2(n)\right]^{1/2}} \tag{3.9}$$

where $x_{1,2}$ are discrete data sequences of length N. For the data in Figure 3.12, the cross-correlation coefficient $\rho_{1,2}$ is -0.99, which shows an extremely strong inverse correlation between the effective average dispersion and the energy enhancement factor of the DM soliton.

It is known that, for the lossless case, the DM soliton energy is dependent on average dispersion [110] and here we have demonstrated that for the lossy case, the DM soliton energy is dependent on the effective average dispersion. In the lossless model, where nonlinearity is invariant with propagation distance as stated previously, for single map strength (S) (and minimum pulse width) there exists only a single $\beta^{(2)}_{ea}$. Hence this is the reason why S can be used effectively to calculate the DM soliton energy [105, 113], for the lossless case. However, because of the modification of the nonlinearity which occurs with propagation distance, resulting from fibre loss and periodic amplification, means that the bandwidth evolution and hence $\beta^{(2)}_{ea}$ depend critically on the amplifier location within the dispersion map for fixed S and τ_{min}. Therefore in amplified systems, S no longer provides an accurate quantity in characterising DM solitons because it neglects the differing bandwidth evolutions that result from amplifier placement within the dispersion map.

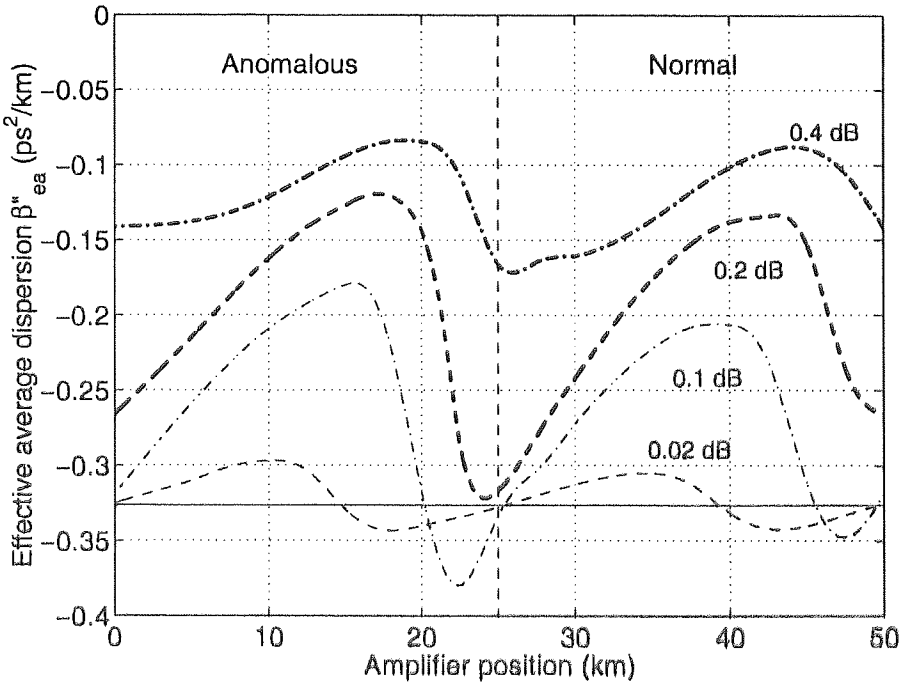

Figure 3.13: Diminishing variations in the effective average dispersion with increasing fibre loss. The numbers indicate the fibre loss per km, with the lossless case being shown by the thin continuous line, for $S = 4$, $\tau_{min} \approx 5$ ps.

Using the concept of effective average dispersion, we determine how fibre loss influences the effective average dispersion. Figure 3.13 illustrates how $\beta^{(2)}_{ea}$ varies with different fibre losses

as a function of the amplifier position within the dispersion map, where the lossless case has been added for completeness. In Figure 3.13, we observe a general trend that as the fibre loss increases, $\beta^{(2)}_{ea}$ approaches $\beta^{(2)}_{ave}$, which is intuitive from our understanding of the effects of fibre loss. In addition, we observe a type of resonant behaviour which peaks for a fibre loss of 0.1 dB, that can produce a $\beta^{(2)}_{ea}$ that is greater than the lossless model, hence η will be larger than for the lossless model. Therefore, if we look only at specific amplifier positions, one could observe either an ascending or descending energy enhancement factor depending on the amplifier location. For example, if the amplifier was positioned at 10 km, then with increasing fibre loss a decreasing energy enhancement factor of the DM soliton, would be observed. Whereas if the amplifier was located at 22 km then the energy enhancement factor of the DM would initially increase before reducing as fibre loss increases. Figure 3.13 concurs with the observations of Refs. [146, 147].

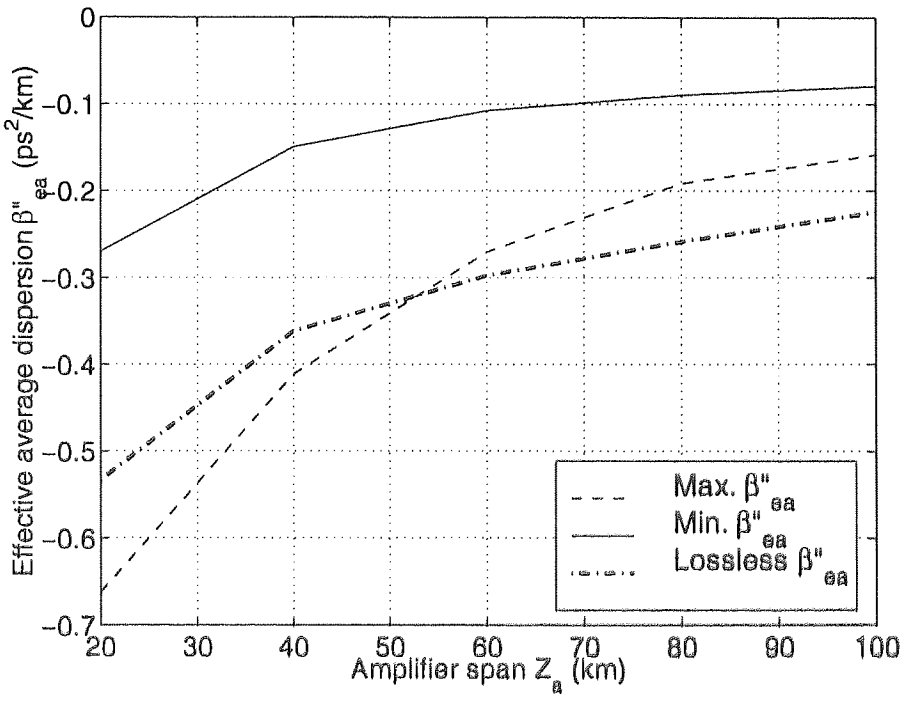

Figure 3.14: Asymptotic convergence of the effective average dispersion to the "linear" average dispersion as Z_a increases for $S = 4$ and $\tau_{min} = 5$ ps.

Next, we determine how Z_a influences the effective average dispersion. Here, we fix the minimum pulse width ($\tau_{min} = 5$ ps), the fibre loss 0.2 dB/km and vary only the local dispersion

to maintain a fixed map strength of 4. Figure 3.14 illustrates how the minimum and maximum effective average dispersions, found as a function of amplifier position, vary as Z_a increases, where the effective average dispersion for the lossless case has been included. In Figure 3.14, we find that for short Z_a we observe large variations in $\beta^{(2)}_{ea}$ resulting from the high local dispersion, but as Z_a increases (reducing local dispersion) we find the minimum and maximum $\beta^{(2)}_{ea}$ converge. Also, as Z_a increases, $\beta^{(2)}_{ea}$ becomes smaller than the lossless case, and thus for all amplifier positions η will be less than the lossless model. This demonstrates, along with Figure 3.13, that it is not only the amplifier position that is important in determining η, but also the fibre loss is an important consideration.

Finally, we show how the effective average dispersion depends on map strength. From Figure 3.15, we can clearly see the general trend of increasing $\beta^{(2)}_{ea}$ with S and again $\beta^{(2)}_{ea}$ is extremely sensitive on amplifier location which grows with increasing S. An interesting feature of Figure 3.15 is the movement of the central trough of each of the curves, which as S increases traverses from the anomalous to the normal dispersion fibre. Also, Figure 3.15 illustrates that a consequence of increasing S is the divergence of $\beta^{(2)}_{ea}$ and $\beta^{(2)}_{ave}$, as $\beta^{(2)}_{ea}$ increases in magnitude. This reinforces our intuitive understanding on why DM soliton transmission can be supported with a normal average dispersion for strong S [119].

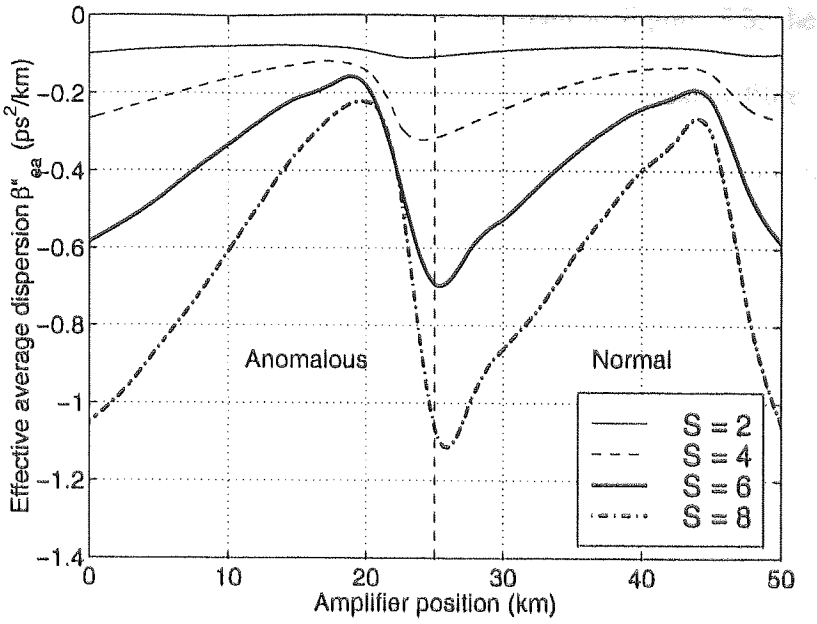

Figure 3.15: Dependence of the effective average dispersion on map strength as a function of amplifier position for τ_{min} = 5 ps and Z_a = 50 km.

Therefore, we have shown that the energy enhancement of the dispersion-managed soliton can be explained in terms of the effective average dispersion. We have shown that in amplified systems the simple relationship between the DM soliton energy and the map strength no longer holds, as it does for the lossless model, as the definition of map strength (S) neglects the modification in nonlinearity that occurs. To accurately characterise and understand DM soliton propagation in amplified systems we must use the concept of effective average dispersion ($\beta_{ea}^{(2)}$). This concept provides a means to interpret the results of previous studies [146, 147].

3.6.2 Reconstruction of the lossless dynamics

As detailed in section 3.6.1, the amplifier position within the dispersion map determines the energy of the DM soliton. It is unsurprising then, that the dynamics of the DM soliton are affected by the positioning of the amplifier.

In the lossless case, there is only a single DM soliton solution for each dispersion map, due to the constant nonlinearity, provided that the condition $|\beta^{(2)}_{a,n}| >> |\beta^{(2)}_{ave}|$ is satisfied [149].

For lossless propagation, the dynamics of which can be seen in Figure 3.3, the DM soliton has the chirp-free points at the mid-points of the anomalous and dispersion fibre sections and the pulse width displays a symmetric evolution about the centre of the dispersion map.

In contrast, when fibre loss and periodic amplification is introduced into the system we observe differing DM soliton dynamics, as the amplifier occupies a different location in the dispersion map. This is shown in Figure 3.16, which details the evolution of the width, chirp and bandwidth of the pulse. From Figure 3.16 it is clear that the pulse width evolution displays an asymmetrical evolution that changes as the amplifier position moves through the dispersion map. Therefore, if the amplifier is located at the points where the asymmetry in the pulse width dynamics changes, then the lossless dynamics should be reconstructed. Figure 3.17 confirms this observation, which contrasts the lossy and lossless dynamics for the two amplifier positions (one in the anomalous dispersion fibre and one in the normal dispersion fibre), where the pulse width dynamics are symmetrical. It is apparent that the lossy dynamics are extremely similar to lossless dynamics with the exception of a small region around one of the minima in Figure 3.17(a) and one of the maxima in Figure 3.17(b). These points, where the lossless dynamics are reconstructed correspond to the point where coherent interactions are minimised.

(a)

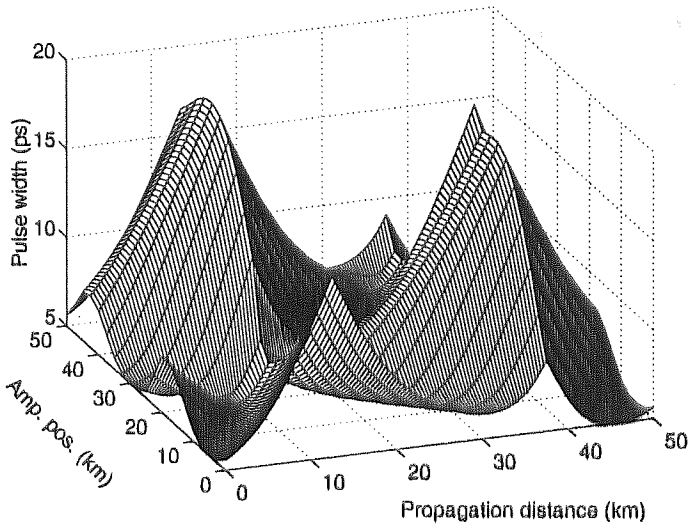

(b)

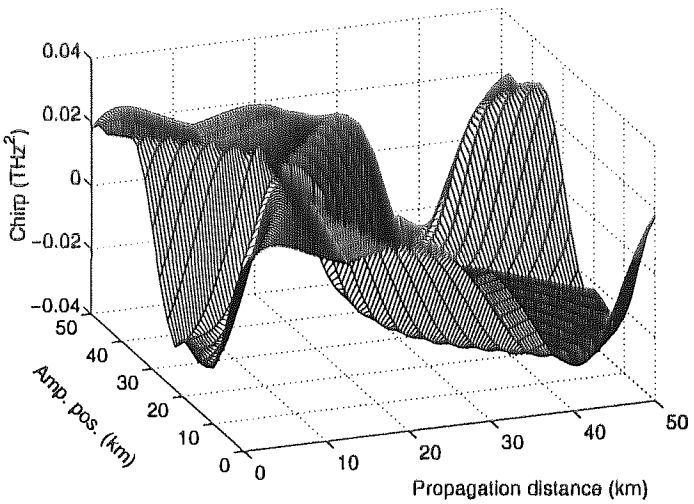

(c)

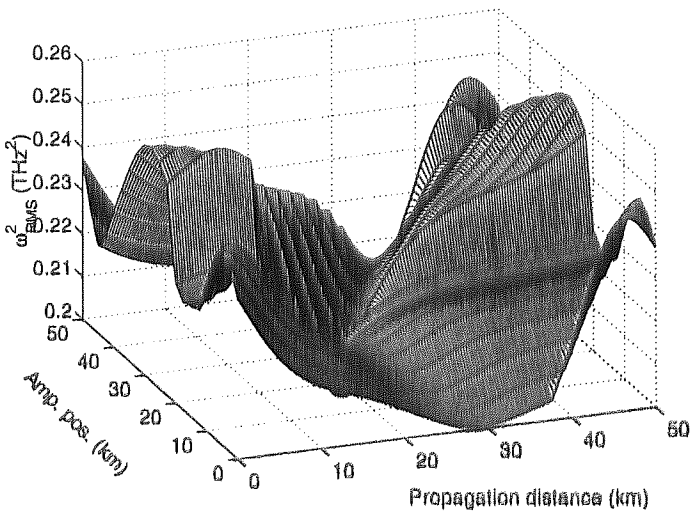

Figure 3.16: Evolution of the DM soliton dynamics over a single dispersion management period as the amplifier occupies different positions in the dispersion map. (a) Pulse width evolution, (b) chirp evolution, and (c) bandwidth evolution.

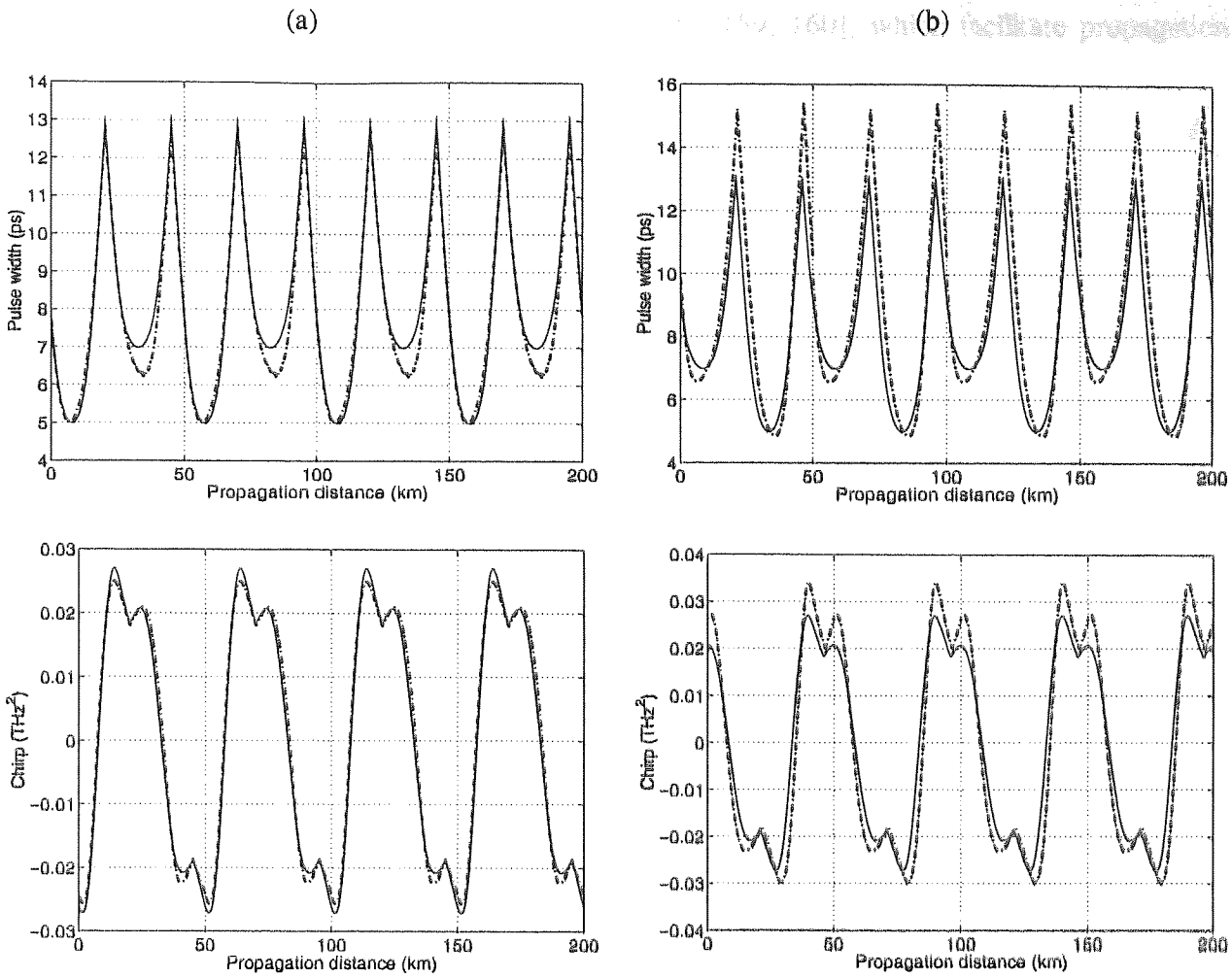

Figure 3.17: Reconstruction of the lossless dynamics for two specific amplifier locations in the dispersion map. (solid line) lossless dynamics and (dot and dash line) dynamics with periodic loss and amplification. (a) Amplifier at 5.5 km in the anomalous dispersion fibre, and (b) amplifier at 28 km in the normal dispersion fibre.

3.7 DM Soliton control techniques

Analogous to the classical soliton, various control techniques can be applied to the DM soliton to further improve system performance. A common control technique in dispersion-managed system is that of fixed frequency [150-153] and sliding frequency filtering [150, 154, 155], which reduces the accumulation of timing jitter. In the regime of weak dispersion management ($S < 3$), similar control techniques that can be applied to classical soliton propagation can also be used to reduce interactions such as phase modulation and amplitude modulation [156-158]. Also, device based techniques such as amplitude modulators [10] and saturable absorbers [83] can also improve performance. In additional, the soliton-like nature of DM solitons allows the

use of optical regenerators as described in Refs. [98, 159, 160], which facilitate propagation over virtually unlimited distances.

3.8 Variational approaches to modelling of dispersion managed systems

Like other partial differential equations, numerical integration of the NLS equation is often costly in terms of both time and computation power. This often limits the parameter space that can be explored by numerical simulations. However, this computation burden can be reduced making a variational approximation of the NLS that effectively reduces the NLS into a set of coupled ordinary differential equations. These ordinary differential equations that determine the evolution of the key parameters can be quickly and easily integrated using a simple integration technique such as the Runge-Kutta method.

This technique was first applied to classical soliton propagation in optical fibre by Anderson [161] and later generalised in terms of dispersion managed systems by Shapiro *et al.* [162]. Since then a huge amount of work has been undertaken investigating DM soliton propagation employing this approach [110, 119, 120, 148, 163-166], with specific analysis of intra channel interactions [129, 135, 136, 167], inter channel interactions [58, 168], DM soliton control [152, 169, 170], and system modelling [171, 172]. However, whilst the variational approach yields a good approximation of DM soliton behaviour under certain conditions, more complicated effects such as FWM and SRS have not yet been included in the model. This method also neglects the continuum dynamics that are often a source of instability, especially when control elements such as filters are included. Although the variational approximation provides a good understanding of the physical mechanisms of DM soliton propagation, until effects such as FWM are included into the model, then accurate estimations of system performance at high data rates does not remain a possibility.

3.9 Conclusion

We have reviewed some of the basic principles of dispersion management and introduced the soliton-like pulse that exists in such systems called the DM soliton. We have then investigated the properties of DM soliton propagation in a regime called SPDM that is suitable for ultra-high speed transmission. This regime is characterised by $Z_p << Z_a$, which confines pulse breathing thus allowing DM solitons to exist for short pulse width and practical amplifier spans. These properties are then used to help design and understand the ultra high-speed transmission systems in chapters 4, 5 and 6.

This chapter also investigated the implications of the amplifier location within the dispersion map. We described how the energy enhancement of the DM soliton, in the lossey case, can be more accurately described using the concept of effective average dispersion. In addition, we also showed that by locating the amplifier at specific points in the dispersion map, the dynamics of the lossless DM soliton could be achieved.

Chapter 4 80 Gbit/s transmission

4.1 Introduction

The seeds of DM soliton transmission were sown in the pioneering experiments of KDD Laboratories undertaken during the mid-1990s [173-175], which demonstrated for the first time transoceanic transmission at 10 Gbit/s. These experiments and the subsequent progress on DM transmission drew heavily on the research into propagation of *classical* solitons in optical fibres that had been under taken during the previous decade [176-182]. The subsequent years have born witness to a massive explosion in both transmission capacity and transmission distance, with many experiments demonstrating successful 10 Gbit/s [133, 183-189], 20 Gbit/s [80, 175, 190-193] and 40 Gbit/s transmission [194-201]. Partially a result of technology advances and partially a consequence of dispersion management, massive WDM experiments emerged with capacities in excess of 1 Tbit/s [97, 202, 203].

Although some systems display a total transmission capacity exceeding 1 Tbit/s, it has largly been achieved using many wavelength channels each operating a low data rate. However, there exists the potential to increase the spectral efficiency of these systems by utilising the same spectrum but with fewer wavelength channels each operating at a much higher data rate. In addition, arguments regarding system cost and complexity support this approach. With this in mind, this chapter investigates ultra high speed channel transmission at 80 Gbit/s. Such high transmission rates require a change in the design of dispersion managed transmission systems because of the short pulse widths required. The manifestations of this problem are evident in 40 Gbit/s systems [204, 205], where due to the short pulse widths and large dispersion of installed standard fibre, transmission occurs in a quasi-linear regime where the propagating pulses lose many of their *soliton-esque* properties. This propagation regime has the additional disadvantage

of being limited by FWM, which imposes limitations on the maximum transmission distance achievable [205]. Currently only a small amount of published literature exists focussing on 80 Gbit/s transmission [83, 141], with even fewer transmission experiments reported [206-208].

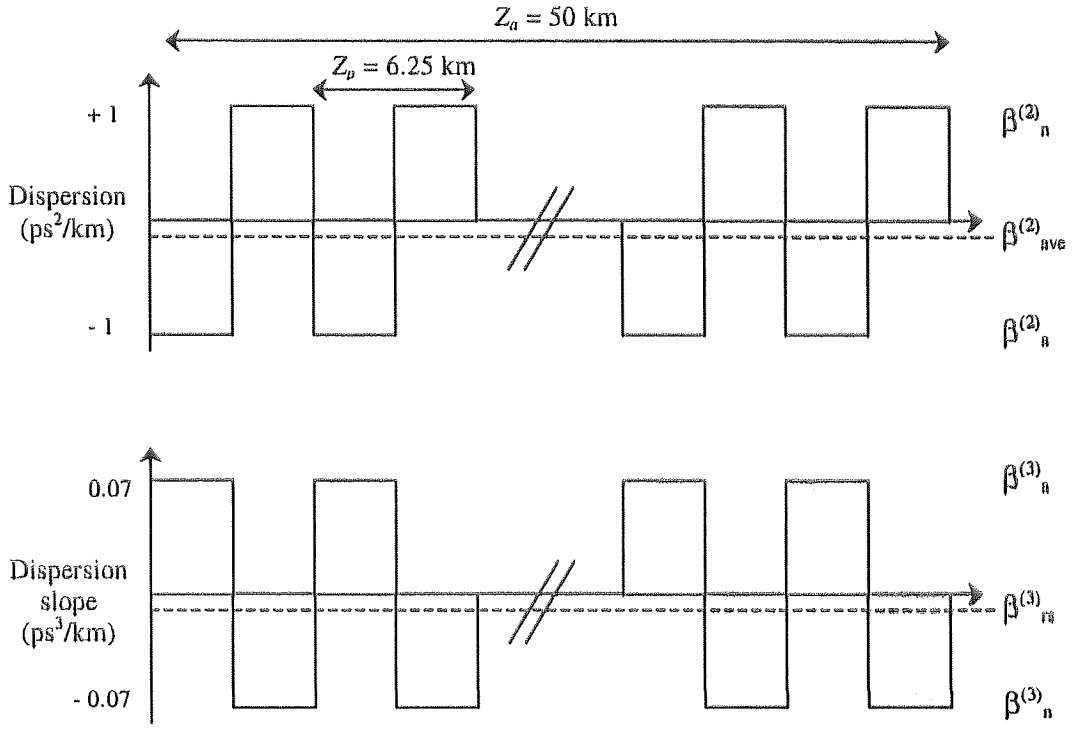

Figure 4.1: Schematic representation of the short period dispersion used for 80 Gbit/s transmission

In this chapter, adopting the novel approach of short period dispersion management, which was detailed in section 3.5.2, we investigate transmission at 80 Gbit/s by numerical simulation. To begin with, we explore and optimise propagation over transoceanic distances determining the conditions under which transmission can be supported. After which we investigate transmission over medium and short haul transmission distances before finally investigating transmission using standard fibre sections.

4.2 Single pulse propagation

The basis of our transmission simulations are formed by finding stable, periodic DM solitons in SPDMs, by applying an averaging method [111] to the numerical integration of the Non-Linear

Schrödinger Equation (NLS) (neglecting higher order dispersive and non-linear terms). Throughout this chapter we consider Z_a = 50 km and fix the following fibre properties: loss, $\alpha \approx$ 0.2 dB/km, effective area, A_{eff} = 50 μm^2 and non-linear index, $n_2 = 2.6 \times 10^{-20}$ m^2/W. We focus on a dispersion map strength S ≈ 1.65, which has been shown to be the optimal map strength to minimise interactions in the lossless case [127]. An example dispersion map is illustrated in Figure 4.1. Fixing the minimum pulse width τ_{min} = 2 ps, to allow a large enough mark-to-space ratio, a freedom still exists to determine the number of dispersion sections per amplifier spacing, $n = 2Z_a/Z_p$. In these systems n should be chosen so that Z_p and $\beta^{(2)}_{a,n}$ are practical, i.e. the map period is not too short, and the dispersion values are not too small.

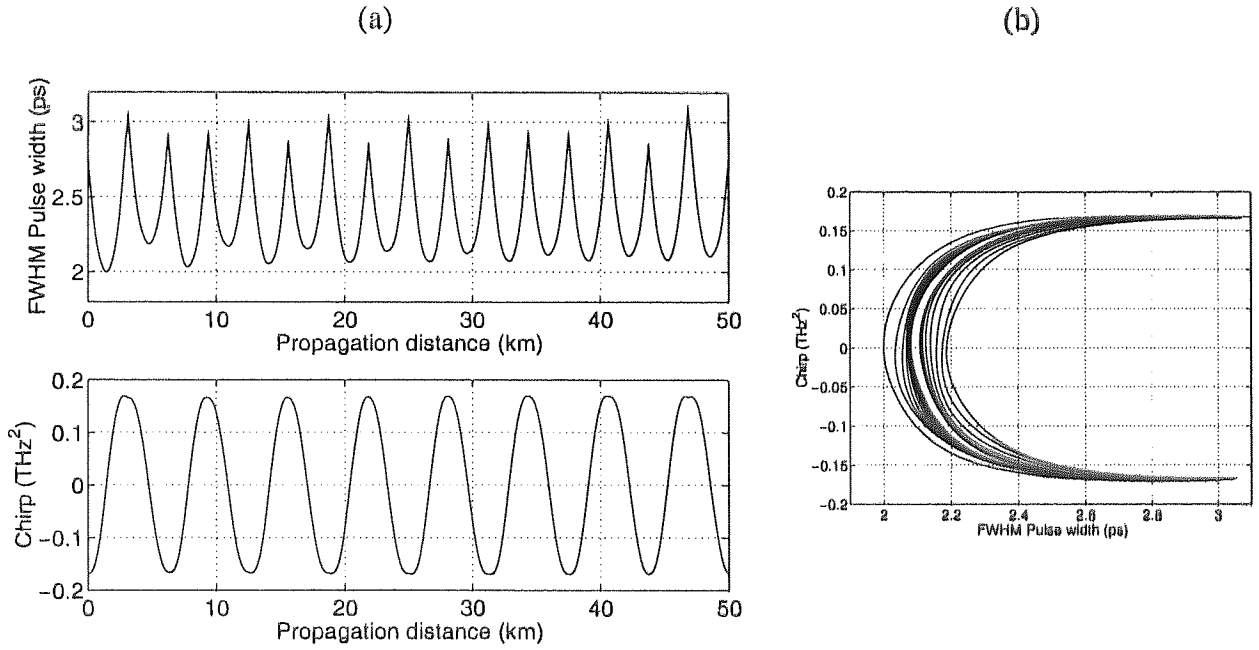

Figure 4.2: DM soliton evolution evolution over Z_a for a 16-section short period dispersion map. (a) Pulse width and chirp evolution (b) Phase plane dynamics.

The evolution of the DM soliton dynamics over Z_a for an SPDM with n = 16, with S = 1.65, $\beta^{(2)}_{ave}$ = -0.02 ps^2/km and τ_{min} = 2 ps is shown in Figure 4.2. In this case, the magnitudes of the local dispersion sections are $\beta^{(2)}_a$ = -1.076 ps^2/km and $\beta^{(2)}_n$ = 1.036 ps^2/km. Unlike the

conventional dispersion management regime ($Z_p \geq Z_a$) the pulse width dynamics are no longer periodic in Z_p (as they are in the lossless model), but are periodic in Z_a. The pulse width evolution over Z_a exhibits a highly regular form with a convergence of the local pulse width minima, and is consistent with a gradual reduction in the nonlinearity across the amplifier span. For identical simulation parameters as used in Figure 4.2, Figure 4.3 illustrates the temporal and spatial evolution over Z_a, where the rapid pulse 'breathing' relative to the amplification span is clearly visible. The evolution of the slow dynamics of the DM soliton can be seen for a propagation distance of 10,000 km in Figure 4.4.

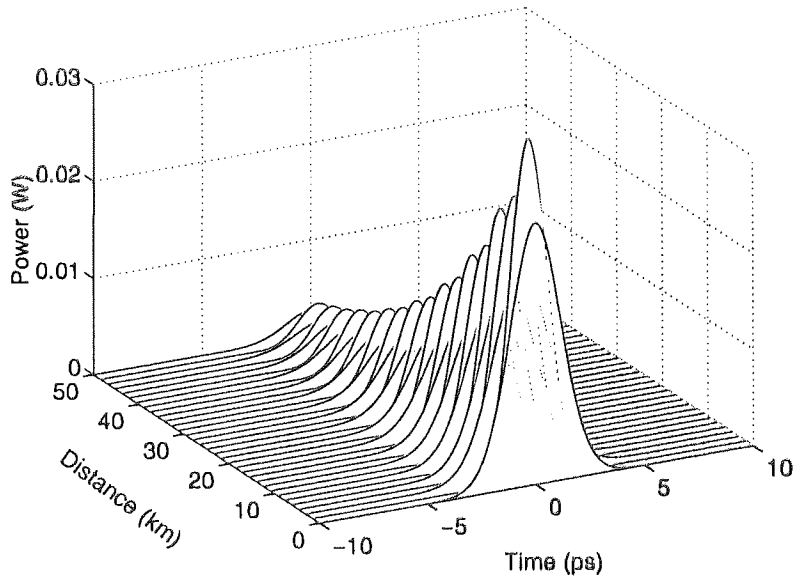

Figure 4.3: DM soliton propagation over a single dispersion management period ($n = 16$).

The selection of the minimum pulse (τ_{min}) width resulted from observation of the interactions between two co-propagating DM solitons. For $\tau_{min} > 2$ ps interaction increases because of the greater overlap between the two DM solitons. The minimum pulse width $\tau_{min} = 2$ ps was selected because it was the longest pulse width for which interactions between adjacent DM solitons were negligible over the domain of interest (< 10,000 km), while reducing the influence of higher order non-linear and dispersive effects that increase as the pulse width becomes shorter. Interactions can also be further reduced by decreasing the average dispersion.

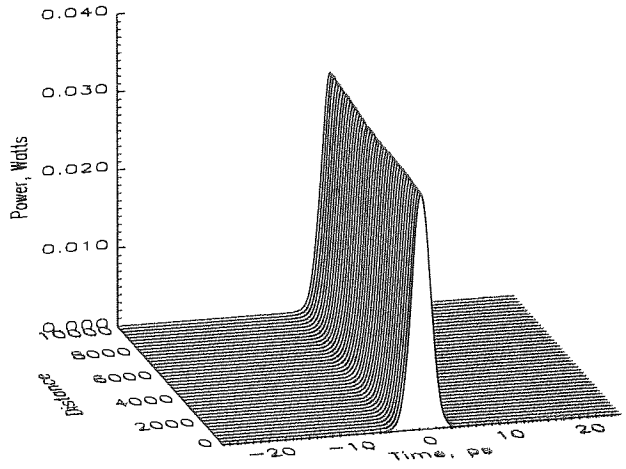

Figure 4.4: Evolution of the slow dynamics of the DM soliton shown over 10,000 km.

4.3 Simulations

For the 80 Gbit/s transmission simulations, we use the Generalised Non-Linear Schrödinger equation (GNLS) [72], which includes the effects of dispersion slope and higher order non-linear effects. Following Refs. [142, 209], dispersion slope compensation is provided by each of the fibre sections having alternative sign dispersion slopes with magnitudes: $\beta^{(3)}_a = -\beta^{(3)}_n = 0.07$ ps^3/km. Therefore dispersion slope compensation occurs over a length scale of Z_p, which becomes an increasingly important factor for short pulse widths. The only control element in the transmission line is a Gaussian filter ($\Omega_{optical}$) of bandwidth 1 THz (FWHM), located directly after each amplifier. A schematic representation of the transmission line is illustrated in Figure 4.5. The noise figure of the amplifiers is taken to be 4.5 dB and the introduction of the filter requires an additional gain of 0.09 dB. The receiver is modelled by a non-optimised Lorentzian electrical filter of bandwidth 50 GHz (62.5 percent of the bit rate). In this system, the amplifier is located at the start of one of the anomalous dispersion fibre sections, and therefore, pulse amplifications and filtering occurs where the DM soliton is highly chirped within its periodic cycle.

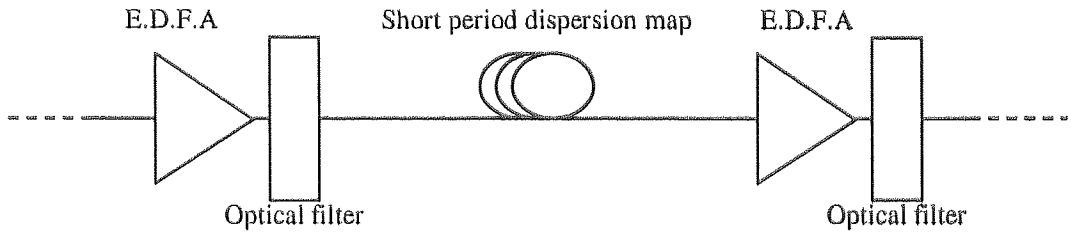

Figure 4.5: Schematic representation of transmission line used for 80 Gbit/s transmission

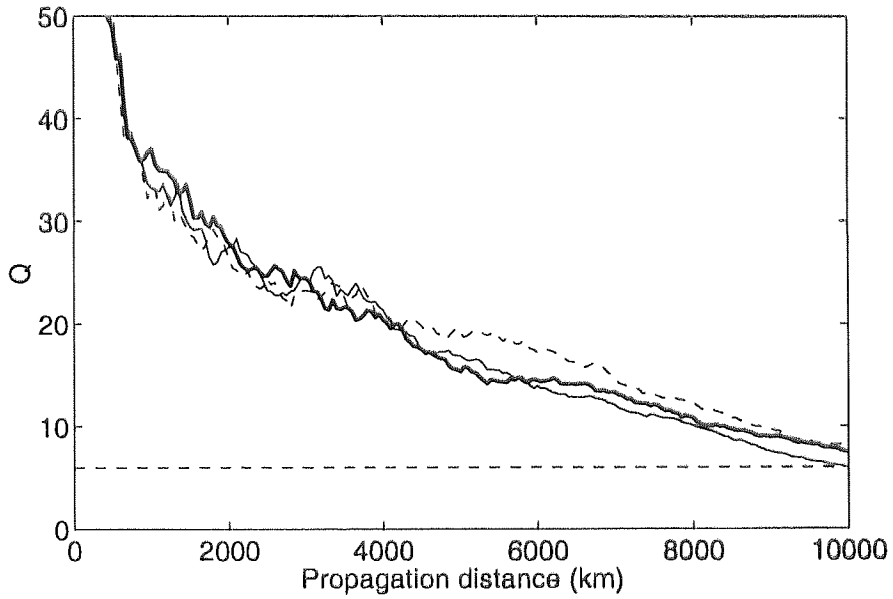

Figure 4.6: Dependence of performance on the dispersion management period for a fixed map strength. (thin solid line) n = 16, (thick solid line) n = 32, and n = 64 (dashed line).

The performance of the transmission system is evaluated using Q-value estimates based on a 2^7 - 1 bit pseudo random sequence, with the computation applied to 4 blocks each containing 32 bits. The Q-values are defined from the equation

$$Q = \frac{\mu_1 - \mu_0}{\sigma_1 + \sigma_0} \tag{4.1}$$

where $\mu_{1,0}$ are the respective mean levels of the 1 and 0, and $\sigma_{1,0}$ are standard deviations of the 1 and 0 respectively. The standard deviations are calculated using:

$$\sigma_1 = \sqrt{\frac{\sum_{i=1}^{n}(p_i - \mu_1)^2}{(n-1)}} \tag{4.2}$$

where n is the number of 1's in the data pattern, p_i is the peak power of the pulse i and μ_1 is the mean level of the 1's. These Q values can then be equated to the Bit Error Rate (B.E.R) that is used in laboratory experiments, assuming a Gaussian distribution in the 1's and 0's, then the relationship between BER and Q can be given as

$$BER = \frac{1}{2\pi}\frac{\exp\left(-\frac{Q^2}{2}\right)}{Q} \tag{4.3}$$

Using equation (4.3) a BER of 10^{-9} is equivalent to a Q value of 6. Although the distribution of the 1's and 0's may possess an alternate statistical distribution [210, 211], for soliton-like transmission, equation (4.3) provides an adequate approximation of a physical system.

The system performance as a function of propagation distance is illustrated in Figure 4.6 for n = 16, 32 and 64. The simulation parameters S = 1.65, $\beta^{(2)}_{ave}$ = -0.02 ps^2/km, $\beta^{(3)}_a = -\beta^{(3)}_n$ = 0.07 ps^3/km, $\Omega_{optical}$ = 1 THz and the corresponding local dispersions for n = 16, 32 and 64 are $\beta^{(2)}_{a,n}$ ≈ ± 1 ps^2/km, ± 2 ps^2/km and ± 4 ps^2/km respectively. Considering the stochastic nature of the simulation, the performance of the three dispersion maps in Figure 4.6 is fairly similar. This is a consequence of the DM soliton energy saturation that occurs for large n, as detailed in section 3.5.2. Thus, in the case of single channel transmission, we can simulate the computationally less intensive map (n = 16) and generalise the results for n = 32 and 64. However, this

approximation is not valid if multiple wavelengths are used as in WDM, this is because the inter channel FWM efficiency is dependant on the magnitudes of the local dispersion. Therefore, throughout the rest of the chapter we shall be exclusively concerned with the map $n = 16$ only. We observe that after the initial steep decline in performance that occurs for short transmission distances (< 1,000 km), which occurs due to the initial introduction of noise, the system performance degrades gradually with propagation distance. The performance of the system is limited by the accumulation of timing jitter and the growth of continuous wave background instabilities that arise from the strong filtering. Nevertheless, for all three SPDMs we have found that transmission with Q > 6 can be achieved for distances in excess of 9,000 km.

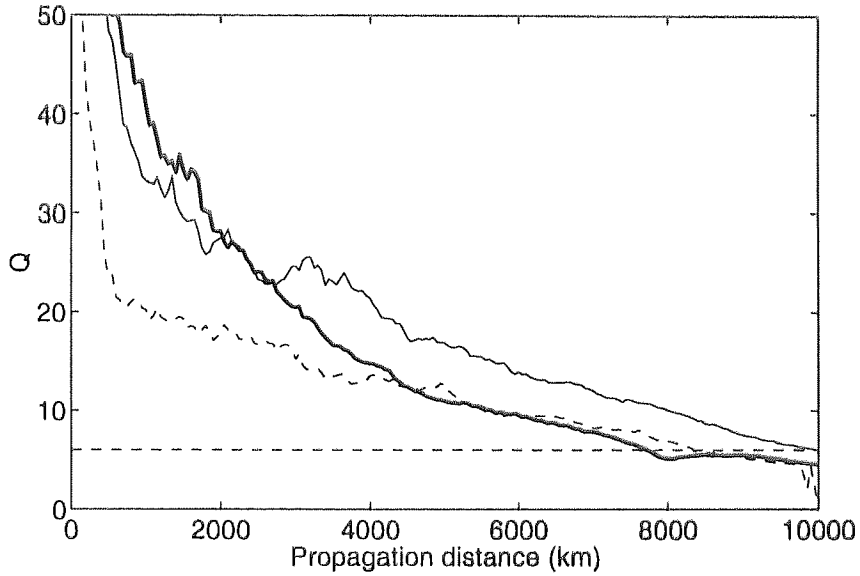

Figure 4.7: Depedence of system performance on average dispersion. (dashed line) $\beta^{(2)}_{ave}$ = -0.005 ps^2/km, (thin solid line) $\beta^{(2)}_{ave}$ = -0.02 ps^2/km, and (thick solid line) $\beta^{(2)}_{ave}$ = –0.05 ps^2/km.

The dependence of system performance on average dispersion ($\beta^{(2)}_{ave}$) is shown in Figure 4.7, as a function of propagation distance, the rest of the simulation parameters remain invariant. It can be seen that there is a clear optimal average dispersion for $\beta^{(2)}_{ave}$ = -0.02 ps^2/km and that movement either side of this value results in a significant reduction in system performance. When $\beta^{(2)}_{ave}$ < -0.02 ps^2/km, interactions between adjacent pulses increase which limits

performance and when $\beta^{(2)}_{ave}$ > -0.02 ps^2/km, the system suffers from a poor Signal-to-Noise Ratio (SNR) which leads to increased timing jitter. The sensitivity to average dispersion in this system arises from the short pulse width (τ_{min} = 2 ps), which means that the DM soliton energy scales more rapidly with $\beta^{(2)}_{ave}$. This sensitivity could be reduced by increasing the pulse width but this leads to increased interactions at S = 1.65, in this system for 80 Gbit/s transmission.

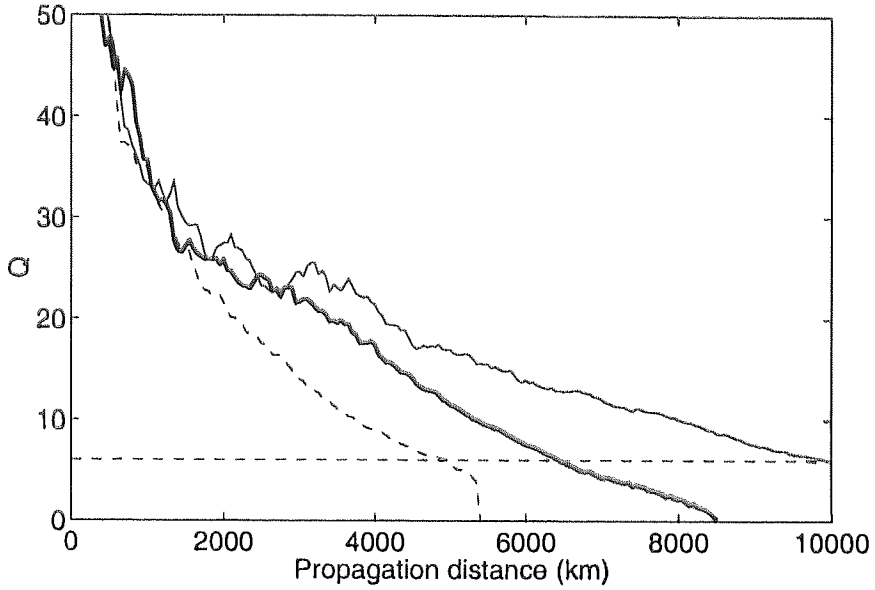

Figure 4.8: System performance as a function of filter bandwidth. (dashed line) $\Omega_{optical}$ = 0.8 THz, (thin solid line) $\Omega_{optical}$ = 1 THz and (thick solid line) $\Omega_{optical}$ = 2 THz

Next, we consider the influence of the filter on the performance of the system. Figure 4.8 shows system performance as a function of propagation distance for filter FWHM bandwidths, $\Omega_{optical}$ = 0.8 THz, 1 THz and 2 THz. For $\Omega_{optical}$ = 0.8 THz the performance is similar to $\Omega_{optical}$ = 1 THz over short propagation distances, but rapidly deteriorates as a result of the increased growth of continuous wave background instability resulting from the strong filtering. The result of the instabilities in the continuous wave background, as described in Ref. [212], can be seen in Figure 4.9. The problem introduced is that the transmitted pulses become indistinguishable from the background resulting in information loss. If the filter is too wide, as for $\Omega_{optical}$ = 2 THz, then performance degrades even more rapidly due to timing jitter and the concomitant interactions.

Nevertheless, for $\Omega_{optical}$ = 1 THz a balance is struck between these two limiting factors described for the $\Omega_{optical}$ = 0.8 THz and 2 THz, and a combination of these limiting factors ultimately kills the performance at ~10,000 km.

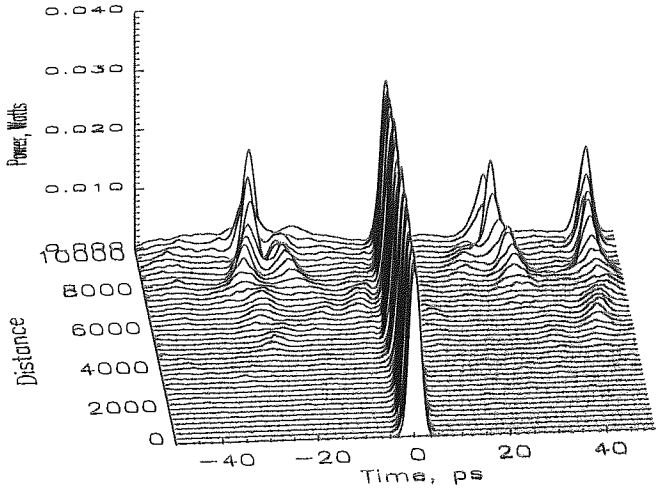

Figure 4.9: Growth of the continuous wave background due to strong optical filtering

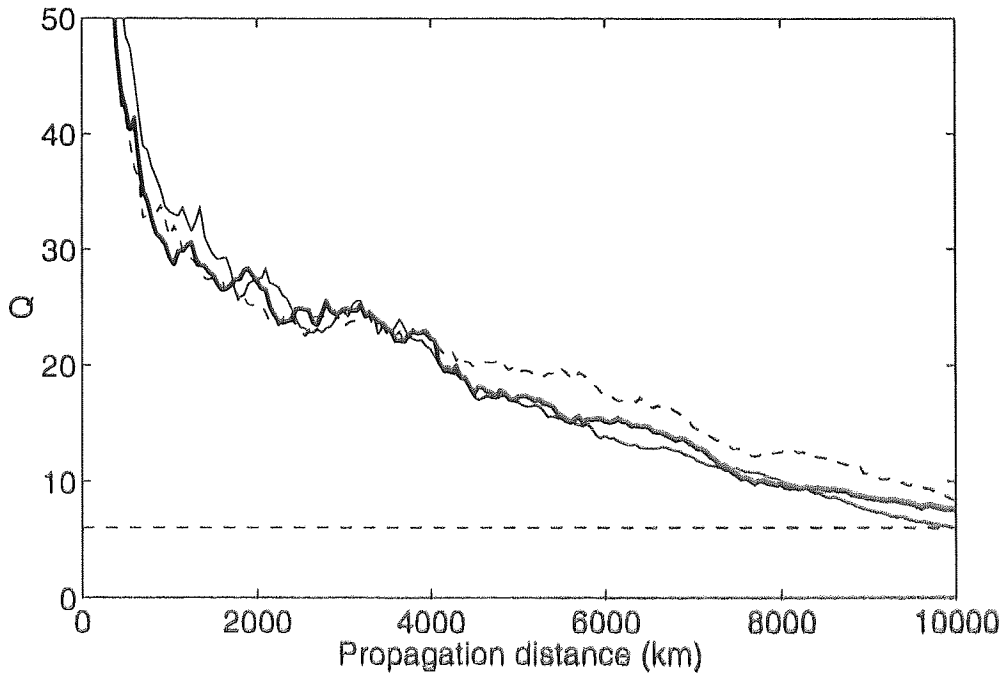

Figure 4.10: Robustness of system performance due to imperfect dispersion slope compensation. (thin solid line) $\beta^{(3)}_{rs}$ = 0 ps^3/km, (dashed line) $\beta^{(3)}_{rs}$ = 0.01 ps^3/km, and (thick solid line) $\beta^{(3)}_{rs}$ = 0.03 ps^3/km

4.4 Higher order non-linear and dispersive effects

At this point in the investigation we have worked on the assumption that we have a zero residual dispersion slope, defined as $\beta^{(3)}_{rs} = (\beta^{(3)}_{a} + \beta^{(3)}_{n})/2$ (as $l_1 = l_2$), by assuming the dispersion slopes in the anomalous and normal dispersion have identical magnitudes $\beta^{(3)}_{a} = -\beta^{(3)}_{n}$. We now break this relationship so that $\beta^{(3)}_{a} \neq -\beta^{(3)}_{n}$, and investigate the tolerance of the optimised system performance to imperfect dispersion slope compensation. With increasing data rates, which use shorter pulse widths, higher order dispersive effects like the dispersion slope begin to play an increasingly important role. In Figure 4.10 the residual dispersion slopes are constructed from the following dispersion slopes in each of the fibre sections $\beta^{(3)}_{rs} = 0$ ps^3/km ($\beta^{(3)}_{a} = -\beta^{(3)}_{n} = 0.07$ ps^3/km), $\beta^{(3)}_{rs} = 0.01$ ps^3/km ($\beta^{(3)}_{a} = 0.07$ ps^3/km, $\beta^{(3)}_{n} = -0.05$ ps^3/km) and $\beta^{(3)}_{rs} = 0.03$ ps^3/km ($\beta^{(3)}_{a} = 0.08$ ps^3/km, $\beta^{(3)}_{n} = -0.02$ ps^3/km). From Figure 4.10 it is apparent that for residual dispersion slopes < 0.03 ps^3/km the system performance remains relatively unaffected and these residual dispersion slopes are of the same order of those previously manufactured (0.004 ps/nm^2/km) in Ref. [142].

We extended our investigation by removing the higher order dispersion compensation, $\beta^{(3)}_{rs} = \beta^{(3)}_{a} = \beta^{(3)}_{n}$, in the SPDM. In Figure 4.11 the residual dispersion slopes are constructed as $\beta^{(3)}_{rs} = 0$ ps^3/km ($\beta^{(3)}_{a} = -\beta^{(3)}_{n} = 0.07$ ps^3/km), $\beta^{(3)}_{rs} = 0.04$ ps^3/km ($\beta^{(3)}_{a} = \beta^{(3)}_{n} = 0.04$ ps^3/km), and $\beta^{(3)}_{rs} = 0.07$ ps^3/km ($\beta^{(3)}_{a} = \beta^{(3)}_{n} = 0.07$ ps^3/km). Figure 4.11 demonstrates that system performance remains relatively unaffected by $\beta^{(3)}_{rs} = 0.04$ ps^3/km but for large dispersion slopes $\beta^{(3)}_{rs} \geq 0.07$ ps^3/km system performance has significantly deteriorated. Figure 4.12 illustrates how the dispersion affects pulse propagation for $\beta^{(3)}_{rs} = 0.07$ ps^3/km. It can be seen that the dispersion slope breaks the uniform evolution of the slow pulse dynamics as shown in Figure 4.4, and induces a more complex evolution in these slow dynamics resulting in the DM soliton shedding radiation.

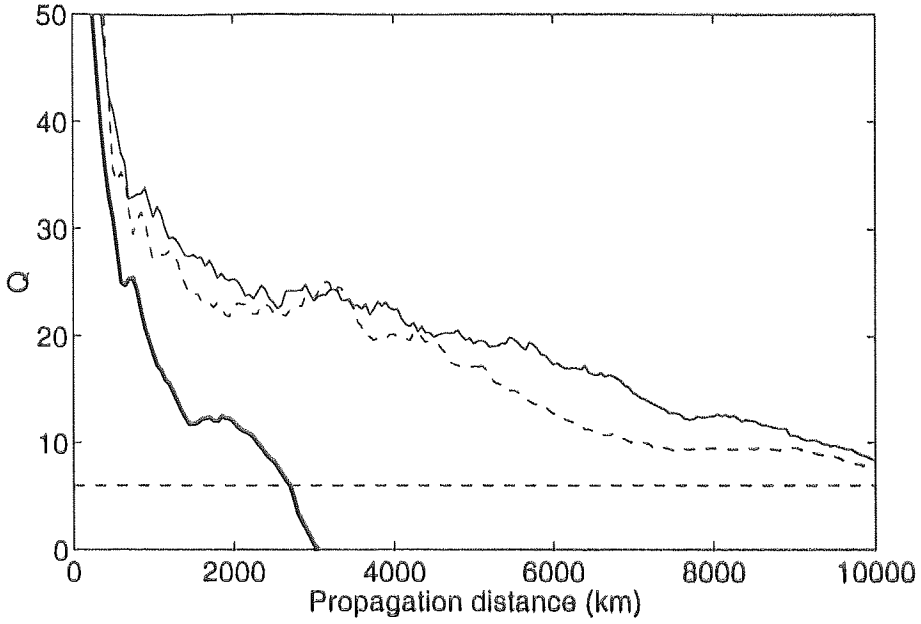

Figure 4.11: Robustness of system performance without dispersion slope compensation. (thin solid line) $\beta^{(3)}_{rs} = 0$ ps^3/km, (dashed line) $\beta^{(3)}_{rs} = 0.04$ ps^3/km, and (thick solid line) $\beta^{(3)}_{rs} = 0.07$ ps^3/km.

Following Ref. [213], we compare the relative contributions of the average dispersion and dispersion slope by their respective dispersion lengths $L_D = \tau^2_{min}/|\beta^{(2)}_{ave}|$ and $L_D' = \tau^3_{min}/|\beta^{(3)}_{rs}|$.

We are only concerned with the length scale of the residual dispersion slope because dispersion slope compensation occurs on the length scale Z_p and generally the condition $Z_p << \tau^2_{min}/|\beta^{(3)}_{a,n}|$ is satisfied. For this system, the simulations showed that the influence of the residual dispersion slope was negligible under the conditions $L_D \geq L_D'$ and only became significant for $L_D < L_D'$.

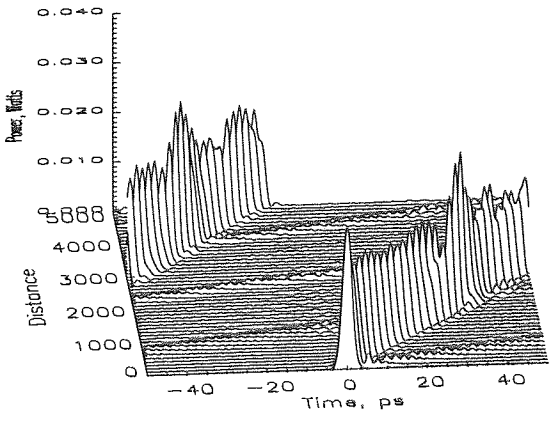

Figure 4.12: Effects of dispersion slope on 2 ps pulse propagation. Noiseless propagation is shown with no dispersion compensation ($\beta^{(3)}_a = \beta^{(3)}_n = \beta^{(3)}_{rs} = 0.07$ ps^3/km).

Thus far, our transmission simulations have included higher order non-linear effects. Until this point, we have not established how SRS influences transmission performance. By switching the Raman coefficients of the GNLS on and off we are able to isolate the effects of SRS. The simulation results indicate that SRS is having a negligible impact on transmission performance with little effect being observable in both single pulse propagation and transmission simulations. However, for completeness we continue to include the Raman coefficients in our numerical integration, even though their role is only minor and could be neglected.

Another influential effect that so far in the discussion has been neglected is polarisation mode dispersion. We simulate PMD by integration of the 2-dimensonal birefringent NLS [214, 215] with the effects of random mode coupling simulated by a random rotation of the birefringent axis and a random phase shift being applied to the propagating pulse on a length scale much shorter than L_D. Figure 4.13 illustrates the dependence of system performance on various values of PMD. For large values of PMD we observe that performance is significantly reduced, however for lower and more moderate values of PMD long haul transmission is still feasible. Therefore, this indicates the requirement for PMD to be controlled to less than 0.05 ps/√km for transoceanic transmission.

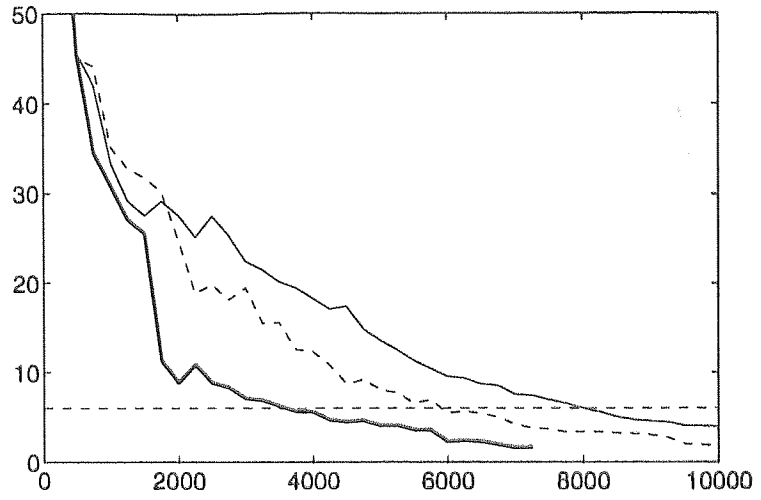

Figure 4.13: The effect of polarisation mode dispersion on 80 Gbit/s transmission. (thin solid line) PMD = 0.02 ps/√km, (dashed line) PMD = 0.05 ps/√km, and (thick solid line) PMD 0.07 ps/√km.

The optimised performance of the system and its limiting factors can be quantitatively observed in Figure 4.14, which shows the eye diagrams shown at propagation distances of 1,000 km, 3,000 km, 5,000 km and 8,000 km where higher order non-linear and dispersive effects have been included with a residual dispersion slope $\beta^{(3)}_{rs}$ = 0.03 ps^3/km. At 1,000 km, we observe an extremely clean eye with little amplitude jitter, and by 3,000 km the increasing timing jitter is clearly observable. At 5,000 km, this timing jitter has increased further and finally at 8,000 km the pulses exhibit considerable timing jitter, with a small amount of amplitude jitter also being present and the continuous wave background instabilities are present.

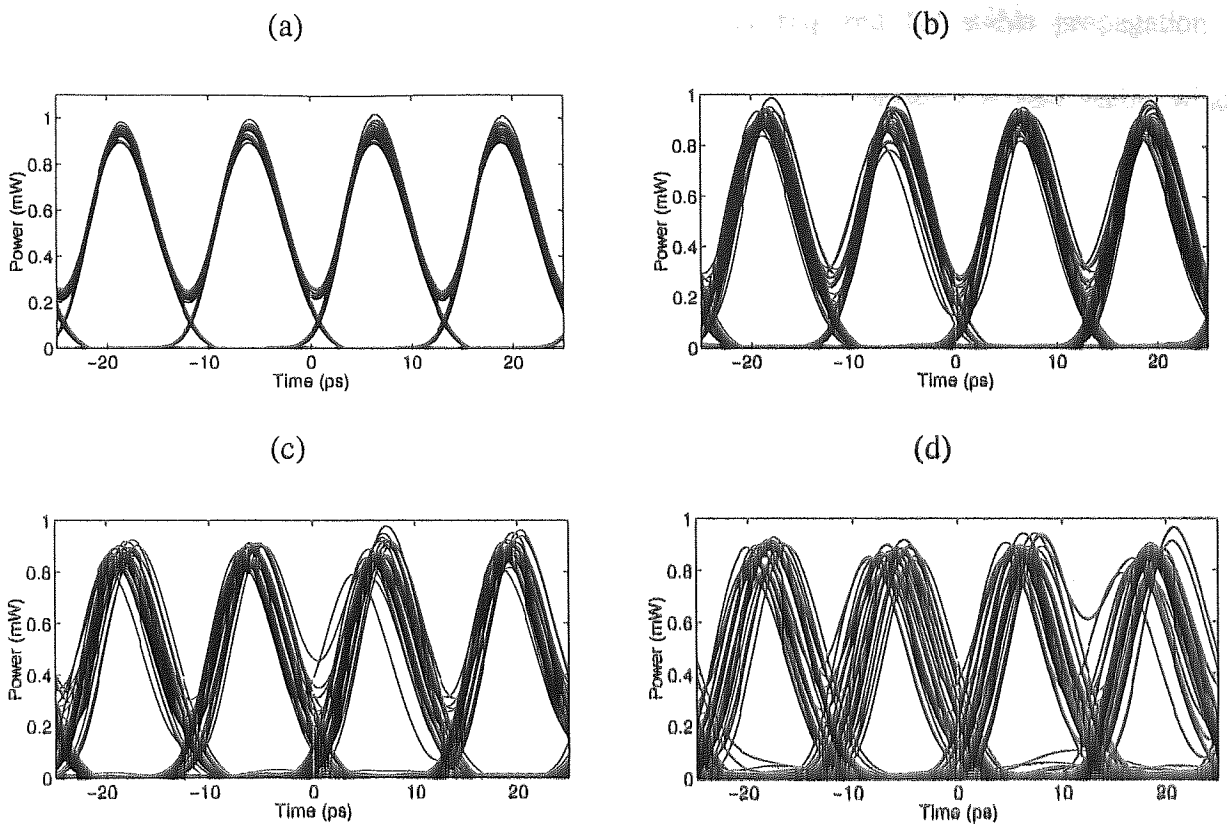

Figure 4.14: Eye diagrams taken at (a) 1,000 km, (b) 3,000 km, (c) 5,000 km and (d) 8,000 km.

An important consideration is the experimental realisation of the theoretical transmission link. Until this point, we have made the assumptions that the pulses possess the exact DM soliton shape. However, the reality is that in the laboratory such complex pulse shapes may prove difficult to generate, whereas Gaussian shaped pulses can be generated relatively easily. Therefore, we should investigate how the substitution of the DM soliton shape for a Gaussian shape influences the performance of the system. Taking the initial chirp found using the averaging method described previously, we perform a sweep of the initial power of the Gaussian pulse against the average dispersion for the optimised system parameters. The simulation results can be observed in Figure 4.15, which also gives an indication of how sensitive the system is on initial conditions. It can be seen in Figure 4.15 that transoceanic transmission is possible using Gaussian shaped pulses. It is also clear that when the initial power is not in the region of that required for a DM soliton for that particular average dispersion, then system performance is poor due to the propagation characteristics. Also, for normal average dispersions performance is again extremely poor, although DM solitons do exist with a normal average dispersion [110,

115, 116, 119], when loss is present the initial power required for stable propagation is extremely high. At high powers, the rapid decline in system performance is also visible which results from increased interactions between neighbouring pulses.

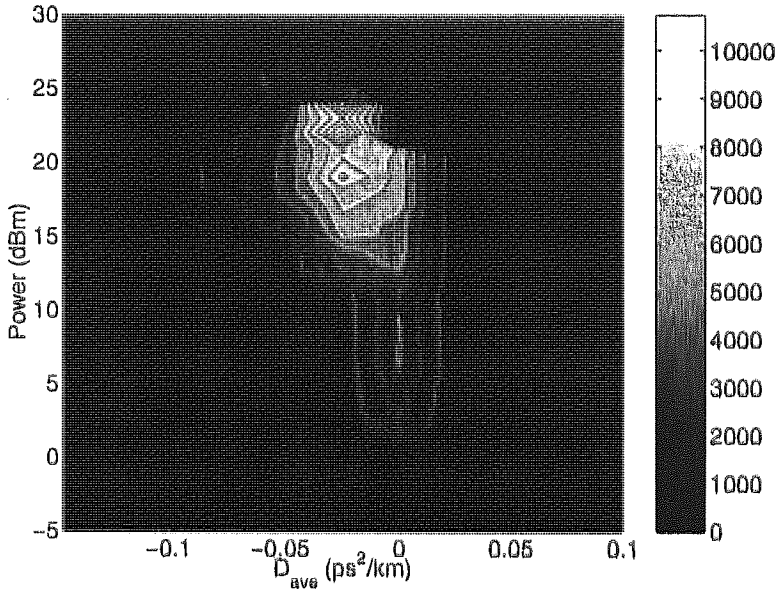

Figure 4.15: Contour plot revealing systems performance as a function of average dispersion and initial power for Guassian shaped pulses. Contour lines indicate the maximum achievable propagation distance in km.

4.5 Medium haul transmission

Apart from transoceanic transmission, two other transmission distances are important for 80 Gbit/s transmission, namely medium haul (~3,000 km) and short haul (~1,000 km). We shall defer discussion of short haul transmission to section 4.6, and focus on medium haul transmission. In both this section and section 4.6, we once again replace the exact DM soliton shape with a Gaussian pulse of the same pulse width, energy and chirp.

We compare the performance of the two systems each with identical dispersion management periods of Z_p = 6.25 km but differing amplification spans of Z_a = 50 km and Z_a = 75 km so we can gauge the impact of SNR on system performance. Figure 4.16 illustrates the transmission performance as a function of minimum pulse width and initial power over a fixed link of 3,000 km for the two different amplification spans. For each of the pulse widths we fix

the average dispersion $\beta^{(2)}_{ave}$ = -0.02 ps^2/km, adjust the local dispersion such that S = 1.65, and fix the ratio between the pulse width and the inverse filter bandwidth. As with the previous simulations we include higher order non-linear effects and introduce a residual dispersion slope of 0.02 ps^3/km. For the case Z_a = 50 km, it can be seen that for a broad range of pulses widths and powers, performance in excess of Q = 6 is achieved with optimum performance being achieved for a pulse width of 2 ps and initial power of 27 dBm. For the case Z_a = 75, we observe a similar dependence to Z_a = 50 km but with a Q factor penalty of ≈ 15, with a slightly longer optimum pulse width of 2.5 ps and a slightly lower initial power of 22 dBm. For both Z_a = 50 km and Z_a = 75 km, we observe the classical DM soliton dependence of increasing power with shortening pulse width. At low powers, SNR and propagation characteristics limit performance whereas at high powers, interactions dominate the decline in transmission performance observed. In addition, for longer pulse widths, interactions become more significant due to the overlap between adjacent pulses whereas for shorter pulse widths higher order non-linear and dispersive effects significantly influence performance.

(a)

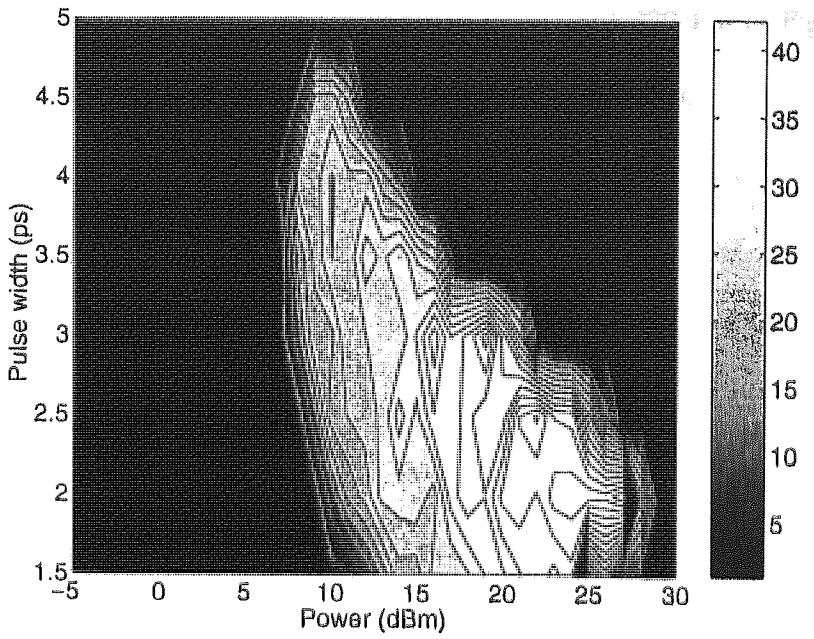

(b)

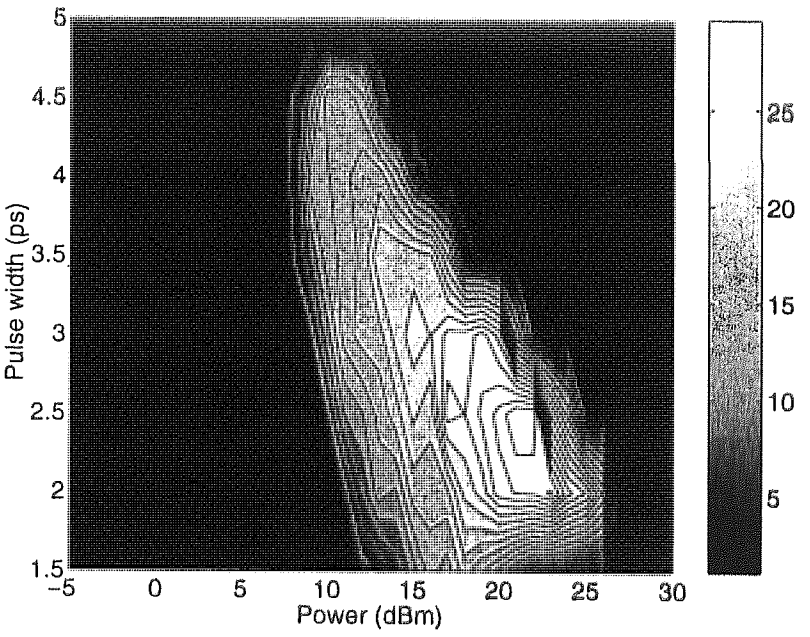

Figure 4.16: Dependence of transmission performance on initial conditions for 80 Gbit/s transmission over 3,000 km using Gaussian shaped pulses. (a) Z_a = 50 km and (b) Z_a = 75 km. Contour lines indicate the Q value estimate after 3,000 km.

4.6 Short haul transmission

Analogous to section 4.5, we provide the same comparison for Z_a = 50 km and Z_a = 75 km using identical simulation parameters for a transmission distance of 1,000 km in Figure 4.17. Again, for both amplification spans, it can be seen that general dependence is similar to those observed in Figure 4.16, and that in both cases a large region for which Q ≥ 6 exists. In the case of Z_a = 50 km, an optimum Q values > 90 is achieved for a pulse width of 2 ps and an initial power of 27 dBm. For the longer amplification span of Z_a = 75 km, the optimum pulse width is increased to 2.5 ps, the optimum power has been reduced to 23 dBm and the Q value has fallen to 60. It is also clear from a comparison of Figure 4.17 and Figure 4.7 that over 1,000 km the range for which error free transmission is supported is larger. These results indicate that short period dispersion managed systems that allow high powered DM solitons to propagate at low average dispersions demonstrate a robustness to the influence of noise, which manifests itself in the form of SNR and timing jitter.

(a)

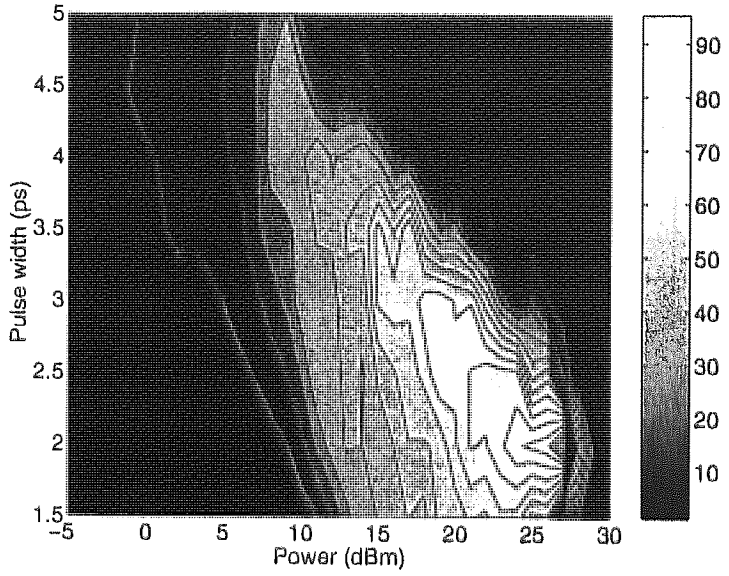

(b)

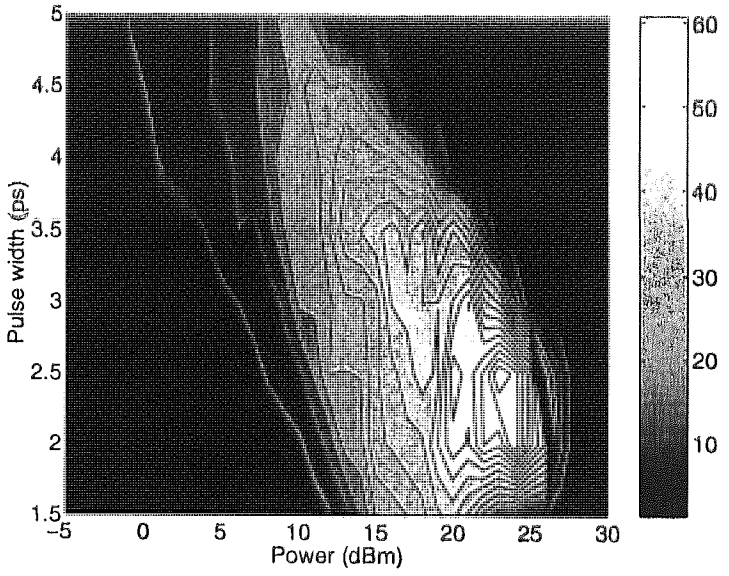

Figure 4.17: Dependence of transmission performance on initial conditions for 80 Gbit/s transmission over 1,000 km using Gaussian shaped pulses. (a) Z_a = 50 km and (b) Z_a = 75 km. Contour lines indicate the Q value estimate after 1,000 km.

4.7 Transmission using standard fibre

	Standard Monomode Fibre (SMF)	Reverse Dispersion Fibre (RDF)
Dispersion at 1550 nm (ps/nm/km)	18	-18
Dispersion Slope at 1550 nm (ps/nm^2/km)	0.06	-0.06
Effective area A_{eff} (μm)	80	30
Fibre loss (dB/km)	0.18	0.24

Table 4.1: Fibre dimensions of Standard Monomode Fibre (SMF) and Reverse Dispersion Fibre (RDF).

As well as using specially manufactured fibre as the cases of Ref. [142], short period dispersion managed transmission can be accomplished using commercially available standard fibre (SMF) and reverse dispersion fibre (RDF) by simply splicing together the fibre sections. The fibre dimensions for SMF and RDF are shown in Table 4.1. We also introduce a splice loss (α_s) into our model and as the effective areas of SMF and RDF are so different we set α_s = 0.2 dB. Setting the amplifier span Z_a = 50 km, the sections of SMF and RDF are cut down to 0.5 km sections producing a dispersion management period Z_p = 1 km. We then launch chirp free Gaussian pulses at the mid-point of the anomalous dispersion fibre sections and set the gain of the amplifiers to equal the fibre loss plus the splice loss ($\alpha.Z_a + n.\alpha_s$). Figure 4.18 illustrates the performance of 80 Gbit/s single channel transmission as a function of pulse width and initial power for transmission over 1,000 km for an average dispersion D_{ave} = 0.02 ps/nm/km. It is evident that for a large region of Figure 4.18 transmission with Q ≥ 6 can be achieved.

In contrast to Figure 4.16 and Figure 4.17, Figure 4.18 maintains a fixed dispersion map, which means that varying the pulse width alters the map strength. From Figure 4.18, the optimum performance is obtained for a pulse width of 2 ps and an initial power of 20 dBm. These optimum conditions correspond to a map strength of $S \sim 6$, which is far stronger than the optimum strength for which interactions are minimised. Such a strong S can be explained in terms that a higher SNR is required due to the additional splice loss and secondly as the length

of the transmission link is only 1,000 km it is still shorter than the collision distance, even for strong S. We observe that in this particular case, for $S = 2$ performance is some what lesser than the optimum conditions. Away from the optimum conditions, good performance is still achieved for longer pulse widths (increasing spectral efficiency) by reducing pulse power. This illustrates the potential of creating short dispersion managed systems from splicing together commercially available fibre sections.

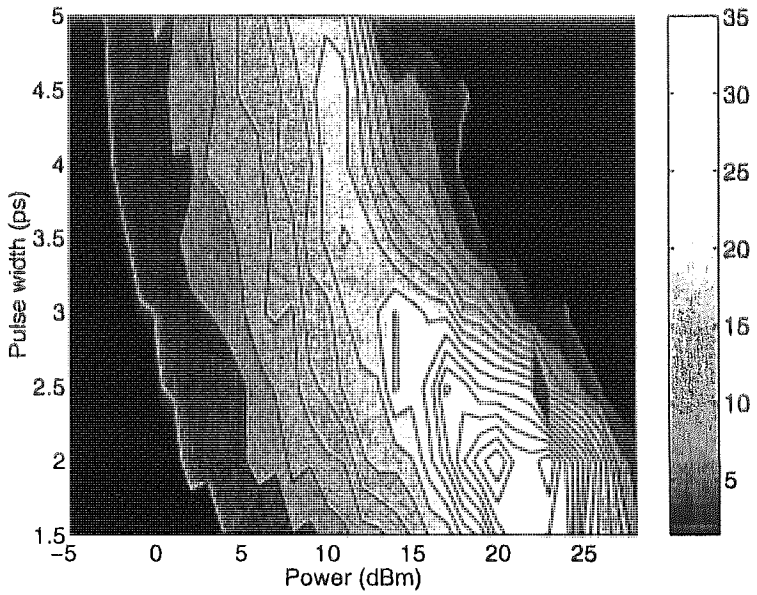

Figure 4.18: Dependence of transmission performance on initial conditions for 80 Gbit/s transmission over 1,000 km using sections of SMF and RDF spliced together. Contour lines indicate the Q value estimate after 1,000 km.

4.8 Conclusion

In conclusion, we have demonstrated, by numerical simulations, the feasibility of 80 Gbit/s single channel transmission over distances in excess of 9,000 km using short period dispersion management. This performance has been achieved by careful optimisation of the system parameters and we have identified the need for careful control of the average dispersion. We have demonstrated the robustness of the system to the dispersion slope, with and without compensation, and shown that by optimisation of the system parameters improved performance

compared to other SPDM simulations at this transmission rate [141] can be achieved. In addition, we investigated transmission over short and medium haul distances, and demonstrated a robustness of these systems to noise. Finally, we investigated a short period dispersion managed system using commercially available SMF and RDF fibre demonstrating that whilst continuous drawn short period dispersion managed fibre, as in Ref. [142], achieves the best performance, enhancements can still be achieved creating the short period dispersion map by splicing together fibre sections.

Chapter 5 160 Gbit/s transmission

5.1 Introduction

In the preceding chapter, we demonstrated the possibility of transoceanic single channel transmission at 80 Gbit/s. The next logical challenge is to further increase the data rate to 160 Gbit/s. Since the last chapter elucidated the effectiveness of short period dispersion management, we continue to use this technique for increasing bit rates. This chapter investigates the feasibility, through optimisation of the system parameters, of single channel transmission at 160 Gbit/s over transoceanic distances. In addition, we investigate transmission over short and medium haul distances.

Although by utilising WDM techniques, transmission capacities of 160 Gbit/s and beyond are common in the literature (see Refs. [154, 216-219] for example), to date there has been little investigation into single channel transmission at data rates as high as 160 Gbit/s. Previous investigations have been concerned with 160 Gbit/s single channel transmission and short period dispersion management [220]. However, a short period dispersion map with an exponentially decaying profile was used and only a transmission distance of 2,000 km was predicted. Experimental transmission at 160 Gbit/s has been demonstrated by Feiste *et al.* [221] over 42 km of standard fibre. However, at slightly lower transmission rates short period dispersion managed transmission has been experimentally demonstrated at 100 Gbit/s [142, 222].

At ultra high data rates, transmission performance is significantly hindered by the problems of system scaling that have been outlined by Marcuse *et al.* [223]. As pulse widths become shorter, propagation becomes increasingly affected by higher order non-linear and dispersive effects. Furthermore, the effect of PMD becomes increasing important. Interactions between DM solitons also become more prevalent at higher data rates resulting from the

increasing map strength, although this effect can be controlled using short period dispersion management.

5.2 Single pulse propagation

Initially we investigate pulse propagation using pulse widths suitable for use in 160 Gbit/s transmission. As the basis of our simulations, we find stable, periodic DM soliton solutions in the SPDM using an averaging method [111], (neglecting higher-order non-linear and dispersive effects). Again, we make the distinction that when we refer to the DM soliton we mean the exactly periodic DM soliton found by the averaging method. Therefore, the energy can be uniquely defined by the minimum pulse width, average dispersion, the depth of the dispersion map, and amplifier position within the dispersion map [109, 110, 224].

For the simulations we fix the amplifier period Z_a = 50 km and the following fibre properties: loss = 0.2 dB/km, effective area = 50 μm^2 and non-linear index, 2.6 x 10^{-20} cm^2/W. We elect to operate with a dispersion map strength $S \approx 1.65$ (defined previously in section 3.4), to minimise interactions [127]. Therefore within the bounds of practical limitations we are free to vary the minimum pulse width (τ_{min}) and the number of dispersion sections n, which determines the dispersion management period (Z_p) and local dispersion ($\beta^{(2)}_{a,n}$).

(a)

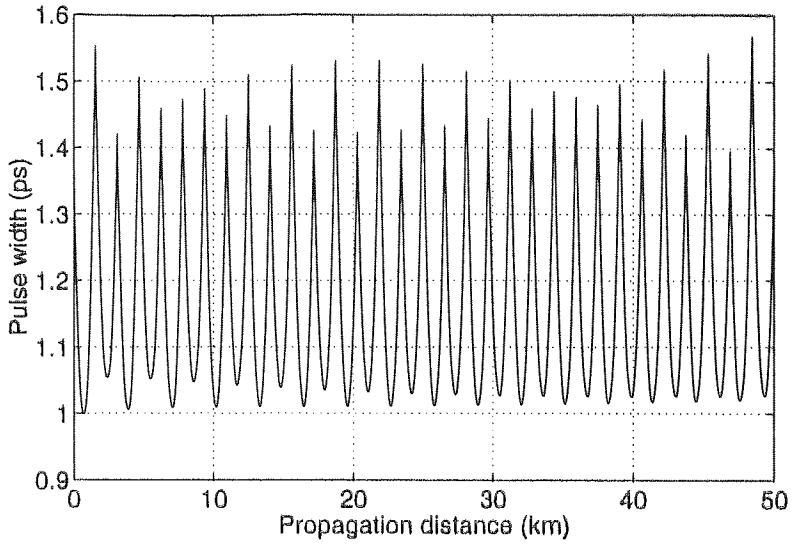

(b)

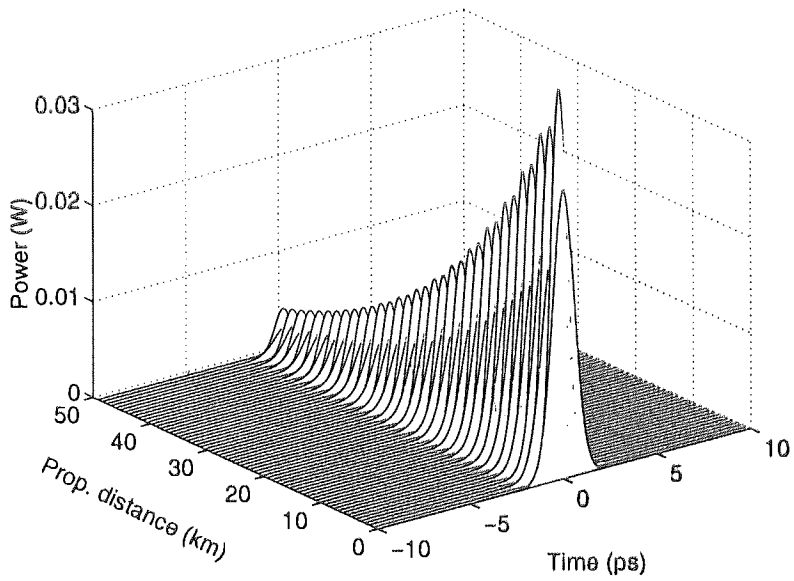

Figure 5.1: Dynamical evolution of the DM soliton over Z_a. (a. left) Pulse width evolution and (b. right) Pulse evolution over Z_a. Simulation parameters: $\beta^{(2)}{}_a = -1.25$ ps^2/km, $\beta^{(2)}{}_n = 1.24$ ps^2/km, $\beta^{(2)}{}_{ave} = -0.05$ ps^2/km, $\tau_{min} = 1$ ps and $Z_a = 50$ km.

Figure 5.1 shows how the DM soliton pulse width evolves over a single amplifier period Z_a with $n = 32$, for which $\beta^{(2)}{}_a = -\beta^{(2)}{}_n \approx -0.5$ ps^2/km, $\beta^{(2)}{}_{ave} = -0.005$ ps^2/km and $\tau_{min} = 1$ ps. It can be seen that the pulse width evolution displays a regular form, and has a breathing ratio of approximately 1.55:1 between the minimum and maximum pulse widths.

Along with the various properties that DM solitons in short period dispersion maps possess relating to the dispersion management period Z_p, as detailed in section 3.5.2, an

interesting feature is the saturation of the DM soliton energy that occurs as Z_p decreases for a fixed map strength. This is a similar feature to that observed by Nijhof *et al.* [113] in conventional dispersion managed systems. In the short period dispersion management regime, this phenomenon provides two main benefits that occur for a fixed map strength and large n: (i) local dispersion ($\beta^{(2)}_{a,n}$) and dispersion management period (Z_p) can be traded freely without significantly affecting performance, in the case of single channel transmission, and (ii) as a direct result of (i) more rapid computation can be achieved by increasing Z_p, thus reducing the computation step in ΔZ, and generalising the results for shorter Z_p.

5.3 Transmission simulations

For the transmission simulations at 160 Gbit/s, we use the Generalised Non-Linear Schrödinger equation (GNLS) [72], including higher order non-linear and dispersive effects. Following Refs. [142, 209], dispersion slope compensation is provided by an alternate sign of dispersion slope in each fibre section with magnitudes: $\beta^{(3)}_a = -\beta^{(3)}_n = -0.07$ ps^3/km. We introduce an amplifier noise figure of 4.5 dB and place a Gaussian filter directly after each amplifier, introducing additional amplifier gain as a result of the inclusion of the filter. The receiver is modelled as a non-optimised Lorentzian electrical filter of bandwidth of 0.14 THz (87.5 percent of the bit rate). In the simulations, we place the amplifier at the beginning of the anomalous dispersion fibre sections as this location has previously been shown to be optimal for transmission performance [225]. The performance of the transmission system is evaluated using Q-value estimates based on a $2^7 - 1$ bit pseudo random binary sequence.

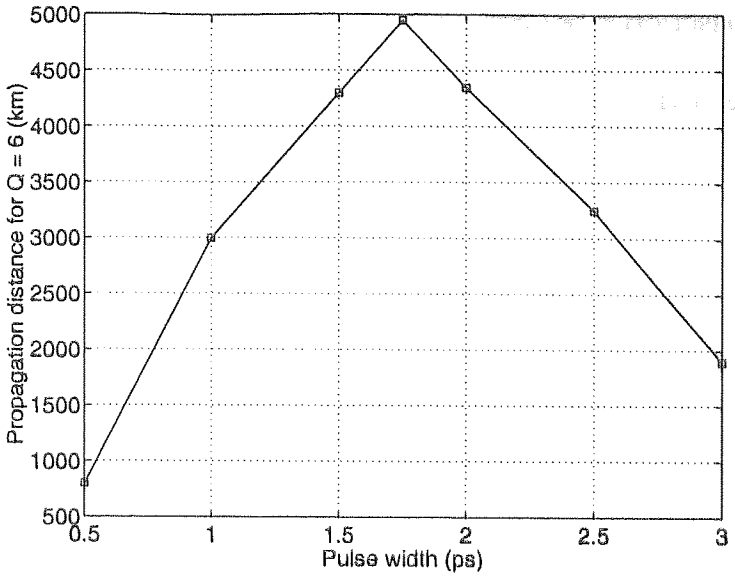

Figure 5.2: System performance as a function of minimum pulse width. To reduce the influence of the filter we fix the ratio between τmin {0.5, 1, 1.5, 1.75, 2, 2.5, 3} (ps) and Ωf {9 4.5 3 2.63 1.26 1.81 1.5} (THz). Simulation parameters: S = 1.65, β(2)ave = -0.05 ps2/km and Za = 50 km.

Optimising the performance of dispersion managed systems presents an arduous task resulting from the shear number of parameters that exist. To be completely assured of optimal performance, one must simulate the system using all reasonable values for each of the parameters, which is currently too computationally demanding. With this in-mind, we adopt the following methodology to optimise the performance of the system. Firstly locate the optimum pulse width, then in turn taking this optimum pulse we then seek to optimise performance in terms of the average dispersion and filter bandwidth. We then repeat the procedure for values of τ_{min} near to the optimum. Therefore, when we refer to optimal performance we mean optimal relative to this procedure.

Initially we determine the system dependence on pulse width. As a result of the amplifier spontaneous emission noise we include wide filters, however at this point we do not want the filters to influence system performance so for each pulse width we fix the ratio of minimum pulse width to inverse filter bandwidth (τ_{min}(ps): $1/\Omega_f$(THz)) to be 1:4 which is sufficient to achieve this. Figure 5.2 illustrates how system performance depends on the minimum pulse width for S = 1.65, where it clearly can be seen that an optimum pulse width exists for τ_{min} = 1.75 ps. For longer pulse widths, interactions dominate and we observe this increasing with τ_{min}

.For shorter pulse widths higher order dispersive effects limit the performance. However even at the optimal pulse width of τ_{min} = 1.75 ps transmission performance is limited to below 5,000 km.

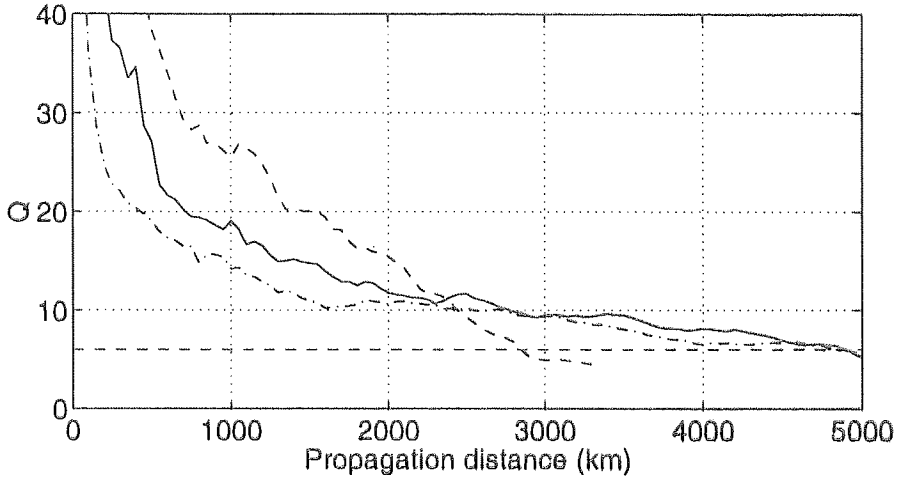

Figure 5.3: System performance as a function of average dispersion for τ_{min} = 1.75 ps. (*dashed line*) $\beta^{(2)}_{ave}$ = -0.01 ps^2/km, (*continuous line*) $\beta^{(2)}_{ave}$ = -0.005 ps^2/km and (*dot and dashed line*) $\beta^{(2)}_{ave}$ = -0.0025 ps^2/km.

Utilising the information from Figure 5.2 that the optimal pulse width is in the region of 1.75 ps we investigate the dependence of system performance on the average dispersion. Figure 5.3 demonstrates the system dependence on average dispersion for $\beta^{(2)}_{ave}$ = -0.0025, -0.005, -0.01 ps^2/km. It is immediately apparent that the optimal average dispersion varies for different propagation lengths. For example, over relatively short transmission distances ≈ 1,000 km higher average dispersions show improved performance, resulting from the greater signal-to-noise ratio (SNR). However, over longer propagation distances the greater energy of the DM solitons is causing an increase in interactions, thus limiting the propagation distance. With low average dispersions, performance is limited by SNR and although a greater propagation distance is achieved, performance over short-medium distances is inferior. The optimum average dispersion is achieved by balancing interactions and SNR.

Exploiting the results of Figure 5.2 and Figure 5.3, we then seek to optimise the bandwidth of the filters located directly after the amplifiers. The system requires the use of

filters to reduce the significant timing jitter that accumulates over the transmission distance. As stated previously we investigate pulse widths close to the optimum and find that the best performance is achieved for τ_{min} = 1.5 ps. Figure 5.4 demonstrates how dependent system performance is upon filter bandwidth (Ω_f). When the filter bandwidth is excessively wide (Ω_f = 3 THz) noise significantly degrades system performance, the resulting collisions between adjacent pulses are clearly evident. Alternatively, when the filter bandwidth is too narrow then transmission performance is limited by the growth of the continuous-wave background instability. Balancing these limiting factors, with a filter bandwidth Ω_f = 1.273 THz FWHM, one can achieve performance in excess of 9,000 km, as seen in Figure 5.4.

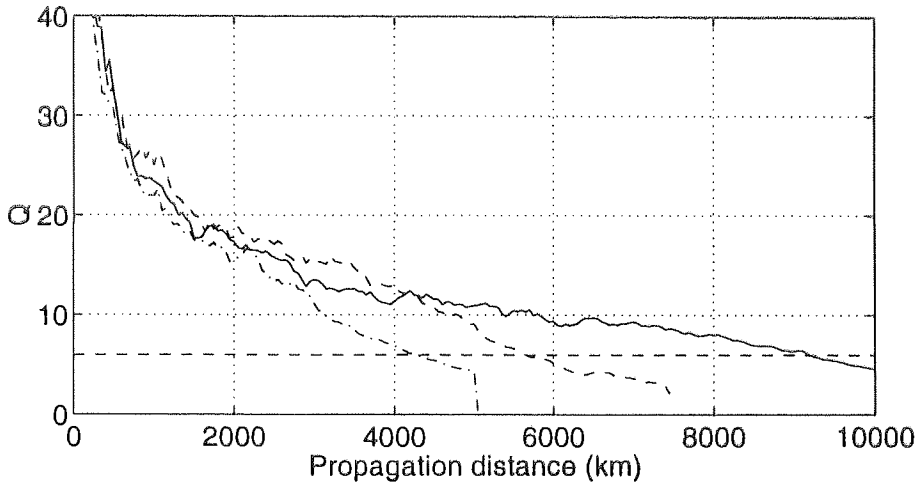

Figure 5.4: System performance as a function of filter bandwidth. (dashed line) Ω_f = 0.9 THz, excess gain coefficient Δg = 0.18 dB, (continuous line) Ω_f = 1.273 THz, excess gain coefficient Δg = 0.1 dB and (dot and dashed line) Ω_f = 3 THz, excess gain coefficient Δg = 0.02 dB.

Figure 5.5 shows the eye diagrams at 1,000 km, 3000 km, 5,000 km and 8,000 km that illustrate the system performance for the optimised system. It can be seen that for distances up to 3,000 km the eye diagrams are very clean, but at 5,000 km we begin to observe some jitter on the pulses, as well as the first signs of the continuous wave background instability generated by strong filtering. At 8,000 km, the degradation of performance is evident as the eye diagram shows severe jitter and large growth in the continuous wave background instability.

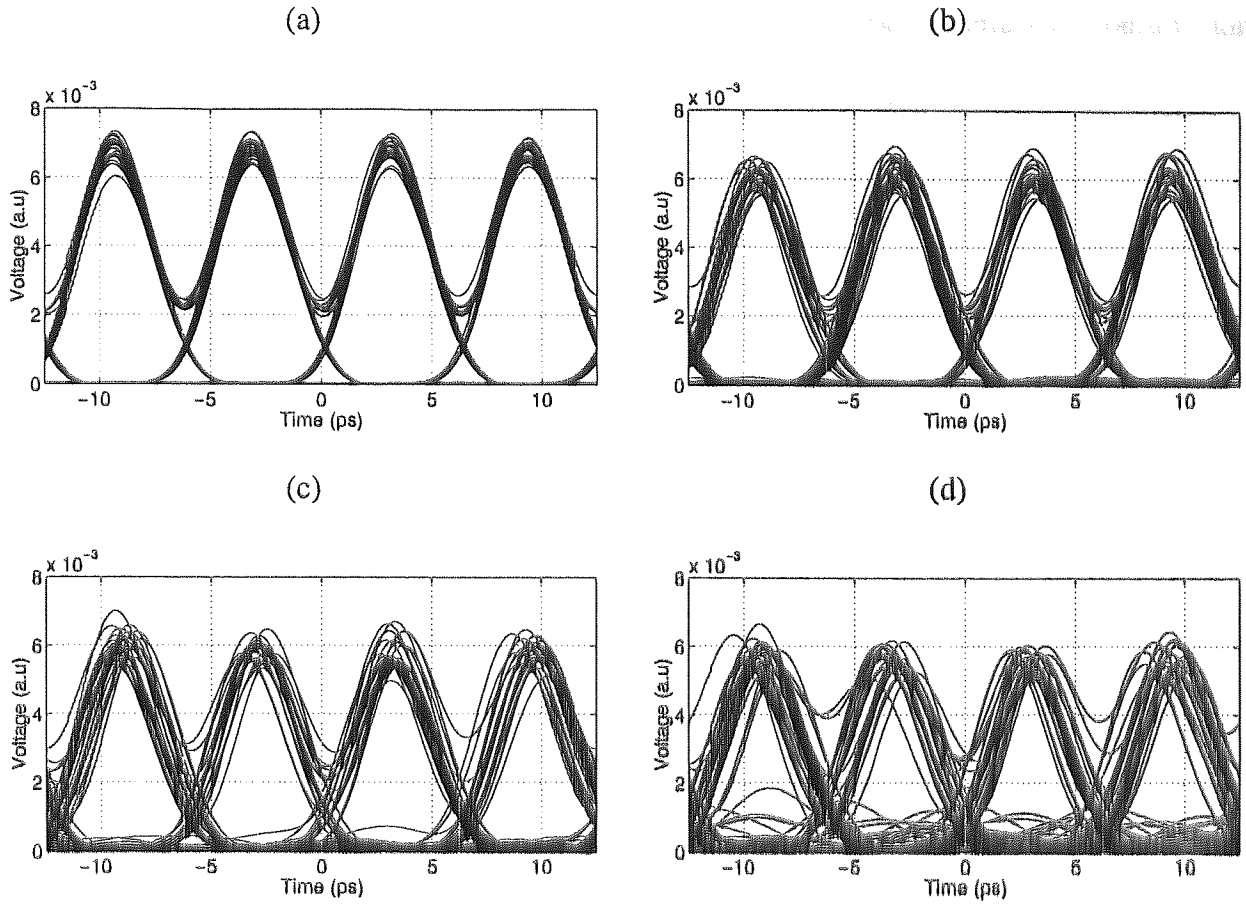

Figure 5.5: Eye diagrams taken at (a) 1,000 km, (b) 3,000 km, (c) 5,000 km and (d) 8,000 km. Simulation parameters: S = 1.65, $\beta^{(2)}_{ave}$ = -0.005 ps^2/km, Ω_f = 1.273 THz, excess gain coefficient Δg = 0.1 dB.

5.4 Higher order non-linear and dispersive effects

With the optimised transmission, we then focus on the tolerance of the system to higher order non-linear and dispersive effects. As the bit rate increases, dispersion slope compensation becomes evermore critical as the dispersion slope length $L_D' = \tau^3 / |\beta^{(3)}|$ becomes increasingly short. The result of which is that for large dispersion slopes non-linear interactions greatly increase [226]. At this point, we have only considered the case $\beta^{(3)}_a = -\beta^{(3)}_n = -0.07$ ps^3/km. Figure 5.6a demonstrates the sensitivity of performance on the residual dispersion slope, where the residual dispersion slope over Z_p is defined as $\beta^{(3)}_{res} = (\beta^{(3)}_a l_a + \beta^{(3)}_n l_n) / (l_a + l_n)$. Likewise the accumulated residual dispersion slope over Z_a is simply $(^n/_2)\beta^{(3)}_{res}$. It is clearly evident that as

the residual dispersion increases we observe a rapid decline in performance resulting from the increased interactions. Although for small residual dispersion slopes, the effect on transmission performance is negligible, for trans-oceanic transmission it must be confined to the region ± 0.01 ps^3/km. Although this condition imposes serious constraints on the manufacture of fibre, they are in excess of those manufactured in Ref. [142].

(a)

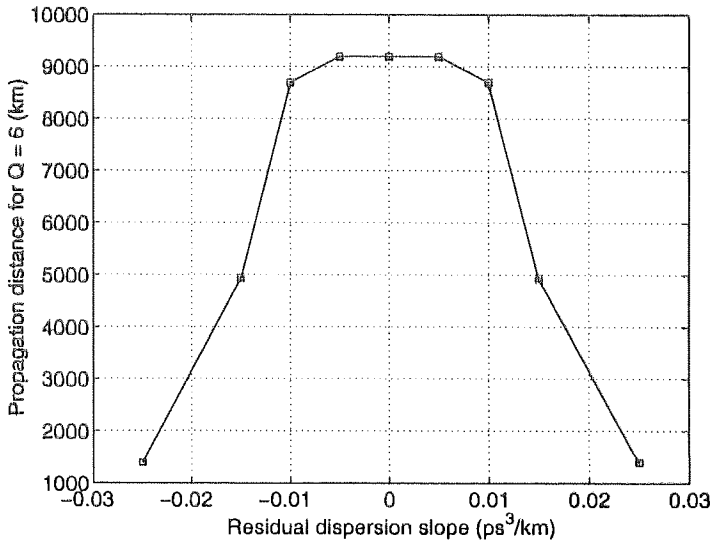

(b)

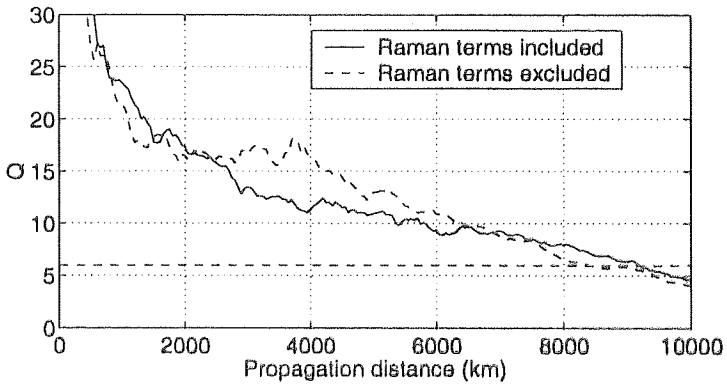

Figure 5.6: (a) Tolerance of system performance to residual dispersion slope. (b) Influence of stimulated Raman Scattering (SRS) on system performance. Simulation parameters: $S = 1.65$, $\beta^{(2)}_{ave} = -0.005$ ps2/km, $\Omega_f = 1.273$ THz, excess gain coefficient Δg.

So far, the simulations have included the effects of Stimulated Raman Scattering (SRS) but to establish the effect of SRS on transmission performance, we turn off the Raman coefficients in the GNLS. From Figure 5.6b, it can be seen that the performances of the two

cases in question are broadly similar which shows that the SRS is only playing a relatively minor role in limiting system performance.

An important physical effect that we have not considered so far is that of Polarisation Mode Dispersion (PMD). We simulate the effects of PMD by numerical integration of the 2-dimensional birefringent GNLS. Following [214, 215], the effects of random mode coupling are simulated by breaking the fibre into equal length sections of 200 m, where the fields are rotated by θ (with a uniform distribution in $[0 : \pi]$) and a random phase difference ϕ imposed between the two orthogonal components (with a uniform distribution in $[0 : \pi]$). Including SRS and $\beta^{(3)}_{res}$ = 0.005 ps^3/km, Figure 5.7 illustrates the performance for different values of PMD. For low values of PMD (0.02 ps/$\sqrt{}$km), the maximum transmission distance is reduced by around 1,000 km to 8,000 km. However, as the PMD is increased, a dramatic reduction in performance is observed where for PMD = 0.05 ps/$\sqrt{}$km performance is limited to 5,000 km and for PMD = 0.07 ps/$\sqrt{}$km only a transmission distance of 2,500 km can be achieved. Therefore PMD imposes severe limitations on system performance which must controlled to be less than 0.02 ps/$\sqrt{}$km to support trans-oceanic transmission.

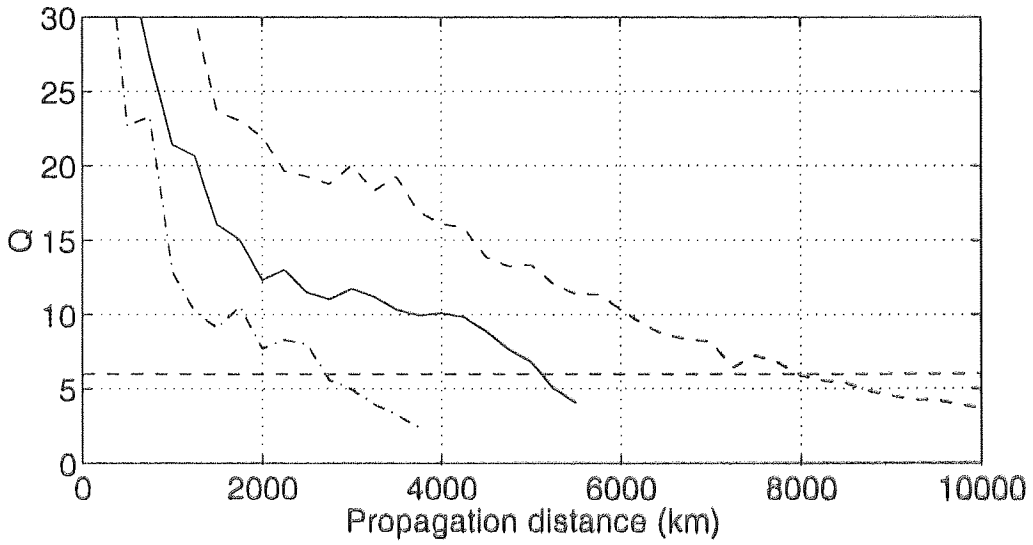

Figure 5.7: System tolerance to Polarisation Mode Dispersion (PMD). (*dashed line*) PMD = 0.02 ps/$\sqrt{}$km, (*continuous line*) PMD = 0.05 ps/$\sqrt{}$km and (*dot and dashed line*) PMD = 0.07 ps/$\sqrt{}$km. Simulation parameters (including SRS): S = 1.65, τ_{min} = 1.5 ps, $\beta^{(2)}_{ave}$ = -0.005 ps^2/km, $\beta^{(3)}_{res}$ = 0.005 ps^3/km, Ω_f = 1.273 THz, A_g = 0.1 dB.

5.5 Noise induced interactions

Until this point in the discussion, we have overlooked the main limiting factor of the system, in the absence of PMD, which is noise induced interactions. Recall our previous observation, which stated that as the filter bandwidth increased, interactions between neighbouring DM solitons also increased. This phenomenon was first considered in the case of classical soliton propagation by Georges [227]. In this particular system, we observe the recurrence of this phenomenon as a key limiting factor for two reasons: (1) the large bandwidth of the propagating DM soliton and (2) the close proximity of neighbouring DM solitons.

We formulate this observation explicitly in Figure 5.8, which shows a pair of DM solitons with the initial conditions of the optimal system. For clarity, we have neglected higher order and non-linear effects. In the case of noiseless propagation, we observe no interaction over 20,000 km, however when ASE noise is introduced by the amplifiers (noise figure = 4.5 dB and Ω_f = 3 THz) the DM solitons collide at approximately 9,000 km. The source of this interaction results from the accumulation of jitter inside of the filter bandwidth. Therefore, to optimise performance the filter bandwidth must be selected to reduce as much of the jitter as possible without exciting instabilities in the continuous wave background. In addition, we found that the pattern propagation length was shorter than the collision length for a pair of DM solitons and that as anticipated, the inclusion of a residual dispersion slope further increases the interactions. Increasingly, for higher bit rates this phenomenon will become more dominant. A possible control technique that can be used to reduce interactions between neighbouring DM solitons is phase-alternation [104]. Figure 5.8c demonstrates this technique for the case of a 5 THz filter and shows that even in the presence of noise the pulses still maintain their phase dependence.

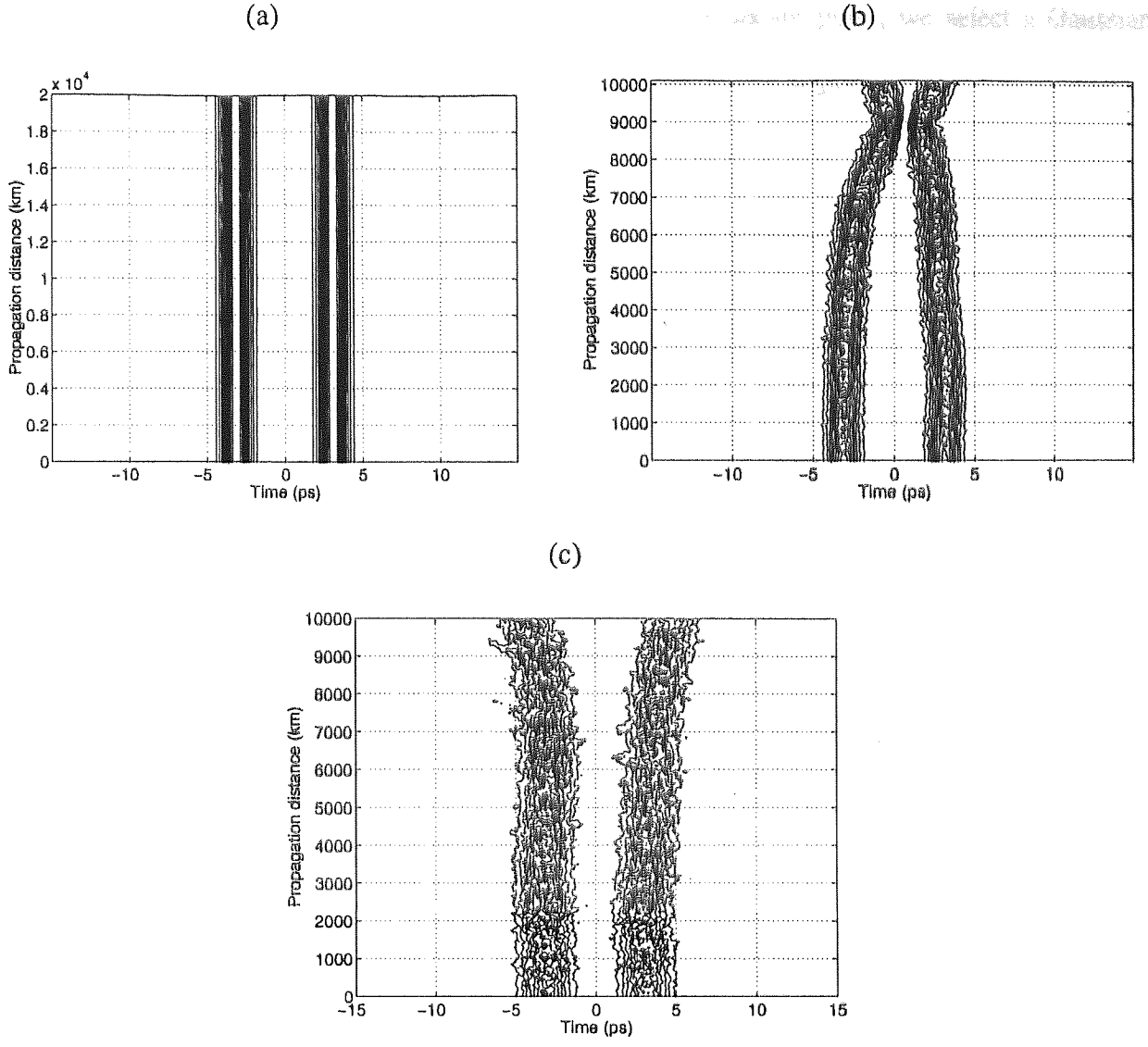

Figure 5.8: Reduction in the collision length between a pair of DM solitons resulting from noise. (*a left*) No amplifier noise, no third order dispersion, no filter and (*b right*) amplifier noise figure = 4.5 dB, no third order dispersion and broad filter. (c bottom) With phase alternation. Simulation parameters as Figure 5.5.

5.6 Robustness of transoceanic transmission

So far in this chapter, we have only considered propagation using the exactly periodic DM soliton. However, under experimental conditions the DM soliton shape cannot be replicated easily. Therefore based on our knowledge of the optimised conditions for DM soliton propagation, we investigate transmission where the DM soliton has been replaced by a Gaussian shaped pulse with the initial parameters. Although at low map strengths the time-bandwidth

product of the DM soliton is closer to that of a hyperbolic secant pulse, we select a Gaussian pulse shape as this is more commonly used in the laboratory environment.

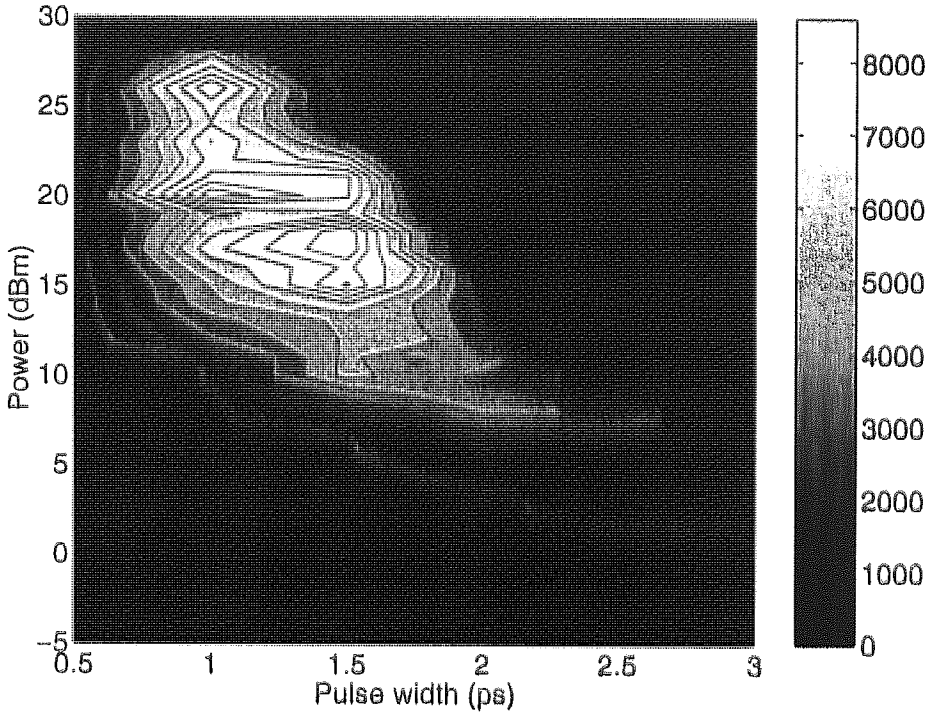

Figure 5.9: Contour plot detailing the dependence of system performance as a function of pulse width and initial power. For each of the pulse widths S is fixed to 1.65 by adjusting the local dispersion. Simulation parameters (SRS included): $\beta^{(2)}_{ave}$ = -0.005 ps^2/km and $\beta^{(3)}_{res}$ = 0.005 ps^3/km. Contour lines indicate the maximum achievable propagation distance.

We use this section to confirm our observations of the previous sections and validate our approach of investigating 160 Gbit/s long haul transmission using only the exactly period DM soliton. Firstly, we investigate the dependence of system performance on the initial power and pulse width of the DM soliton. With both Z_a (= 50 km) and Z_p (= 1.5625 km) fixed, we follow our previous approach and adjust the local dispersion to fix S = 1.65 for each pulse width. We also introduce phase alternation between consecutive pulses in order to reduce interactions. In Figure 5.9 we include SRS, a residual dispersion slope $\beta^{(3)}_{res}$ = 0.005 ps^3/km and set the average dispersion $\beta^{(2)}_{ave}$ = -0.005 ps^2/km (which was the optimised condition from Figure 5.3). As in Figure 5.2, we fix the ratio between minimum pulse width and inverse of the filter bandwidth so that at τ_{min} = 1.5 ps we have the optimised filter bandwidth of 1.273 THz. Figure 5.9 illustrates the typical behaviour we expect to observe in the pulse width – initial power plane for DM

solitons. It is apparent that the optimum transmission performance is achieved for τ_{min} = 1.5 ps and that as the power deviates significantly from that of the exactly periodic DM soliton, performance declines rapidly. Also visible in Figure 5.9 is the rapid growth in interactions at high powers and the increasing penalties due to higher order non-linear and dispersive effects that occur for short pulse widths. Contrasting Figure 5.4 and Figure 5.9, there appears to be little penalty in terms of transmission distance for trading the exact DM soliton shape for a Gaussian pulse shape.

Examining closer the behaviour at the optimised pulse width τ_{min} = 1.5 ps, Figure 5.10 investigates the dependence on average dispersion. It can be seen that the optimal conditions are extremely dependant on both the initial power and average dispersion. The limiting factors have been included in Figure 5.10. In the regions labelled 'propagation stability', transmission performance is extremely poor due to the fact that DM soliton propagation cannot be sustained for any considerable distance, i.e. there is a mismatch between the initial power of the pulse and the average dispersion. This behaviour is demonstrated in Figure 5.11, which illustrates the pulse evolution for three specific locations in Figure 5.10. Additionally, at low powers, performance is limited by SNR and at high powers intra channel interactions dominate.

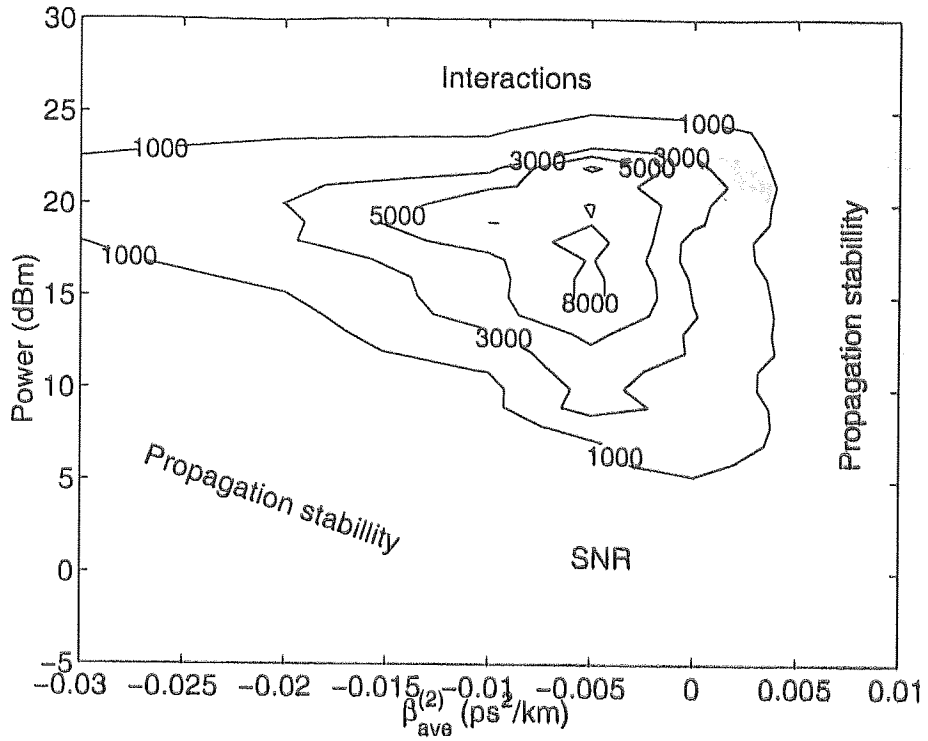

Figure 5.10: Contour plot showing system performance as a function of average dispersion and initial power. Simulation parameters (SRS included): $S = 1.65$, $\tau_{min} = 1.5$ ps, $\beta^{(3)}_{res} = 0.005$ ps^3/km, $\Omega_f = 1.273$ THz, $\Delta g = 0.1$ dB. Contour lines indicate the maximum achievable propagation distance.

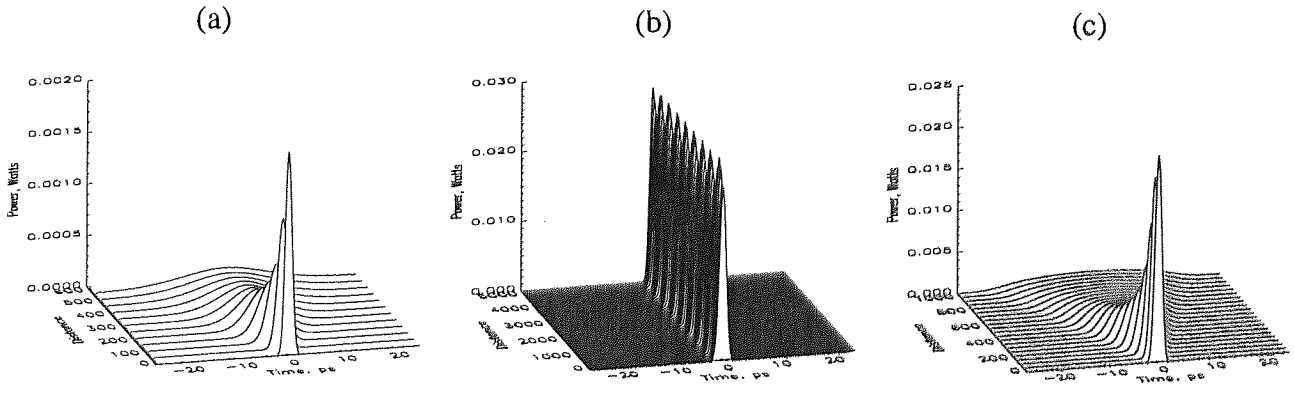

Figure 5.11: Single pulse propagation (a) initial power = 5 dBm, $\beta^{(2)}_{ave} = -0.02$ ps^2/km, (b) initial power = 16 dBm, $\beta^{(2)}_{ave} = -0.005$ ps^2/km (c) initial power = 16 dBm, $\beta^{(2)}_{ave} = 0.005$ ps^2/km.

5.7 Medium haul transmission

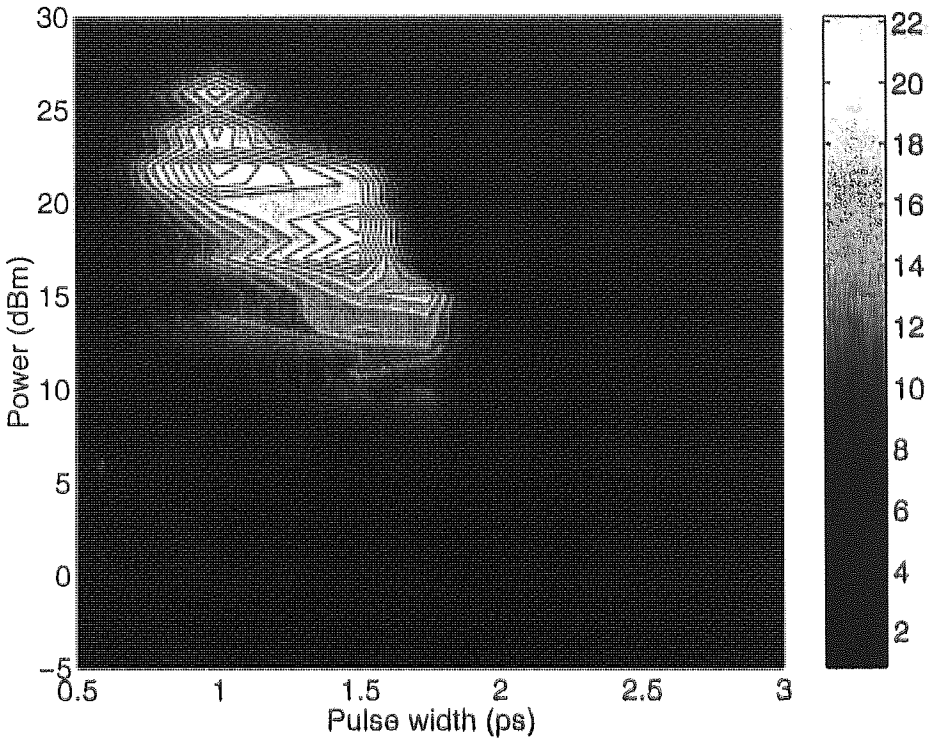

Figure 5.12: Transmission performance over 3,000 km as a function initial power and pulse width. Contour lines indicate the Q value estimates at 3,000 km.

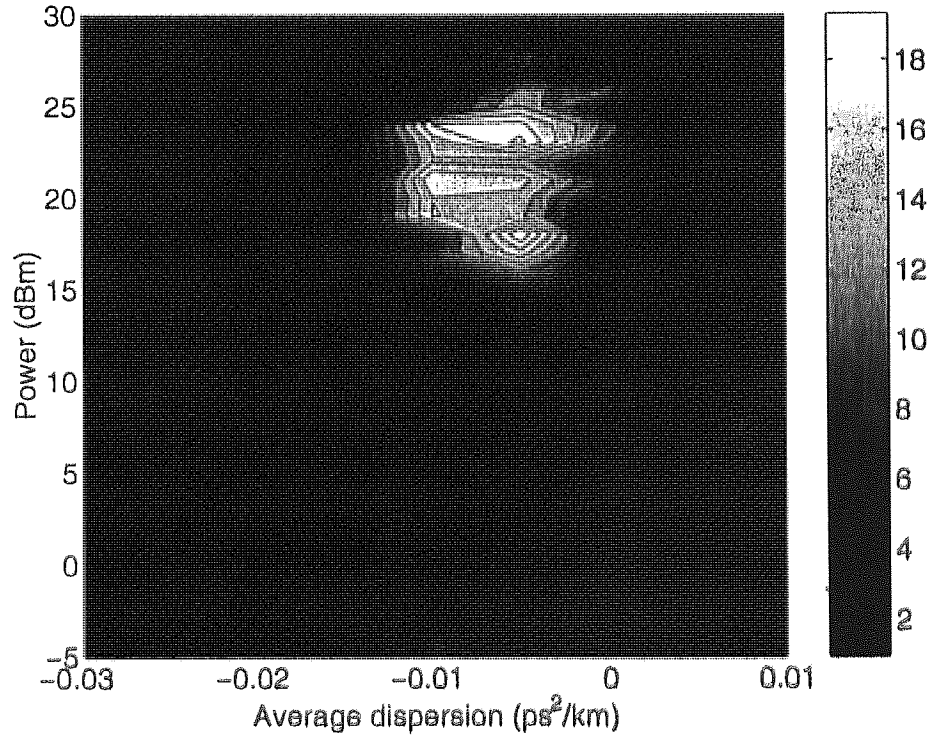

Figure 5.13: Transmission performance over 3,000 km as a function of initial power and average dispersion for τ_{min} = 1 ps. Contour lines indicate the Q value estimates at 3,000 km.

Transmission over transoceanic distances imposes stringent conditions on propagation, and it allows us to understand the limitations of performance, although often transmission distances over a smaller distance is all that is required. Now we investigate propagation over a fixed transmission distance of 3,000 km utilising our knowledge of transoceanic transmission. Figure 5.12 illustrates system performance as a function of initial power and pulse width for a fixed average dispersion of –0.005 ps^2/km. It is evident that optimum performance is achieved for a 1 ps pulse which is shorter than the optimum pulse width of 1.5 ps for transoceanic transmission. For longer pulse widths, interactions due to the pulse overlap limit performance and for very short pulse widths, the higher order non-linear and dispersive effects force a rapid decline in system performance. It is evident from Figure 5.12 that a large region exists for which $Q \geq 6$ showing that the system maintains a certain degree of robustness. When we evaluate system performance in terms of the initial power and average dispersion for the optimum pulse width of 1 ps, as in Figure 5.13, a different pattern begins to emerge. Here we observe that system performance depends critically on average dispersion and that slight deviations from the optimum results in a rapid decline in performance. This sensitivity to average dispersion is a direct consequence of the short pulse being used, therefore longer pulse widths would create larger transmission regions. However at the optimum average dispersion a reasonable range of initial powers can be tolerated to achieve transmission for $Q \geq 6$.

5.8 Short haul transmission

Another target distance that is important to optical communications is 1,000 km. In a similar manner to section 5.7 we illustrate performance as a function of initial power and pulse width over 1,000 km for $\beta^{(2)}_{ave}$ = -0.005 ps^2/km. Contrasting Figure 5.14 and Figure 5.12 we see that

there is a broadly similar dependence in the general performance characteristics, but with Figure 5.14 having twice the performance observed in Figure 5.12. Again we find the optimum pulse width is 1 ps with an initial power of 21 dBm, but now as a result of the shorter propagation distance the transmission region for which $Q \geq 6$ has increased. Utilising the optimum pulse width of 1 ps we then proceed to map out performance in terms of initial power and average dispersion, which can be seen in Figure 5.15. Here we observe a much broader transmission region compared to Figure 5.13, and that the optimal average dispersion has increased to –0.01 ps^2/km. This indicates that over short transmission distances SNR can be traded for increased interactions leading to improved performance.

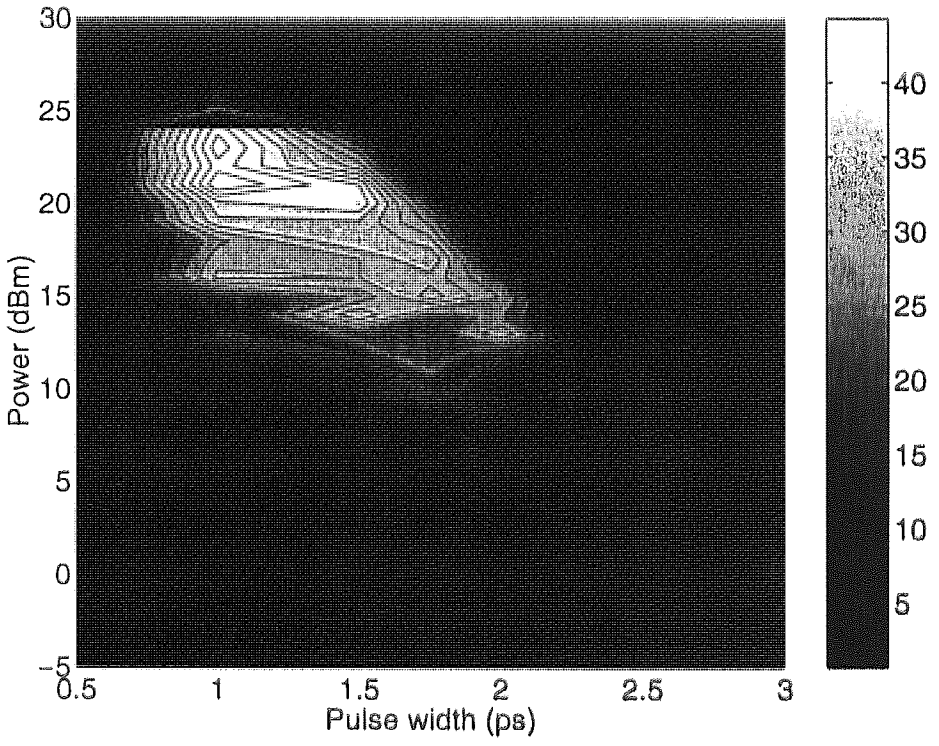

Figure 5.14: Transmission performance over 1,000 km as a function of initial power and initial pulse width. Contour lines indicate the Q value estimates at 1,000 km.

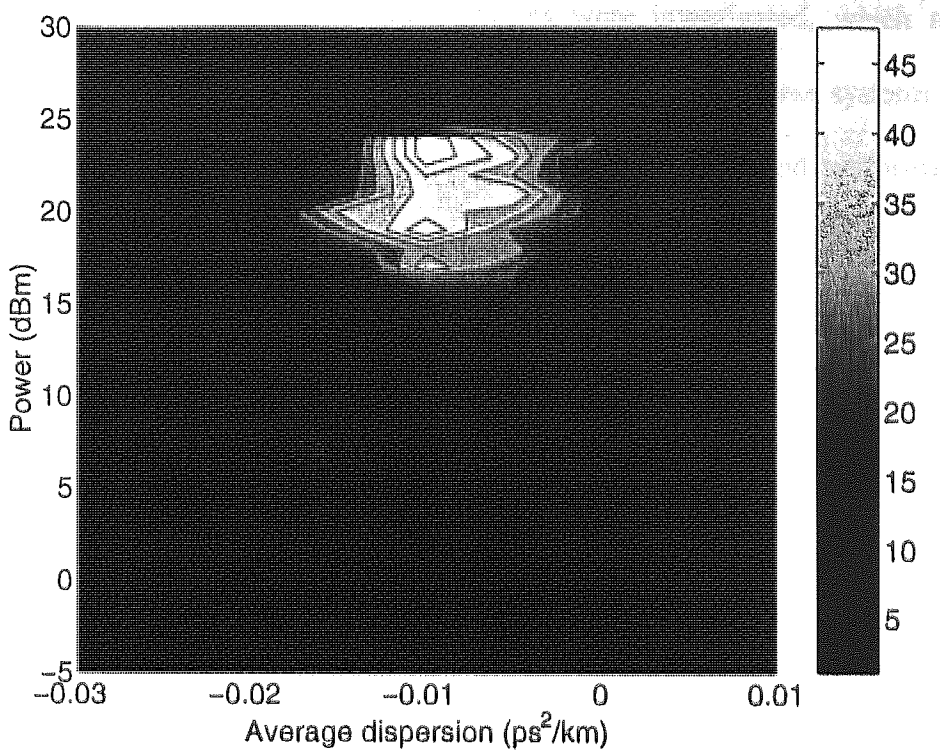

Figure 5.15: Transmission performance over 1,000 km as a function of initial power and average dispersion. Contour lines indicate the Q value estimates at 3,000 km.

5.9 Conclusions

In conclusion, we have demonstrated numerical simulations of 160 Gbit/s single channel transmission over trans-oceanic distances. This performance was achieved by using short period dispersion management, which supports short pulse propagation and reduces interactions between neighbouring DM solitons. We demonstrated that by optimising the system parameters of pulse width, average dispersion and filter bandwidth, that the transmission distance can be significantly increased. We then substituted the exact form of the DM soliton with a Gaussian pulse shape and verified that only a small penalty was incurred. We investigated the tolerance of the optimised system to higher order non-linear and dispersive effects and found that transmission performance was sensitive to both the residual dispersion slope ($\beta^{(3)}_{res}$) and polarisation mode dispersion (PMD). However, trans-oceanic transmission is still possible if these two factors can be confined to some tolerable limits that have been defined. In addition,

transmission over medium and short haul distances were investigated, which revealed that system performance was quite robust to initial conditions. However, these systems did exhibit a sensitivity to average dispersion that must be closely controlled if good performance is to be achieved.

Chapter 6 320 Gbit/s transmission

6.1 Introduction

In the preceding chapters, we have focused on single channel transmission at 80 Gbit/s and 160 Gbit/s. In this chapter, we now increase the data rate again to investigate single channel transmission at 320 Gbit/s. Although transmission capacity in excess of 320 Gbit/s is becoming more commonplace amongst the published literature [202, 218, 219, 228-230], however, most of these approaches involve massive WDM strategies. To date, relatively little published material has focussed on ultra high speed single channel transmission [143, 231].

In this chapter, we continue our approach of using short period dispersion management and investigate transmission using numerical simulations. We determine the distances over which 320 Gbit/s single channel transmission is feasible and then focus specifically on short haul transmission.

6.2 Single pulse propagation

As in the previous two chapters, we initially investigate single pulse propagation by finding stable, period DM solitons using an averaging method [111]. Again we fix the amplifier span Z_a = 50 km and the following fibre properties: fibre loss α = 0.2 dB/km, effective area A_{eff} = 50 μm^2 and non-linear index $n_2 = 2.6 \times 10^{-20}$ m^2/W. To minimise interactions between neighbouring DM solitons we operate at a map strength of 1.6.

Following the logic applied in the previous two chapters, we focus initially on a 64 section short period dispersion map, which equates to Z_p = 1.5625 km. Figure 6.1 provides a schematic representation of the dispersion map used for 320 Gbit/s transmission with the pulse

width evolution for the exactly periodic DM soliton being shown in Figure 6.2. It can easily be seen that the pulse width oscillates extremely rapidly and that we begin to observe additional dynamics creeping into the pulse width evolution that were not observed in previous chapters. With the extremely rapid oscillation in pulse width, Figure 6.3 shows that the pulse evolution over Z_a looks more akin to that of the classical soliton than the DM soliton. Even though the number of dispersion sections per amplifier span has greatly increased we still find that these DM soliton solutions are stable and can propagation over distances in excess of 10,000 km, as shown in Figure 6.4.

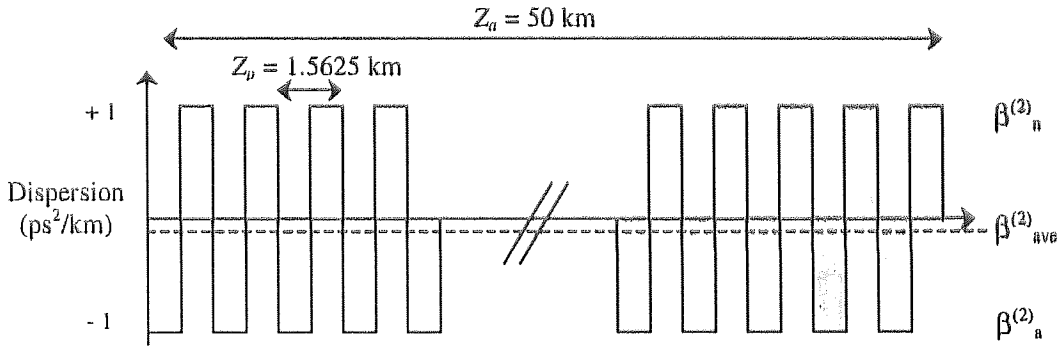

Figure 6.1: Schematic representation of the short period dispersion map used for 320 Gbit/s transmission.

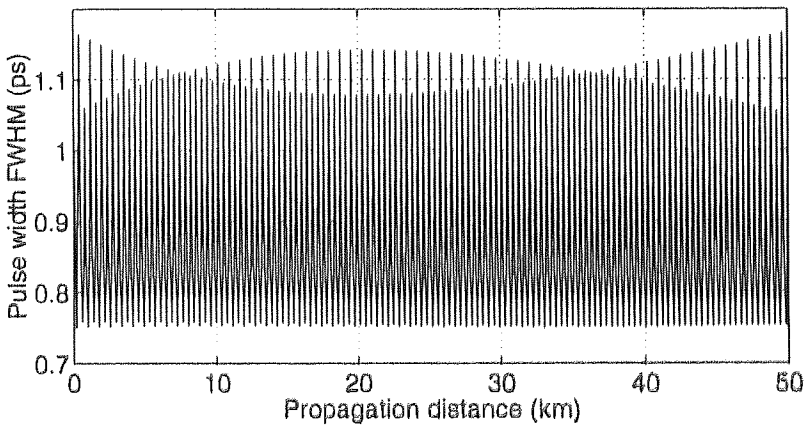

Figure 6.2: Pulse width evolution over Z_a for a 64 section SPDM.

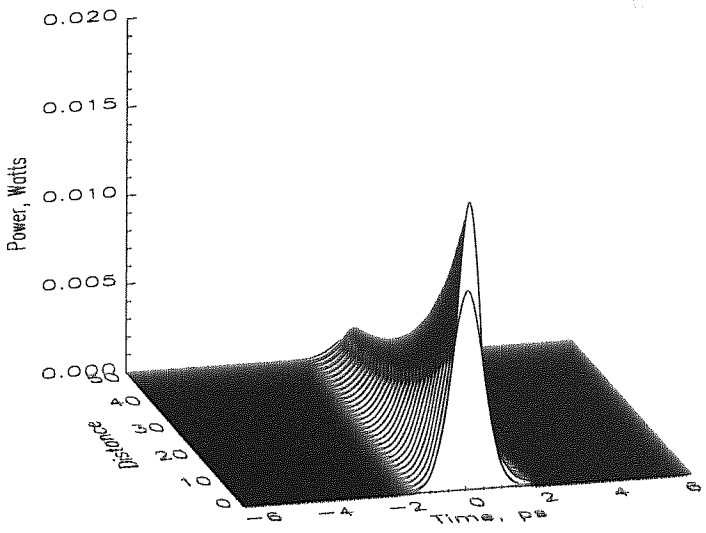

Figure 6.3: Dynamical evolution of the DM soliton over Z_a.

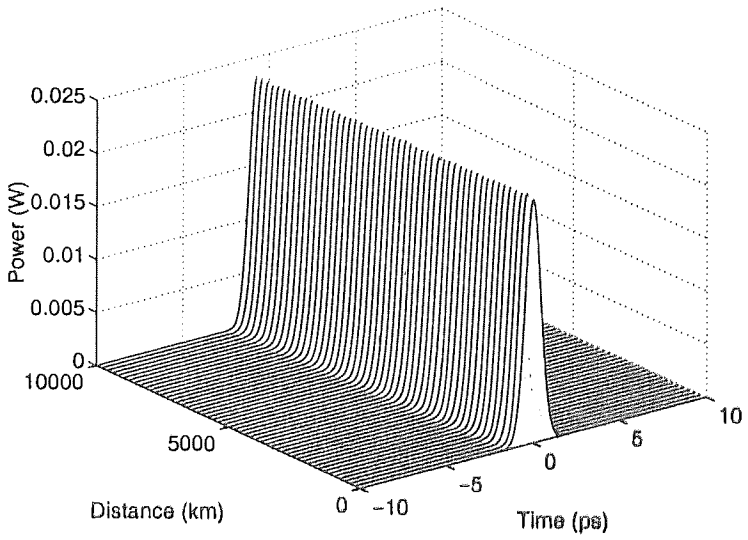

Figure 6.4: DM soliton propagation over 10,000 km shown stroboscopically at the amplifiers.

6.3 Transmission simulations

For the transmission simulations at 320 Gbit/s we use the Generalised Non-Linear Schrödinger equation (GNLS) including higher order non-linear and dispersive effects. Again as in the

previous chapters, dispersion slope compensation is provided by an alternate sign of dispersion slope in each fibre section with magnitudes: $\beta^{(3)}_a = -\beta^{(3)}_n = 0.07$ ps^3/km. We take the noise figure of the amplifier to be 4.5 dB and place a Gaussian filter after each amplifier to suppress the accumulation of ASE noise, as detailed in Figure 6.5. Once again, the receiver is modelled by a non-optimised Lorentzian electrical filter of 280 GHz (87.5 percent of the bit rate). In this particular system, we place the amplifiers at the beginning of the anomalous dispersion fibre section and therefore pulse amplification and filtering occurs where the pulse width is relatively broad.

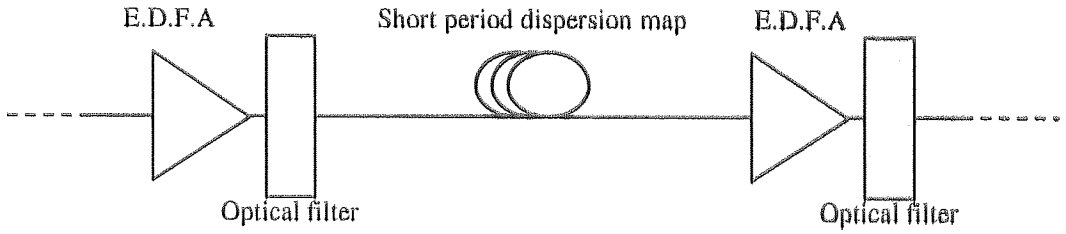

Figure 6.5: Schematic representation of transmission line used for 320 Gbit/s transmission

The performance of the system is evaluated using Q value estimates taken from a 2^7-1 bit pseudo random binary sequence. Initially we determine the dependence of system performance on the minimum pulse width τ_{min} for a fixed map strength of $S = 1.65$. To allow for the differing spectral bandwidths and to reduce the effect filters have on propagation, we fix the ratio of minimum pulse width to inverse filter bandwidth ($\tau_{min} : \Omega_f$) to be 0.25, such that the filters are broad relative to the pulse width at that point. Figure 6.6 details the dependence of system performance on minimum pulse width. It is clear that an optimum minimum pulse width exists for $\tau_{min} = 1.5$ ps and that for longer pulse widths interactions increase limiting performance. For shorter pulse widths performance declines as a result of higher order non-linear and dispersive effects. At the optimum minimum pulse width a balance is obtained between interactions and higher order effects, thus a transmission distance of 3,400 km is achieved.

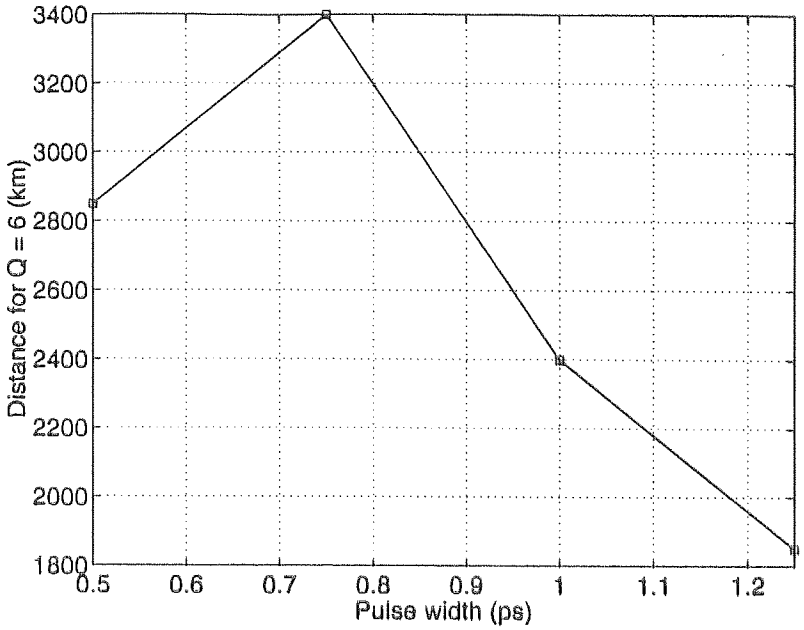

Figure 6.6: System performance as a function of minimum pulse width.

Taking the optimum minimum pulse width from Figure 6.6, we then seek to optimise system performance for this specific pulse width. Firstly we optimise the performance in terms of average dispersion, which can be seen Figure 6.7. It is apparent from Figure 6.7, that for average dispersions that are greater in magnitude than the optimum average dispersion, we observe that although performance improves over shorter distances (< 1,000 km), for longer propagation distances, declines rapidly due to interactions. The performance of the optimum average dispersion over short haul distances is considerably poorer due to SNR, however the lower energy of these DM solitons facilitates longer propagation distances before interactions become significant. For average dispersions that are smaller in magnitude than the optimum, SNR severely limits performance.

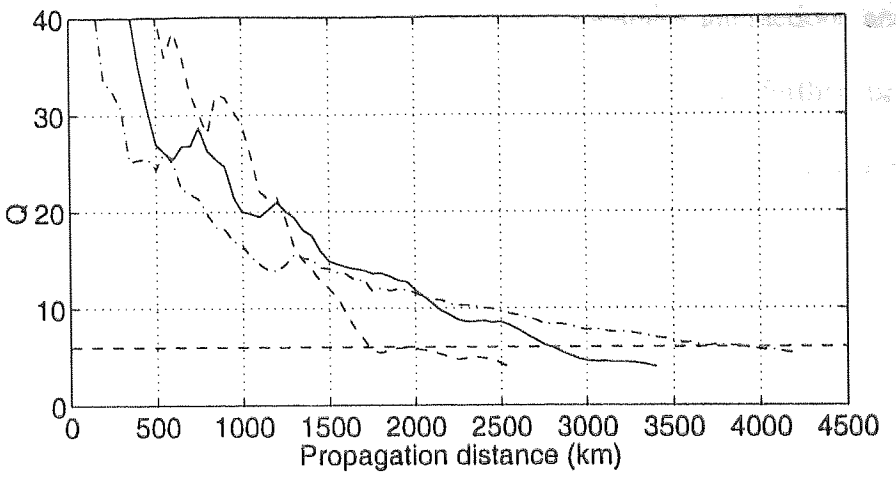

Figure 6.7: Dependence of system performance on average dispersion.(dashed line) $\beta^{(2)}_{ave}$ = -0.004 ps^2/km, (solid line) $\beta^{(2)}_{ave}$ = -0.002 ps^2/km and (dot and dash line) $\beta^{(2)}_{ave}$ = -0.001 ps^2/km.

By breaking the relation $\beta^{(3)}_a = \beta^{(3)}_n$, a residual dispersion slope $\beta^{(3)}_{rs}$ is created which allows the tolerable limits of system performance to $\beta^{(3)}_{rs}$ to be investigated. Figure 6.8 illustrates the sensitivity of the system to the residual dispersion slope. Transmission performance is significantly affected by the residual dispersion slope, so much so that when $|\beta^{(3)}_{rs}| = 0.005$ ps^3/km propagation is limited to 1500 km.

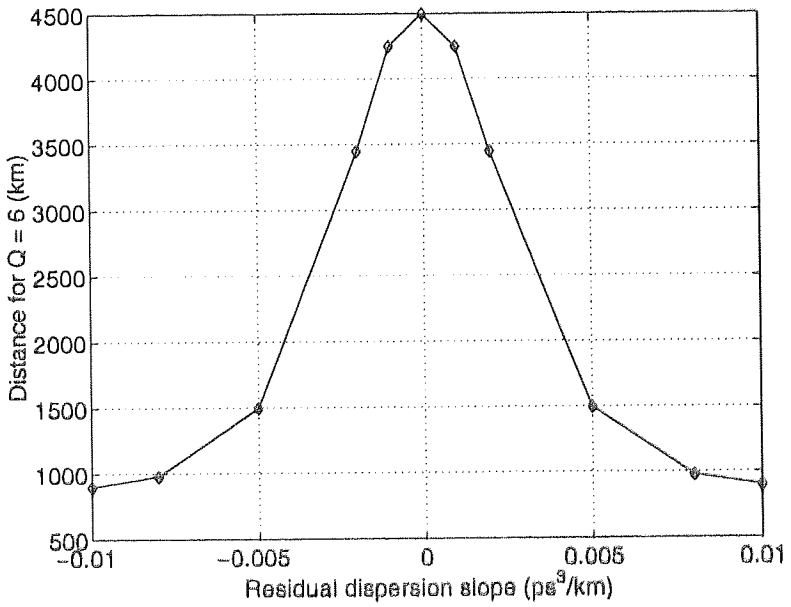

Figure 6.8: Tolerance of system performance to residual dispersion slope.

At this point, we have optimised the system to minimise interactions and higher order effects, and maximise SNR. The performance of the system can further be enhanced by optimising the bandwidth of the optical filters that are located after each amplifier. In this particular system, the role of filters is to simply suppress the ASE noise generated by the amplifiers, which reduces the timing jitter of the pulses [62, 63] and does not suppress the frequency shift of interacting solitons [55, 232]. The effects that filter bandwidth has on propagation is demonstrated in Figure 6.9. For $\Omega_f = 2$ THz, it can be seen that whilst the noise in the DM soliton spectra is significantly reduced, the narrow bandwidth of the filter excites the Continuous-Wave (CW) background instability [212] which destroys the transmitted information as the DM solitons become less distinguishable from the background. The other extreme is observable in Figure 6.9(c), where $\Omega_f = 5$ THz, in this case the filter is so wide that the continuum is not excited, but the noise in the spectrum leads to a significant accumulation of timing jitter. In this scenario, we seek a balance between these two effects which is shown in Figure 6.9(d), where the greatest amount of noise is removed from the spectrum without leading to significant build up of the continuum until relatively large propagation distances have been achieved.

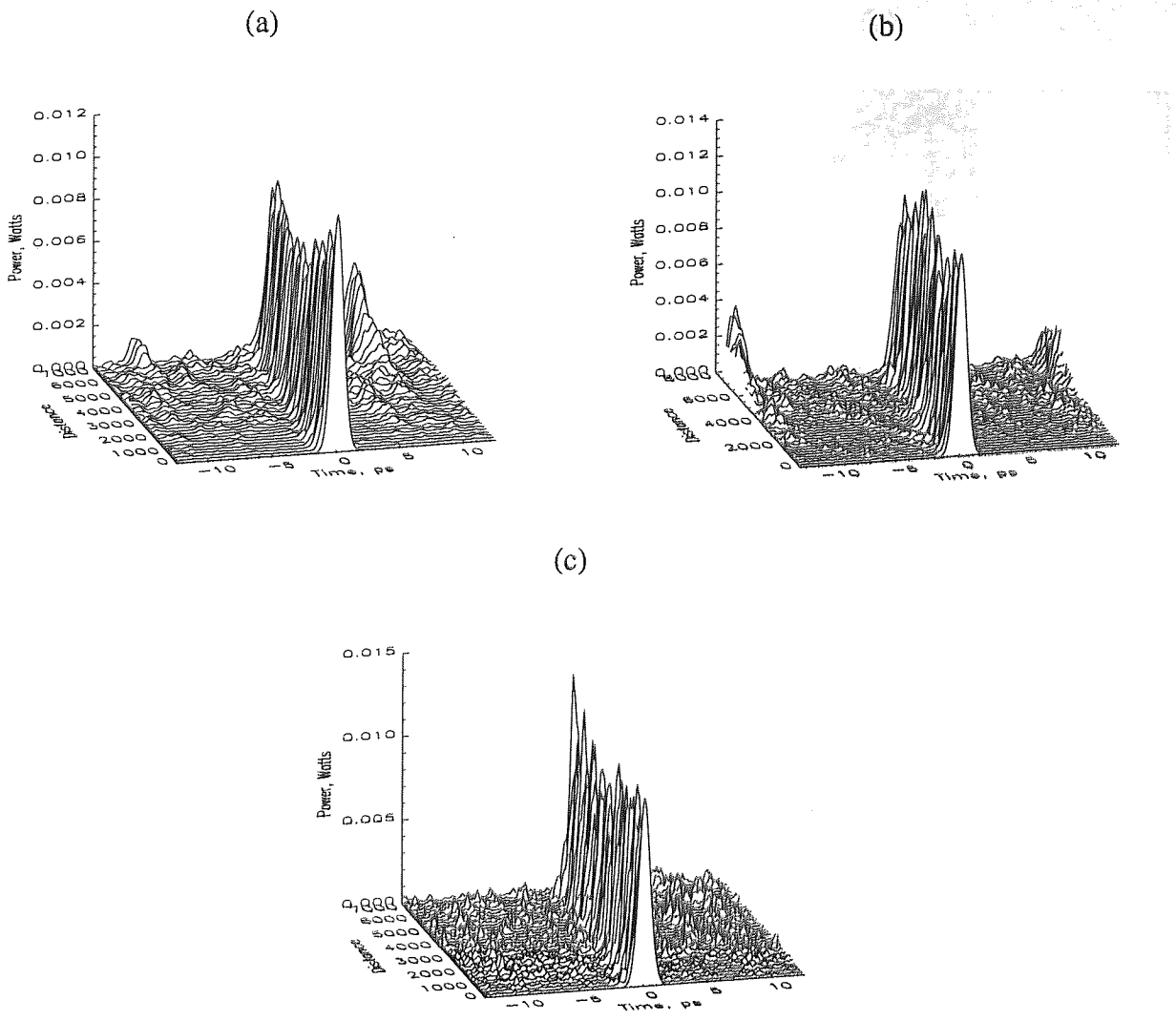

Figure 6.9: The effect of filter bandwidth on DM soliton propagation. (a) $\Omega_f = 2$ THz, (b) $\Omega_f = 3$THz and (c) $\Omega_f = 5$THz.

As stated previously, ASE noise manifests itself in the form of timing jitter that can be observed from the eye diagram at the receiver. However, when DM solitons have a broad spectrum (short pulse widths), then as we observed in the previous chapter the timing jitter leads to interactions between solitons. These induced interactions can be seen in Figure 6.10. Again, we see that the collision distance can clearly be related to the amount of noise in the DM soliton spectrum. Without ASE noise and filters, the collision distance for a pair of DM solitons is greater than 10,000 km where as with ASE noise and no filters the collision distance is reduced to less than 4,000 km.

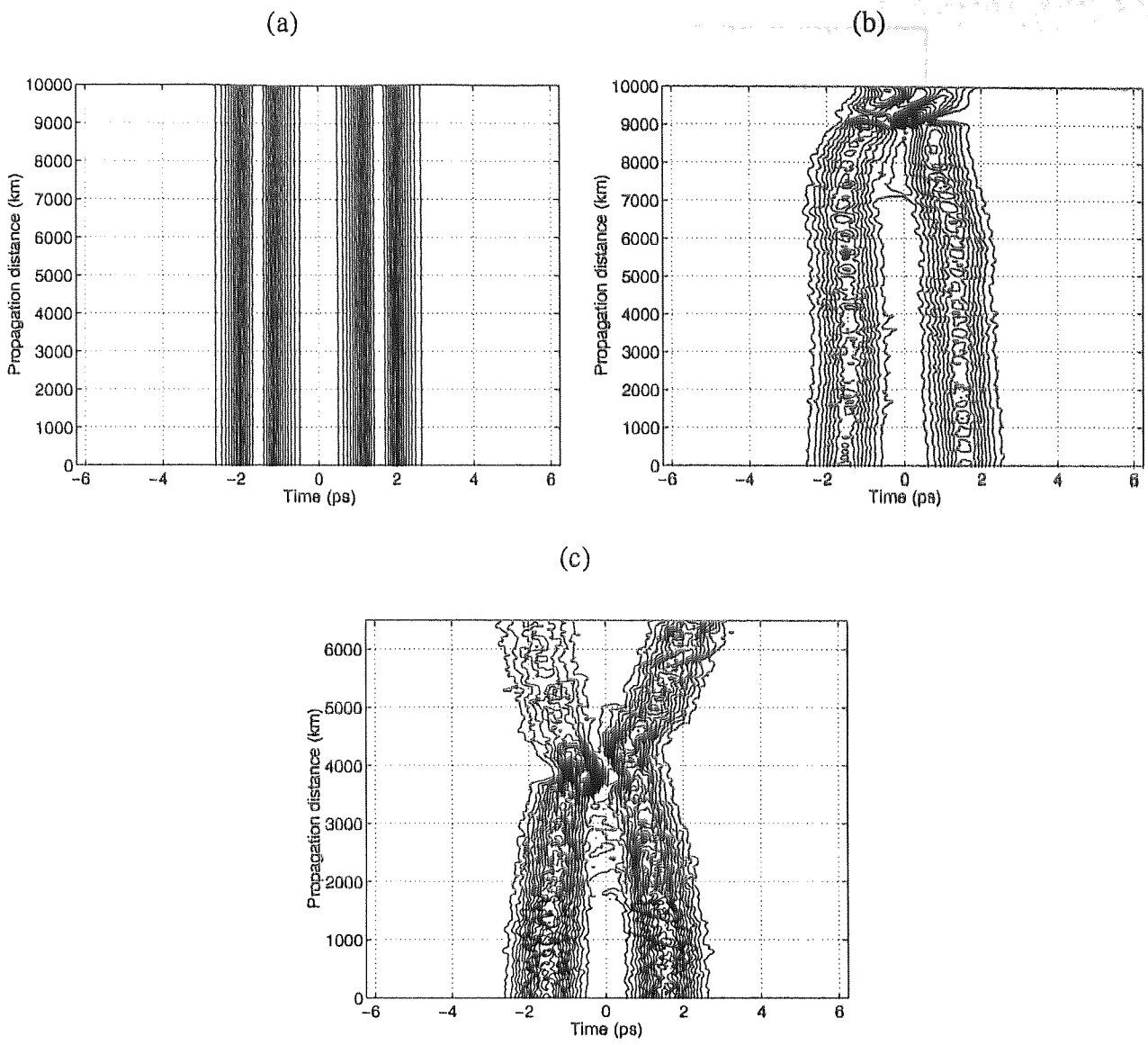

Figure 6.10: Reduction of the collision distance between a pair of DM solitons due to noise. (a) No ASE noise, no filter, (b) ASE noise, 3 THz filter, and (c) ASE noise, no filter.

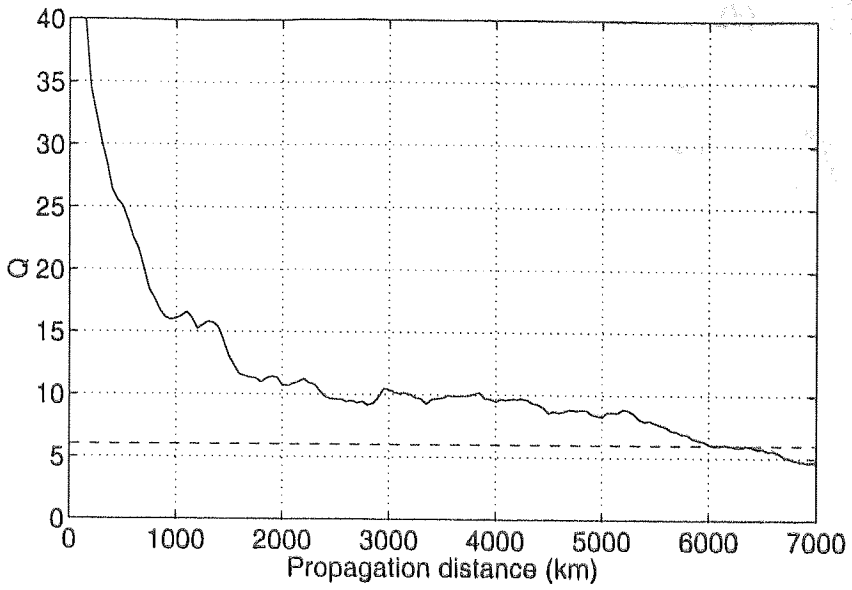

Figure 6.11: Optimal system performance as a function of propagation distance.

Using the optimised conditions for τ_{min}, $\beta^{(2)}_{ave}$ and Ω_f, Figure 6.11 details system performance as a function of propagation distance. It is observable that propagation over 6,500 km can be achieved under optimal conditions. A more detailed look at the transmission performance can be seen in Figure 6.12 that shows the eye diagrams at 1,000 km intervals. From Figure 6.11 and Figure 6.12, it can be seen that the effects of accumulated noise kill the performance. For propagation distances between 3,000 km and 6,000 km, the increasing timing jitter of the pulses is clearly observable. At 6,000 km the CW background instabilities become visible. By 7,000 km, interactions stimulated by the noise are evident in the eye diagram along with the increasing growth of the CW background.

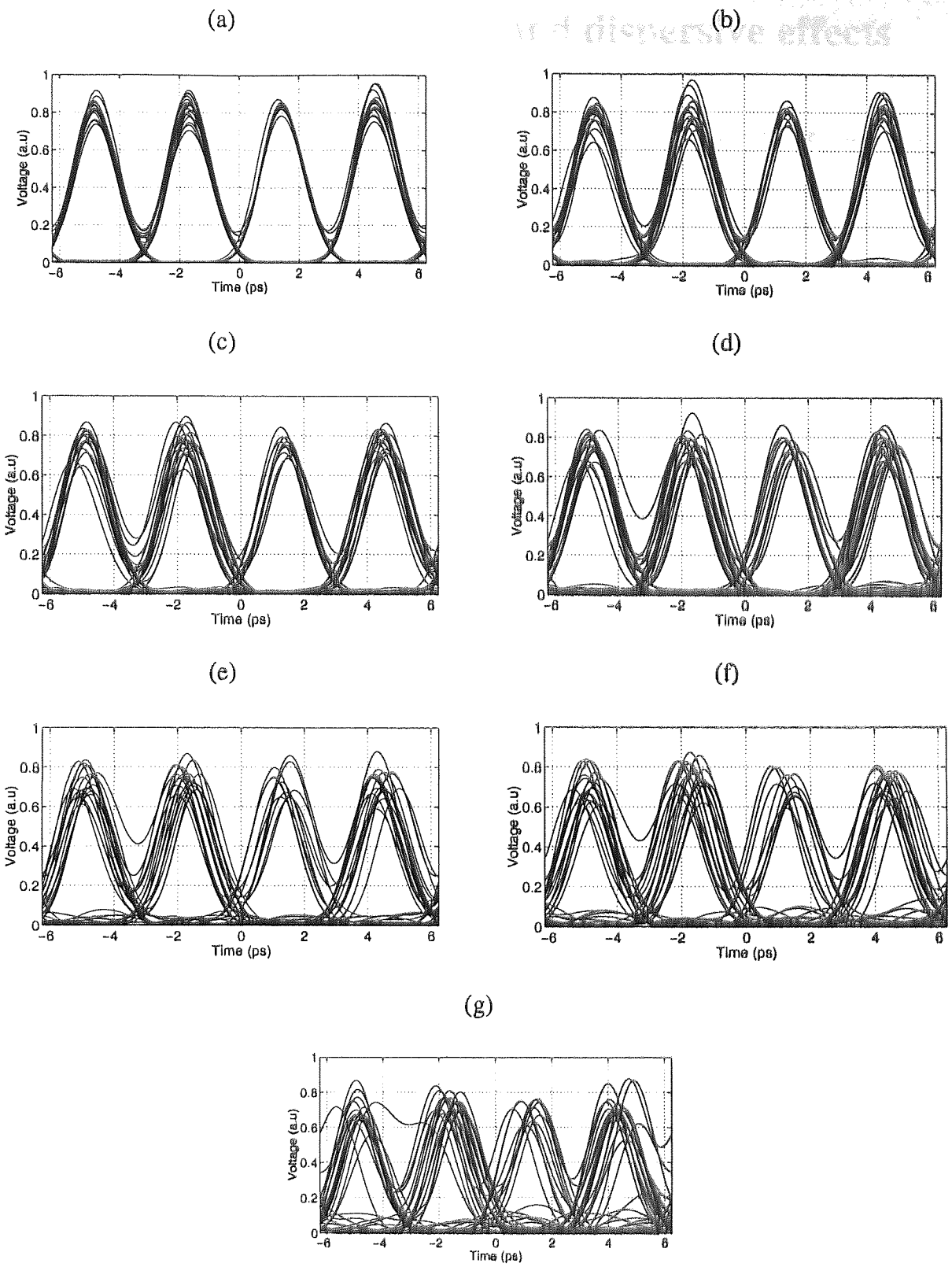

Figure 6.12: Eye diagrams of optimal transmission performance at (a) 1,000 km, (b) 2,000 km, (c) 3,000 km, (d) 4,000 km, (e) 5,000 km, (f) 6,000 km and (g) 7,000 km.

6.4 Higher order non-linear and dispersive effects

Having determined the optimal conditions for transmission performance, we now turn our attention to the robustness of this system to higher order non-linear and dispersive effects. Firstly, we investigate the effects of dispersion slope. As stated previously, in this system, dispersion slope compensation is provided on the length scale of Z_p, which becomes increasingly important as the pulse width becomes shorter. In this particular case, we are mainly concerned with the residual dispersion slope $\beta^{(3)}_{rs}$, as the dispersion lengths associated with each of the dispersion slopes of the individual fibre sections is much smaller than Z_p ($L_D' < Z_p$). However due to the short pulse width, we are faced with an incredibly short dispersion length associated with $\beta^{(3)}_{rs}$ relative to desirable transmission lengths of 1,000 km and upwards. The effects of the residual dispersion slope on propagation can be seen in Figure 6.13. In the case of $\beta^{(3)}_{rs} = 0.005$ ps^3/km, $L_D' \approx 84$ km, we observe that even for propagation distances $>> L_D'$ only a small amount of radiation is shed and propagation largely remains unaffected. As $\beta^{(3)}_{rs}$ increases, the effect on propagation becomes more noticeable. For $\beta^{(3)}_{rs} = 0.025$ ps^3/km, $L_D' \approx$ 17 km, the smooth propagation of the DM soliton is destroyed and instead we observe a pseudo-random evolution of the slow DM soliton dynamics which sheds a lot of radiation. Increasing $\beta^{(3)}_{rs}$ further, we observe the DM soliton shedding a large amount of radiation which eventually destroys the propagating pulse.

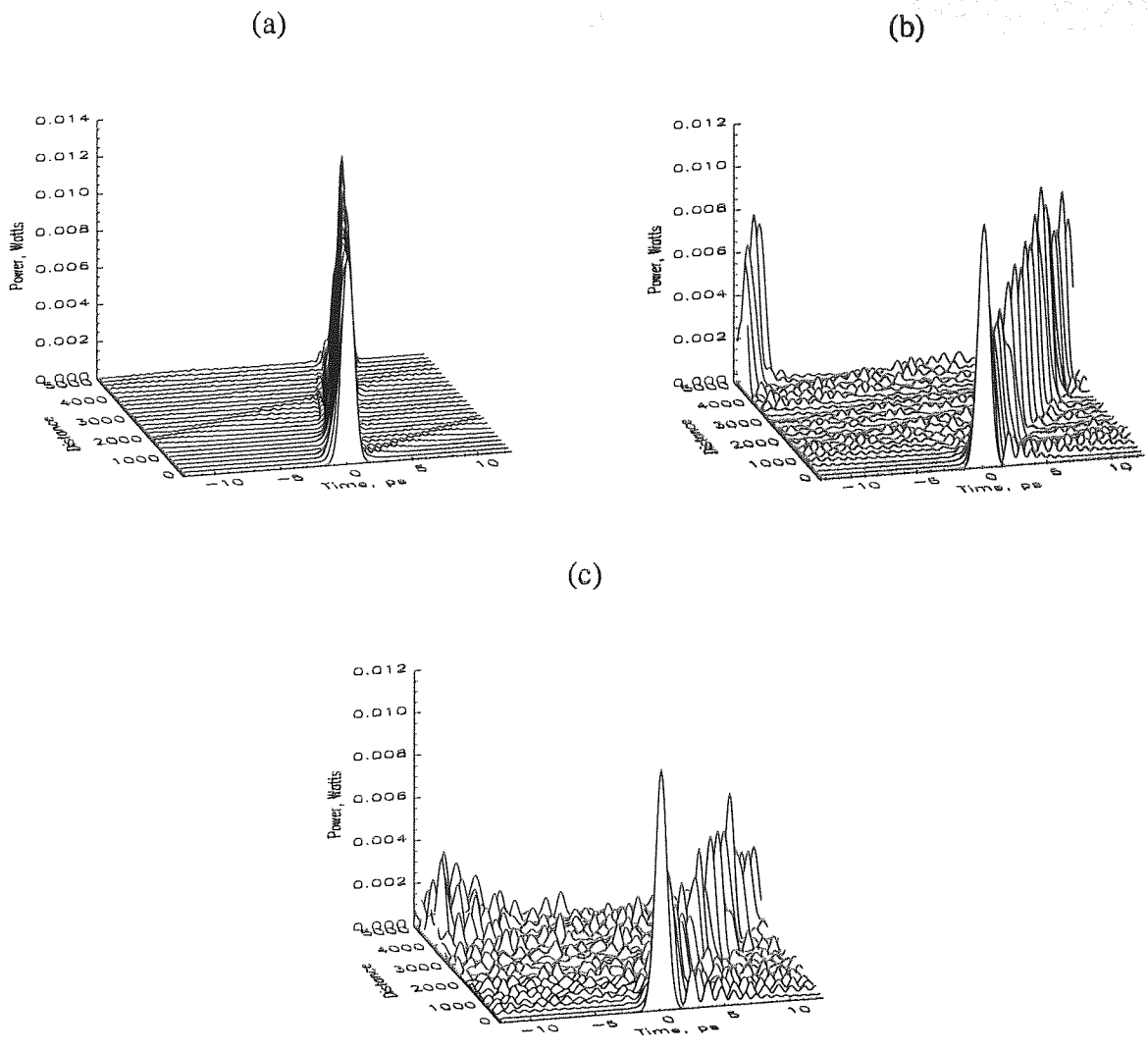

Figure 6.13: Effect of residual dispersion slope on propagation. (a) $\beta^{(3)}_{rs} = 0.005$ ps^3/km, (b) $\beta^{(3)}_{rs} = 0.025$ ps^3/km, (c) $\beta^{(3)}_{rs} = 0.05$ ps^3/km.

The effects of Stimulated Raman Scattering (SRS) become increasingly important for short pulse widths. Figure 6.14 illustrates noiseless propagation of the optimal DM soliton including the effects of SRS. From Figure 6.14(a) no filter has been included and it appears the SRS has little effect on propagation. However, from Figure 6.14(b) and Figure 6.14(c) the SRS induced frequency shift becomes visible. In this case, the observed frequency shift is small due to the relatively lower power of the DM soliton making the SRS process inefficient. Nevertheless this is not always the case as is detailed in section 6.5.

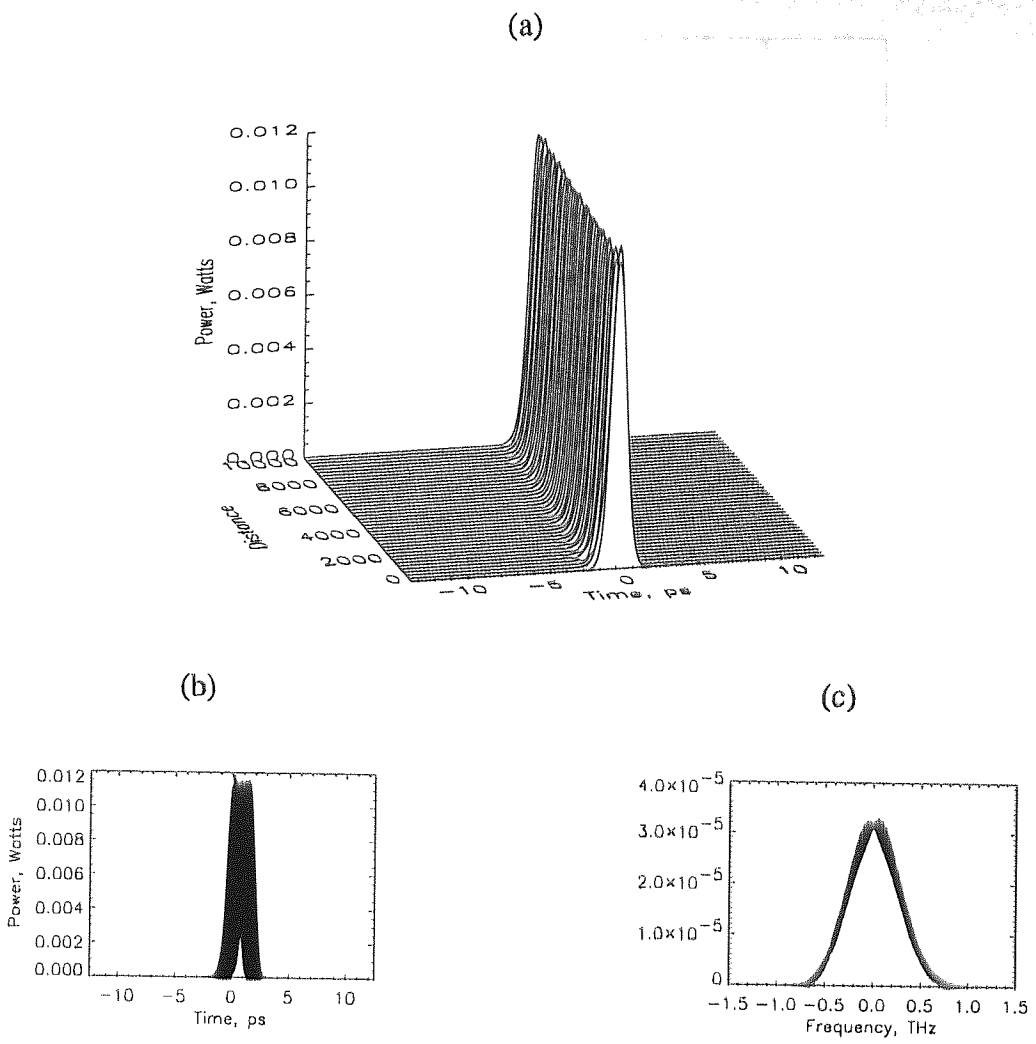

Figure 6.14: Effect of SRS on short pulse propagation with no noise and no filter. (a) 3D evolution, (b) 2D evolution showing temporal shift due to SRS, (c) Frequency shift.

Polarisation Mode Dispersion (PMD) is another limiting factor that must be considered. As in previous chapters, we use the birefringent 2-dimensional GNLS including the effects of random mode coupling. Figure 6.15 demonstrates how influential polarisation mode dispersion is on single channel transmission at 320 Gbit/s. For relatively low values of PMD we observe that transmission is limited to around 4,500 km, which is a reduction of 1,500 km. However, performance declines rapidly as the PMD increases due to the instability of the propagating pulse [215]. For PMD = 0.07 ps/$\sqrt{\text{km}}$, only a small transmission distance of around 250 km is possible, which indicates that for short pulses the main performance limiting factor is the PMD induced instability of the propagating pulse.

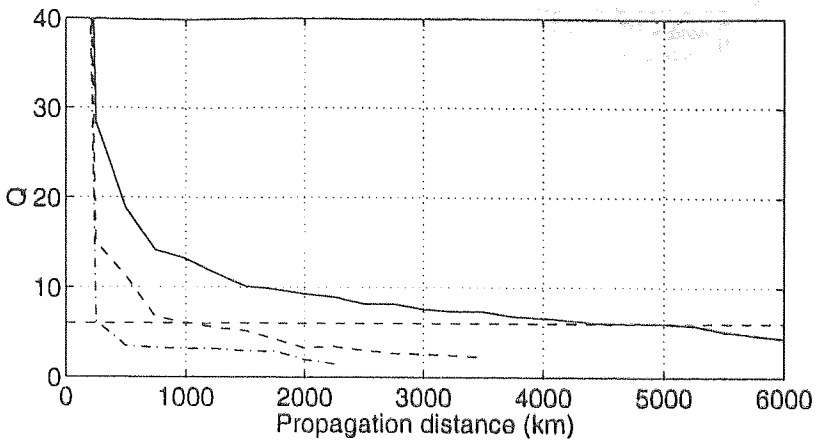

Figure 6.15: The effect of polarisation mode dispersion on 320 Gbit/s transmission. (solid line) PMD = 0.02 ps/√km, (dashed line) PMD = 0.05 ps/√km, and (dot and dashed line) PMD = 0.07 ps/√km.

6.5 Long haul transmission

Following the convention adopted in the preceding two chapters, we investigate transmission at 320 Gbit/s using a Gaussian shaped pulse with the initial conditions of the DM soliton. The difference in profile of the exactly periodic DM soliton and a Gaussian pulse with the same initial conditions are shown in Figure 6.16. It is apparent that over the core (centre) of the pulse there is little to distinguish between the two pulses, but the Gaussian pulse has tails that decay much faster than those of the DM soliton. Whilst this may reduce interactions that originate from overlapping of pulses, it also induces a quasi-periodic motion in the slow dynamics of the propagating DM soliton. These dynamics can be seen in Figure 6.17.

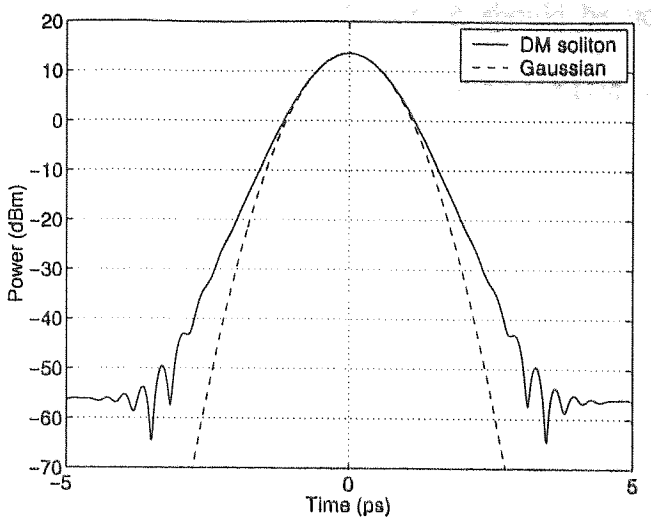

Figure 6.16: Comparison of shape profiles for the exact DM soliton shape (solid line) and a Gaussian shape pulse (dashed line).

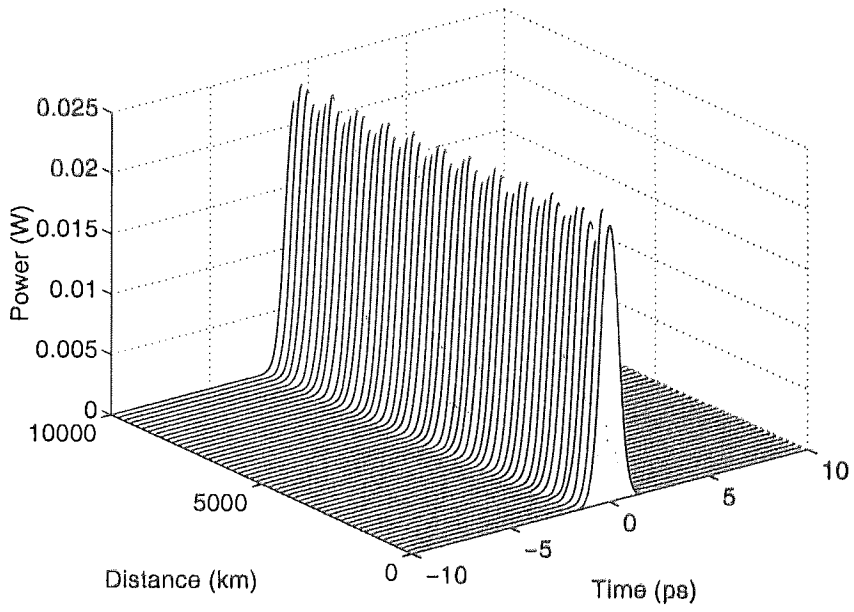

Figure 6.17: Propagation of a Gaussian shaped pulse with the initial conditions of the DM soliton.

We investigate transmission distance for which Q ≥ 6 as a function of the average dispersion and initial pulse power. These simulation results for τ_{min} = 0.75 ps are observable in Figure 6.18. Clearly, performance is incredibly sensitive to average dispersion and only small average dispersions can be tolerated. At the optimum point in Figure 6.18, a transmission distance greater than 6,000 km can be achieved. Figure 6.18 exhibits the same general shape that we have observed in previous chapters and therefore we shall not dwell too much on limiting

factors discussed in the previous chapters. In addition, it should be noted that the optimum average dispersion in Figure 6.18 is identical to that found using the DM soliton in Figure 6.7.

An interesting feature of Figure 6.18 is that the optimum conditions of the propagation using Gaussian pulses are not those of the exactly periodic DM soliton. For Gaussian pulses, optimum performance is achieved for an initial power of 19 dBm, whereas the DM soliton power is 10 dBm. This is quite astonishing when we investigate the effect of SRS at high powers. Figure 6.19 illustrates noiseless propagation (without any filters) for Gaussian shaped pulses with the initial conditions of the DM soliton and those of the optimum conditions observed in Figure 6.18. We can see that in the case of the high power Gaussian pulse, the SRS process is extremely efficient with a large frequency shift being observable, which is a direct result of the increased power. In contrast, Figure 6.19(b) exhibits little variation in propagation characteristics with only a small frequency shift visible. Therefore how come we achieve improved performance with an increased amount of SRS?. The answer becomes evident in Figure 6.20, when we include an optical filter of 3THz located directly after the amplifier, analogous to the previous studies [233, 234]. We observe that the SRS induces a frequency shift that causes some of the spectrum to be cut away by the filter. Therefore, we undergo a form of SRS enhanced regeneration of the propagating pulse.

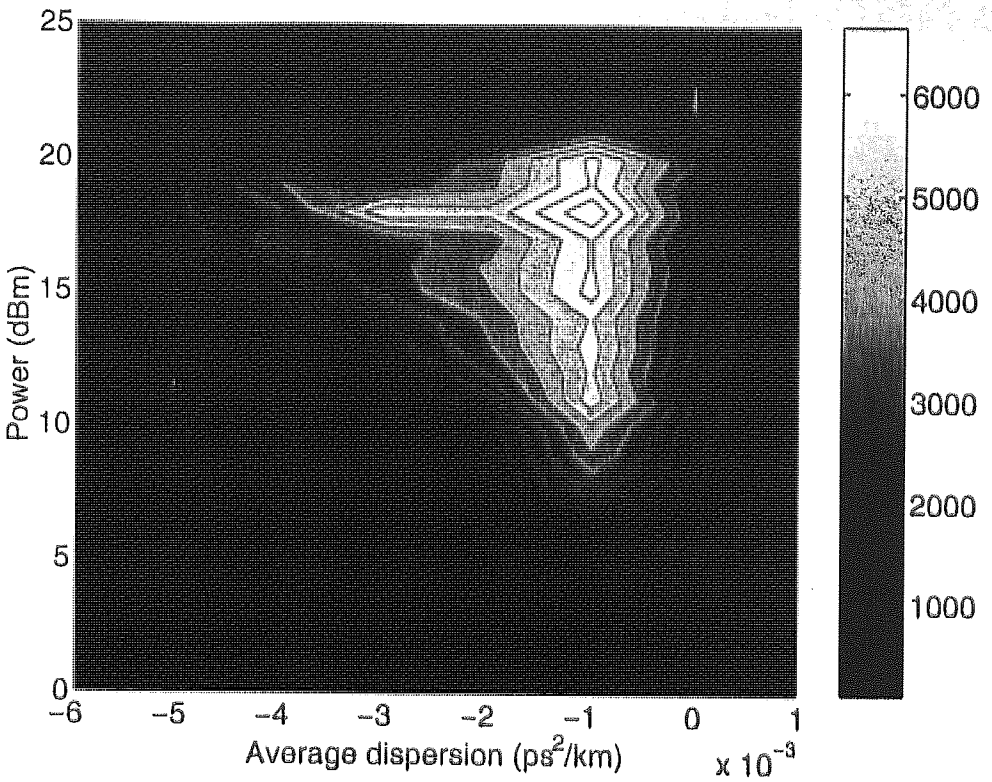

Figure 6.18: Dependence of transmission performance on average dispersion and initial power for $\tau = 0.75$ ps. Contour lines indicate the maximum achievable propagation distance in km.

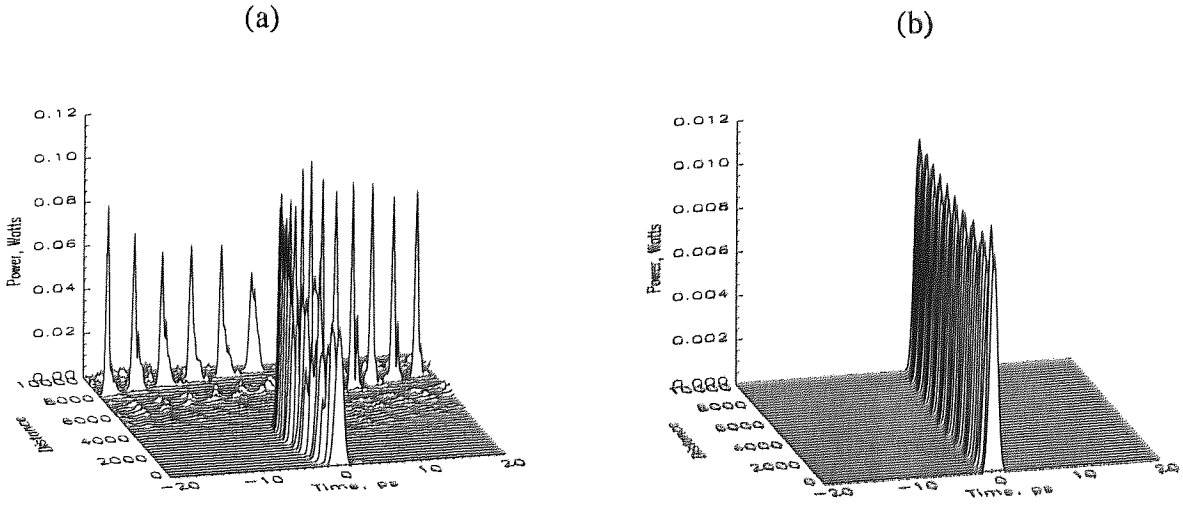

Figure 6.19: SRS effects visible in pulse propagation (a) initial power = 18 dBm, (b) initial power = 10 dBm.

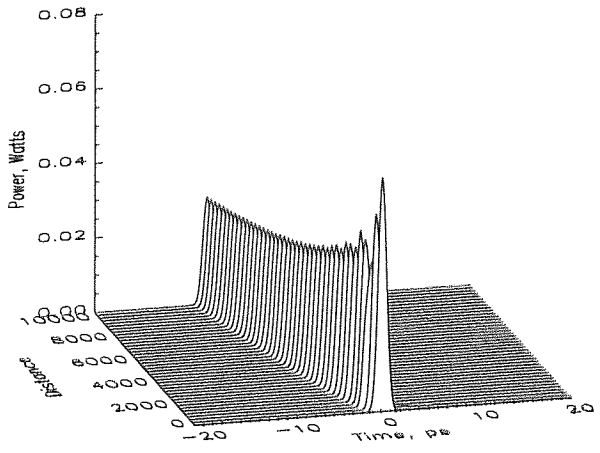

Figure 6.20: Control of SRS for a Gaussian pulse of initial power 18 dBm by using a 3 THz filter located after each amplifier

6.6 Short haul transmission over 1,000 km

In addition to long haul transmission, we focus here on short haul transmission at 320 Gbit/s. The constraints on short haul transmission are often more relaxed than for transoceanic systems, with this in mind we use two different pulse widths to investigate performance. Figure 6.21 and Figure 6.22 illustrate the transmission performance over 1,000 km as a function of initial power and average dispersion for τ_{min} = 0.75 ps and τ_{min} = 1 ps respectively. In each case, the initial conditions of the Gaussian pulses were that taken from the exact DM soliton with S fixed to 1.65 and higher order non-linear and dispersive effects were included. Once again, the general dependence of Figure 6.21 and Figure 6.22 is broadly similar to those observed in previous chapters but with a vastly reduced set of tolerable average dispersions. It is clear that transmission is supported over a larger region for τ_{min} = 0.75 than for τ_{min} = 1 ps. This indicates that the overwhelming limiting factor is interactions between adjacent pulses as τ_{min} = 1 ps exhibits a greater tolerance to higher order non-linear and dispersive effects. In addition, the lower optimum power for τ_{min} = 1 ps is also indicative of the system being interaction limited.

Although the optimum performance is similar in both cases, the optimum region is far larger in Figure 6.21, which is more desirable. Therefore, at a transmission rate 320 Gbit/s little additional freedom is gained when we reduced the transmission distance to only 1,000 km. However, what is apparent when Figure 6.21 is compared to Figure 6.18 is the greater optimum average dispersion for transmission over 1,000 km compared to long-haul transmission.

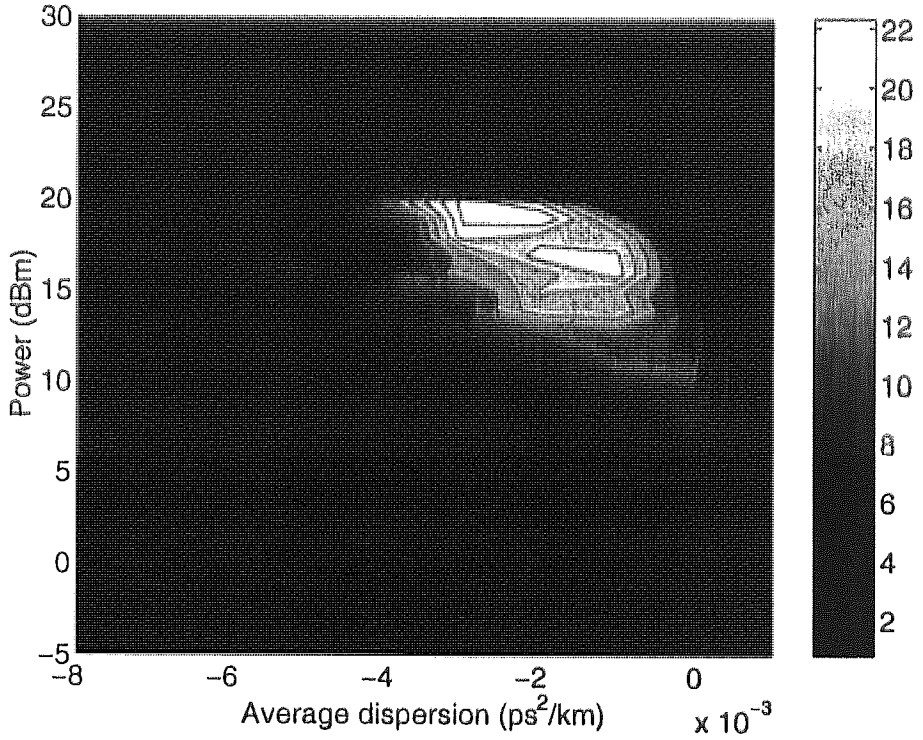

Figure 6.21: Contour plot detailing system performance as a function of initial power and average dispersion for τ = 0.75 ps over 1,000 km. Contour lines indicate the Q values at the receiver.

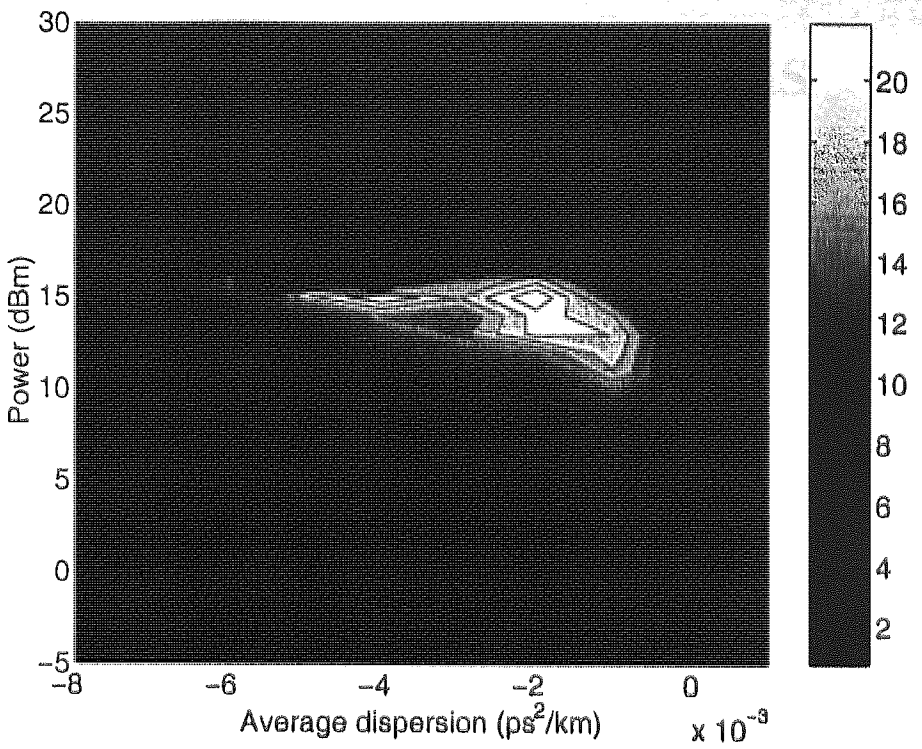

Figure 6.22: Contour plot detailing system performance as a function of initial power and average dispersion for τ = 1 ps over 1,000 km. Contour lines indicate the Q values at the receiver.

6.7 Conclusion

In conclusion, we demonstrated the possibility of 320 Gbit/s single channel transmission over distances in excess of 6,000 km. This performance was achieved by methodical optimisation of the system parameters. We found that performance was limited mainly by noise induced interactions although the system was extremely sensitive to higher order dispersive effects. In order to achieve reasonable performance, the average dispersion must be tightly controlled. Also the use of optical filters can be used along with SRS to improve performance. Over short haul distances, good transmission performance can be achieved for a relatively large parameter space. In addition, we have shown that system performance is severely limited by PMD. In the case of strong PMD, stable pulses cannot be supported and shatter after only a relatively short propagation distance. However, transmission in excess of 4,000 km is possible if the PMD is below the tolerable limit defined in the chapter.

Chapter 7 Quasi-linear versus dispersion managed soliton propagation

7.1 Introduction

In the previous chapters, our work has focussed specifically on DM soliton transmission systems. Nevertheless, dispersion managed systems support a whole spectrum of propagation regimes that range from quasi-linear to non-linear soliton-like propagation. As described previously, DM solitons exist for low to moderate dispersion map strengths (S), however, as S increases beyond a certain threshold, DM soliton propagation is no longer supported [110]. The reason for this is that for strong S, the energy required to create a DM soliton is too great. However, in this region of strong S ($S > 12$), another form of propagation exists, which is referred to as quasi-linear propagation. In quasi-linear propagation, the pulses have an energy that is far below that required for the formation of a DM soliton, and therefore non-linear effects significantly impair the performance of these systems. Quasi-linear behaviour can still be observed for low to moderate map strengths by simply reducing the energy of the pulses.

Interest in quasi-linear propagation arises from the combination of commercially available fibres (including legacy fibres) with large dispersions at 1550 nm, and the desire for ever increasing data rates. Typically, fibre types such as SMF, RDF, DCF and their variants continue to dominate the fibre market. Adopting the conventional design of dispersion managed systems where $Z_p \geq Z_a$, although $Z_p = Z_a$ is more commonly found amongst the published literature, then for practical amplifier spans ($Z_a \geq$ 35 km) and increasing transmission rates (implying shorter pulse widths), the strength of the dispersion management soon exceeds the limit for DM solitons. Therefore, in such systems, the quasi-linear propagation regime is

imposed on the designers of such systems. For this reason, propagation in this regime has received considerable attention [96, 98, 138, 173, 194, 204, 235]. Although this propagation regime has the advantage, compared to soliton-like systems of reduced interactions [138], this propagation regime is significantly limited by Intra Channel Four Wave Mixing (ICFWM) [205, 236], a phenomena that is virtually nonexistent in soliton-like propagation.

Quasi-linear propagation, often referred to as "pulse-overlapped" transmission, is characterised by pulses which experience massive breathing where pulses overlap a significant number of their nearest neighbours. It is during the periods where the pulses are overlapped that the ICFWM builds, which manifests itself in the form of amplitude jitter and formation of "ghost" pulses.

In this chapter, we contrast the performance of quasi-linear propagation, with soliton-like propagation for 40 Gbit/s based transmission for both single channel and WDM transmission. In addition, we investigate means by which performance can be improved in both soliton-like and quasi-linear systems by optimisation of the carrier pulse shape.

7.2 Comparison of propagation regimes

In order to contrast the propagation regimes, we construct the dispersion maps from fixed fibre types, namely SMF and RDF. The reasons for the selections arise from the availability of such fibres and because of the alternate sign dispersion slopes of each fibre. The different propagation regimes are therefore achieved by altering the dispersion management period (which conversely varies S) for a fixed amplifier span, Z_a = 40 km. The four dispersion maps investigated are shown in Figure 7.1.

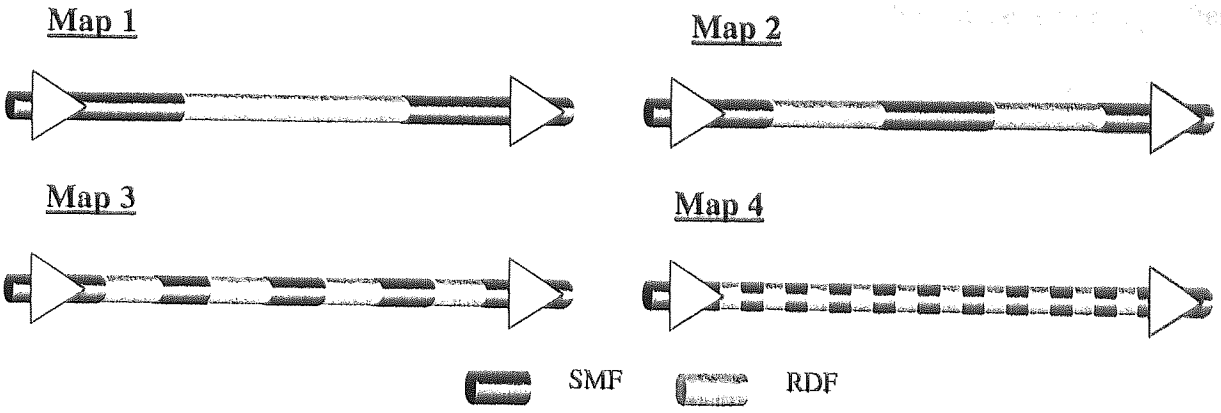

Figure 7.1: Schematic representation of the dispersion maps investigated. Each map is constructed using sections of SMF and RDF with Z_a = 40 km. Map 1: Z_p = 40 km, Map 2: Z_p = 20 km, Map 3: Z_p = 10 km, and Map 4: Z_p = 4 km.

In the case of map 1, we have $Z_p = Z_a = 40$ km, therefore S is strong and pulse propagation will be quasi-linear in nature. In map 2, the dispersion management period is reduced to $Z_p = 20$ km, therefore $S_{map2} = S_{map1}/2$ and consequently the propagation will still be quasi-linear but with more confined breathing of the pulse. For the map 3, we start to approach a more non-linear propagation regime with $Z_p = 10$ km and $S_{map3} = S_{map1}/4$. Finally, in the case of map 4, $Z_p << Z_a$ meaning that we are into the regime of short period dispersion management and for suitable pulse widths DM soliton behaviour should be observable.

7.3 Single channel transmission

For each of the four dispersion maps illustrated in Figure 7.1, performance is evaluated using Q value estimates based on a 2^7-1 PRBS. The amplifiers are taken to have a noise figure of 4.5 dB, with a wide Gaussian filter of 1.5 THz, located directly after the amplifier, to remove the accumulation of ASE noise. Including higher order non-linear and dispersive effects we introduce a residual dispersion slope of D_s = 0.01 ps/nm^2/km. Fixing the average dispersion, D_{ave} = 0.05 ps/nm/km, we compare the system performance for each of the dispersion maps.

Propagation in dispersion map 1 is illustrated in Figure 7.2, which depicts the evolution of both a single pulse and the Q value. It can be seen that the propagating pulse exhibits massive expansions and contractions in pulse width, with the original pulse shape emerging after propagation over nZ_a. It is clear that when the pulse width is at its maximum, it extends over many neighbouring bit periods. The Q value evolution also provides an interesting insight into propagation in this regime, where it can be seen that only periodically is the transmitted data pattern reconstructed, with these points of reconstruction corresponding to the points where the pulse is most compressed. For all other points, the pulses are so overlapped that they become indistinguishable from each other. Also from Figure 7.2(b), the changing periodicity of the reconstruction of the data pattern is clearly evident which is due to SPM.

The dependence of transmission performance on pulse width and initial power for map 1 can be seen in Figure 7.3. We observe that broadly the dependence is that of the DM soliton where initial power increases with shortening pulse width, and improved performance being achieved for stronger map strengths. At high powers, non-linear effects limit performance and at short pulse widths, low powers impede performance.

Moving onto propagation in map 2, shown in Figure 7.4, the breathing of the pulse is now more confined and therefore extends over fewer of the adjacent pulses. Examination of the Q value evolution in Figure 7.4 shows that although we still have this periodic reconstruction of the transmitted paper, this period is far shorter than in map 1. Again, we see the effect of SPM that gradually increases this reconstruction period. From Figure 7.5, it is clear that map 2 displays a similar behaviour to map 1, but with a reduced transmission distance. Also, we do not observe the increasing performance for shorter pulse widths, with optimum performance being achieved for longer pulse widths.

Propagation in map 3 represents a departure from the behaviour observed for maps 1 and 2, this behaviour can be seen in Figure 7.6. The breathing of the pulse is now rapid and well confined, giving the appearance of more soliton-like propagation. This behaviour is also evident in the evolution of the Q factor, where it can be seen that although the small amount of breathing

leads to some variation in the Q values, generally the transmitted pattern can be detected at any point along the propagation. The evidence of more soliton-like behaviour is also evident in Figure 7.7, where a solitary peak of optimal performance can be seen. Away from this peak, the dependence shows similarities with those from maps 1 and 2.

True DM soliton behaviour is observable in map 4, which can be seen in Figure 7.8. In this case, the high-powered pulses display a short rapid breathing motion that results in the transmitted pattern being maintained continuously throughout propagation. This is evident from the Q value evolution in Figure 7.8(b). Observation of Figure 7.9 confirms the soliton-like nature of the propagation in map 4 due to the sharp peaks that are clearly evident. The strongest of the peaks in Figure 7.9 occurs for the critical map strength $S_c = 1.65$ where interactions between neighbouring DM solitons are minimised [127]. An interesting feature is that for $S = S_c/2$ and $S = 2S_c$ we observe two resonant performance peaks. Away from these peaks, performance is considerably degraded.

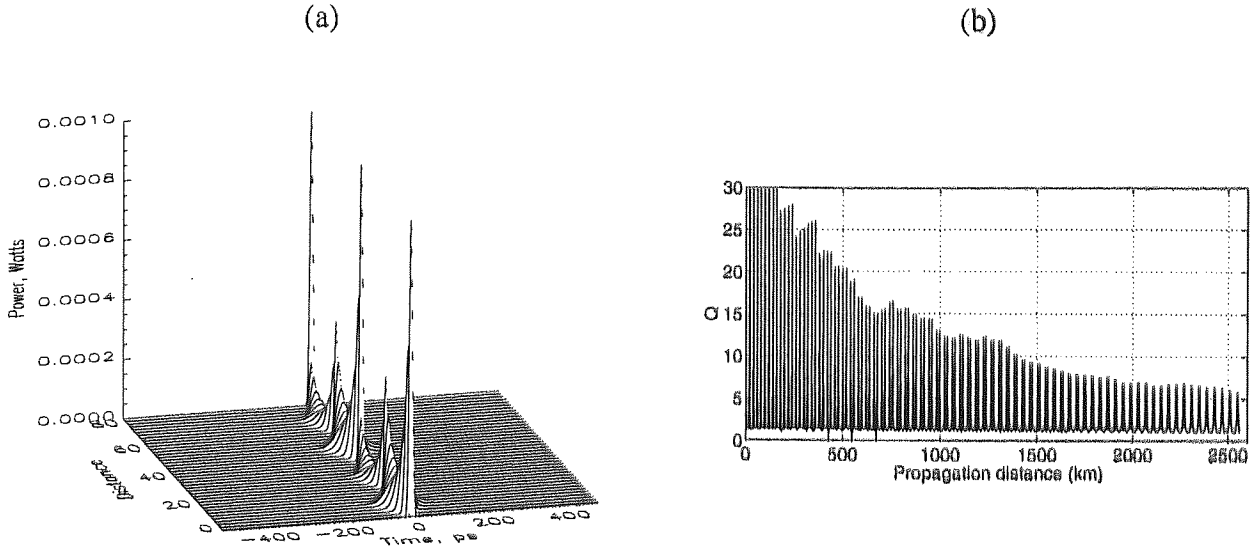

Figure 7.2: Propagation in dispersion map 1. (a) Single pulse propagation over 2 dispersion management periods (τ = 10 ps) and (b) evolution of Q as a function of propagation distance for P_0 = 0 dBm and τ = 10 ps.

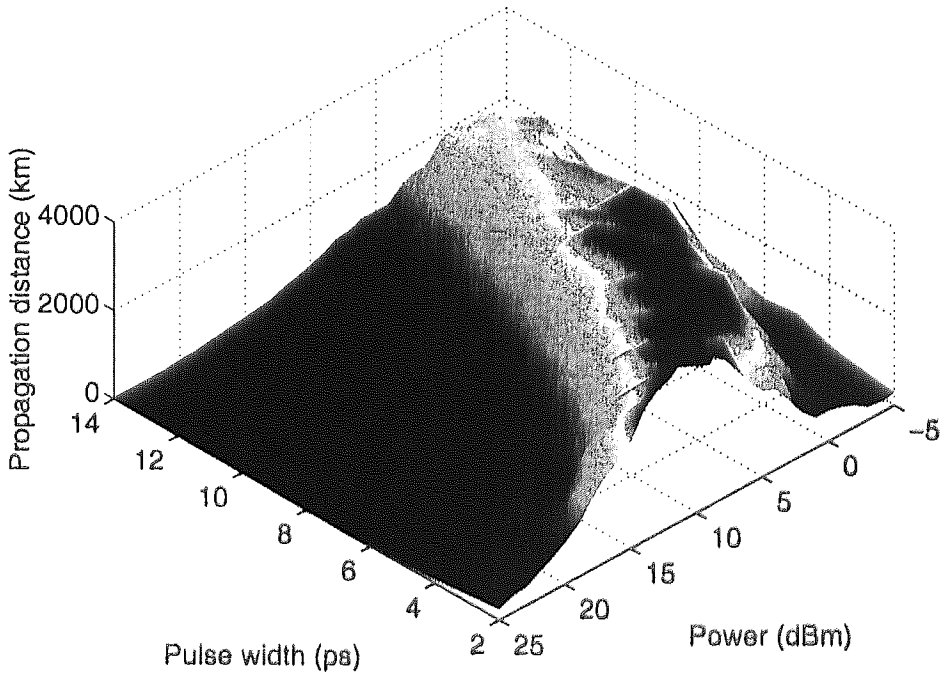

Figure 7.3: Surface plot detailing the system dependence on pulse width and initial power for 40 Gbit/s transmission using dispersion map 1.

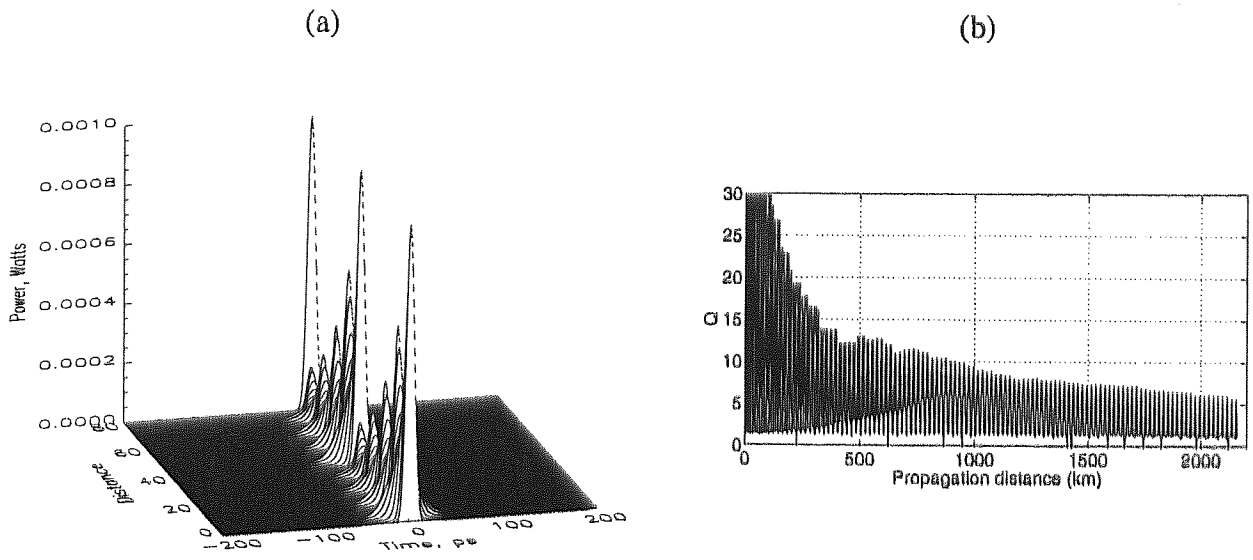

Figure 7.4: Propagation in dispersion map 2. (a) Single pulse propagation over 2 dispersion management periods (τ = 10 ps) and (b) evolution of Q as a function of propagation distance for P_0 = -2 dBm and τ = 10 ps.

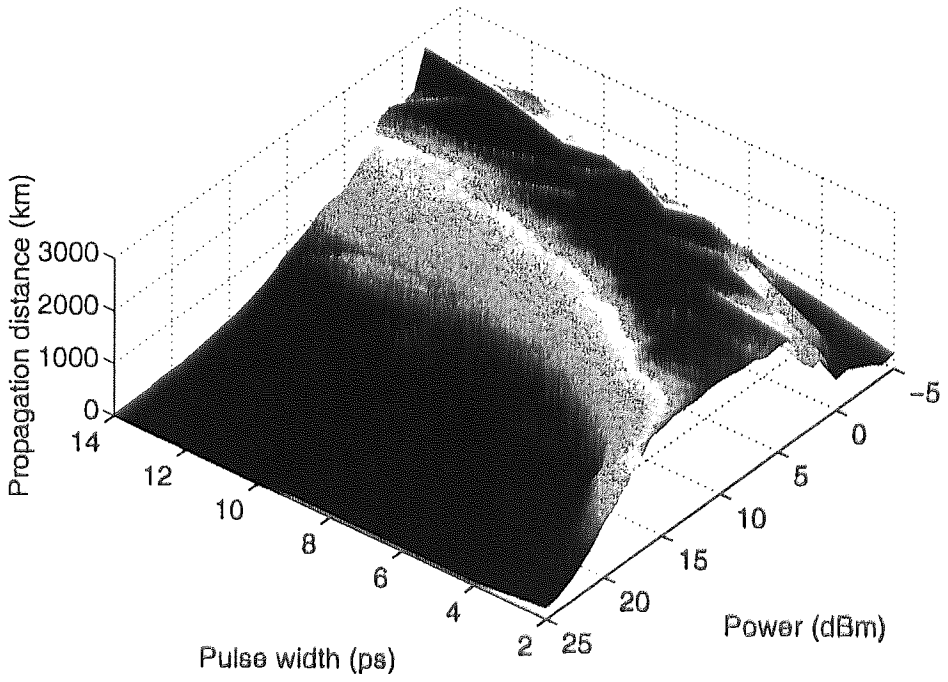

Figure 7.5: Surface plot detailing the system dependence on pulse width and initial power for 40 Gbit/s transmission using dispersion map 2.

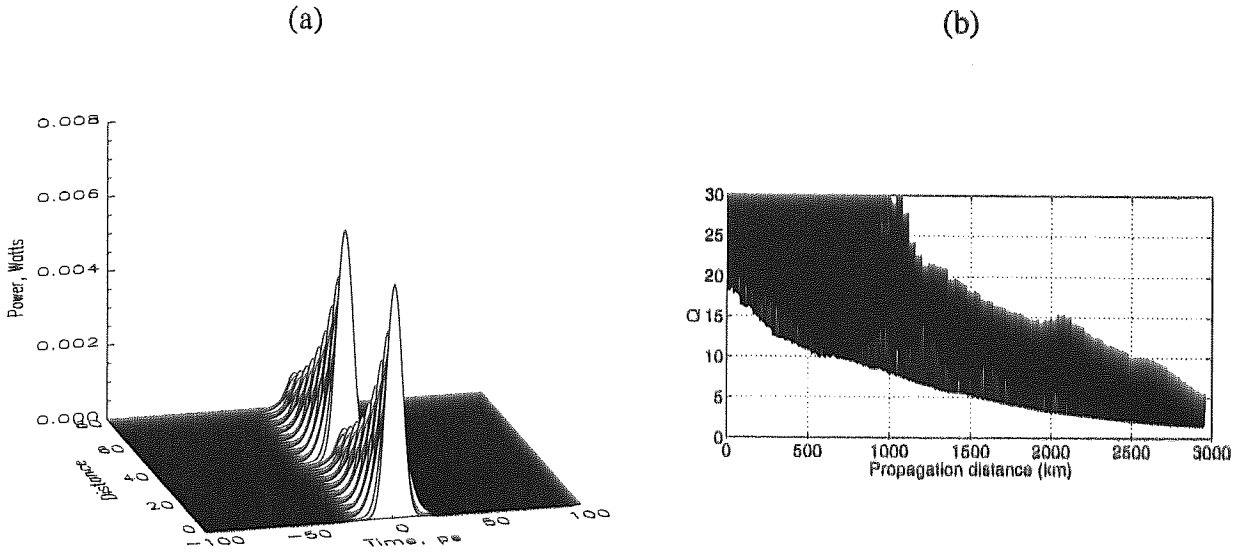

Figure 7.6: Propagation in dispersion map 3. (a) Single pulse propagation over 2 dispersion management periods (τ = 10 ps) and (b) evolution of Q as a function of propagation distance for P_0 = 6 dBm and τ = 10 ps.

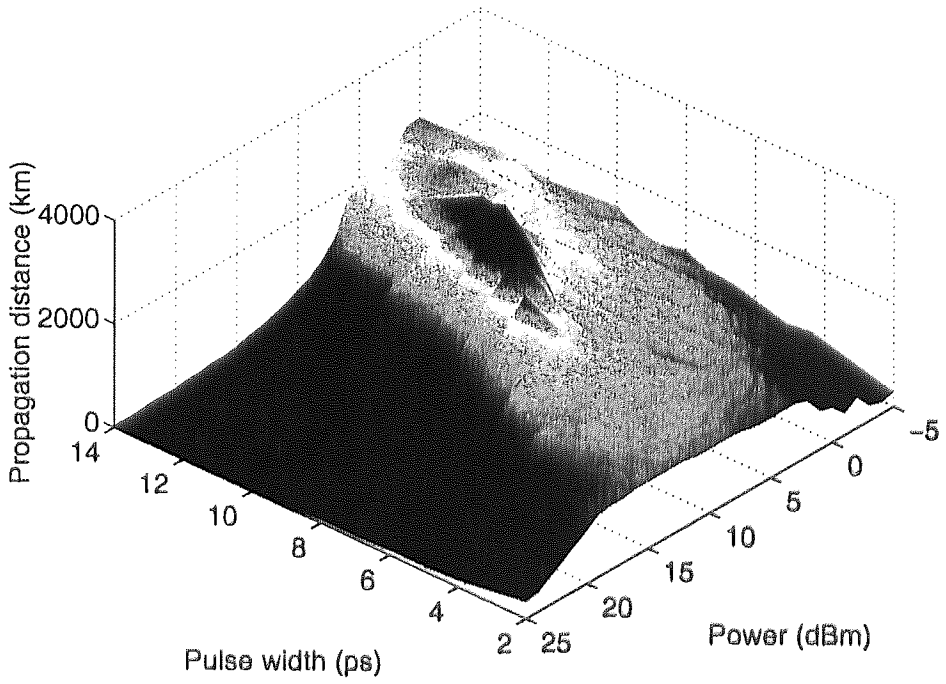

Figure 7.7: Surface plot detailing the system dependence on pulse width and initial power for 40 Gbit/s transmission using dispersion map 3.

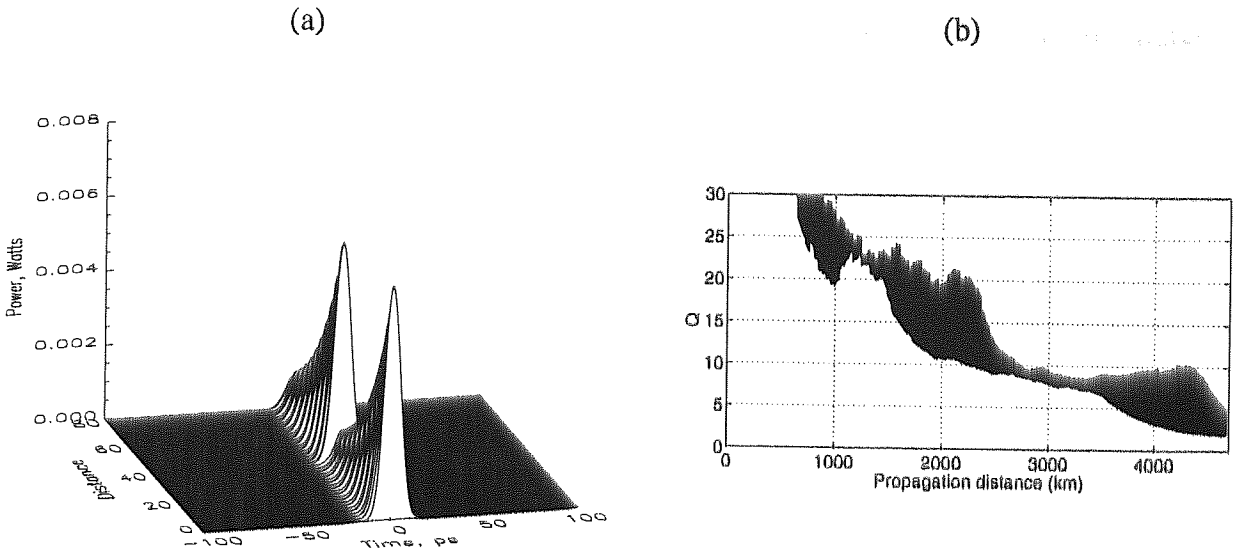

Figure 7.8: Propagation in dispersion map 4. (a) Single pulse propagation over 2 dispersion management periods (τ = 10 ps) and (b) evolution of Q as a function of propagation distance for P_0 = 7 dBm and τ = 10 ps.

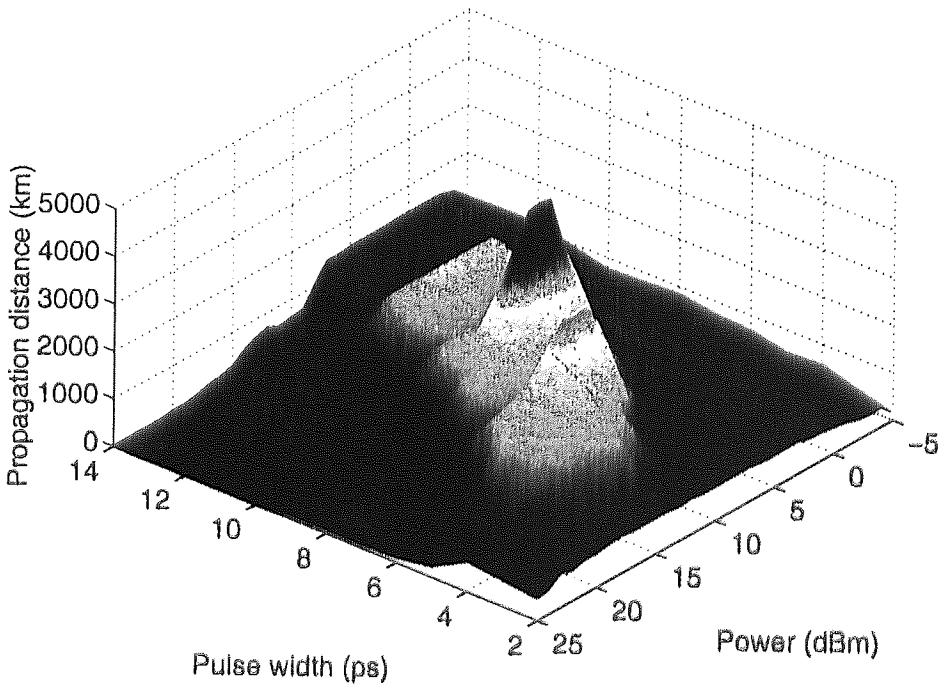

Figure 7.9: Surface plot detailing the system dependence on pulse width and initial power for 40 Gbit/s transmission using dispersion map 4.

7.4 WDM Transmission

Having investigated single channel transmission at 40 Gbit/s, we take a subset of the pulse widths used in section 7.3 and investigate WDM transmission using 4 channels. Throughout, we fix the channel spacing ΔC = 150 GHz, which scales to achieve 1 Tbit/s transmission capacity from a single EDFA window. Figure 7.10 through to Figure 7.13 display both 1x40 Gbit/s single channel and 4x40 Gbit/s transmission for pulse widths τ = 8, 9, 10, 12, 14 ps for maps 1 to 4.

In the case of map 1, we observe that in general WDM performance is limited by that of the single channel, which in this case is Intra-Channel Four Wave Mixing (ICFWM). Also it can be seen that the maximum propagation distance achieved is similar for each of the pulse widths investigated. Another interesting point from Figure 7.10 is that the optimal power for WDM transmission is far greater than the power for optimal single channel performance.

A similar phenomenon is noticeable in Figure 7.11 but with a general reduction in performance relative to map 1. Again, there appears to be little sensitivity of the WDM performance on pulse width, but this is a result of the poor performance of the single channel.

In Figure 7.12, we observe a departure from the previous behaviour of Figure 7.10 and Figure 7.11. It can be seen that the optimal initial power now coincides for both single channel and WDM transmission and that a large WDM penalty is incurred. In general, the maximum achievable transmission distance for WDM is approximately half that achievable for single channel transmission.

For the soliton-like propagation in Figure 7.13, it can clearly be seen that a large WDM penalty is occurring at the optimal initial power. For certain pulse widths the maximum WDM distance is approximately a quarter of the maximum single channel transmission distance. In addition, whilst the single channel transmission displays a dependence on the pulse width, the WDM performance remains largely invariant with respect to the pulse widths investigated.

Therefore, if we take a pulse width of 10 ps and contrast the performance obtained from each of the dispersion maps, we observe that although significant variations in single channel

performance, the maximum achievable WDM distance is extremely similar. However, what is different is the limiting factors of the systems. For maps 1 and 2, we observe that WDM performance is limited by the performance of the single channel, i.e. ICFWM. For maps 2 and 3, where the propagation is more soliton like, we observe large penalties occurring from inter channel effects such as FWM and XPM.

From the previous analysis, it is apparent that the inter channel interaction process behaves differently for each of the dispersion maps investigated. We can achieve a better understanding of this interaction process by investigating the interactions between a pair of propagating pulses, separated by a channel spacing ΔC = 150 GHz. Figure 7.14 illustrates the frequency shift as a function of propagation distance for two pulses, with an initial temporal separation of 500 ps. The different inter channel collision mechanisms are clearly visible in Figure 7.14. For map 1, the interaction process takes place over a long distance, due to the large breathing of the pulses, however, from the frequency shift we can see that the collisions are not too severe, due to the low intensities of the pulses during temporal overlap. At the other extreme, in map 4 we observe that the inter channel collisions are shorter and more severe, which is a result of the reduced breathing and increased intensities of the pulses during temporal overlapping. Between the extremes of maps 1 and 4, we observe that for maps 2 and 3 a trade off between collision severity and collision length occurring. The post collision residual frequency shift is also increasing as the severity of the interaction increases. From Figure 7.14 it can be seen that the inter channel collision process can be controlled by adjusting the dispersion management period. Therefore, this offers the potential to optimise WDM transmission performance.

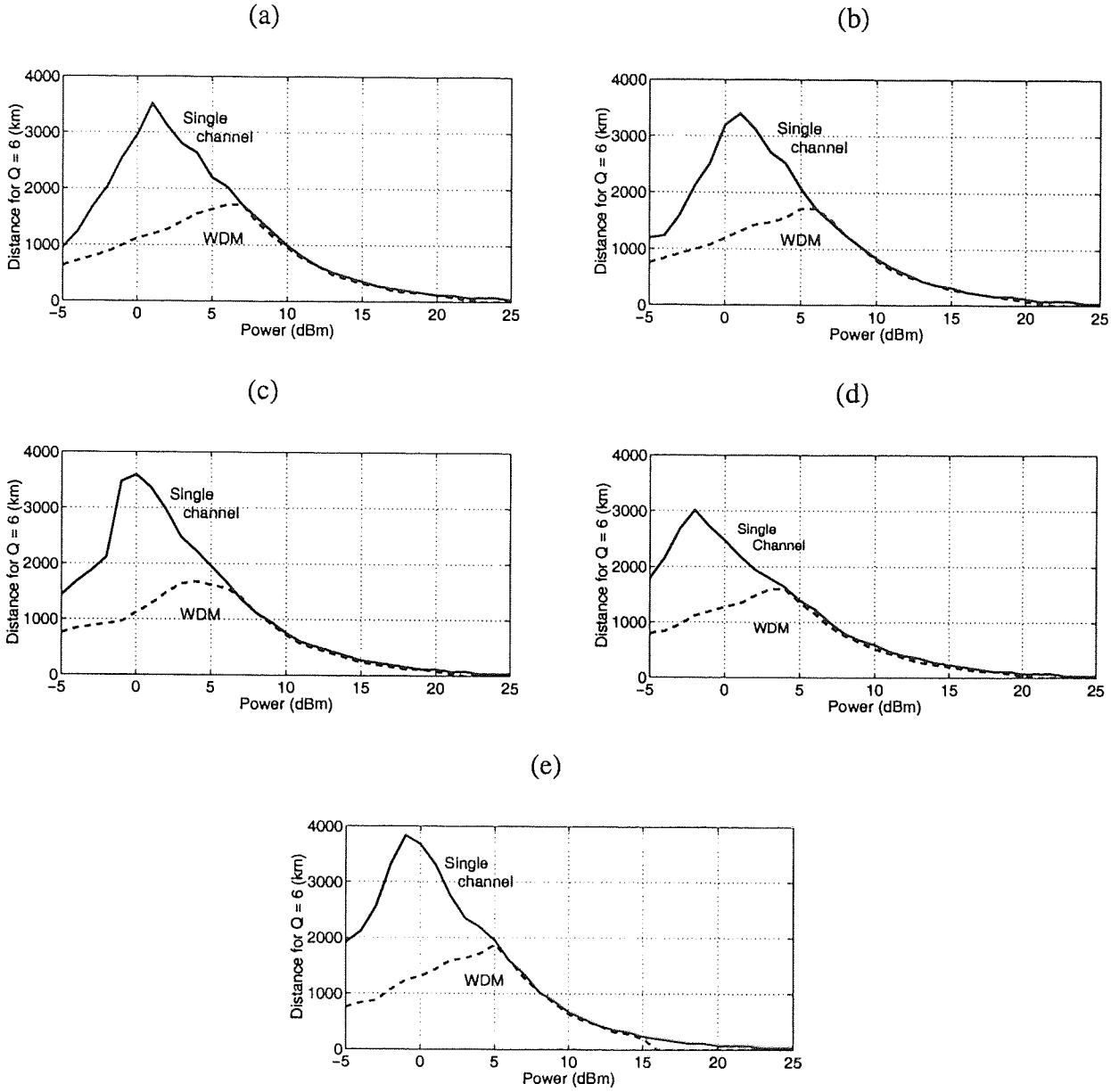

Figure 7.10: System performance as a function of input power for single channel 40 Gbit/s transmission and 4x40 Gbit/s WDM transmission for map 1, (a) $\tau = 8$ ps, (b) $\tau = 9$ ps, (c) $\tau = 10$ ps, (d) $\tau = 12$ ps and (e) $\tau = 14$ ps.

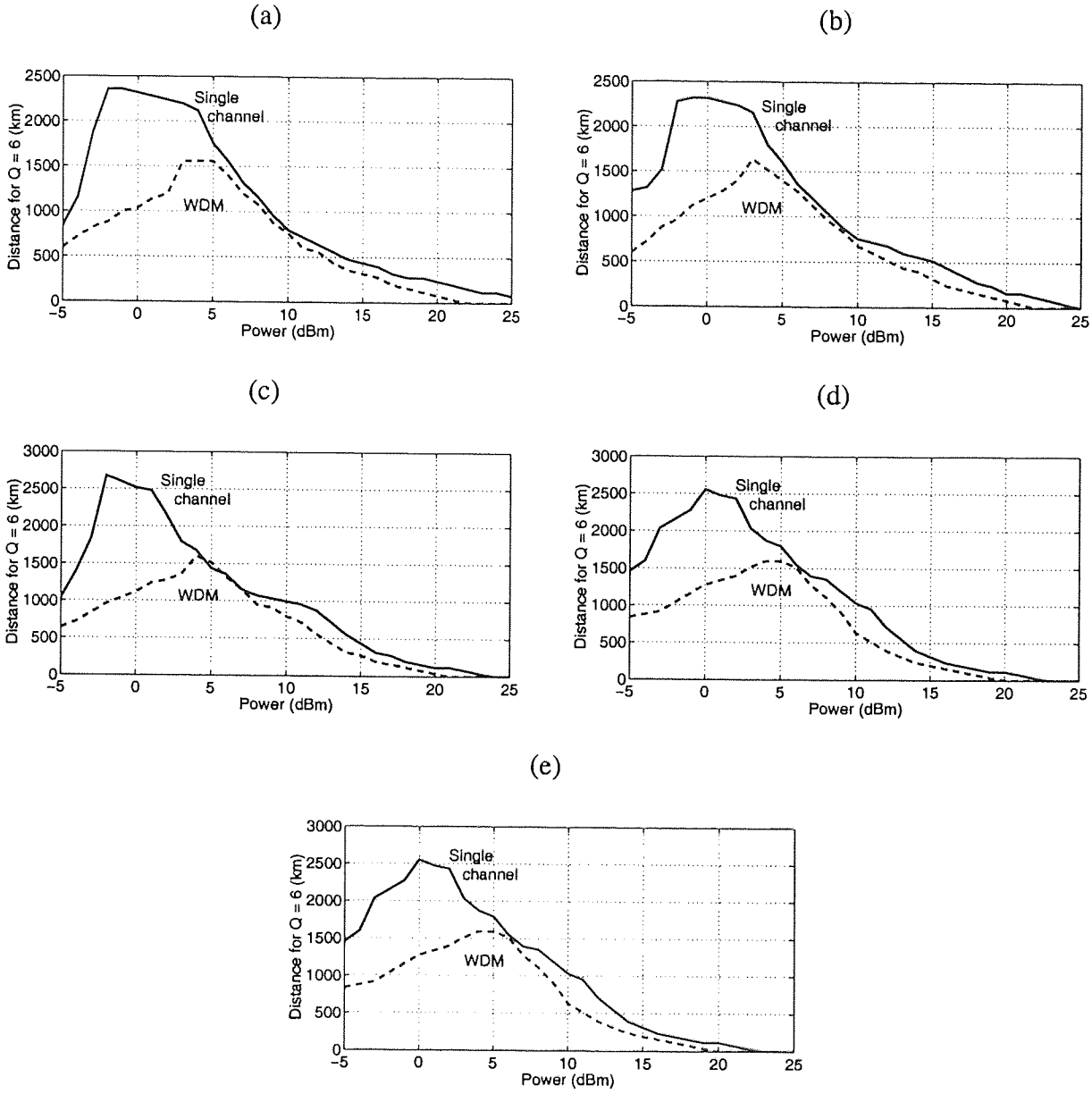

Figure 7.11: System performance as a function of input power for single channel 40 Gbit/s transmission and 4x40 Gbit/s WDM transmission for map 2, (a) $\tau = 8$ ps, (b) $\tau = 9$ ps, (c) $\tau = 10$ ps, (d) $\tau = 12$ ps and (e) $\tau = 14$ ps.

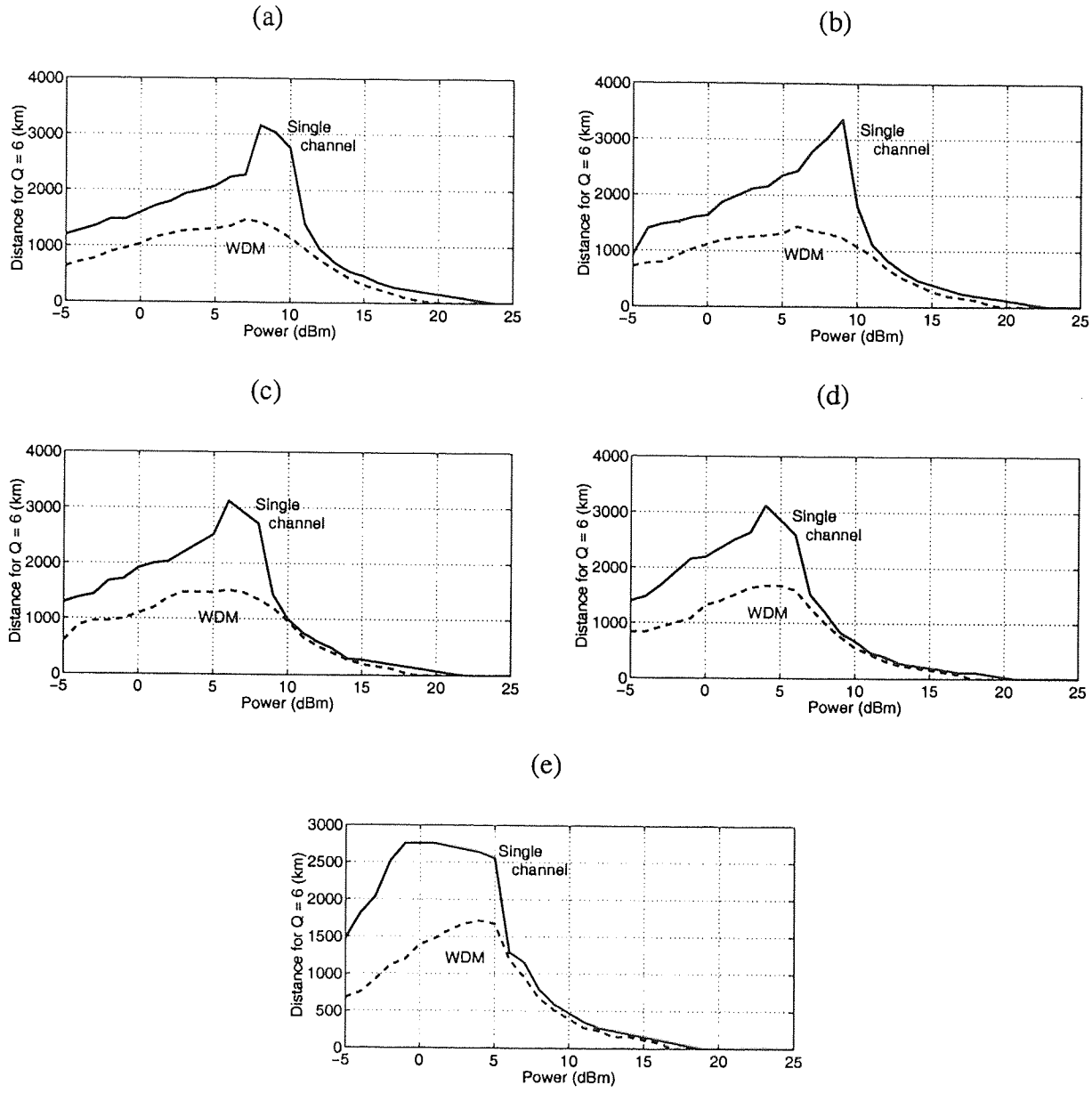

Figure 7.12: System performance as a function of input power for single channel 40 Gbit/s transmission and 4x40 Gbit/s WDM transmission for map 3, (a) $\tau = 8$ ps, (b) $\tau = 9$ ps, (c) $\tau = 10$ ps, (d) $\tau = 12$ ps and (e) $\tau = 14$ ps.

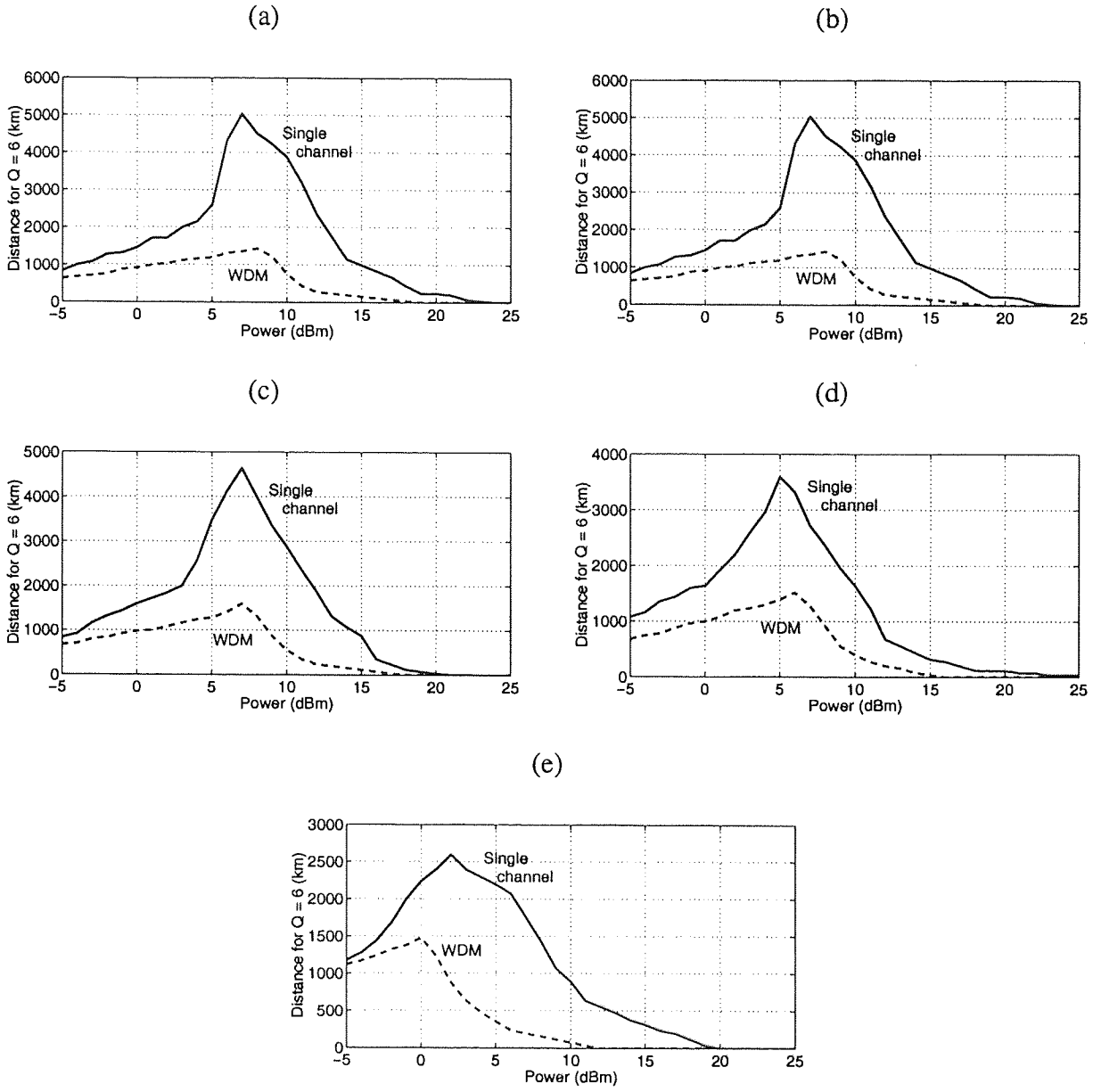

Figure 7.13: System performance as a function of input power for single channel 40 Gbit/s transmission and 4x40 Gbit/s WDM transmission for map 4, (a) $\tau = 8$ ps, (b) $\tau = 9$ ps, (c) $\tau = 10$ ps, (d) $\tau = 12$ ps and (e) $\tau = 14$ ps.

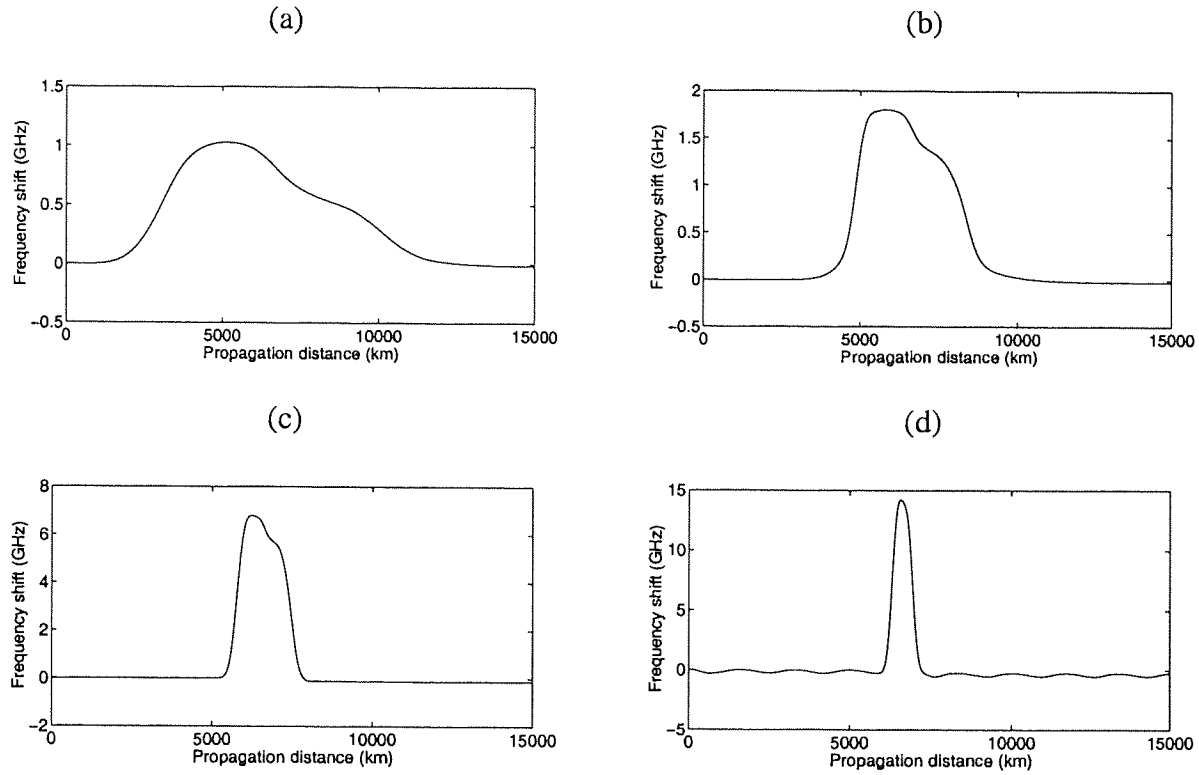

Figure 7.14: The frequency shift resulting from the inter channel interactions between a pair of DM solitons separated by a channel spacing of 150 GHz. (a) Map 1, (b) map 2, (c) map 3 and (d) map 4.

7.5 Optimisation of average dispersion

In the previous sections, we contrasted performance for a fixed average dispersion. However, each of the propagation regimes has differing values of optimal average dispersion. Therefore, to truly contrast propagation ranging from quasi-linear to soliton-like, we must optimise the average dispersion for each regime. Based on the findings in section 7.4, we confine our analysis to focus on pulse widths of 10 ps. Figure 7.15 illustrates the single channel performance as a function of average dispersion and initial power for each of the dispersion maps using a 10 ps pulse. For map 1, we observe the quasi-linear type dependence on average dispersion, i.e. reasonably insensitive, with an optimum corresponding to a normal average dispersion of –0.04

ps/nm/km. Map 2 shows a movement from the quasi-linear to the more soliton like propagation regime, in that performance is highly dependant on average dispersion and also contains a large performance peak for zero average dispersion. For map 3, this soliton-like dependence continues with the optimal average dispersion moving firmly into anomalous dispersion region. Also, we have a small region of high performance with performance declining rapidly as we move away from the optimal conditions. Finally, map 4 again exhibits strong single channel soliton-like performance. In addition, as the maps range from 1 to 4, it can be seen that the maximum achievable propagation also increases, where for soliton propagation a distance in excess of 7,000 km can be achieved.

Having optimised the average dispersion, we then seek to investigate how this influences the WDM performance. Figure 7.16 contrasts the optimal single channel and WDM performance for maps 1–4. Evident from Figure 7.16 is that large WDM penalties are incurred in maps 1 and 4, which arise from the inter channel collision processes described in section 7.4. For maps 2 and 3, we see that the differences in optimal performances between single channel and WDM are much smaller, so we are seeing the benefits of trading inter channel interaction severity with interaction length. The optimal WDM performance is actually achieved using map 3, with map 1 displaying the worst performance. However, only map 4 displays the potential of significantly increasing propagation distance for larger channel spacing, which would be required in transoceanic systems. It appears that for any significant propagation distance, the soliton-like propagation characteristics appear to exhibit the best performance.

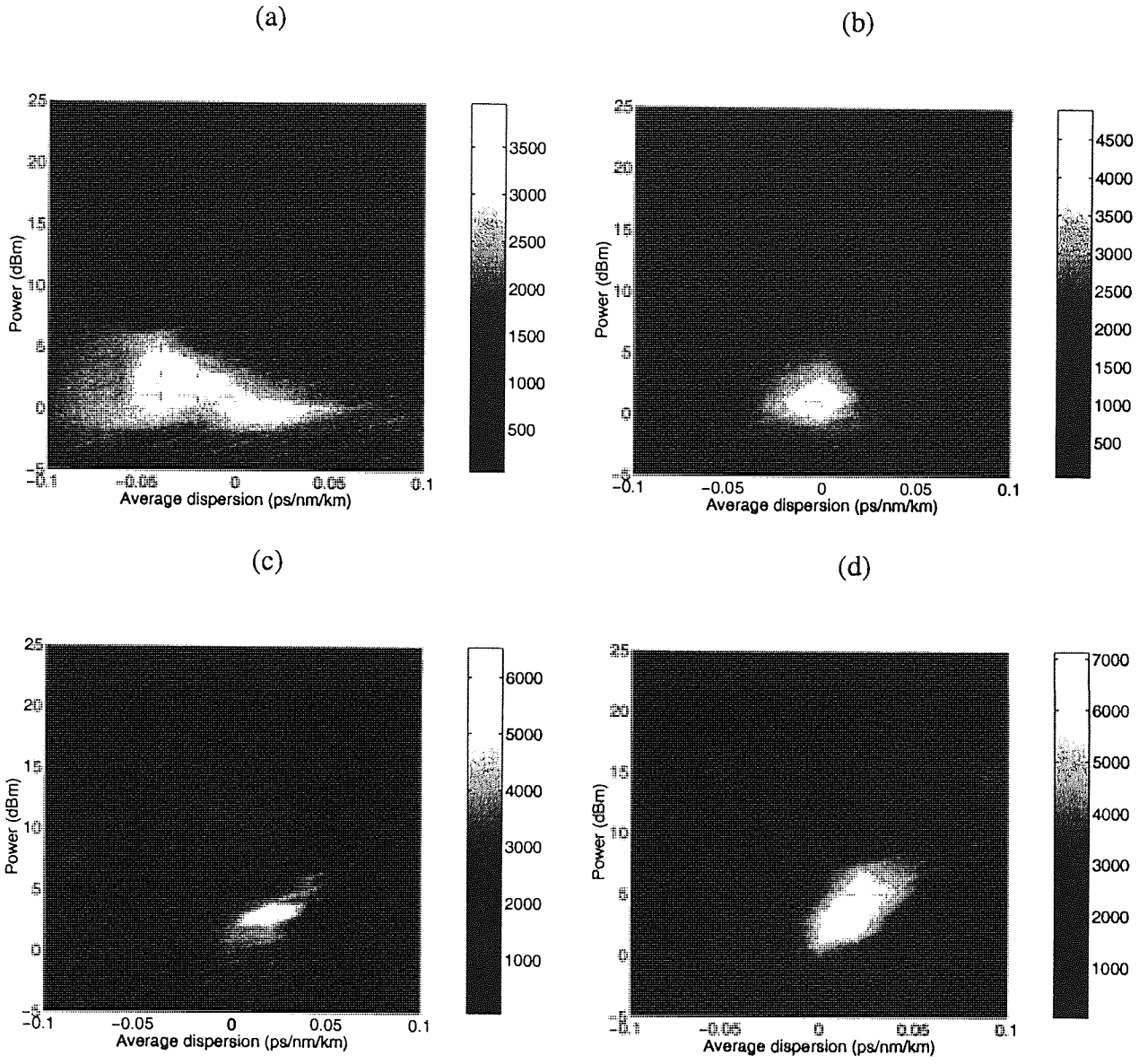

Figure 7.15: Optimisation of transmission distance as a function of average dispersion (D_{ave}) and initial power for a pulse width (τ) of 10 ps. (a) Map 1, (b) map 2, (c) map 3 and (d) map 4.

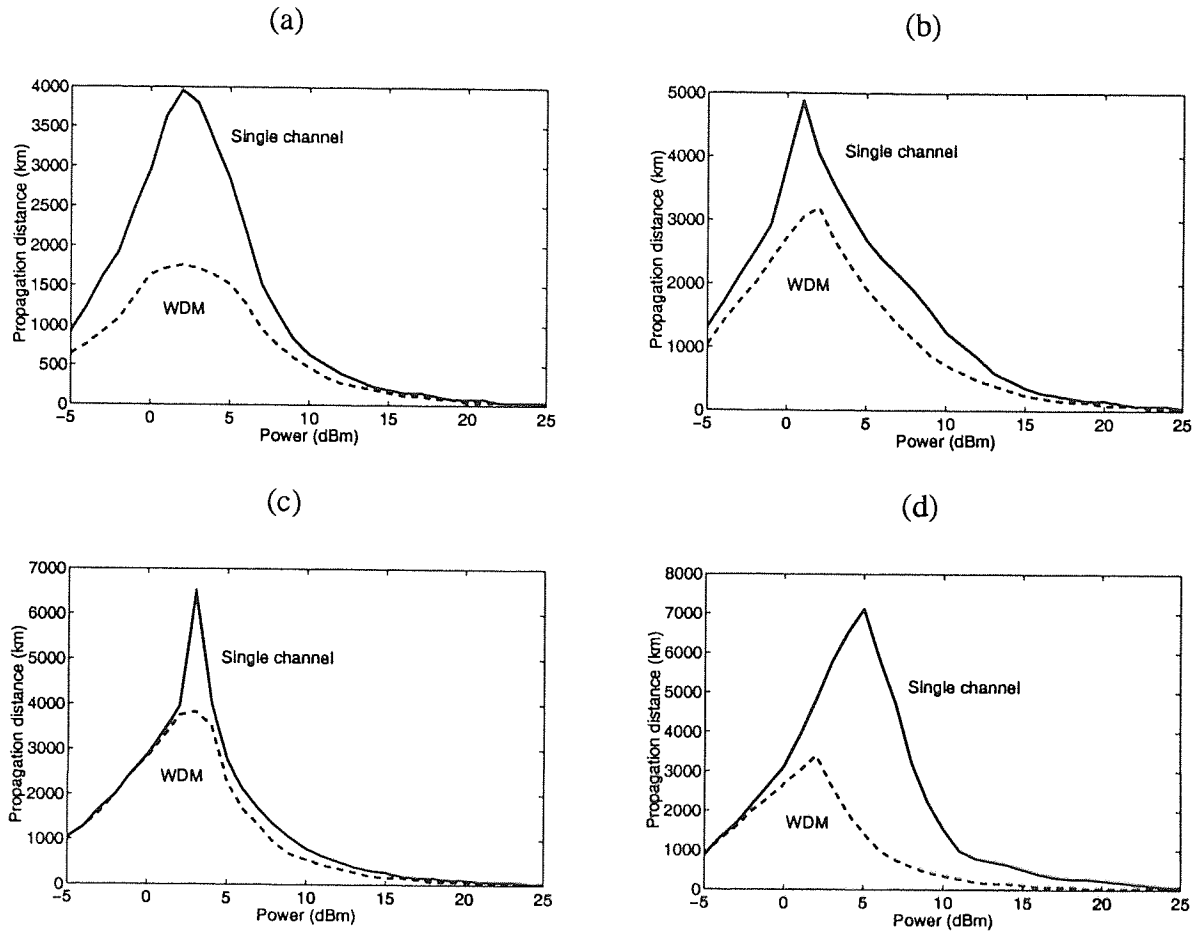

Figure 7.16: Optimal single channel and WDM performance for a pulse width (τ) of 10 ps. (a) Map 1, D_{ave} = -0.04 ps/nm/km, (b) map 2, D_{ave} = 0 ps/nm/km, (c) map 3, D_{ave} = 0.02 ps/nm/km, and (d) map 4, D_{ave} = 0.02 ps/nm/km,

7.6 Optimisation of quasi-linear transmission

Having contrasted the performance of both quasi-linear and DM soliton transmission, we next focus on how performance of quasi-linear systems, which appear abundantly in the published literature [10, 198, 237-239], can be improved. As demonstrated in the previous section, quasi-linear propagation is severely limited by non-linear effects, which impose severe restrictions on the achievable transmission distance. Our motivation is to investigate techniques that can be applied in general to quasi-linear systems.

To investigate the quasi-linear regime we select a dispersion map as shown in Figure 7.17. This dispersion map is constructed from SMF and RDF fibre sections with $Z_p = Z_a = 40$ km and is analogous to map 1 from section 7.2. In such a dispersion map, the dispersion is high enough to enable quasi-linear propagation for pulse widths suitable for 40 Gbit/s transmission.

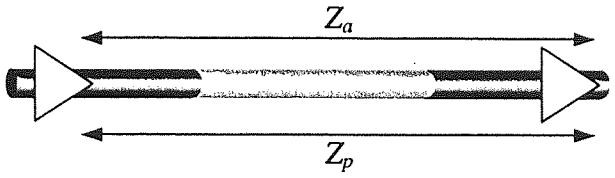

Figure 7.17: Schematic representation of the dispersion map used to investigate quasi-linear propagation. $Z_a = Z_p =$ 40 km.

As described previously in this chapter, the overwhelming limiting factor in quasi-linear systems is Intra-channel Four Wave Mixing (ICFWM), which results in both amplitude jitter and the generation of ghost pulses. Although regimes have been identified for which ICFWM is minimised [240], it still seriously limits the reach of these systems. As ICFWM manifests through the Kerr nonlinearity, which is also responsible for SPM and XPM, reducing the non-linear phase shift should also decrease ICFWM. A prediction from the analytical work of Zakharov *et al.* [241] suggests that the non-linear phase shift decreases with increasing S and therefore subsequent improvements in transmission should be achieved. This hypothesis is tested using the dispersion illustrated in Figure 7.17 for 40 Gbit/s transmission, where performance is equated using Q value estimates taken from a 2^7-1 PRBS, with the inclusion of higher order non-linear and dispersive effects. The Simulation results are shown in Figure 7.18.

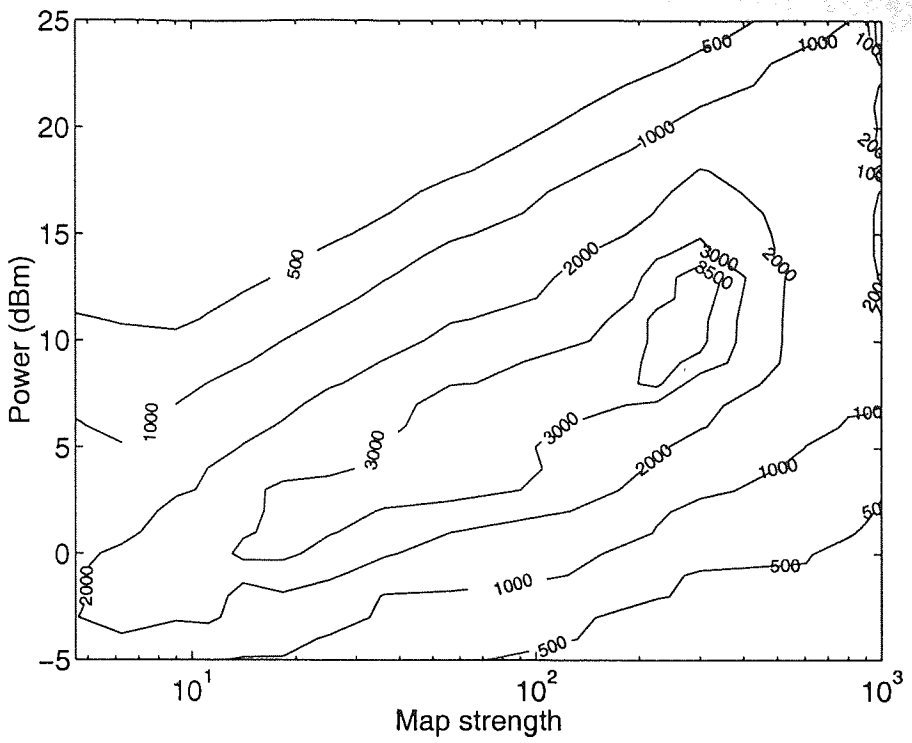

Figure 7.18: System performance illustrated as a function of initial power and map strength. Simulation parameters D_{ave} = 0.05 ps/nm/km and D_{rs} = 0.01 ps/nm^2/km.

Figure 7.18 illustrates the dependence of quasi-linear propagation on the strength of the dispersion management, where S is varied by adjustment of the pulse width only. The predicted strong dependence of transmission performance on S is clearly visible, with performance increasing with S up to a region where optimal performance is achieved for $S \approx$ 200-300. For stronger values of S (> 300), we observe a saturation in the reduction of the non-linear phase shift and also higher order non-linear effects become increasingly important, although the rapid decline in performance, that would be observed in a soliton-based system under these conditions, is not apparent, due to the massive breathing of the pulses. Therefore, provided that the pulse width does not become too short, improvements in performance can be gained by increasing S.

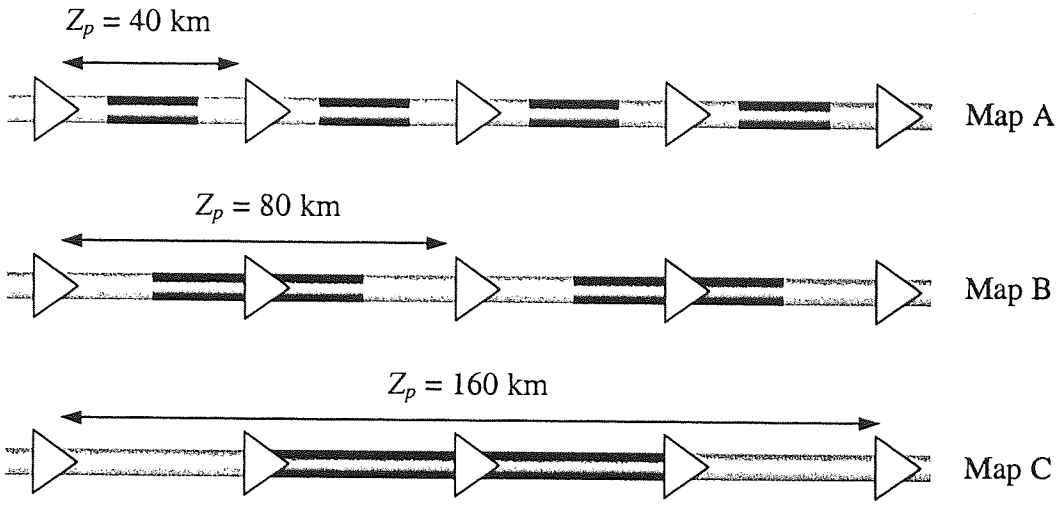

Figure 7.19: Schematic representation of the 3 dispersion maps constructed from SMF and RDF fibre sections, used to investigate the effects of increasing the dispersion management period for a fixed amplifier span.

Figure 7.18 indicates that stronger map strengths, up to the point where higher order non-linear effects become significant, are better for quasi-linear transmission. In a dispersion-managed system, the simplest means by which S can be varied is to alter Z_p (assume Z_a is fixed). Therefore continuing with the SMF and RDF fibre types, we investigate three different dispersion management periods, as illustrated in Figure 7.19. For map A, Z_p = 40 km, for map B, Z_p = 80 km and for map C, Z_p = 160 km, therefore in terms of map strength, map B is twice as strong as map A and map C is twice as strong as map B. Figure 7.20 demonstrates the effect changing Z_p has on transmission performance for 10 ps pulses. Figure 7.20 reveals that the dependence of system performance on S is more complex and cannot be universally extrapolated from the results in Figure 7.18. The inferior performance observed for increasing Z_p can be attributed to the amount of physical time that the pulses remain overlapped, which increases ICFWM. With these constraints in mind, the results indicate that increasing the magnitude of the fibre dispersion may be a superior way of increasing the map strength in quasi-linear systems.

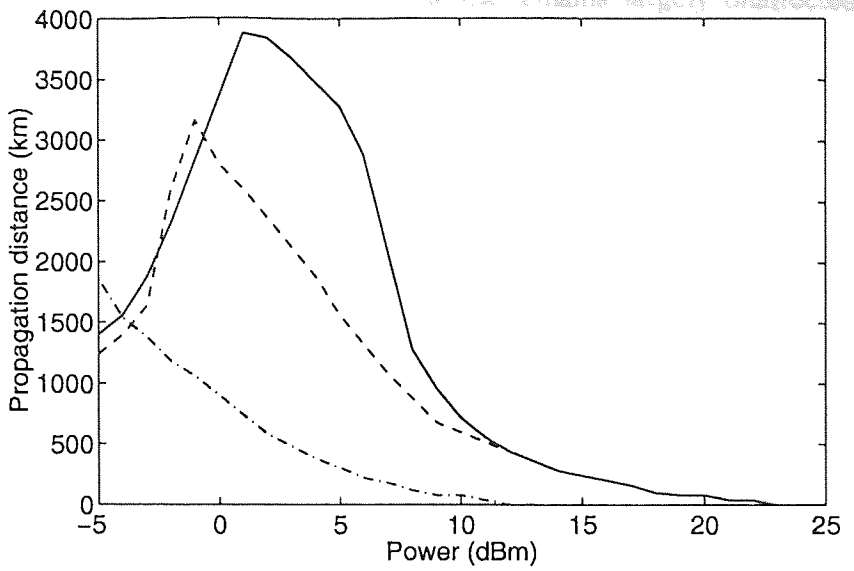

Figure 7.20: System performance at 40 Gbit/s as a function of initial power for $\tau = 10$ ps and $Z_a = 40$ km. (*solid line*) Map A, $Z_p = 40$ km, (*dashed line*) Map B, $Z_p = 80$ km and (*dot and dash line*) Map C, $Z_p = 160$ km.

7.6.1 Pulse shape optimisation for quasi-linear transmission

Another prediction from the analytics of Zakharov *et al.* [241], was that the non-linear phase shift is also dependant on the spectral intensity of the pulse. In other words, for a fixed pulse width, the spectral intensity can be changed by varying the pulse shape. Therefore, the steeper the edges of the pulses are then the larger the bandwidth, which in turn reduces the intensity of the constituent frequency components.

Again using SMF and RDF fibre sections with $Z_a = Z_p = 40$ km, $D_{rs} = 0$ ps/nm/km and $\tau = 10$ ps (FWHM) transmission performance is contrasted again at 40 Gbit/s for hyperbolic secant and super Gaussian shaped pulses. The simulations results are shown in Figure 7.21. Observations of Figure 7.21 reveal that although the general dependence is broadly similar, the region of optimal performance is considerably larger for the super Gaussian pulses of order 2 and above. Simulations results showed that the Gaussian and hyperbolic secant pulses displayed an extremely similar dependence. Likewise, for super Gaussian pulses of order 2 and above, transmission performance exhibited a similar behaviour, which indicates a saturation of the phenomenon. Also apparent from Figure 7.21, and the simulations of the other pulse shapes, is

that performance away from the optimal conditions remains largely unaffected by the shape, indicating that other effects dominate performance in these regions.

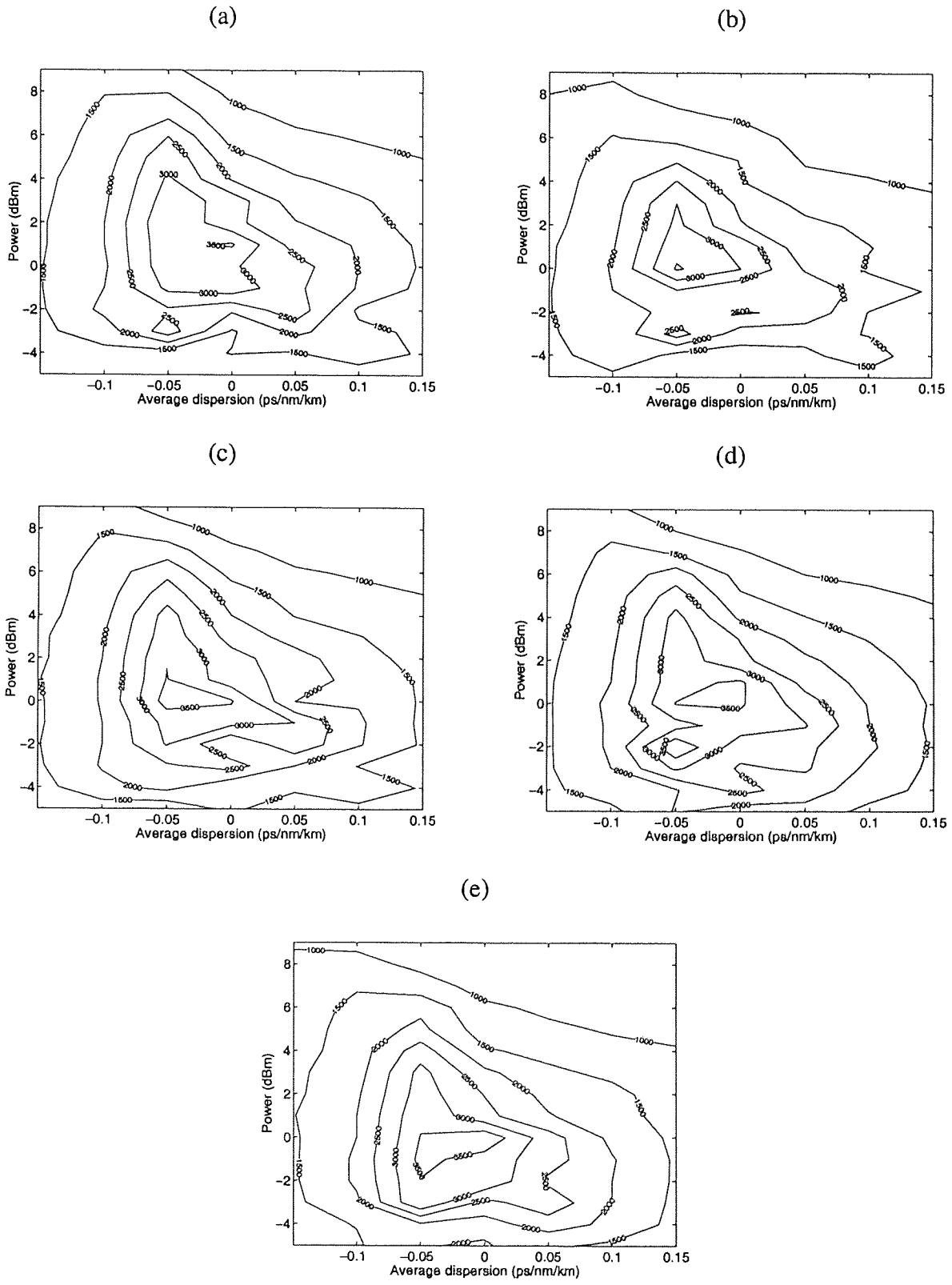

Figure 7.21: Propagation distance as a function of initial power and average dispersion for a pulse width of 10 ps (FWHM). (*a*) Gaussian pulse, (*b*) Hyperbolic secant pulse, (*c*) a super Gaussian pulse of order 2, (*d*) a super Gaussian pulse of order 3 and (*e*) super Gaussian pulse of order 100.

7.7 Pulse shape optimisation for soliton-like transmission

Having demonstrated in section 7.6.1 the performance improvements achieved from optimisation of the pulse shape, we next focus on ways in which the pulse shape can be optimised for soliton-like systems. Transmission using soliton-like propagation is limited mainly by interactions between adjacent pulses. Interactions in such systems manifest through a combination of coherent and incoherent interactions. In incoherent interactions, the process takes place through the nonlinearity whereas for coherent interactions, although the process is identical, it is aided by overlapping of pulse tails. When the motivation is spectral efficiency, adjacent pulse tails overlap which fuels coherent interactions. Previously, techniques such as phase alternation have been used to reduce the coherence of the pulse tails, thus reducing interactions [156]. However, influence of coherent interactions could be diminished by simply reducing the tails of the pulses, for an identical FWHM pulse width. Suitable pulse shapes for comparison are hyperbolic secant, Gaussian and parabolic, which are illustrated in Figure 7.22. Clearly evident are the reduced tails of the parabolic shaped pulses relative to those of the hyperbolic secant and Gaussian pulse shapes.

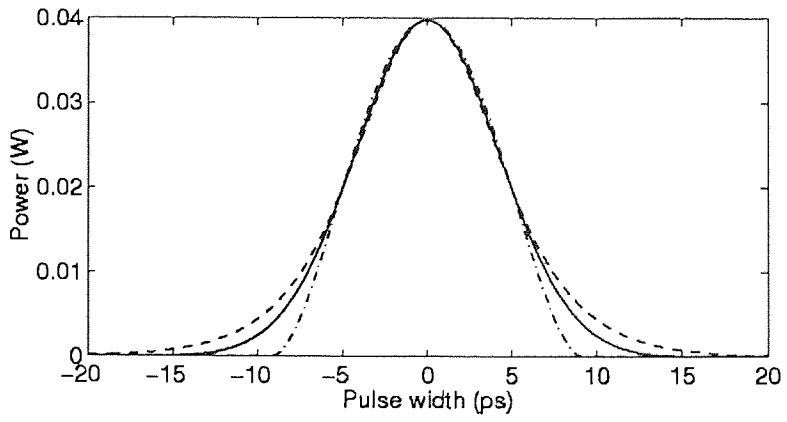

Figure 7.22: Comparison of shapes for a 10 ps (FWHM) pulse. (*dashed line*) hyperbolic secant, (*solid line*) Gaussian and (*dot and dash line*) parabolic.

To maintain continuity with the rest of the results in this chapter, we investigation this propagation regime using SMF and RDF fibre sections with the condition $Z_a = 5Z_p$, where Z_a = 40 km. Therefore, the dispersion map strength is close to the optimal conditions for interactions as described in Ref. [127]. Figure 7.23 illustrates transmission performance as a function of initial power for the three pulse shapes detailed in Figure 7.22. It is apparent that the hyperbolic secant shaped pulses have the worst performance of the three pulses. The Gaussian shaped pulses exhibit a similar dependence to the hyperbolic secant pulses at low powers, but as the power increases, improved performance is achieved by the Gaussian pulses. This improvement of performance can be directly attributed to the reduced tails of the Gaussian pulse relative to the hyperbolic secant pulse.

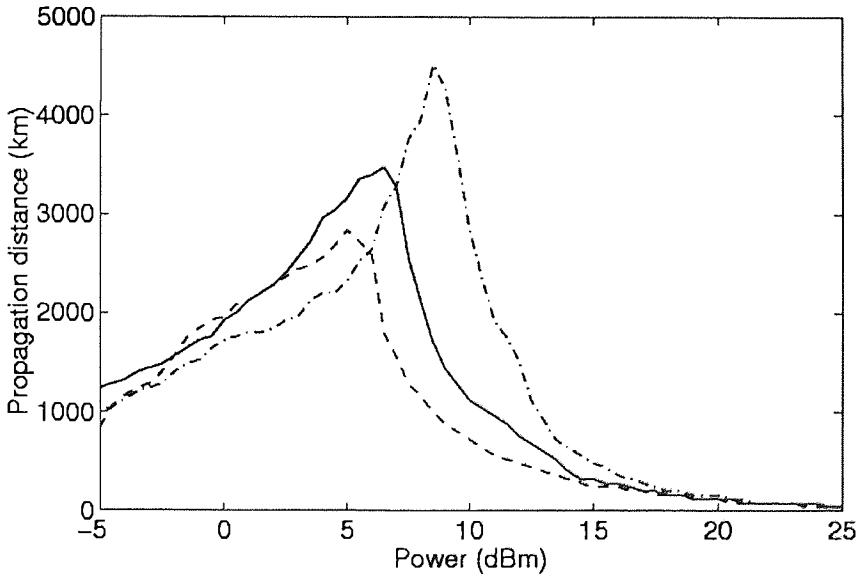

Figure 7.23: A comparison of transmission performance at 40 Gbit/s using 10 ps FWHM pulses. (*dashed line*) hyperbolic secant, (*solid line*) Gaussian and (*dot and dash line*) parabolic.

The best performance in Figure 7.23 is achieved using parabolic pulses. Also it can be seen that the optimal initial power has increased which shows that SNR is improved as a consequence of reduced interactions. Another interesting feature of Figure 7.23 is that for lower powers the parabolic shaped pulse performs worse than the Gaussian and hyperbolic secant

pulses. This poorer performance can be attributed to the imbalance between the non-linear and dispersive effects for this pulse shape at these lower powers. For stronger map strengths, interactions tend to be dominated by coherent interaction, unless the pulses are extremely well separated, in such cases the use of parabolic pulses will bring little improvement in system performance.

7.8 Conclusion

In conclusion, we have investigated dispersion managed propagation regimes ranging from quasi-linear to soliton-like. The simulation results indicate that for the case of a fixed average dispersion all 4 dispersion maps have similar achieved propagation distances for WDM transmission. However, for each of the maps, we observed different constraints on the systems. For quasi-linear transmission, performance was limited by ICFWM, whereas for soliton-like propagation inter channel effects dominated. Analysis of the inter channel interaction process revealed that the in quasi-linear systems the interaction process takes place over a long length of time, where as for soliton propagation this process is much swifter. For the regimes between these 2 extremes, we found that the length and severity of the inter channel collisions could be exchanged, leading to an improvement in performance. We demonstrated this by optimising the average dispersion for each propagation regime, where we found that the best performance was achieved using map 3, which had the smallest WDM penalty. In addition, only map 4 displays the potential of significantly increasing propagation distance for larger channel spacing, which would be required in transoceanic systems.

We also demonstrated that transmission performance in quasi-linear systems could be further improved by optimising both the dispersion map strength and the pulse shape. We observed that performance increases with increasing S until higher order non-linear effects become significant, and that the dependence on S is not unconditional, where for long Z_p, ICFWM builds due to the amount overlapping between pulses. In addition, enhancements in

performance can be achieved by optimisation of the carrier pulse shape to reduce the non-linear phase shift. These simulation results are in good agreement with previous analytical results [241].

For soliton based systems, we showed that transmission performance could be improved by using a pulse shape which has smaller tails than the conventional pulse shapes used in dispersion managed systems.

Chapter 8 Conclusion

This thesis has presented the results of numerical simulations of high bit rate dispersion managed optical communication systems. Initially, the background theories of pulse propagation in optical fibres and dispersion management were presented in chapters 2 and 3. The results of the thesis can be broadly grouped into 2 main areas. Firstly, soliton-like propagation in short period dispersion managed system is investigated in chapters 3, 4, 5 and 6. Secondly, the performance of soliton-like and quasi-linear propagation is contrasted for both single channel and WDM transmission is investigated in chapter 7.

Chapter 3 investigated how the properties of the DM soliton depend on the ratio Z_p:Z_a in a short period dispersion management regime characterised by $Z_p << Z_a$. The results showed that DM solitons in SPDMs exhibited a similar behaviour relative to DM solitons in the conventional dispersion management regime characterised by $Z_p \geq Z_a$. The DM solitons in SPDMs displayed a greater SNR for an identical map strength, which is a direct consequence of the increased depth of the dispersion map, with the dependence on map depth taking a similar form as predicted for conventional dispersion managed systems. Thus, interactions between neighbouring solitons also increased. In addition, as Z_p becomes increasingly smaller than Z_a, DM solitons become less dependant on the amplifier position within the dispersion map.

Additionally in this chapter, the implication of the amplifier location with dispersion maps was investigated. It was found that when periodic fibre loss and amplification are introduced into DM systems, the classic definition of the dispersion map strength no longer accurately characterises DM soliton propagation. In this case, the more complex definition of the effective average dispersion is required for accurate characterisation.

Chapter 4 determined the conditions under which single channel transmission at 80 Gbit/s could be achieved using soliton-like pulses in short period dispersion maps. The

simulation results indicated that transmission in excess of 9,000 km could be achieved by optimisation of the key system parameters, which was more robust that previous system simulations at 80 Gbit/s [141]. The main limiting factor of the system was the accumulation of noise generated by the amplifiers, due to the short pulse widths required to reduce interactions. Therefore, optimisation of the ASE filters was a critical factor in achieving the maximum propagation distance. Over shorter transmission distances, it was found that additional freedoms exist to trade interactions for SNR, thus improving the overall performance and tolerance of the system.

Embracing the results of chapter 4, chapter 5 determines the conditions under which transmission at 160 Gbit/s using short period dispersion management can be supported. At this data rate, the mark to space ratio is confined by the higher order non-linear and dispersive effects. Therefore, the jitter arising from the accumulation of noise along the transmission link is sufficient to induce interactions between adjacent DM solitons, which is main limiting factor of the system. The effects of polarisation mode dispersion also became increasingly important. However, the simulations demonstrated that transmission over transoceanic distances was still possible, although the performance depended critically on the initial conditions of the system.

Chapter 6 examines the robustness of short period dispersion managed transmission to a data rate of 320 Gbit/s. The short pulse width is now the overwhelming dominating factor, in terms of the increased higher order non-linear and dispersive effects, and the scaling of the DM soliton energy with the average dispersion. Therefore, both the residual dispersion and average dispersion must be strictly controlled. Limiting the accumulation of noise is also critical factor along with polarisation mode dispersion. The system is also sensitive to initial conditions. If the polarisation mode dispersion can be confined to the tolerable limits defined in chapter 6, then propagation in excess of 4,000 km can be achieved.

Finally, in chapter 7 the optimal propagation regimes for single channel and WDM 40 Gbit/s based transmission were investigated. The simulations show that in the case of single channel transmission, performance improved as the propagation became more soliton-like.

However, in the case of WDM transmission, the soliton-like propagation regime suffered large inter channel penalties, with the main limitation of quasi-linear systems arising from the inter channel interactions. Optimal performance was achieved by a propagation regime that lay between these two extremes of soliton-like and quasi-linear. In addition, ways in which transmission performance could be improved by optimising the carrier pulse shape in both soliton-like and quasi-linear propagation was investigated. In the case of soliton-like propagation, parabolic shaped pulses reduced interactions, whereas in the case of quasi-linear transmission systems, ICFWM could be reduced using super Gaussian shaped pulses.

8.1 Future work

One area of future work concerning the topics addressed in this thesis, is that of random variations of the fibre parameters in dispersion managed systems [242, 243], with specific reference to short period dispersion management [244, 245]. This is an important subject because of the process involved in the manufacture of short period dispersion maps. As Z_p becomes increasingly small, it becomes impractical to produce short period dispersion maps from splicing fibre section together due to both splicing loss and complexity. Therefore fibre where the short period dispersion maps are drawn into the fibre [142, 209], are required. However, a consequence of this manufacturing process is that random variations in the fibre parameters occur, which significantly impairs transmission performance, especially in short period dispersion maps where these perturbations accumulate more rapidly [245]. Therefore, work defining the tolerable limits of such variations would be of great importance.

Another area of future work would relate to investigating WDM transmission at 80, 160 and 320 Gbit/s, using the short period dispersion maps detailed in chapters 3,4 and 5. These systems offer the potential benefit of requiring less wavelengths to be used, which would require less guard bands between the wavelengths and improve overall spectral efficiency. The scope of this could be broadened to encompass data rates such as 20 and 40 Gbit/s, in order to find the

optimum data rate – number of channels combination for dispersion managed transmission [246].

Appendix A – Publications

- L.J. Richardson, W. Forysiak and N.J. Doran, "Energy dependence of dispersion managed solitons in short period dispersion maps", *Fourteenth Quantum Electronics Conference, Manchester (QE-14), UK, P2-30, p. 209*, Sept. 1999.

- L.J. Richardson, W. Forysiak and N.J. Doran, "Energy enhancement of short-period dispersion managed solitons", *Conference on Lasers and Electro-Optics (CLEO 2000), San Francisco, USA*, CMF7, pp. 32-33, May. 2000.

- L.J. Richardson and W. Forysiak, "Dispersion managed soliton propagation in amplified systems: A physical interpretation", *Conference on Lasers and Electro-Optics (CLEO 2000), San Francisco, USA*, CMF2, pp. 27-28, May. 2000.

- L.J. Richardson and W. Forysiak, "80 Gbit/s dispersion managed soliton transmission using short period dispersion management", *Postgraduate Research in Electronics and Photonics Conference (PREP 2000)*, Nottingham, UK, pp. 52-56, April 2000.

- L.J. Richardson, W. Forysiak and N.J. Doran, "Ultra high-speed 160 Gbit/s dispersion managed soliton transmission over 6,000 km using short period dispersion management", *Fifth OptoElectronics and Communications Conference (OECC 2000)*, Makuhari Messe, Chiba, Japan, 13A1-2, pp. 336-337, July 2000.

- L.J. Richardson and W. Forysiak, "Short period dispersion management", *Workshop on the Dispersion Managed Soliton*, Makuhari Messe, Chiba, Japan, July 2000.

- L.J. Richardson, W. Forysiak and N.J. Doran, "Dispersion-managed soliton propagation in short-period dispersion maps", *Optics Letters*, 25(14), pp. 1010-1012, 2000.

- L.J. Richardson, W. Forysiak and N.J. Doran, "320 Gbit/s single channel transmission over 4,500 km using short period dispersion management", *26th European Conference on Optical Communications (ECOC2000)*, Munich, West Germany, pp. 187-188, September 2000.

- V.K. Mezentsev, L.J. Richardson and S.K. Turitsyn, "Nonlinear regimes of high-bit-rate (80 and above Gb/s) optical data transmission", (Invited paper) *Research group on Optical Soliton Communications (ROSC) symposium*, Hakone, Japan, September 2000.

- S.K. Turitsyn, L.J. Richardson, E. Seve, V.K. Mezentsev, "System optimisation of 40 Gb/s per channel WDM transmission" (Invited paper) *Research Group on Optical Soliton Communications (ROSC) symposium*, Hakone, Japan, September 2000.

- L.J. Richardson, W. Forysiak and K.J. Blow, "Single channel 320 Gbit/s short period dispersion managed transmission over 6,000 km", *Electronics Letters*, 36(24), pp.2029-2030, 2000.

- L.J. Richardson and W.Forysiak, "Trans-oceanic 80 Gbit/s single channel transmission using short period dispersion management" *IEE Journal of Optoelectronics*, 147(6), pp.417-422, 2000.

- L.J. Richardson, V.K. Mezentsev and S.K. Turitsyn, "Limitations of 40 Gbit/s based WDM transmission: DM soliton versus quasi-linear propagation", *Optical Fibre Communications conference* (OFC 2001), Los Angeles, USA, March 2001.

- L.J. Richardson, W. Forysiak and N.J. Doran, "Trans-oceanic 160 Gbit/s transmission using short period dispersion management", *IEEE Photonics Technology Letters*, 13(3), pp. 209-211, 2001.

- L.J. Richardson, J.H.B. Nijhof and W. Forysiak, "An interpretation of the energy variations of dispersion managed solitons in terms of effective average dispersion", *Optics Communications*, 189(103), pp.63-67, 2001.

- L.J. Richardson, W. Forysiak, N.J. Doran and K.J. Blow, "Long-haul ultra high-speed transmission using dispersion managed solitons", *IEICE Transactions on Communications*, E84B(5), pp. 1159-1166, 2001.

- L.J. Richardson, K.J. Blow and V.K. Mezentsev, "Control of soliton-like propagation in short period dispersion maps with random parameters", *Non-Linear Guided Waves and their applications (NLGW 2001)*, Tampa, USA, March 2001.

- L.J. Richardson, V.K. Mezentsev and S.K. Turitsyn, "Spectral efficiency of dispersion managed solitons: comparison of 20, 40 and 80 Gbit/s based WDM transmission", Conference on Lasers and Electro-Optcs 2001, Baltimore, Maryland, USA, May 2001.

- L.J. Richardson and K.J. Blow, "Optimisation of ultra high-speed single channel dispersion managed systems: 80 Gbit/s versus 160 Gbit/s", *Postgraduate Research in Electronics and Photonics Conference (PREP 2001)*, Keele, UK, April 2000.

- V.K. Mezentsev, L.J. Richardson and S.K. Turitsyn, "Non Guassian statistics in dispersion managed systems", *Workshop on numerical simulation associated with OFC 2001*, Los Angeles, USA, March 2001.

- L.J. Richardson, V.K. Mezentsev, S.K. Turitsyn and K.J. Blow, "Reduction of WDM penalties in long haul transmission by adjustment of the dispersion management period", *European conference on Networks and Optical Communications (NOC 2001)*, Ipswich, UK, June 2001.

- L.J. Richardson and V.K. Mezentsev, "Tuning optimal configurations for short dispersion managed systems", *Optical Amplifiers and their applications conference (OAA'01)*, Stressa, Italy, July 2001.

Appendix B – Numerical simulations

In this section, we review some of the techniques used in the numerical simulations found in this thesis. Several methods can be used to integrate the NLS equation, which fall into two main groups namely, finite difference methods and pseudospectral methods. Generally, the pseudospectral methods are up to an order of magnitude faster for the same accuracy, than the finite difference methods [247]. One of the important pseudospectral methods is the Split Step Fourier Method (SSFM) [247], which obtains its computational speed from employing the Fast Fourier Transform (FFT) algorithm. Throughout the thesis, we use the SSFM method in all of the numerical simulations.

The SSFM method splits the integration into two parts, with separate differential operators accounting for the non-linear and dispersive effects. Therefore, the NLS equation (2.35) can be written in terms of

$$\frac{\partial A}{\partial z} = \left(\hat{D} + \hat{N}\right)A \tag{B.4}$$

where $\hat{D}$ is the differential operator that accounts for dispersion and absorption in a linear medium and $\hat{N}$ is the non-linear operator that governs the effects of fibre nonlinerities. These operators are given by

$$\hat{D} = -\frac{i}{2}\beta_2 \frac{\partial^2}{\partial T^2} - \frac{\alpha}{2} \tag{B.5}$$

$$\hat{N} = i\gamma|A|^2 \tag{B.6}$$

The SSFM makes the approximation that the nonlinearity and dispersion act independently, which is reasonable approximation, provided the step size h is short. More specifically, the

propagation from z to $z+h$ is carried in two steps. In the first step, the nonlinearity acts alone and $\hat{D} = 0$, and in the second step the dispersion acts alone $\hat{N} = 0$. Mathematically this is given by

$$A(z+h,T) = \exp(h\hat{D})\exp(h\hat{N})A(z,T) \tag{B.7}$$

The non-linear operator is evaluated in the Fourier domain, which when employing the FTT algorithm improves the computational efficiency of the SSFM. The accuracy of the SSFM can be improved further by including the effects of nonlinearity in the middle of the dispersive steps [248], which can be shown as

$$A(z+h,T) \approx \exp\left(\frac{h}{2}\hat{D}\right)\exp\left(\int_{z}^{z+h}\hat{N}(z')dz'\right)\exp\left(\frac{h}{2}\hat{D}\right)A(z,T) \tag{B.8}$$

Equation (B.8) is known as the Symmetrised Split Step Fourier Method (SSSFM) due the symmetric place of the dispersive operators.

To successfully utilise the SSFM, the temporal and spectral resolution, and the step size have to be decided. The temporal/spectral resolution is dependant on the bandwidth of the propagating signal. In the case of WDM simulations, where the signal occupies a much wider bandwidth, then a higher resolution is required. The best approach for determining the step size is to use a method that measures physical quantities of the propagation [249]. For example, the bandwidth of a propagating pulse provides an indication of how non-linear the problem is, although for WDM, unless the individual channel bandwidths are measured, then this method will give overly small step sizes. However, too large steps in WDM simulations produce spurious FWM products that degrade system performance [249]. Also in single channel transmission, too large step sizes produce sidebands that are phase matched to the step length. In the simulations used in this thesis, we employ a stepper algorithm to continually determine the required step size. The algorithm is based on the spurious side-band formation [249] by

calculating how linear and non-linear the propagation is. The nonlinearity is calculated in terms of the non-linear coefficient, the total intensity of the light and how concentrated it is and the linearity is measured from the energy in the fibre and the loss of the fibre.

Analogous to scalar model, the SSFM can be applied to the vector (birefringent) NLS under the conditions of high and low birefringence [250]. The effects of random mode coupling can be simulated by fixing the SSFM step size to be smaller than the characteristic length of the random coupling [214]. Under this condition, the coupling between the polarisation modes can be neglected when solving the propagation within a single step. After each step, the birefringent axes are randomly rotated and a random phase shift is introduced between the fields [214, 215, 251, 252].

Bibliography

[1] J. X. Cai, M. Nissov, A. N. Piliperskii, A. J. Lucero, C. R. Davidson, D. Foursa, H. Kidorf, M. A. Mills, H. Menges, P. C. Corbett, D. Sutton, and N. S. Bergano, "2.4 Tb/s (120 x 20 Gb/s) transmissionover transoceanic distance using optimum FEC overhead and 48 % spectral efficiency," *OFC 2001. Optical Fiber Communication Conference, Postdeadline papers, PD 20, 2001.*

[2] T. Ito, K. Fukuchi, K. Sekiya, D. Ogasahara, R. Ohhira, and T. Ono, "6.4 Tb/s (160 x 40 Gb/s) WDM transmission experiment with 0.8 bit/s/Hz spectral efficiency," *26th European Conference on Optical Communication, ECOC'00, 2000.*

[3] G. Vareille, F. Pitel, and J. F. Marcerou, "3 Tbit/s (300 x 11.6 Gbit/s) transmission over 7380 km using C + L band with 25 GHz channel spacing and NRZ format," *OFC 2001. Optical Fiber Communication Conference, Postdeadline papers, PD 22, 2001.*

[4] Y. Zhu, W. S. Lee, C. Scahill, C. Fludger, D. Watley, M. Jones, J. Homan, B. Shaw, and A. Hadjifotiou, "1.28 Tbit/s (32 x 40 Gbit/s) transmission over 1000 km with only 6 spans," *26th European Conference on Optical Communication, ECOC'00, 2000.*

[5] T. Miyakawa, I. Morita, K. Tanaka, H. Sakata, and E. Edagawa, "2.56 Tbit/s (40 Gbit/s x 64 WDM) unrepeatered 230 km transmission with 0.8 bit/s/Hz spectral efficiency using low-noise fiber Raman amplifier and 170um2-Aeff fiber," *OFC 2001. Optical Fiber Communication Conference, Postdeadline papers, PD 26, 2001.*

[6] N. Robinson, "Optical transmission system design: from the begining toward the future," *OFC'97. Optical Fiber Communication Conference, Tutoral papers, 1997*, pp. 43-60.

[7] B. Bakhshi, M. Vaa, E. A. Golovchenho, W. Patterson, R. L. Maybach, and N. S. Bergano, "Comparison of CRZ, RZ and NRZ modulation formats in a 64x12.3 Gb/s WDM transmission experiment over 9000 km," *OFC 2001. Optical Fiber Communication Conference, WF4, 2001.*

[8] F. Matera and M. Settembre, "Comparison of the performance of optical systems operating in long links encompassing dispersion shifted fibers," *Optics Communications*, 128(4-6), pp. 216-22, 1996.

[9] M. Nakazawa, E. Yamada, H. Kubota, T. Yamamoto, and A. Sahara, "Numerical and experimental comparison of soliton, RZ pulse and NRZ pulses under two-step dispersion allocation," *Electronics Letters*, 33(17), pp. 1480-2, 1997.

[10] M. Nakazawa, H. Kubota, K. Suzuki, E. Yamada, and A. Sahara, "Ultrahigh-speed long-distance TDM and WDM soliton transmission technologies," *IEEE Journal of Selected Topics in Quantum Electronics*, 6(2), pp. 363-96, 2000.

[11] D. Marcuse, *Light Transmission Optics*. New York: Van Nostrad Reinhold, 1982.

[12] J. M. Senior, *Optical Fiber Communications Principles and applications (Second Edition)*: Prentice Hall international series in optoelectronics, 1992.

[13] G. P. Agrawal, *Nonlinear Fibre Optics (2nd Edition)*. San Diego: Academic Press, p. 3, 1995.

[14] A. Simon and R. Ulrich, "Evolution of polarisation along a single mode fibre," *Applied Physics Letters*, 31, pp. 517-520, 1977.

[15] I. P. Kaminow, "Polarization in optical fibers," *IEEE Journal of Quantum Electronics*, 17, pp. 15-21, 1981.

[16] E. Iannone, F. Matera, A. Mecozzi, and M. Settembre, *Nonlinear Optical Communication Networks*: Wiley Series in Microwave and Optical Engineering, p. 32, 1998.

[17] S. C. Rasleigh, W. K. Burns, R. P. Moeller, and R. Ulrich, "Polarization holdinh in birefringent single mode fibers," *Optics Letters*, 7, pp. 40-42, 1982.

[18] E. Iannone, F. Matera, A. Mecozzi, and M. Settembre, *Nonlinear Optical Communication Networks*: Wiley Series in Microwave and Optical Engineering, pp. 34-35, 1998.

[19] E. Iannone, F. Matera, A. Mecozzi, and M. Settembre, *Nonlinear Optical Communication Networks*: Wiley Series in Microwave and Optical Engineering, p. 36, 1998.

[20] G. P. Agrawal, *Nonlinear Fibre Optics (2nd Edition)*. San Diego: Academic Press, p. 16, 1995.

[21] E. Iannone, F. Matera, A. Mecozzi, and M. Settembre, *Nonlinear Optical Communication Networks*: Wiley Series in Microwave and Optical Engineering, pp. 36-37, 1998.

[22] G. P. Agrawal, *Nonlinear Fibre Optics (2nd Edition)*. San Diego: Academic Press, p. 29, 1995.

[23] C. Menyuk, "Stabiliity of solitons in birefringent optical fibers. i: Equal propagation amplitudes," *Optics Letters*, 12(pp. 614-616, 1987.

[24] G. P. Agrawal, *Nonlinear Fibre Optics (2nd Edition)*. San Diego: Academic Press, p. 37, 1995.

[25] G. P. Agrawal, *Nonlinear Fibre Optics (2nd Edition)*. San Diego: Academic Press, p. 41, 1995.

[26] G. P. Agrawal, *Nonlinear Fibre Optics (2nd Edition)*. San Diego: Academic Press, p. 43, 1995.

[27] P. A. K. Wai and C. Menyuk, "Polarization mode dispersion, decorrelation, and diffusion in optical fibres with randomly varying birefringence," *Journal of Lightwave Technology*, 14, pp. 148-157, 1996.

[28] C. D. Poole, "Statistical treatment of polarization dispersion in single-mode fiber," *Optics Letters*, 13, pp. 687-689, 1988.

[29] A. Yariv, *Quantum Electronics (3rd Edition)*. New York: Wiley, 1989.

[30] E. Iannone, F. Matera, A. Mecozzi, and M. Settembre, *Nonlinear Optical Communication Networks*: Wiley Series in Microwave and Optical Engineering, p. 56, 1998.

[31] G. P. Agrawal, *Nonlinear Fibre Optics (2nd Edition)*. San Diego: Academic Press, pp. 61-63, 1995.

[32] G. P. Agrawal, *Nonlinear Fibre Optics (2nd Edition)*. San Diego: Academic Press, p. 65, 1995.

[33] G. P. Agrawal, *Nonlinear Fibre Optics (2nd Edition)*. San Diego: Academic Press, pp. 75-77, 1995.

[34] G. P. Agrawal, *Nonlinear Fibre Optics (2nd Edition)*. San Diego: Academic Press, pp. 89-90, 1995.

[35] G. P. Agrawal, *Nonlinear Fibre Optics (2nd Edition)*. San Diego: Academic Press, pp. 316-362, 1995.

[36] G. P. Agrawal, *Nonlinear Fibre Optics (2nd Edition)*. San Diego: Academic Press, pp. 370-399, 1995.

[37] V. E. Zakharov and A. B. Shabat, "Exact theory of two dimensional self focussing and one-dimensional self modulation of waves in nonlinear media," *Zhurnal Eksperimentalnoi i Teoreticheskoi Fiziki*, 34, pp. 62-69, 1972.

[38] A. Hasegawa and F. Tappert, "Transmission of stationary nonlinear optical pulses in dispersive dielectric fibres 1. anomalous dispersion," *Applied Physics Letters*, 23, pp. 142-144, 1973.

[39] L. F. Mollenauer, R. H. Stolen, and J. P. Gordon, "Experimental observation of picosecond pulse narrowing and solitons in optical fibres," *Physical Review Letters*, 45, pp. 1095-1098, 1980.

[40] G. P. Agrawal, *Nonlinear Fibre Optics (2nd Edition)*. San Diego: Academic Press, p. 145, 1995.

[41] G. P. Agrawal, *Nonlinear Fibre Optics (2nd Edition)*. San Diego: Academic Press, pp. 145-148, 1995.

[42] R. J. Essiambre and G. P. Agrawal, "Ultrahigh-bit-rate soliton communication systems using dispersion-decreasing fibers and parametric amplifiers," *Optics Letters*, 21(2), pp.

116-18, 1996.

[43] D. J. Richardson, L. Dong, R. P. Chamberlin, A. D. Ellis, T. Widdowson, and W. A. Pender, "Periodically amplified system based on loss compensating dispersion decreasing fibre," *Electronics Letters*, 32(4), pp. 373-4, 1996.

[44] M. Nakazawa, "Optical soliton transmission systems," *Journal of the Institute of Electronics & Communication Engineers of Japan*, 74(3), pp. 229-34, 1991.

[45] A. Okhrimchuk, G. Onishchukov, and F. Lederer, "Long-haul soliton transmission in a standard fiber at 1.3 mu m with distributed Raman amplification," *Conference on Lasers and Electro-Optics (CLEO 2000). Technical Digest. Postconference Edition. TOPS Vol.39 (IEEE Cat. No.00CH37088). Opt. Soc. America. 2000*, pp. 343-4.

[46] E. Desurvire and R. J. Simpson, "Amplification of spontenious emmission in erbium doped singe mode fiber amplifiers," *Journal of Lightwave Technology*, 7, pp. 835-845, 1989.

[47] K. J. Blow and N. J. Doran, "Average soliton dynamics and the operation of soliton systems with lumped amplifiers," *IEEE Photonics Technology Letters*, 3(4), pp. 369-71, 1991.

[48] A. Hasegawa and Y. Kodama, "Guiding-center soliton in fibers with periodically varying dispersion," *Optics Letters*, 16(18), pp. 1385-7, 1991.

[49] N. J. Smith, K. J. Blow, and I. Andonovic, "Sideband generation through perturbations to the average soliton model," *Journal of Lightwave Technology*, 10(10), pp. 1329-33, 1992.

[50] J. P. Gordon, "Interaction forces among solitons in optical fibers," *Optics Letters*, 8, pp. 596-598, 1983.

[51] K. J. Blow and N. J. Doran, "Bandwidth limits of nonlinear (soliton) optical communication systems," *Electronics Letters*, 19, pp. 429-430, 1983.

[52] F. M. Mitschke and L. F. Mollenauer, "Experimental observation of interaction forces between solitons in optical fibers," *Optics Letters*, 12(5), pp. 355-7, 1987.

[53] K. Bertilsson and P. A. Andrekson, "Numerical study of moderate distance high bit-rate alternating-amplitude soliton systems," *Journal of Lightwave Technology*, 14(3), pp. 237-42, 1996.

[54] C. Desum and P. L. Chu, "Soliton interaction in the presence of loss and periodic amplification in optical fibers," *Optics Letters*, 12, pp. 349-351, 1987.

[55] T. Georges and F. Favre, "Modulation, filtering, and initial phase control of interacting solitons," *Journal of the Optical Society of America B-Optical Physics*, 10(10), pp. 1880-9, 1993.

[56] F. Matera, M. Settembre, M. Tamburrini, M. Zitelli, and S. K. Turitsyn, "Reduction of the four wave mixing in optically amplified links by limiting pulse overlapping," *OFC '00. Optical Fiber Communication Conference and Exhibit. Technical Digest. Conference Edition. 2000 OSA Technical Digest Series. Opt. Soc. America. 2000.*

[57] A. M. Niculae, W. Forysiak, A. J. Gloag, T. H. B. Nijhof, and N. J. Doran, "Soliton collisions with wavelength-division multiplexed systems with strong dispersion management," *Optics Letters*, 23(17), pp. 1354-6, 1998.

[58] J. F. L. Devaney, W. Forysiak, A. M. Niculae, and N. J. Doran, "Soliton collisions in dispersion-managed wavelength-division-multiplexed systems," *Optics Letters*, 22(22), pp. 1695-7, 1997.

[59] H. Sugahara, H. Kato, T. Inoue, A. Maruta, and Y. Kodama, "Optimal dispersion management for a wavelength division multiplexed optical soliton transmission system," *Journal of Lightwave Technology*, 17(9), pp. 1547-59, 1999.

[60] E. Iannone, F. Matera, A. Mecozzi, and M. Settembre, *Nonlinear Optical Communication Networks*: Wiley Series in Microwave and Optical Engineering, pp. 155-159, 1998.

[61] J. P. Gordon and H. A. Haus, "Random walk of coherently amplified solitons in optical fiber transmission," *Optics Letters*, 11, pp. 665-667, 1986.

[62] A. Mecozzi, J. D. Moores, H. A. Haus, and Y. Lai, "Soliton transmission control,"

Optics Letters, 16(23), pp. 1841-3, 1991.

[63] Y. Kodama and A. Hasegawa, "Generation of asymptotically stable optical solitons and suppression of the Gordon-Haus effect," *Optics Letters*, 17(1), pp. 31-3, 1992.

[64] D. Marcuse, "Simulations to demonstrate reduction of the Gordon-Haus effect," *Optics Letters*, 17(1), pp. 34-6, 1992.

[65] E. Kolltveit, B. Biotteau, I. Riant, F. Pitel, O. Audouin, P. Brindel, E. Brun, P. Sansonetti, and J. P. Hamaide, "Soliton frequency-guiding by UV-written fiber Fabry-Perot filter in a 2*5 Gb/s wavelength-division multiplexing transmission over transoceanic distances," *IEEE Photonics Technology Letters*, 7(12), pp. 1498-500, 1995.

[66] L. F. Mollenauer, J. P. Gordon, and S. G. Evangelides, "The sliding-frequency guiding filter: an improved form of soliton jitter control," *Optics Letters*, 17(22), pp. 1575-7, 1992.

[67] E. A. Golovchenko, A. N. Pilipetskii, C. R. Menyuk, J. P. Gordon, and L. F. Mollenauer, "Soliton propagation with up- and down-sliding-frequency guiding filters," *Optics Letters*, 20(6), pp. 539-41, 1995.

[68] P. V. Mamyshev and L. F. Mollenauer, "Stability of Soliton Propagation with Sliding-Frequency Guiding Filters," *Optics Letters*, 19(24), pp. 2083-2085, 1994.

[69] F. Favre and V. Chandrakumar, "Comparison between analytical and numerical simulations for sliding filter damped soliton jitter," *Optics Communications*, 126(1-3), pp. 34-7, 1996.

[70] E. Iannone, F. Matera, A. Mecozzi, and M. Settembre, *Nonlinear Optical Communication Networks*: Wiley Series in Microwave and Optical Engineering, pp. 43-45, 1998.

[71] E. Iannone, F. Matera, A. Mecozzi, and M. Settembre, *Nonlinear Optical Communication Networks*: Wiley Series in Microwave and Optical Engineering, pp. 45-46, 1998.

[72] K. J. Blow and D. Wood, "Theoretical description of transient stimulated Raman scattering in optical fibers," *IEEE Journal of Quantum Electronics*, 25(12), pp. 2665-73, 1989.

[73] G. P. Agrawal, *Nonlinear Fibre Optics (2nd Edition)*. San Diego: Academic Press, pp. 404-407, 1995.

[74] P. V. Mamyshev and L. F. Mollenauer, "Pseudo-phase-matched four-wave mixing in soliton wavelength-division multiplexing transmission," *Optics Letters*, 21(6), pp. 396-8, 1996.

[75] G. Aubin, T. Montalant, J. Moulu, B. Nortier, F. Pirio, and J. B. Thomine, "Soliton transmission at 10 Gbit/s with a 70 km amplifier span over one million kilometres," *Electronics Letters*, 30(14), pp. 1163-5, 1994.

[76] H. Kubota and M. Nakazawa, "Soliton transmission control in time and frequency domains," *Electronics & Communications in Japan, Part 2: Electronics (English Translation of Denshi Tsushin Gakkai Ronbunshi)*, 76(11), pp. 1-13, 1993.

[77] G. Aubin, T. Montalant, J. Moulu, B. Nortier, F. Pirio, and J. B. Thomine, "Record amplifier span of 105 km in a soliton transmission experiment at 10 Gbit/s over 1 Gm," *Electronics Letters*, 31(3), pp. 217-19, 1995.

[78] G. Aubin, T. Montalant, J. Moulu, F. Pirio, J. B. Thomine, and F. Devaux, "40 Gbit/s OTDM soliton transmission over transoceanic distances," *Electronics Letters*, 32(24), pp. 2188-9, 1996.

[79] S. Bigo, O. Leclerc, P. Brindel, G. Vendrome, E. Desurvire, P. Doussiere, and T. Ducellier, "All-optical regenerator for 20 Gbit/s transoceanic transmission," *Electronics Letters*, 33(11), pp. 975-6, 1997.

[80] O. Leclerc, P. Brindel, S. Bigo, E. Brun-Maunand, and E. Desurvire, "2*20 Gbit/s, 3500 km regenerated WDM soliton transmission with all-optical Kerr fibre modulation," *Electronics Letters*, 34(2), pp. 199-201, 1998.

[81] M. Nakazawa, K. Suzuki, H. Kubota, A. Sahara, and E. Yamada, "160 Gbit/s WDM (20 Gbit/s*8 channels) soliton transmission over 10000 km using in-line synchronous

modulation and optical filtering," *Electronics Letters*, 34(1), pp. 103-4, 1998.

[82] T. Widdowson, D. J. Malyon, A. D. Ellis, K. Smith, and K. J. Blow, "Soliton shepherding: all-optical active soliton control over global distances," *Electronics Letters*, 30(12), pp. 990-1, 1994.

[83] S. Bennett and A. J. Seeds, "Error free 80 Gb/s soliton transmission over trans-oceanic (>8,000 km) distances using fast saturable absorbers and dispersion decreasing fibre," *OFC/IOOC'99. Optical Fiber Communication Conference and the International Conference on Integrated Optics and Optical Fiber Communications (Cat. No.99CH36322). IEEE. Part vol.2, 1999*, pp. 50-2 vol.

[84] D. S. Govan, N. J. Smith, F. M. Knox, and N. J. Doran, "Stable propagation of solitons with increased energy through the combined action of dispersion management and periodic saturable absorption," *Journal of the Optical Society of America B-Optical Physics*, 14(11), pp. 2960-6, 1997.

[85] D. Atkinson, W. H. Loh, V. V. Afanasjev, A. B. Grudinin, A. J. Seeds, and D. N. Payne, "Increased Amplifier Spacing in a Soliton System with Quantum- Well Saturable Absorbers and Spectral Filtering," *Optics Letters*, 19(19), pp. 1514-1516, 1994.

[86] M. Matsumoto, H. Ikeda, and A. Hasegawa, "Suppression of Noise Accumulation in Bandwidth-Limited Soliton Transmission by Means of Nonlinear Loop Mirrors," *Optics Letters*, 19(3), pp. 183-185, 1994.

[87] F. X. Kartner and U. Keller, "Stabilization of solitonlike pulses with a slow saturable absorber," *Optics Letters*, 20(1), pp. 16-18, 1995.

[88] A. Hirano, H. Kobayashi, H. Tsuda, A. Takahashi, M. Asobe, K. Sato, and K. Hagimoto, "10 Gbit/s RZ all-optical discrimination using refined saturable absorber optical gate," *Electronics Letters*, 32(2), pp. 198-199, 1998.

[89] H. Tsuda, A. Hirano, A. Takahashi, K. Sato, and K. Hagimoto, "2.4 Gbit/s all-optical pulse discrimination experiment using a high-speed saturable absorber optical gate," *Electronics Letters*, 32(4), pp. 365-366, 1996.

[90] C. G. Goedde, W. L. Kath, and P. Kumar, "Periodic amplification and conjugation of optical solitons," *Optics Letters*, 20(12), pp. 1365-7, 1995.

[91] C. Chen and S. Chi, "Improving the soliton transmission by optical phase conjugation in a polarization-division multiplexing system," *Optik*, 110(1), pp. 29-32, 1999.

[92] S. Wen and S. Chi, "Undoing of soliton interaction by optical phase conjugation," *Electronics Letters*, 30(8), pp. 663-4, 1994.

[93] W. Forysiak and N. J. Doran, "Reduction of Gordon-Haus jitter in soliton transmission systems by optical phase conjugation," *Journal of Lightwave Technology*, 13(5), pp. 850-5, 1995.

[94] N. J. Doran and W. Forysiak, "Phase conjugation for jitter and soliton-soliton compensation in soliton communications," *CLEO '94. Summaries of Papers Presented at the Conference on Lasers and Electro-Optics. Vol.8. 1994 Technical Digest Series. Conference Edition (Cat. No.94CH3463-7). Opt. Soc. America. 1994*, pp. 367-8.

[95] A. Mostofi and P. L. Chu, "Reversal of soliton interactions in optically phase-conjugated systems with unequal-amplitude and alternating-phase solitons," *Optics Communications*, 141(5-6), pp. 259-64, 1997.

[96] K. Suzuki, H. Kubota, A. Sahara, and M. Nakazawa, "640 Gbit/s (40 Gbit/s*16 channel) dispersion-managed DWDM soliton transmission over 1000 km with spectral efficiency of 0.4 bit/Hz," *Electronics Letters*, 36(5), pp. 443-5, 2000.

[97] M. Nakazawa, H. Kubota, K. A. Suzuki, E. Yamada, and A. Sahara, "Recent progress in soliton transmission technology," *Chaos*, 10(3), pp. 486-514, 2000.

[98] O. Leclerc, P. Brindel, D. Rouvillain, B. Dany, E. Pincemin, E. Desurvire, C. Duchet, A. Shen, F. Blache, F. Devaux, A. Coquelin, M. Goix, S. Bouchoule, and P. Nouchi, "Dense WDM (0.27 bit/s/Hz) 4*40 Gbit/s dispersion-managed transmission over 10000 km with in-line optical regeneration by channel pairs," *Electronics Letters*, 36(4), pp. 337-8, 2000.

[99] I. Morita, M. Suzuki, N. Edagawa, K. Tanaka, and S. Yamamoto, "Long-haul soliton

WDM transmission with periodic dispersion compensation and dispersion slope compensation," *Journal of Lightwave Technology*, 17(1), pp. 80-5, 1999.

[100] A. Hasegawa, S. Kumar, and Y. Kodama, "Reduction of collision-induced time jitters in dispersion-managed soliton transmission systems," *Optics Letters*, 21(1), pp. 39-41, 1996.

[101] S. Kumar, Y. Kodama, and A. Hasegawa, "Optimal dispersion management schemes for WDM soliton systems," *Electronics Letters*, 33(6), pp. 459-61, 1997.

[102] Y. Kodama and A. Maruta, "Optimal design of dispersion management for a soliton-wavelength-division-multiplexed system," *Optics Letters*, 22(22), pp. 1692-4, 1997.

[103] W. Forysiak, J. F. L. Devaney, N. J. Smith, and N. J. Doran, "Dispersion management for wavelength-division-multiplexed soliton transmission," *Optics Letters*, 22(9), pp. 600-2, 1997.

[104] A. Hasegawa, Y. Kodama, and A. Maruta, "Recent progress in dispersion-managed soliton transmission technologies," *Optical Fiber Technology*, 3(3), pp. 197-213, 1997.

[105] N. J. Smith, N. J. Doran, F. M. Knox, and W. Forysiak, "Energy-scaling characteristics of solitons in strongly dispersion-managed fibers," *Optics Letters*, 21(24), pp. 1981-3, 1996.

[106] S. K. Turitsyn, T. Schafer, and V. K. Mezentsev, "Self-similar core and oscillatory tails of a path-averaged chirped dispersion-managed optical pulse," *Optics Letters*, 23(17), pp. 1351-3, 1998.

[107] N. J. Smith, F. M. Knox, N. J. Doran, K. J. Blow, and I. Bennion, "Enhanced power solitons in optical fibres with periodic dispersion management," *Electronics Letters*, 32(1), pp. 54-5, 1996.

[108] V. S. Grigoryan, T. Yu, E. A. Golovchenko, C. R. Menyuk, and A. N. Pilipetskii, "Dispersion-managed soliton dynamics," *Optics Letters*, 22(21), pp. 1609-11, 1997.

[109] J. H. B. Nijhof, N. J. Doran, W. Forysiak, and F. M. Knox, "Stable soliton-like propagation in dispersion managed systems with net anomalous, zero and normal dispersion," *Electronics Letters*, 33(20), pp. 1726-7, 1997.

[110] A. Berntson, N. J. Doran, W. Forysiak, and J. H. B. Nijhof, "Power dependence of dispersion-managed solitons for anomalous, zero, and normal path-average dispersion," *Optics Letters*, 23(12), pp. 900-2, 1998.

[111] J. H. B. Nijhof, W. Forysiak, and N. J. Doran, "The averaging method for finding exactly periodic dispersion-managed solitons," *IEEE Journal of Selected Topics in Quantum Electronics*, 6(2), pp. 330-6, 2000.

[112] T. Yu, E. A. Golovchenko, A. N. Pilipetskii, and C. R. Menyuk, "Dispersion-managed soliton interactions in optical fibers," *Optics Letters*, 22(11), pp. 793-5, 1997.

[113] M. Nakazawa, H. Kubota, A. Sahara, and K. Tamura, "Marked increase in the power margin through the use of a dispersion-allocated soliton," *IEEE Photonics Technology Letters*, 8(8), pp. 1088-90, 1996.

[114] J. H. B. Nijhof, N. J. Doran, W. Forysiak, and A. Berntson, "Energy enhancement of dispersion-managed solitons and WDM," *Electronics Letters*, 34(5), pp. 481-2, 1998.

[115] J. H. B. Nijhof, N. J. Doran, and W. Forysiak, "Dispersion-managed solitons in the normal dispersion regime: a physical interpretation," *24th European Conference on Optical Communication. ECOC '98 (IEEE Cat. No.98TH8398). Telefonica. Part vol.1, 1998*, pp. 103-4 vol.

[116] J. N. Kutz and S. G. Evangelides, "Dispersion-managed breathers with average normal dispersion," *Optics Letters*, 23(9), pp. 685-687, 1998.

[117] V. S. Grigoryan and C. R. Menyuk, "Dispersion-managed solitons at normal average dispersion," *Optics Letters*, 23(8), pp. 609-11, 1998.

[118] M. Nakazawa, H. Kubota, and K. Tamura, "Nonlinear pulse transmission through an optical fiber at zero-average group velocity dispersion," *IEEE Photonics Technology Letters*, 8(3), pp. 452-4, 1996.

[119] S. K. Turitsyn and E. G. Shapiro, "Dispersion-managed solitons in optical amplifier transmission systems with zero average dispersion," *Optics Letters*, 23(9), pp. 682-4,

1998.
[120] J. H. B. Nijhof, W. Forysiak, and N. J. Doran, "Dispersion-managed solitons in the normal dispersion regime: a physical interpretation," *Optics Letters*, 23(21), pp. 1674-6, 1998.
[121] S. K. Turitsyn and E. G. Shapiro, "Variational approach to the design of optical communication systems with dispersion management," *Optical Fiber Technology*, 4(2), pp. 151-88, 1998.
[122] T. Georges, "Extended path-averaged soliton regime in highly dispersive fibers," *Optics Letters*, 22(10), pp. 679-81, 1997.
[123] G. M. Carter, J. M. Jacob, C. R. Menyuk, E. A. Golovchenko, and A. N. Pilipetskii, "Timing-jitter reduction for a dispersion-managed soliton system: experimental evidence," *Optics Letters*, 22(8), pp. 513-15, 1997.
[124] N. J. Smith, W. Forysiak, and N. J. Doran, "Gordon-Haus jitter reduction in enhanced power soliton systems," *Conference on Optical Fiber Communications. Technical Digest. Postconference Edition. 1997 OSA Technical Digest Series. Vol.6 (IEEE Cat. No.97CH36049). Opt. Soc. America. 1997*, p. 309.
[125] M. Suzuki, I. Morita, N. Edagawa, S. Yamamoto, H. Taga, and S. Akiba, "Reduction of Gordon-Haus timing jitter by periodic dispersion compensation in soliton transmission," *Electronics Letters*, 31(23), pp. 2027-9, 1995.
[126] J. N. Kutz and P. K. A. Wai, "Ideal amplifier spacing for reduction of Gordon-Haus jitter in dispersion-managed soliton communications," *Electronics Letters*, 34(6), pp. 522-3, 1998.
[127] S. Kumar and F. Lederer, "Gordon-Haus effect in dispersion-managed soliton systems," *Optics Letters*, 22(24), pp. 1870-2, 1997.
[128] G. Bento, F. Neddam, and S. Wabnitz, "Role of adjacent-pulse overlap in the interaction between dispersion-managed solitons," *Optics Letters*, 25(3), pp. 144-6, 2000.
[129] T. Georges, "Soliton interaction in dispersion-managed links," *Journal of the Optical Society of America B-Optical Physics*, 15(5), pp. 1553-60, 1998.
[130] S. Kumar, M. Wald, F. Lederer, and A. Hasegawa, "Soliton interaction in strongly dispersion-managed optical fibers," *Optics Letters*, 23(13), pp. 1019-21, 1998.
[131] T. Inoue, H. Sugahara, A. Maruta, and Y. Kodama, "Interactions between dispersion managed solitons in optical-time-division-multiplexed system," *IEEE Photonics Technology Letters*, 12(3), pp. 299-301, 2000.
[132] B. A. Malomed, "Suppression of soliton jitter and interactions by means of dispersion management," *Optics Communications*, 147(1-3), pp. 157-62, 1998.
[133] I. S. Penketh, P. Harper, S. B. Aleston, A. M. Niculae, I. Bennion, and N. J. Doran, "10-Gbit/s dispersion-managed soliton transmission over 16,500 km in standard fiber by reduction of soliton interactions," *Optics Letters*, 24(12), pp. 802-4, 1999.
[134] S. K. Turitsyn, N. J. Doran, E. G. Turitsyna, E. G. Shapiro, and M. P. Fedoruk, "Soliton interaction in optical communication systems with short-scale dispersion management," *Conference on Lasers and Electro-Optics (CLEO 2000). Technical Digest. Postconference Edition. TOPS Vol.39 (IEEE Cat. No.00CH37088). Opt. Soc. America. 2000*, pp. 30-1.
[135] M. Wald, B. A. Malomed, and F. Lederer, "Interaction of moderately dispersion-managed solitons," *Optics Communications*, 172(1-6), pp. 31-6, 1999.
[136] M. Matsumoto, "Analysis of interaction between stretched pulses propagating in dispersion-managed fibers," *IEEE Photonics Technology Letters*, 10(3), pp. 373-5, 1998.
[137] A. M. Niculae, W. Forysiak, and N. J. Doran, "Optimal amplifier location in strong dispersion-managed soliton systems," *Technical Digest. Summaries of papers presented at the Conference on Lasers and Electro-Optics. Postconference Edition. CLEO '99. Conference on Lasers and Electro-Optics (IEEE Cat. No.99CH37013). Opt. Soc. America. 1999*, pp. 236-7.
[138] J. Martensson, M. Westlund, and A. Berntson, "Intra-channel pulse interactions in 40 Gbit/s dispersion-managed RZ transmission system," *Electronics Letters*, 36(3), pp. 244-

6, 2000.
[139] S. K. Turitsyn, I. Gabitov, E. W. Laedke, V. K. Mezentsev, S. L. Musher, E. G. Shapiro, T. Schafer, and K. H. Spatschek, "Variational approach to optical pulse propagation in dispersion compensated transmission systems," *Optics Communications*, 151(1-3), pp. 117-35, 1998.
[140] S. K. Turitsyn, M. P. Fedoruk, and A. Gornakova, "Reduced-power optical solitons in fiber lines with short-scale dispersion management," *Optics Letters*, 24(13), pp. 869-71, 1999.
[141] A. H. Liang, H. Toda, and A. Hasegawa, "High speed soliton transmission in dense periodic fibers," *Optics Letters*, 24(12), pp. 799-801, 1999.
[142] H. Anis, G. Berkey, G. Bordogna, M. Cavallari, B. Charbonnier, A. Evans, I. Hardcastle, M. Jones, G. Pettitt, B. Shaw, V. Srikant, and J. Wakefield, "Continuous dispersion managed fiber for very high speed soliton systems," *25th European Conference on Optical Communication. ECOC '99 Conference. Soc. Electr. Electron. Part vol.1, 1999*, pp. 230-1 vol.
[143] W. I. Kaechele, M. L. Dennis, T. F. Carruthers, and I. N. Duling, III, "200-Gbit/s polarization-multiplexed transmission over 100 km of dense-dispersion-managed fiber," *Conference on Lasers and Electro-Optics (CLEO 2000). Technical Digest. Postconference Edition. TOPS Vol.39 (IEEE Cat. No.00CH37088). Opt. Soc. America. 2000*, pp. 92-3.
[144] A. H. Liang, H. Toda, and A. Hasegawa, "Dense periodic fibers with ultralow four-wave mixing over a broad wavelength range," *Optics Letters*, 24(16), pp. 1094-6, 1999.
[145] F. Favre, D. Le Guen, and T. Georges, "Experimental evidence of pseudoperiodical soliton propagation in dispersion-managed links," *Journal of Lightwave Technology*, 17(6), pp. 1032-6, 1999.
[146] M. K. Chin and X. Y. Tang, "Quasi-stable soliton transmission in dispersion managed fiber links with lumped amplifiers," *IEEE Photonics Technology Letters*, 9(4), pp. 538-40, 1997.
[147] T. Yu, R. M. Mu, V. S. Grigoryan, and C. R. Menyuk, "Energy enhancement of dispersion-managed solitons in optical fiber transmission systems with lumped amplifiers," *IEEE Photonics Technology Letters*, 11(1), pp. 75-7, 1999.
[148] S. K. Turitsyn, V. K. Mezentsev, and E. G. Shapiro, "Dispersion-managed solitons and optimization of the dispersion management," *Optical Fiber Technology*, 4(4), pp. 384-452, 1998.
[149] S. K. Turitsyn, J. H. B. Nijhof, V. K. Mezentsev, and N. J. Doran, "Symmetries, chirp-free points, and bistability in dispersion-managed fiber lines," *Optics Letters*, 24(24), pp. 1871-3, 1999.
[150] M. Matsumoto, "Analysis of filter control of dispersion-managed soliton transmission," *Journal of the Optical Society of America B-Optical Physics*, 15(12), pp. 2831-7, 1998.
[151] A. Tonello, A. D. Capobianco, S. Wabnitz, and S. K. Turitsyn, "Tuning of in-line filter position for dispersion-managed soliton transmission," *Optics Communications*, 175(1-3), pp. 103-8, 2000.
[152] A. Berntson and B. A. Malomed, "Dispersion management with filtering," *Optics Letters*, 24(8), pp. 507-9, 1999.
[153] A. Mecozzi, "Timing jitter in wavelength-division-multiplexed filtered soliton transmission," *Journal of the Optical Society of America B-Optical Physics*, 15(1), pp. 152-61, 1998.
[154] L. F. Mollenauer, P. V. Mamyshev, J. Gripp, M. J. Neubelt, N. Mamysheva, L. Gruner-Nielsen, and T. Veng, "Demonstration of massive wavelength-division multiplexing over transoceanic distances by use of dispersion-managed solitons," *Optics Letters*, 25(10), pp. 704-6, 2000.
[155] L. F. Mollenauer, P. V. Mamyshev, and J. P. Gordon, "Effect of guiding filters on the behavior of dispersion-managed solitons," *Optics Letters*, 24(4), pp. 220-222, 1999.
[156] H. Murai, H. T. Yamada, K. Fujii, and Y. Ozeki, "Analysis on dispersion managed

solitons with initial phase alternation for DWDM transmission systems," *ROSC Symposium, Hakone, Japan*, 2000.

[157] E. Pincemin, F. Neddam, and O. Leclerc, "Efficient reduction of interactions in dispersion-managed links through in-line filtering and synchronous intensity modulation," *Optics Letters*, 25(5), pp. 287-9, 2000.

[158] S. Waiyapot and M. Matsumoto, "Stability analysis of dispersion-managed solitons controlled by synchronous amplitude modulators," *IEEE Photonics Technology Letters*, 11(11), pp. 1408-10, 1999.

[159] B. Dany, P. Brindel, O. Leclerc, and E. Desurvire, "Feasibility of 16*40 Gbit/s dispersion-managed transoceanic systems with high spectral efficiency," *25th European Conference on Optical Communication. ECOC '99 Conference. Soc. Electr. Electron. Part vol.1, 1999*, pp. 152-3 vol.

[160] L. F. Mollenauer, "The many benefits of nonlinearity for the all-optical, terabit, long-distance network," *Nonlinear Optics: Materials, Fundamentals, and Applications. Technical Digest. Postconference Edition. TOPS Vol.46 (IEEE Cat. No.00CH37174). Opt. Soc. America. 2000*, pp. 304-6.

[161] D. Anderson, "Variational Approach to Non-Linear Pulse-Propagation in Optical Fibers," *Physical Review A*, 27(6), pp. 3135-3145, 1983.

[162] E. G. Shapiro and S. K. Turitsyn, "Theory of guiding-center breathing soliton propagation in optical communication systems with strong dispersion management," *Optics Letters*, 22(20), pp. 1544-6, 1997.

[163] A. Berntson, D. Anderson, N. J. Doran, W. Forysiak, and J. H. B. Nijhof, "Power dependence and accessible bandwidth for dispersion-managed solitons in asymmetric dispersion maps," *Electronics Letters*, 34(21), pp. 2054-6, 1998.

[164] T. I. Lakoba, J. Yang, D. J. Kaup, and B. A. Malomed, "Conditions for stationary pulse propagation in the strong dispersion management regime," *Optics Communications*, 149(4-6), pp. 366-75, 1998.

[165] J. N. Kutz, P. Holmes, S. G. Evangelides, Jr., and J. P. Gordon, "Hamiltonian dynamics of dispersion-managed breathers," *Journal of the Optical Society of America B-Optical Physics*, 15(1), pp. 87-96, 1998.

[166] F. Abdullaev and J. G. Caputo, "Validation of the variational approach for chirped pulses in fibers with periodic dispersion," *Physical Review E. Statistical Physics, Plasmas, Fluids, & Related Interdisciplinary Topics*, 58(5), pp. 6637-48, 1998.

[167] T. Inoue, H. Sugahara, A. Marijta, and Y. Kodama, "Interactions between dispersion managed solitons in optical-time-division-multiplexed systems," *Transactions of the Institute of Electronics & Communication Engineers of Japan, Part B*, J83-B(6), pp. 763-8, 2000.

[168] H. Sugahara, H. Kato, and Y. Kodama, "Maximum reductions of collision induced frequency shift in soliton-WDM systems with dispersion compensation," *Electronics Letters*, 33(12), pp. 1065-6, 1997.

[169] M. Matsumoto, "Instability of dispersion-managed solitons in a system with filtering," *Optics Letters*, 23(24), pp. 1901-3, 1998.

[170] A. Tonello, A. D. Capobianco, S. Wabnitz, O. Leclerc, B. Dany, and E. Pincemin, "Stability and optimization of dispersion-managed soliton control," *Optics Letters*, 25(20), pp. 1496-8, 2000.

[171] M. Matsumoto, "Theory of stretched-pulse transmission in dispersion-managed fibers," *Optics Letters*, 22(16), pp. 1238-40, 1997.

[172] T. Georges, F. Favre, and D. L. Guen, "Theoretical and experimental study of soliton transmission in dispersion managed links," *IEICE Transactions on Electronics*, E81-C(2), pp. 226-31, 1998.

[173] I. Morita, M. Suzuki, N. Edagawa, S. Yamamoto, and S. Akiba, "Single-channel 40 Gbit/s, 5000 km straight-line soliton transmission experiment using periodic dispersion compensation," *ECOC '96. 22nd European Conference on Optical Communication (IEEE Cat. No.96TH8217). Telenor. Part vol.2, 1996*, pp. 191-4 vol.

[174] M. Suzuki, I. Morita, S. Yamamoto, N. Edagawa, H. Taga, and S. Akiba, "Timing jitter reduction by periodic dispersion compensation in soliton transmission," *OFC `95 Optical Fiber Communication. Summaries of Papers Presented at the Conference on Optical Fiber Communication. Vol.8. 1995 Technical Digest Series. Postconference Edition. Opt. Soc. America. 1995*, pp. 401-4.

[175] I. Morita, M. Suzuki, N. Edagawa, S. Yamamoto, H. Taga, and S. Akiba, "20-Gb/s single-channel soliton transmission over 9000 km without inline filters," *IEEE Photonics Technology Letters*, 8(11), pp. 1573-4, 1996.

[176] L. F. Mollenauer, S. G. Evangelides, and J. P. Gordon, "Wavelength Division Multiplexing with Solitons in Ultra-Long Distance Transmission Using Lumped Amplifiers," *Journal of Lightwave Technology*, 9(3), pp. 362-367, 1991.

[177] L. F. Mollenauer, E. Lichtman, G. T. Harvey, M. J. Neubelt, and B. M. Nyman, "Demonstration of Error-Free Soliton Transmission over More Than 15000 Km at 5 Gbit/S, Single-Channel, and over More Than 11000 Km at 10 Gbit/S in 2-Channel Wdm," *Electronics Letters*, 28(8), pp. 792-794, 1992.

[178] H. Taga, M. Suzuki, N. Edagawa, Y. Yoshida, S. Yamamoto, S. Akiba, and H. Wakabayashi, "5 Gbit/s optical solution transmission experiment over 3000 km employing 91 cascaded Er-doped fibre amplifier repeaters," *Electronics Letters*, 28(24), pp. 2247-8, 1992.

[179] A. D. Ellis, T. Widdowson, X. Shan, G. E. Wickens, and D. M. Spirit, "Transmission of a true single polarisation 40 Gbit/s soliton data signal over 205 km using a stabilised erbium fibre ring laser and 40 GHz electronic timing recovery," *Electronics Letters*, 29(11), pp. 990-2, 1993.

[180] M. Nakazawa, K. Suzuki, E. Yamada, H. Kubota, and Y. Kimura, "Straight-line soliton data transmissions over 2000 km at 20 Gbit/s and 1000 km at 40 Gbit/s using erbium-doped fibre amplifiers," *Electronics Letters*, 29(16), pp. 1474-6, 1993.

[181] P. A. Andrekson, N. A. Olsson, M. Haner, J. R. Simpson, T. Tanbun-Ek, R. A. Logan, D. Coblentz, H. M. Presby, and K. W. Wecht, "32 Gb/s optical soliton data transmission over 90 km," *IEEE Photonics Technology Letters*, 4(1), pp. 76-9, 1992.

[182] M. Suzuki, N. Edagawa, H. Taga, H. Tanaka, S. Yamamoto, and S. Akiba, "Feasibility demonstration of 2O Gbit/s single channel soliton transmission over 11500 km using alternating-amplitude solitons," *Electronics Letters*, 30(13), pp. 1083-4, 1994.

[183] P. Harper, F. M. Knox, P. N. Kean, I. Bennion, and N. J. Doran, "10-Gbit/s soliton propagation over 5250 km in standard fiber with dispersion compensation," *Conference on Optical Fiber Communications. Technical Digest. Postconference Edition. 1997 OSA Technical Digest Series. Vol.6 (IEEE Cat. No.97CH36049). Opt. Soc. America. 1997*, pp. 304-5.

[184] P. Harper, I. S. Penketh, S. B. Alleston, I. Bennion, and N. J. Doran, "10 Gbit/s dispersion managed soliton propagation over 200 Mm without active control," *Electronics Letters*, 34(21), pp. 1997-9, 1998.

[185] J. M. Jacob, E. A. Golovchenko, A. N. Pilipetskii, G. M. Carter, and C. R. Menyuk, "10-Gb/s transmission of NRZ over 10000 km and solitons over 13500 km error-free in the same dispersion-managed system," *IEEE Photonics Technology Letters*, 9(10), pp. 1412-14, 1997.

[186] L. F. Mollenauer, P. V. Mamyshev, and M. J. Neubelt, "Demonstration of soliton WDM transmission at 6 and 7*10 Gbit/s, error free over transoceanic distances," *Electronics Letters*, 32(5), pp. 471-3, 1996.

[187] L. E. Nelson, L. D. Garrett, A. B. Chraplyvy, and R. W. Tkach, "NZ-DSF dispersion maps in 2000-km 8*10 Gb/s WDM transmission," *24th European Conference on Optical Communication. ECOC '98 (IEEE Cat. No.98TH8398). Telefonica. Part vol.1, 1998*, pp. 315-16 vol.

[188] M. Suzuki, "Long-haul soliton transmission beyond 10 Gbits/s," *OFC `95 Optical Fiber Communication. Summaries of Papers Presented at the Conference on Optical Fiber Communication. Vol.8. 1995 Technical Digest Series. Postconference Edition. Opt. Soc.*

America. 1995, pp. 303-4.

[189] H. Toda, Y. Inada, Y. Kodama, and A. Hasegawa, "10 Gbit/s optical soliton transmission experiment in a comb-like dispersion profiled fiber loop," *IEICE Transactions on Communications*, E82-B(10), pp. 1541-3, 1999.

[190] G. M. Carter, M. Ruomei, V. Grigoryan, P. Sinha, C. R. Menyuk, T. F. Carruthers, M. L. Dennis, and I. N. Duling, III, "20 Gb/s transmission of dispersion-managed solitons over 20,000 km," *OFC/IOOC'99. Optical Fiber Communication Conference and the International Conference on Integrated Optics and Optical Fiber Communications (Cat. No.99CH36322). IEEE. Part vol.2, 1999*, pp. 32-4 vol.

[191] N. Edagawa, I. Morita, and M. Suzuki, "20 Gbit/s soliton-based RZ transmission experiment using a 8,100 km straight-line transmission line with periodic dispersion compensation," *KDD Technical Journal*157), pp. 5-16, 1997.

[192] F. Favre, D. Le Guen, and T. Georges, "20 Gbit/s soliton transmission over 5200 km of non-zero-dispersion-shifted fibre with 106 km dispersion-compensated span," *Electronics Letters*, 34(2), pp. 201-2, 1998.

[193] L. F. Mollenauer and P. V. Mamyshev, "Massive wavelength-division multiplexing with solitons," *IEEE Journal of Quantum Electronics*, 34(11), pp. 2089-102, 1998.

[194] S. B. Alleston, P. Harper, I. S. Penketh, I. Bennion, N. J. Doran, and A. D. Ellis, "1000 km transmission of 40 Gbit/s single channel RZ data over dispersion managed standard (non-dispersion shifted) fibre," *Electronics Letters*, 35(10), pp. 823-4, 1999.

[195] P. A. Andrekson, "40 Gbit/s soliton transmission on installed fiber lines," *IEE Colloquium on High Speed and Long Distance Transmission (Ref. No.1999/022). IEE. 1999*, pp. 10/1-6.

[196] A. D. Ellis, T. Widdowson, and X. Shan, "Wavelength dependence of 40 Gbit/s solitonic transmission over distances greater than 2000 km," *Electronics Letters*, 32(4), pp. 381-2, 1996.

[197] F. Favre, D. Le Guen, M. L. Moulinard, M. Henry, T. Georges, and F. Devaux, "40 Gbit/s, 5*100 km span straight line soliton transmission experiment without in-line control," *Electronics Letters*, 32(12), pp. 1115-16, 1996.

[198] I. Morita, M. Suzuki, N. Edagawa, S. Yamamoto, and S. Akiba, "Single-channel 40 Gbit/s, 5000 km straight-line soliton transmission experiment using periodic dispersion compensation," *Electronics Letters*, 33(8), pp. 698-9, 1997.

[199] A. Sahara, T. Inui, T. Komukai, H. Kubota, and M. Nakazawa, "40-Gb/s RZ transmission over a transoceanic distance in a dispersion managed standard fiber using a modified inline synchronous modulation method," *Journal of Lightwave Technology*, 18(10), pp. 1364-73, 2000.

[200] K. Suzuki, H. Kubota, T. Komukui, E. Yamada, T. Imai, K. Tamura, A. Sahara, and M. Nakazawa, "40 Gbit/s soliton transmission field experiment over 1360 km using in-line soliton control," *Electronics Letters*, 34(22), pp. 2143-5, 1998.

[201] M. Zitelli, F. Matera, and M. Settembre, "40-Gbit/s transmission in dispersion-management links with step-index fiber and linear compensation," *Optics Letters*, 24(16), pp. 1169-71, 1999.

[202] D. Le Guen, S. Del Burgo, L. Moulinard, D. Grot, M. Henry, F. Favre, and T. Georges, "Narrow band 1.02 Tbit/s (51*20 Gbit/s) soliton DWDM transmission over 1000 km of standard fiber with 100 km amplifier spans," *OFC/IOOC'99. Optical Fiber Communication Conference and the International Conference on Integrated Optics and Optical Fiber Communications (Cat. No.99CH36322). IEEE. Part Suppl., 1999*, pp. D4/1-3 Suppl.

[203] M. Suzuki and K. Sakai, "Recent progress of wavelength division multiplexing technology in Tera-bit/s transoceanic undersea cable systems," *Optical Review*, 7(1), pp. 1-8, 2000.

[204] D. S. Govan, W. Forysiak, and N. J. Doran, "Long-distance 40-Gbit/s soliton transmission over standard fiber by use of dispersion management," *Optics Letters*, 23(19), pp. 1523-5, 1998.

[205] P. V. Mamyshev and N. A. Mamysheva, "Pulse-overlapped dispersion-managed data transmission and intrachannel four-wave mixing," *Optics Letters*, 24(21), pp. 1454-6, 1999.

[206] M. Nakazawa, K. Suzuki, and H. Kubota, "Single-channel 80 Gbit/s soliton transmission over 10000 km using in-line synchronous modulation," *Electronics Letters*, 35(2), pp. 162-4, 1999.

[207] K. Suzuki and M. Nakazawa, "80-160 Gbit/s ultrahigh speed soliton transmission and related soliton technology," *20th Australian Conference on Optical Fibre Technology (ACOFT '95). Proceedings. IREE Soc. 1995*, pp. 347-50.

[208] L. F. Mollenauer, "Dispersion maps for ultra long distance, terabit capacity WDM," *Conference on Lasers and Electro-Optics (CLEO 2000). Technical Digest. Postconference Edition. TOPS Vol.39 (IEEE Cat. No.00CH37088). Opt. Soc. America. 2000*, p. 137.

[209] K. J. Blow and D. Wood, "Theoretical Description of Transient Stimulated Raman-Scattering in Optical Fibers," *IEEE Journal of Quantum Electronics*, 25(12), pp. 2665-2673, 1989.

[210] A. F. Evans, "Novel fibers for soliton communications," *OFC '98. Optical Fiber Communication Conference and Exhibit. Technical Digest. Conference Edition. 1998 OSA Technical Digest Series Vol.2 (IEEE Cat. No.98CH36177). Opt. Soc. America. 1998*, pp. 22-3.

[211] T. Georges, "Bit Error Rate Degradation of Interacting Solitons Owing to Non-Gaussian Statistics," *Electronics Letters*, 31(14), pp. 1174-1175, 1995.

[212] T. Georges, "Study of the non-Gaussian timing jitter statistics induced by soliton interaction and filtering," *Optics Communications*, 123(4-6), pp. 617-23, 1996.

[213] N. J. Smith and N. J. Doran, "Modulational instabilities in fibers with periodic dispersion management," *Optics Letters*, 21(8), pp. 570-2, 1996.

[214] G. P. Agrawal, *Nonlinear Fibre Optics (2nd Edition)*. San Diego: Academic Press, pp. 76-77, 1995.

[215] S. G. Evangelides, L. F. Mollenauer, J. P. Gordon, and N. S. Bergano, "Polarization Multiplexing with Solitons," *Journal of Lightwave Technology*, 10(1), pp. 28-35, 1992.

[216] M. Matsumoto, Y. Akagi, and A. Hasegawa, "Propagation of solitons in fibers with randomly varying birefringence: effects of soliton transmission control," *Journal of Lightwave Technology*, 15(4), pp. 584-9, 1997.

[217] M. Nakazawa, K. Suzuki, and H. Kubota, "160 Gbit/s (80 Gbit/s*2 channels) WDM soliton transmission over 10000 km using in-line synchronous modulation," *Electronics Letters*, 35(16), pp. 1358-9, 1999.

[218] M. Suzuki, I. Morita, K. Tanaka, N. Edagawa, S. Yamamoto, and S. Akiba, "160 Gbit/s (8*20 Gbit/s) soliton WDM transmission experiments using dispersion flattened fibre and periodic dispersion compensation," *Electronics Letters*, 34(5), pp. 475-6, 1998.

[219] F. Favre, D. Le Guen, M. L. Moulinard, M. Henry, and T. Georges, "320 Gbit/s soliton WDM transmission over 1300 km with 100 km dispersion-compensated spans of standard fibre," *Electronics Letters*, 33(25), pp. 2135-6, 1997.

[220] T. Matsuda, M. Murakami, and T. Imai, "340 Gbit/s (34*10 Gbit/s) WDM transmission over 8,514 km using broadband gain equalisation technique for transoceanic systems," *Electronics Letters*, 35(13), pp. 1090-1, 1999.

[221] T. Hirooka, T. Nakada, and A. Hasegawa, "Feasibility of densely dispersion managed soliton transmission at 160 Gb/s," *IEEE Photonics Technology Letters*, 12(6), pp. 633-5, 2000.

[222] U. Feiste, R. Ludwig, C. Schbert, J. Berger, S. Diez, C. Schmidt, and H. G. Weber, "160 Gbit/s transmission using 160 to 40 Gbit/s OTDM and 40 to 10 Gbit/s ETDM demux-techniques," *26th European Conference on Optical Communication. ECOC '00 Conference. Soc. Electr. Electron. Postdeadline Papers, 2000.*

[223] W. K. Kaechele, M. L. Dennis, R. B. Jenkins, T. F. Carruthers, and I. N. Duling, III, "Dispersion-managed transmission of 100 Gb/s time-division-multiplexed return-to-zero

format data," *Optical Fiber Communication Conference. Technical Digest Postconference Edition. Trends in Optics and Photonics Vol.37 (IEEE Cat. No. 00CH37079). Opt. Soc. America. Part vol.1, 2000*, pp. 232-4 vol.

[224] D. Marcuse and C. R. Menyuk, "Simulation of single-channel optical systems at 100 Gb/s," *Journal of Lightwave Technology*, 17(4), pp. 564-9, 1999.

[225] L. J. Richardson and W. Forysiak, "Energy variation of dispersion-managed solitons in amplified systems: a physical interpretation," *Conference on Lasers and Electro-Optics (CLEO 2000). Technical Digest. Postconference Edition. TOPS Vol.39 (IEEE Cat. No.00CH37088). Opt. Soc. America. 2000*, pp. 27-8.

[226] L. J. Richardson, W. Forysiak, and N. J. Doran, "Energy enhancement of short-period dispersion-managed solitons," *Conference on Lasers and Electro-Optics (CLEO 2000). Technical Digest. Postconference Edition. TOPS Vol.39 (IEEE Cat. No.00CH37088). Opt. Soc. America. 2000*, pp. 32-3.

[227] H. Toda, I. Akiyoshi, N. Yamaguchi, and A. H. Liang, "On the dispersion slope compensation in dense dispersion managed solitons," *Technical Digest. 5th Optoelectronics and Communications Conference. OECC '00 Organizing Committee. 2000*, pp. 338-339, 2000.

[228] T. Georges, "Amplifier Noise Jitter of 2 Interacting Solitons," *Optics Communications*, 85(2-3), pp. 195-201, 1991.

[229] H. S. Chung, H. Kim, S. E. Jin, E. S. Son, D. W. Kim, K. M. Lee, H. Y. Park, and Y. C. Chung, "320-Gb/s WDM transmission with 50-GHz channel spacing over 564 km of short-period dispersion-managed fiber (perfect cable)," *IEEE Photonics Technology Letters*, 12(10), pp. 1397-9, 2000.

[230] K. Fukuchi, M. Kakui, A. Sesaki, T. Ito, Y. Inada, T. Tsuzaki, T. Shitomi, K. Fujii, S. Shikii, H. Sugahara, and A. Hasegawa, "1.1-Tb/s (55*20-Gb/s) dense WDM soliton transmission over 3,020 km widely-dispersion-managed transmission line employing 1.55/1.5- mu m hybrid repeaters," *25th European Conference on Optical Communication. ECOC '99 Conference. Soc. Electr. Electron. Part Suppl., 1999*, pp. 42-3 Suppl.

[231] G. C. Gupta, K. Fukuchi, and T. Ogata, "Highly efficient 1 Tb/s (50 ch*20 Gb/s)-2000 km RZ transmission experiment by suppressing XPM with optimized pulsewidth," *Optical Fiber Communication Conference. Technical Digest Postconference Edition. Trends in Optics and Photonics Vol.37 (IEEE Cat. No. 00CH37079). Opt. Soc. America. Part vol.1, 2000*, pp. 152-4 vol.

[232] E. Yoshida, T. Yamamoto, A. Sahara, and M. Nakazawa, "320 Gbit/s TDM transmission over 120 km using 400 fs pulse train," *Electronics Letters*, 34(10), pp. 1004-5, 1998.

[233] Y. Kodama and S. Wabnitz, "Reduction and suppression of soliton interactions by bandpass filters," *Optics Letters*, 18(16), pp. 1311-13, 1993.

[234] K. J. Blow, N. J. Doran, and D. Wood, "Suppression of the soliton self-frequency shift by bandwidth-limited amplification," *Journal of the Optical Society of America B-Optical Physics*, 5(6), pp. 1301-4, 1988.

[235] M. Nakazawa, K. Kurokawa, H. Kubota, and E. Yamada, "Observation of the trapping of an optical soliton by adiabatic gain narrowing and its escape," *Physical Review Letters*, 65(15), pp. 1881-4, 1990.

[236] D. Le Guen, A. O'Hare, S. Del Burgo, D. Grot, F. Favre, and T. Georges, "Narrowband 640 Gbit/s soliton DWDM transmission over 1200 km of standard fibre with 100 km -21 dB amplifier spans," *Electronics Letters*, 34(24), pp. 2345-6, 1998.

[237] S. K. Turitsyn, E. G. Turitsyna, and M. P. Fedoruk, "Path-average theory of intra-channel four-wave mixing," *Conference on Lasers and Electro-Optics (CLEO 2000). Technical Digest. Postconference Edition. TOPS Vol.39 (IEEE Cat. No.00CH37088). Opt. Soc. America. 2000*, p. 27.

[238] F. Favre, D. Le Guen, M. L. Moulinard, M. Henry, P. L. Francois, F. Devaux, and T. Georges, "Single-wavelength 40 Gbit/s, 8*100 km-span soliton transmission without any in-line control," *Electronics Letters*, 33(5), pp. 407-8, 1997.

[239] I. Morita, K. Tanaka, N. Edagawa, and M. Suzuki, "40 Gb/s single-channel soliton transmission over transoceanic distances by reducing Gordon-Haus timing jitter and soliton-soliton interaction," *Journal of Lightwave Technology*, 17(12), pp. 2506-11, 1999.

[240] S. B. Alleston, P. Harper, I. S. Penketh, I. Bennion, and N. J. Doran, "40 Gbit/s single channel dispersion managed pulse propagation in standard fibre over 509 km," *Electronics Letters*, 35(1), pp. 57-9, 1999.

[241] F. Merlaud and S. K. Turitsyn, "Intra-channel four wave mixing ang ghost pulse generation: time domain approach," *26th European Conference on Optical Communication. ECOC '00, 2000.*

[242] V. E. Zakharov and S. V. Manakov, "On propagation of short pulses in strong dispersion managed optical lines," *Pis'Ma V Zhurnal Eksperimental'Noi i Teoreticheskoi Fiziki*, 70(9), pp. 573-6, 1999.

[243] F. Abdullaev and B. B. Baizakov, "Disintegration of a soliton in a dispersion-managed optical communication line with random parameters," *Optics Letters*, 25(2), pp. 93-5, 2000.

[244] M. Matsumoto and H. A. Haus, "Stretched-pulse optical fiber communications," *IEEE Photonics Technology Letters*, 9(6), pp. 785-7, 1997.

[245] L. J. Richardson and W. Forysiak, "Short period dispersion management," *Workshop on the dispersion managed soliton (associated with OECC) 2000.*

[246] L. J. Richardson, K. J. Blow, and V. K. Mezenrsev, "Control of soliton-like propagation in short period dispersion maps with random parameters," *Nonlinear guided waves and their applications (NLGW) 2001.*

[247] L. J. Richardson, V. K. Mezenrsev, and S. K. Turitsyn, "Spectral efficiency of dispersion managed solitons: comparison of 20, 40 and 80 Gbit/s based WDM transmission," *Conference on Lasers and Electro-Optics (CLEO) 2001.*

[248] G. P. Agrawal, *Nonlinear Fibre Optics (2nd Edition)*. San Diego: Academic Press, pp. 50-55, 1995.

[249] G. P. Agrawal, *Nonlinear Fibre Optics (2nd Edition)*. San Diego: Academic Press, pp. 51-52, 1995.

[250] F. Forghieri, "Modeling of wavelength multiplexed lightwave systems," *Conference on Optical Fiber Communications. Technical Digest. Postconference Edition. 1997 OSA Technical Digest Series. Vol.6 (IEEE Cat. No.97CH36049). Opt. Soc. America. 1997. (Tutorial sessions)*, pp. 3-40.

[251] E. Iannone, F. Matera, A. Mecozzi, and M. Settembre, *Nonlinear Optical Communication Networks*: Wiley Series in Microwave and Optical Engineering, pp. 57-58, 1998.

[252] P. A. K. Wai and C. R. Menyuk, "Stabillity of solitons in randomly varying birefringent fibres," *Optics Letters*, 16(pp. 1231-1233, 1991.

[253] C. De Angelis, F. Matera, and S. Wabnitz, "Soliton instabilities from resonant random mode coupling in birefringent optical fibers," *Optics Letters*, 17(12), pp. 850-2, 1992.